MATHEMATICAL MODELING OF THE EVOLUTION OF THERMAL FIELD DURING START-UP PHASE OF THE DIRECT CHILL CASTING PROCESS FOR AA5182 SHEET INGOTS

by

JOYDEEP SENGUPTA

B. Tech., Regional Engineering College, Warangal, India, 1992
M. Tech., Indian Institute of Technology, Kharagpur, India, 1994

A THESIS SUBMITTED IN PARTIAL FULFILLMENT OF
THE REQUIREMENTS FOR THE DEGREE OF

DOCTOR OF PHILOSOPHY

in

THE FACULTY OF GRADUATE STUDIES

(Department of Metals and Materials Engineering)

We accept this thesis as conforming
to the required standard

THE UNIVERSITY OF BRITISH COLUMBIA
December 2002

(Joydeep Sengupta)

Department of Metals and Materials Engineering
The University of British Columbia
Vancouver, Canada

Date: 19th December 2002

Abstract

The control of the thermal cooling conditions at the start-up phase of the Direct Chill (DC) casting process for aluminum sheet ingots is difficult, and is critical from the standpoint of defect formation. Firstly, boiling water heat transfer governs the secondary cooling experienced by the ingot surfaces as they emerge from the mould. This results in varying rates of heat transfer from the ingot faces as the surface temperature of the ingot changes with time during the start-up phase. Moreover, if the ingot surface temperature at locations below the point of water impingement is high enough to promote film boiling, the water is ejected away from the surface. This can result in a sudden decrease in heat transfer and the formation of local hot spots. Also, the chill water may enter into the gap formed between the ingot base and the bottom block with the evolution of the butt curl. This process of water incursion alters the heat transfer from the base of the ingot, and in turn affects the surface temperature of the ingot faces.

A comprehensive mathematical model has been developed to describe heat transfer during the start-up phase of the D.C. casting process. The model, based on the commercial finite element package ABAQUS, includes primary cooling to the mould, secondary cooling to water, and ingot base cooling. The algorithm used to account for secondary cooling to the water includes boiling curves that are a function of surface temperature, water flow rate, impingement point temperature, and position relative to the point of water impingement. In addition, the secondary cooling algorithm accounts for water ejection, which can occur at low water flow rates (low heat extraction rates). The algorithm used to describe ingot base cooling includes the drop in contact heat transfer due to base deformation (butt curl), and also the increase in heat transfer due to the process of water incursion between the ingot base and bottom block.

The model has been extensively validated against temperature measurements obtained from two 711 x 1680 mm AA5182 ingots, cast under different start-up conditions (non typical "cold" practice and non-typical "hot" practice). Temperature measurements were taken at various locations on the ingot rolling and narrow faces, ingot base, and top surface of the bottom block. Ingot base deflection data were also obtained for the two test conditions. Comparison of the model predictions with the data collected from the cast/embedded thermocouples indicates that the model that accounts for the processes of water ejection and water incursion, is capable of describing the flow of heat in the early stages of the casting process, satisfactorily.

The research programme represents a significant improvement over existing thermal models that do not quantitatively describe the important phenomena related to the effects of water ejection and water incursion, which are specific to the transient start-up phase of the process. The thermal model, which has been extensively validated by the industrial data, not only provides an insight into the link between ingot base cooling and secondary water cooling heat transfer during the start-up phase, but also emerges as a basis for the development of thermomechanical models, based on fundamental principles, which can be used as a powerful tool for process optimization and quality control.

Table of Contents

List of Tables

List of Figures

List of Symbols

Latin Symbols	Description	Units
A	a set of differential equations representing a problem	---
B	a set of differential equations representing boundary conditions	---
c_p	specific heat capacity	$Jkg^{-1}K^{-1}$
$[C^e]$	elemental heat capacitance matrix	$Jkg^{-1}K^{-1}$
f	a polynomial function	---
f_s	volume fraction solidified	---
f_{wet}	wetting factor for water incursion	---
h	convective heat transfer coefficient	$Wm^{-2}K^{-1}$
$h_{air\ gap}$	heat transfer coefficient associated with air gap	$Wm^{-2}K^{-1}$
$h_{contact}$	heat transfer coefficient associated with meniscus	$Wm^{-2}K^{-1}$
h_{gap}	gap conductance coefficient at the ingot/bottom block interface	$Wm^{-2}K^{-1}$
h_{water}	boiling water heat transfer coefficient	$Wm^{-2}K^{-1}$
i, j, k	counters in an algorithm	---
k	thermal conductivity	$Wm^{-1}K^{-1}$
k_x, k_y, k_z	component of k in three directions	
$[K_c^e]$	elemental conductance matrix related to conduction	$Wm^{-1}K^{-1}$
$[K_h^e]$	elemental conductance matrix related to convection	$Wm^{-1}K^{-1}$
$[K^e]$	elemental conductance matrix	$Wm^{-1}K^{-1}$
L	latent heat of fusion	Jkg^{-1}
m	number of Gauss points in an element	---
n	number of degrees of freedom	---
n_x, n_y, n_z	direction cosines	---
N	distance between the metal level in the mould and the sensor	m
N_i	shape functions	---
N_{start}	distance between the metal level in the mould and the sensor at the start of a cast	m
q	heat flow rate per unit area	Wm^{-2}
Q	water flow rate per unit length of mould perimeter	$Lmin^{-1}\ cm^{-1}$
$\dot{Q}$	volumetric heat source term	Wm^{-3}
$\{R_Q^e\}$	heat load vector associated with internal heat generation	Wm^{-1}
$\{R_q^e\}$	heat load vector associated with surface heating	Wm^{-1}
$\{R_h^e\}$	heat load vector associated with surface convection	Wm^{-1}
t	time	s
Δt	time step in an FE analysis	s
t_n , t_{n+1}	consecutive time steps in an FE analysis	s
T	temperature	°C
T_o	initial temperature	°C

$T_{bottom\ block}$	temperature of the bottom block	°C
T_{ingot}	temperature of the ingot	°C
T_L	liquidus temperature of AA5182	°C
T_S	solidus temperature of AA5182	°C
T_{sink}	sink temperature	°C
T_{surf}	ingot surface temperature	°C
T^*	initial temperature of the ingot	°C
W_i, W_j, W_k	weighting functions	---
x	direction along the narrow face in the Cartesian coordinate system	---
X_1	half thickness of the ingot	m
X_2	extent of water incursion in the ingot along x direction	m
X_3	extent of water incursion in the bottom block along x direction	m
y	direction along the rolling face in the Cartesian coordinate system	---
Y_1	half width of the ingot	m
Y_2	extent of water incursion in the ingot along y direction	m
Y_3	extent of water incursion in the bottom block along y direction	m
z	direction along the cast length in the Cartesian coordinate system	---
z'	distance from the water impingement point	m
z_{max}	maximum butt curl measured at ingot corner	m

Greek Symbols

Γ	surface enclosing the computational domain	---
θ	weighting factor in a recurrence algorithm	---
ξ, ζ, η	local coordinate system within an isoparametric element	---
ξ_i, ζ_j, η_k	gaussian points within an element	---
ρ	density	kgm^{-3}
ϕ	exact solution	---
$\hat{\phi}$	approximate solution	---
$\dot{\phi}$	time derivative of ϕ	---
ϕ_i	nodal solution values	---
Ω	computational domain	---
Ω^e	elemental domain	---

Acknowledgements

I would like to thank my research supervisors, Dr. Steve Cockcroft, Dr. Mary Wells, and Dr. Daan Maijer, for their guidance and financial support during the course of my research programme. Their opinions and insights are highly valued and often sought. Special thanks to Dr. Maijer, who taught me to "play with ABAQUS". Both Dr. Cockcroft and Dr. Wells have been my true mentors, and have greatly contributed to my professional and personal development at UBC. I am especially thankful to Dr. Wells for inspiring me to be a well-rounded graduate student, by striking a "fine" balance between my academic and extra-curricular activities at UBC.

I would also like to mention Mr. André Larouche, Mr. Yves Caron, Mr. Joseph Langlais, Mr. Thierry Bourgeois, and Mr. Jean-Pierre Martin of Alcan for their whole-hearted commitment to the academic research programme investigating this industrial problem. The knowledge and expertise they shared with me are invaluable. I am thankful to Mr. Daniel Godin of Alcan's Dubuc Experimental Casting Centre, who made sure that all the industrial experiments were carried out smoothly.

I also gratefully acknowledge the expertise of Dr. Mohamed Gadala, Dr. Roger Reed, Dr. Warren Poole, and Dr. Reza Vaziri, who as the members of my doctoral supervisory committee provided critique and feedback. I am grateful to the Faculty of Graduate Studies' UGF scholarship, which supported me financially in the last two years of my research programme.

I am thankful to my parents, Debamitra and Pradeep, and my sister Debapriya for the love and support they constantly shower on me. I also acknowledge my numerous friends in the department, and at UTSAV, and GSS, for the good times I shared with them at Vancouver.

JOYDEEP SENGUPTA

Vancouver

19th December 2002

CHAPTER 1
INTRODUCTION

1.1 Importance of Aluminum Alloys in Automotive Manufacturing

Over the next few years, the use of aluminum in the automotive industry is estimated to increase dramatically. Presently, the use of aluminum in a car averages from 100 kg/vehicle to 115 kg/vehicle, and some forecasts suggest that it will reach 160 kg/vehicle by 2005 and 270 kg/vehicle by 2010[1]. Aluminum is emerging as the material of choice because it is three times lighter than steel, and when alloyed, can approach steel's high strength characteristics. Hence, to realize the dream of "lean" (cars weighing less than 2000 pounds) and "green" (fuel-efficient and emission free engines) automobiles, North American automakers are looking to aluminum as a lightweight alternative to steel. With the development of the innovative Aluminum Structured Vehicle Technology (ASVT)[2] by Alcan International Ltd., the largest Canadian aluminum producer, high strength AA5xxx and AA6xxx aluminum alloys are gaining considerable importance. Automobiles manufactured using ASVT exhibit comparable mechanical properties, stiffness, strength, and crashworthiness at significantly reduced weight compared with conventional vehicles manufactured with steel, while offering increased fuel-economy and improved corrosion resistance.

1.2 Direct Chill Casting Process for Aluminum Sheet Ingots

Typically, commercial production of aluminum sheets for automotive use encompasses several manufacturing steps. These include casting and homogenization of aluminum ingots, hot and cold rolling of the ingots to obtain sheets of required thickness, and finally, heat-treating the sheets to achieve desired mechanical properties. One of the technical challenges in producing these sheets is the ability to cast high strength aluminum sheet ingots economically and free from defects.

The semi-continuous Direct Chill (D.C.) Casting process (**Figure 1.1**[3, 4]) has been used almost exclusively to produce aluminum sheet ingots during the past 60 years owing to its robust nature and relative simplicity. In this process, a bottom block is partially inserted into an open rectangular mould at the start of a cast. Superheated liquid aluminum is poured from a nozzle,

through a distribution bag, into the mould, at a predetermined filling rate. Once the molten metal fills the bottom block to a prescribed height, the bottom block and cast ingot are lowered into a casting pit. The level of the metal in the mould is kept constant by continually adding molten metal.

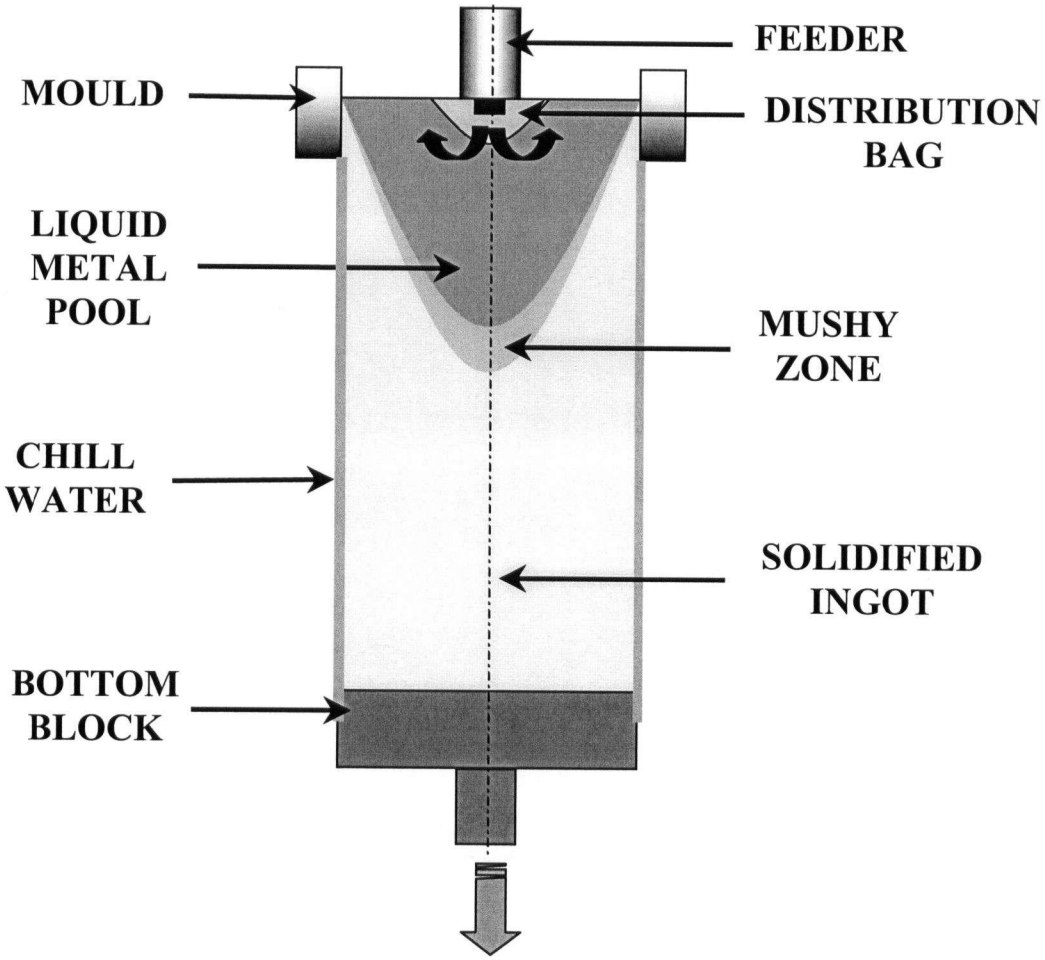

Figure 1.1 – Schematic of the D.C. casting process for aluminum sheet ingots.[3, 4]

The aluminum ingot is subjected to cooling by the transfer of heat to the water-cooled mould (primary cooling), and to cooling through the contact of chill water with the solid shell as it emerges from the mould cavity (secondary cooling). This water comes from a series of holes, which surround the mould at its base. The defining character of the D.C. casting process is the extraction of heat due to this direct impingement of water on the ingot surface – typically ~80% of total heat is removed by this method[3, 4] under steady state conditions, as compared to ~20% of total heat, which is extracted by the mould. The ingot is lowered at a predetermined casting

speed, which varies with time and is tailored to suit the alloy. (Industry uses different casting parameters or "recipes" for different alloys based on their hot tearing/cold cracking susceptibility. These recipes vary from one company to another, and generally, details of these recipes are proprietary and are not made available in published literature.) The process is semi-continuous, in that, once the ingot has the desired length (usually ~4-10 m), the casting is stopped and the ingot is removed from the casting pit, illustrated in **Figure 1.2**[5]. The process is restarted when the metal and machinery are ready again.

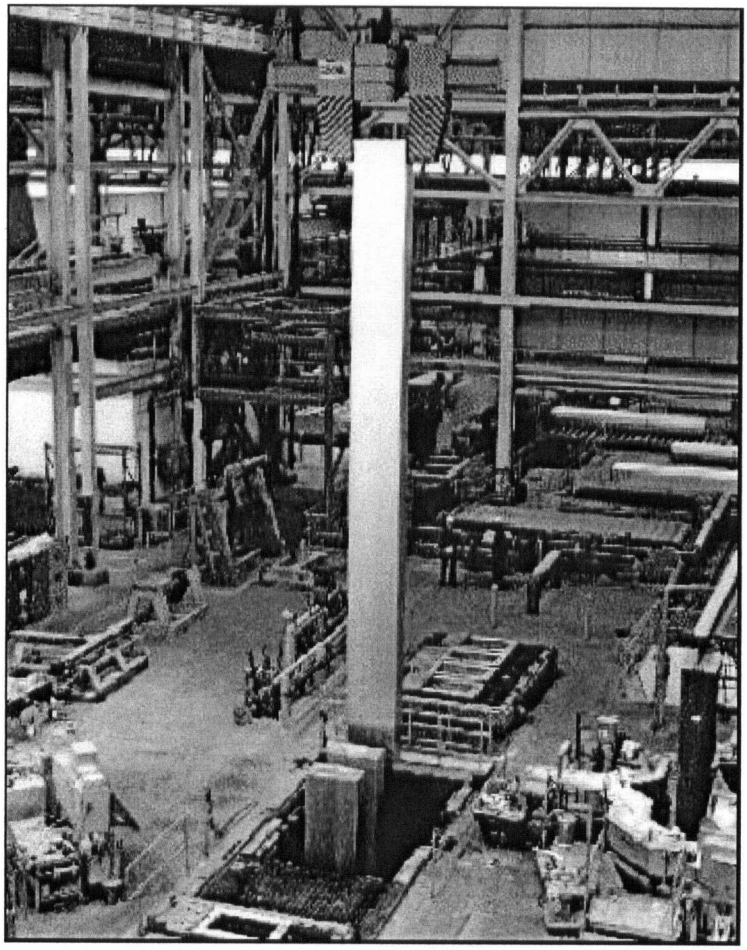

Figure 1.2 – A ~10 m long sheet ingot is removed from casting pit at the end of the D.C. casting process.[5]

In terms of the thermal field evolution, there are two distinct stages in this semi-continuous process. Stage I[3, 4] or the start-up†, during which time the liquid pool profile and thermal field evolve with time relative to the mould; and Stage II[3, 4] or steady state, during which time they remain essentially constant relative to the mould. Steady state operation is usually achieved within a cast length of ~0.5-1 m for a fully developed sump.

1.2.1 Quality Issues in D.C. Cast Ingots

As mentioned earlier, one of the most important considerations in D.C. casting of aluminum sheet ingots is the capability of attaining a defect-free ingot. The quality issues of major concern are[6]:

- hot tearing and cold cracking
- dimensional control.

The thermal stresses and strains in the ingot generated during the start-up phase can play a major role in the initiation of hot tears and cold cracks, especially in the case of high strength alloys, such as AA5182[7]. The hot tears or pre-solidification cracks form in the mushy zone, when a tensile stress is imposed across partially solidified grains, and the surrounding liquid cannot fill the gap between the dendrites. Hence, these cracks are always inter-granular. The cold cracks are considered to initiate at temperatures below the solidus, and are always trans-granular.

It has been observed that high casting speeds favor hot tears and low casting speeds increase the risk of cold cracks in the industry[6]. The formation of hot tears have also been linked with the frictional forces between the ingot and mould (related to mould cleanliness)[8], and the variability in cooling conditions during the transient phase[9, 10]. Hot tearing criteria based on (i) time spent by the alloy in different regimes of the solidification interval, (ii) liquid pressure drop associated with solidification shrinkage, and (iii) tensile stress caused by thermal contraction of the solid phase have been suggested[11-14]. Therefore, quantification of temperature fields, cooling rates, thermal stresses, strains, and strain rates generated in the ingot is essential to predict and control the formation of hot tears in the mushy zone during the cast start-up.

Due to the temperature gradients in the ingot, large thermal stresses can develop in the solidifying metal causing macro-deformation of the ingot. One example is deformation of the

† During the start-up phase, the ingot is additionally cooled by heat conduction to the bowl-shaped bottom block, which is referred to as base cooling.

ingot base, called butt curl (**Figure 1.3**[3, 4]), which occurs during the transient start-up phase. The butt curl is usually seen to develop abruptly when the cooling water hits the ingot surface. Butt curl rate (derivative of displacement w.r.t. time) has been observed to reach a maximum shortly after the water impingement and then to decay to a very low value after a few minutes of the casting process[15].

As reported by Droste and Schneider[16], the production problems related to butt curl include: run outs of the melt, cold shuts, reduced rigid standing (instability) of the ingot on bottom block, and low recovery rates. Ultimately, if the magnitude of butt curl is excessive, the ingot bottom may have to be sawed off. Since the evolution of butt curl is directly linked with the amount of thermal stress generated in the ingot, attempts have been made in the industry to control the amount of curl by employing casting practices that reduce the intensity of cooling during the start-up phase. For example, experiments conducted by Droste and Schneider suggest that the use of very low cooling water volume coupled with very high casting velocities for some alloys can reduce base deformation. However, these practices can cause extreme butt shrinkage and dangerous casting situations.

Butt curl can also be reduced by forming a thick bottom shell, which bends to a lesser extent upon direct impingement of water. This can be achieved by appropriate bottom block design or by using longer filling times[17].

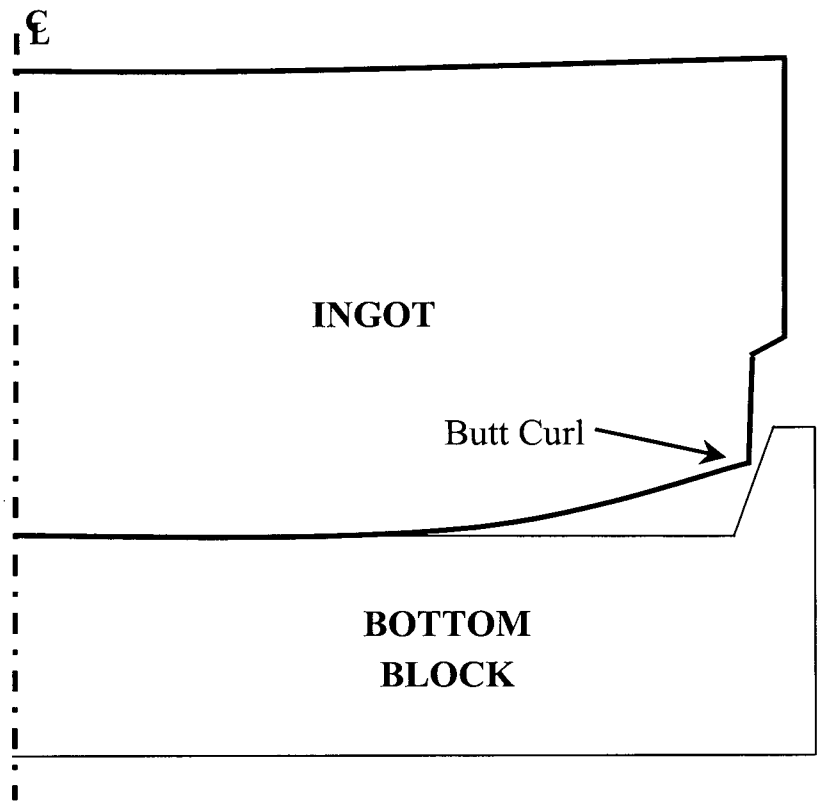

Figure 1.3 – Butt curl phenomenon during the start-up phase of the D.C. casting process.
Note: The magnitude of base displacement has been increased for clarity.[3, 4]

1.2.2 Optimization of the Start-up Phase

From the standpoint of defects, the most critical stage of the D.C. casting process is the start-up phase. Therefore, optimization of this transient phase is the key to the production of defect free ingots. To date, relatively little fundamental work has been done to rationalize the design of the casting process with regards to controlling the final ingot quality. Despite increased use of automation, the control of the thermal cooling conditions at the start is difficult due to the large number of casting parameters involved, as shown in **Figure 1.4**[18], and the individual and combined effects of these parameters on ingot cooling. In order to produce a defect free ingot these parameters must be set at their optimal levels to obtain required ingot cooling conditions.

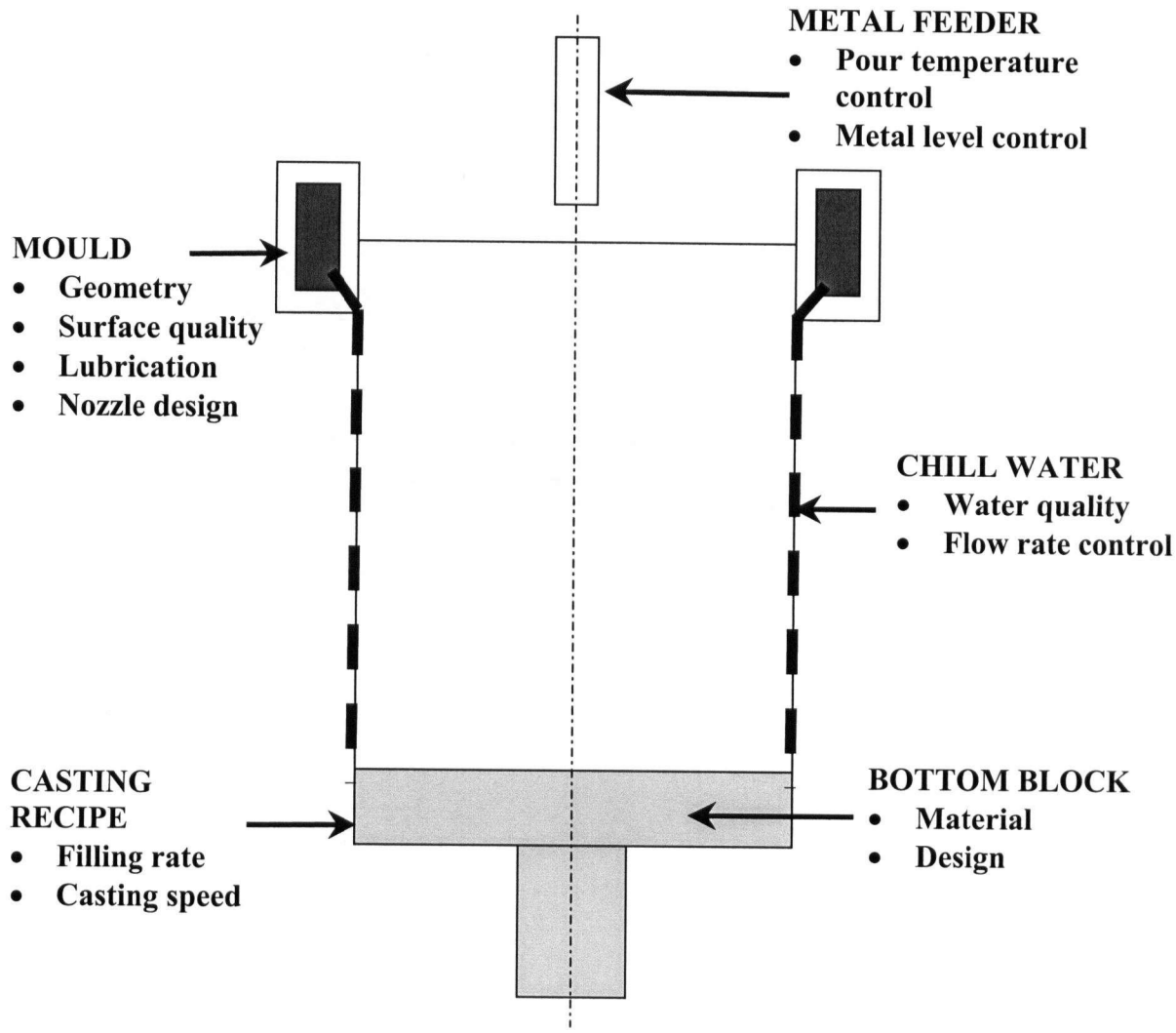

Figure 1.4 – Illustration of various design and process parameters having an impact on the heat transfer process during the cast start-up.[18]

The trend in the industry has been to control the rate of heat transfer by varying the bottom block filling rate, casting speed, and water flow rates during the start-up phase. Additional strategies include the use of a variety of water-cooling systems including Alcoa's CO_2 injection[19], Wagstaff's Turbo process[20], and Alcan's Pulse Water technique[21]. These optimized start-up programs or so-called "casting recipes" governing the start-up procedure, have evolved largely through trial-and-error, and vary with the size of ingots and type of alloy. Attempts have also been made to develop an optimized bottom block shape empirically[22, 23].

A significant part of the problem of developing a fundamentally based approach to optimize the start-up phase lies in the fact that during this transient regime, the ingot is simultaneously cooled by the mould (primary cooling), the chill water (secondary cooling), and the bottom block (base cooling). These three heat transfer paths, shown in **Figure 1.5**, are complex and inter-related. The intensity of primary cooling experienced in the mould can change during the start-up phase. In particular, the upward deformation of the ingot base (butt curl) tends to draw the sides inwards altering heat transfer to the mould and ultimately, introducing variability in ingot surface temperature as it exits the mould. The secondary cooling experienced by the ingot surfaces as they emerge from the mould, is governed by boiling water heat transfer. Referring to **Figure 1.6**[24], this results in varying rates of heat transfer from the ingot faces as the surface temperature of the ingot changes with time during the start-up phase. Moreover, if the ingot surface temperature at the point of water impingement is high enough to promote film boiling, the water film can be ejected away at the surface. This can result in a sudden decrease in heat transfer at the surface of the ingot. Finally, the evolution of butt curl complicates heat extraction from the base of the ingot during the start-up phase. This deformation arises due to the large thermal contraction of the sides of the ingot and leads to "pulling away" of the ingot corners and sides from the bottom block. As butt curl evolves, the heat transfer from the ingot base can initially drop significantly, due to the loss of contact with the bottom block, and then increase as cooling water is drawn into the gap between the base of the ingot and the bottom block, which is known as water incursion.

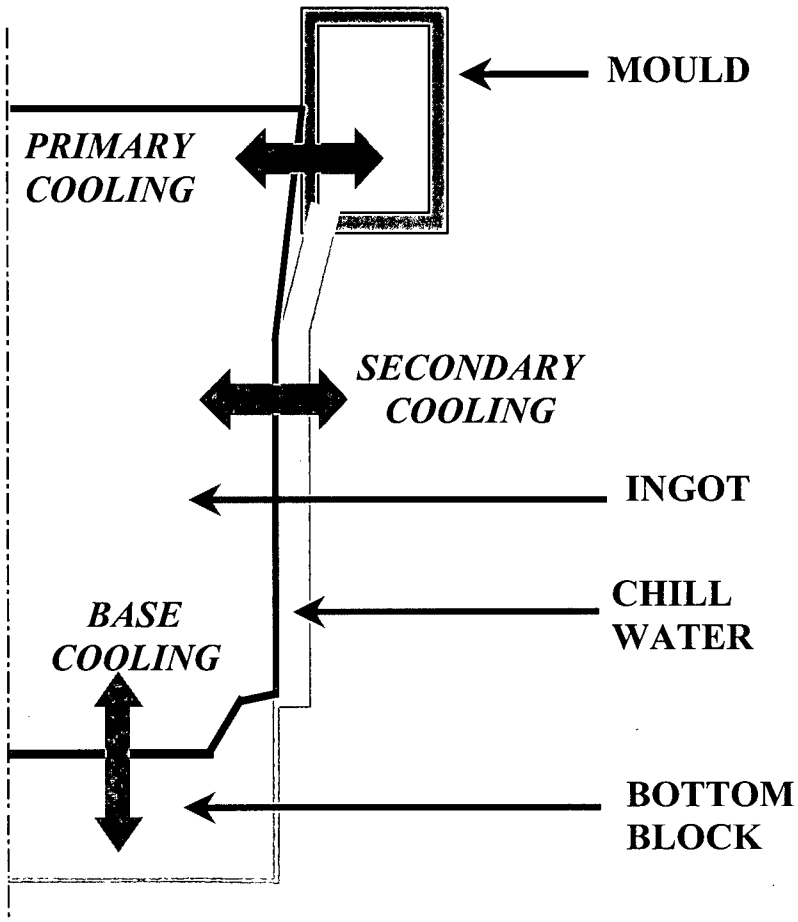

Figure 1.5 – Various cooling processes active during the cast start-up phase.

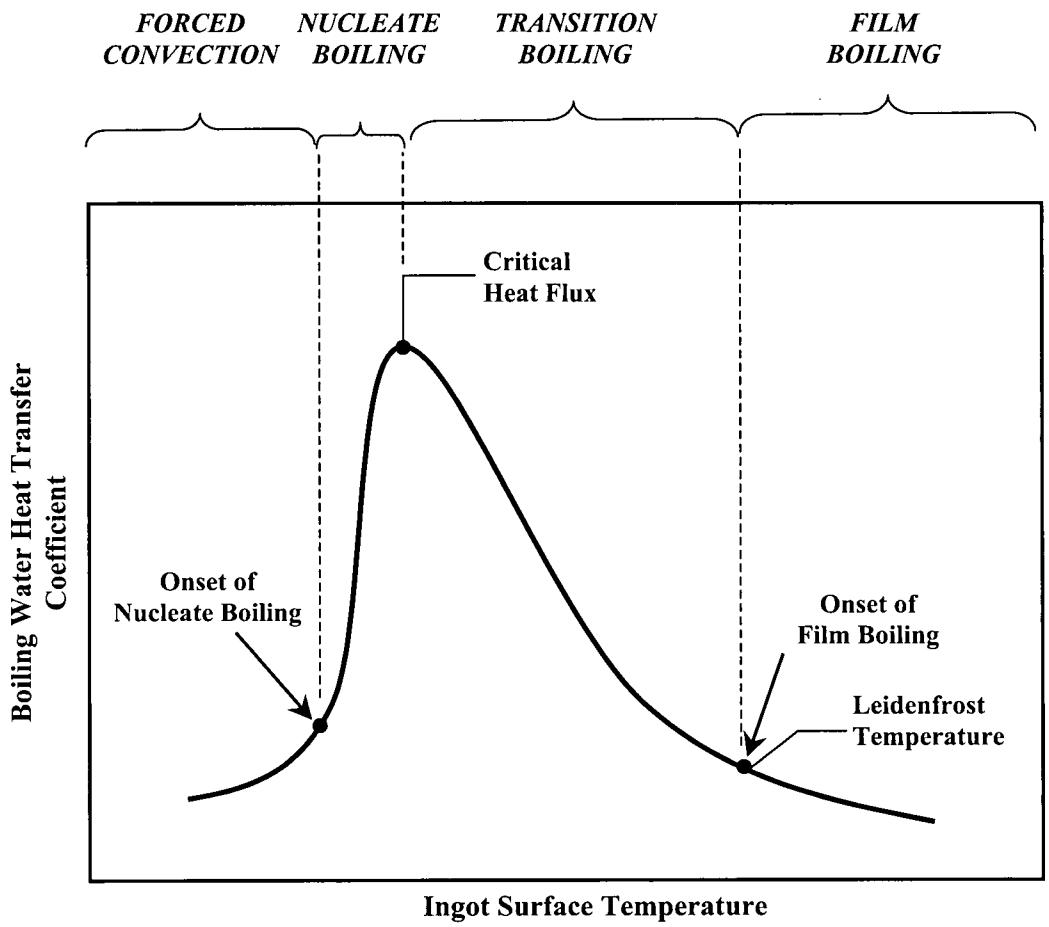

Figure 1.6 – Generic boiling curve indicating the different boiling water heat transfer regimes.[24]

The complexity of the various heat transfer processes described above requires tight control of the ingot cooling during the start-up phase. With the development of sophisticated commercial finite element codes and more powerful computers, mathematical models based on fundamental principles can be developed to predict the temperature distribution and stress/strain fields in the solidifying ingot during the D.C. casting process. This approach not only eliminates immense experimental efforts required to optimize the process, but also addresses the crux of the problem; i.e. describing and analyzing the thermomechanical behavior of the ingot during the start-up phase. It is therefore critical that these mathematical tools capture all of the complexity of the physical phenomena active during the industrial process if they are to ultimately be useful.

As a part of an on-going effort to reduce crack formation in rolling ingots during the D.C. casting process, Alcan International Ltd. has entered into a collaborative research agreement with researchers in the Department of Metals and Materials Engineering at the University of British Columbia to develop a 3-D fully coupled mathematical model describing the evolution of temperature, stress and strain in AA5182[†] aluminum sheet ingots during the start-up phase. This doctoral research programme presents part of this effort. Similar joint efforts between European industries and Universities have been reported in the literature[26, 27]. For example, thermomechanical models for D.C. casting process are being developed concurrently, using commercial finite element packages such as MARC[‡] (by Hoogovens, Netherlands and Péchiney, France), ABAQUS[§] (by EPFL-Lausanne, Switzerland), and ALSIM/ALSPEN (by Institute for Energy Technology, Norway). National laboratories in the United States (Albany Research Center, Oregon, Argonne National Laboratory, Illinois, and Oak Ridge National Laboratory, Tennessee), and University of Kentucky, Lexington, Kentucky have also collaborated recently to develop mathematical models to study ingot stress crack formation and butt deformation[28], and to reduce aluminum ingot scrap[*].

In the chapter that follows, developments in the mathematical modeling of the D.C. casting process during the past two decades are presented and reviewed.

[†]AA5182 is a non-heat treatable aluminum alloy containing a nominal composition of magnesium 4.5 wt% with a small percentage of manganese (0.35 wt%) added to improve strength. At this composition, magnesium remains in the solid solution for the majority of the casting cycle. The two-phase boundary is crossed only at relatively low temperatures where diffusion constraints would limit the extent of Mg_2Al_3 formation during the ingot-cooling period. Therefore, strengthening by the formation of second phase precipitates (*i.e.* Mg_2Al_3) in AA5182 is insignificant. As a result, AA5182 is a relatively ductile alloy wherein strengthening is achieved primarily by work hardening[25].

[‡] Trademark of MARC Analysis Research Corporation, Palo Alto, USA.

[§] Trademark of Hibbit, Karlson and Sorensen, Inc., Providence, USA.

[*] According to the DoE report, D.C. casting process is used for 68% of the aluminum ingots produced in the USA; with ingot scrap, from stress cracks and butt curl, accounting for a 5% loss in production. It is estimated that predictive modeling would lower production losses to 2%, which will result in an estimated annual energy savings of over six trillion Btu and cost savings of over $550 million by 2020.

References

1. Becker, M.N., *Aluminum: New Challenges in Downstream Activities,* JOM, The Minerals, Metals & Materials Society, Warrendale, USA, 1999 (November), pp. 26-38.
2. *The World of Alcan*, General Information Document published by Alcan Inc., Public Relations Group, 1990.
3. Wiskel, J.B., *Thermal Analysis of the Start-up Phase for D.C. Casting of an AA5182 Aluminum Ingot*, Ph. D. Thesis, Dept. of Metals & Materials Engineering, University of British Columbia, Vancouver, Canada, 1996.
4. Drezet, J.-M., *Direct Chill and Electromagnetic Casting of Aluminium Alloys: Thermomechanical Effects and Solidification Aspects*, Ph. D. Thesis, Department of Materials, Ecole Polytechnique Federale de Lausanne, Lausanne, Switzerland, 1996.
5. Alcan Primary Metal British Columbia Website, Alcan Corporate Affairs, B.C. Operations, http://www.sno.net/alcan/, 2002.
6. Grandfield, J.F., and McGlade, P.T., *D.C. Casting of Aluminium: Process Behaviour and Technology,* Materials Forum, 1996, **20**, pp. 29-51.
7. Jacoby, J.E., *Direct Chill Casting Defects,* Proceedings of the 5th Australasian Asian Pacific Conference on Aluminum Cast House Technology (Edited by M. Nilmani, P. Whiteley, and J. Grandfield), The Minerals, Metals & Materials Society, 1997, pp. 245-251.
8. Nofal, A.A., *Surface Defect Formation in the D.C.-cast Aluminum Products,* Advances in Continuous Casting: Research and Technology, Woodhead Publishing Ltd., 1992, pp. 208-215.
9. Wiskel, J.B., and Cockcroft, S. L., *Heat-Flow-Based Analysis of Surface Crack Formation during the Start-up of the Direct Chill Casting Process: Part I. Development of the Inverse Heat-Transfer Model,* Metallurgical and Materials Transactions B, 1996, **27B**, pp. 119-127.
10. Wiskel, J.B., and Cockcroft, S. L., *Heat-Flow-Based Analysis of Surface Crack Formation during the Start-up of the Direct Chill Casting Process: Part II. Experimental Study of an AA5182 Rolling Ingot,* Metallurgical and Materials Transactions B, 1996, **27B**, pp. 129-137.

11. Clyne, T.W., and Davies, G.J., *The Influence of Composition on Solidification Cracking Susceptibility in Binary Alloy Systems,* The British Foundrymen, 1981, **74**, pp. 65-73.

12. Farup, I., Drezet, J-M., and Rappaz, M., *In Situ Observation of Hot Tearing Formation in Succinonitrile-acetone,* Acta Materialia, 2001, **49**, pp. 1261-1269.

13. Rappaz, M., Drezet, J-M., and Gremaud, M., *A New Hot-Tearing Criterion,* Metallurgical and Materials Transactions A, 1999, **30A**, pp. 449-455.

14. Farup, I., and Mo, A., *Two-Phase Modeling of Mushy Zone Parameters Associated with Hot Tearing,* Metallurgical and Materials Transactions A, 2000, **31A**, pp. 1461-1472.

15. Fjær, H.G., and Mo, A., *Mathematical Modeling of Butt Curl Deformation of Sheet Ingots. Comparison with Experimental Results for Different Starter Block Shapes,* Light Metals 1995 (Ed. J. Evans), The Minerals, Metals & Materials Society, Warrendale, USA., 1995, pp. 951-959.

16. Droste, W., and Schneider, W., *Laboratory Investigations about the Influence of Starting Conditions on Butt Curl and Swell of D.C. Cast Sheet Ingots,* Light Metals 1991 (Ed. E.L. Rooy), The Minerals, Metals & Materials Society, Warrendale, USA, 1991, pp. 945-951.

17. Schneider, W., *D.C. Casting of Aluminum Alloys - Past, Present and Future,* Light Metals 2002 (Ed. W. Schneider), The Minerals, Metals & Materials Society, Warrendale, USA, 2002, pp. 953-960.

18. Caron, Y., and Larouche, A., *Importance of Understanding Ingot Butt Cooling Conditions at Cast Start-up: A Case Study,* Light Metals 1996 (Ed. W. Hale), The Minerals, Metals & Materials Society, Warrendale, USA., 1996, pp. 963-969.

19. Yu, H., *A Process to Reduce D.C. Ingot Butt Curl and Swell,* Light Metals 1980, The Minerals, Metals & Materials Society, Warrendale, USA, 1980, pp. 613-628.

20. Wagstaff, *U.S. Patent # 4,693,298*, 1987.

21. Bryson, N.B., *U.S. Patent # 3,411,079*, Casting of Aluminum Ingots, 1969.

22. Schneider, W., and Jensen, E. K., *Investigations about Starting Cracks in D.C. Casting of 6063 Type Billets Part I: Experimental Results,* Light Metals 1990 (Ed. C. M. Bickert), The Minerals, Metals & Materials Society, Warrendale, USA, 1990, pp. 931-936.

23. Schneider, W., Jensen, E. K., and Carrupt, B., *Development of a New Starting Block Shape for the D. C. Casting of Sheet Ingots: Part I. Experimental Results,* Light Metals

1995 (Ed. J. Evans), The Minerals, Metals & Materials Society, Warrendale, USA, 1995, pp. 961-967.

24. White, F.M., *Heat and Mass Transfer*, 1991, A-W Pub. Co.

25. Hatch, J.E.E., *Aluminum: Properties and Physical Metallurgy*, 1999, American Society for Metals, Materials Park, Ohio.

26. Drezet, J.-M., Bughardt, A., Fjær, H. G., and Magnin, B., *Thermomechanical Effects in D.C. Casting of Aluminum Alloy: A Numerical Benchmark Study,* Materials Science Forum, 2000, **329-330**, pp. 493-500.

27. *VIR[CAST] News*, Newsletter edited by Calcom SA, Switzerland, 1st edition, Spring edition, 2002.

28. *Aluminum: Project Fact Sheet*, Newsletter published by Office of Industrial Technologies, Energy Efficiency, and Renewable Energy, U. S. Department of Energy (DoE), Washington, D.C., 2000.

CHAPTER 2

LITERATURE REVIEW

2.1 Introduction

Research into the mathematical modeling of the D.C. casting process has usually been separated into two distinct, but inter-related tasks: (i) computation of the thermal fields, and (ii) calculation of stress state in the ingot during the casting process.

Final successful solution of the stress model is dependent on the thermal analysis in two ways: 1) the correct prediction of the solid-liquid interface position, and 2) the precision with which the thermal model can determine temperature fields within the ingot[1]. Thermal models can be developed independent of stress models in an uncoupled analysis; however, to include the effects of air gap formation between the ingot and mould and butt curl on the heat transfer, the two models should be coupled together.

In the following sections thermal and stress models of the D.C. casting process currently available in the published literature have been critically reviewed.

2.2 Uncoupled Thermal Models

Mathematical models of the D.C. casting process have evolved continuously over the past 25 years. In the 1970s and 1980s, thermal models first became available and typically these models were simple 2-D analyses and represented the steady state regime of the process. Weckman and Niessen[1] did an exhaustive review of the development in the thermal models for the D.C. casting process until the end of the 1980s.

In 1980, Jensen[2] reported the development of a simple 2-D axisymmetric model for 200 mm dia. billets to study the effect of contact heat transfer at the base of ingot on the development of the solidifying shell during the transient phase. In 1981, Katgerman[3] described a 2-D axisymmetric heat flow model for computing the solidification time and fraction solid as a function of the distance along the ingot in order to predict the hot cracking tendencies of several alloys as a function of casting rate and billet diameter. The hot cracking index was found to be the highest for an AA5182 alloy.

In 1982, Weckman and Niessen[4] published a comprehensive heat transfer analysis with well laid out boundary conditions to describe the problem. The authors developed an empirical relationship describing the boiling water heat transfer coefficient as a function of ingot surface temperature, water flow rate, and distance from the point of water impingement. Their experimental studies on AA6063 cast billets revealed that with an increase in casting speed the length of nucleate boiling region on the casting surface was increased, along with the sump depth. They noted that if the casting speeds are too high, or the water flow rates are low enough, the surface temperature of the ingot will rise and surpass a critical temperature, during which time there will be a sudden switch to film boiling and the heat transfer coefficient may drop to a value as low as 400 $Wm^{-2}K^{-1}$. At this point the water will boil off the surface of the ingot, and if the ingot shell is not thick enough, it may not sustain the metallostatic pressure, causing liquid metal breakouts.

Weckman and Niessen attempted to mathematically represent the secondary cooling boundary conditions as a function of water flow rate and saturation temperature of water, using heat transfer theory for a free falling film of water on the surface of a cylindrical ingot. The solid-liquid interface was modeled as a planar heat source where heat input over this plane was proportional to the latent heat of fusion and casting speed, and its position was determined iteratively. This method of describing latent heat was used to accurately represent the interface geometry, which is important when studying hot tearing problems at the base of the sump. The model was verified by experimental thermocouple data and zinc prints of solid-liquid interface. However, both the mathematical model and experiments considered steady state casting conditions, and hence cannot be directly applied to the start-up phase. Moreover, the major drawback of this model is that it could not handle mushy zones. Their work, however, gives an insight into the importance of various factors like water flow rate, position of the water impingement point, and casting speed, which must be considered while determining the boundary conditions for the water-cooled ingot surface.

In 1986, Bakken and Bergström[5] addressed the problem of using semi-empirical formulae developed from laboratory measurements to represent secondary cooling conditions, by determining heat transfer coefficients from in-situ temperature measurements during an actual industrial casting process, and using these coefficients in their 2-D model[6]. The authors argued that direct application of laboratory measurements to D.C. casting thermal models is erroneous,

owing to the fact that cooling rates are much lower in industrial situations. Furthermore, it is wrong to assume that various heat transfer mechanisms (film and nucleate boiling) will be active in exactly the same temperature intervals in laboratory and industrial settings.

In 1989, Tarapore[7] developed a 2-D thermal model to study the effect of three casting variables - metal temperature, casting speed, and water flow rate - on the solidification characteristics of a cast ingot. A base case validated by industrial measurements was developed, which was then used to study the impact of the casting variables.

The need to address the issue of crack/hot tear formation during the cast start-up provided an impetus to model the thermal behavior during the transient state, in the early 1990s. In 1990, Jensen and Schneider[8] used ALSIM2, a 2-D thermal model capable of analyzing both start-up and steady state phases[9] for the purpose of studying the influence of bottom block material and shape on the cracking tendency of AA6063 billets. The authors addressed the heat transfer process between the ingot base and bottom block during the start-up phase, by using a heat transfer coefficient that varied with time. The bottom block was treated as a surface with a constant temperature. A heat transfer coefficient in the range of 3000-2000 $Wm^{-2}K^{-1}$ was used to represent the heat transfer process at the initial stage when the base of the billet is in good contact with the bottom block. The heat transfer coefficient was then reduced to 300 $Wm^{-2}K^{-1}$ to reflect the loss of contact with the outer parts of the bottom block as the billet curls upwards when the cooling water first hits the billet surface.

Jensen and Schneider observed that there was considerable variation in heat flow intensity from one casting to the other for the same thermocouple position, depending on the local filling process and local thermal contact conditions. They linked the tendency to form centre cracks in the transient phase with a maximum sump depth on a sump depth *vs.* time curve calculated by the model. Based on their work, three important observations can be made; the risk for starting cracks can be reduced by (i) changing the bottom block material from steel/cast iron to aluminum, (ii) reducing the initial casting speed, and (iii) changing the bottom block design from a bowl (concave) shape to conical (convex) shape.

While comparing two heat transfer models, TEMPERI (developed by University of Waterloo, Ontario) and FIDAP (developed by FDI, Chicago), Devadas and Grandfield[10] made two important observations. Firstly, they used different heat transfer coefficients ranging from 10-8000 $Wm^{-2}K^{-1}$ for primary cooling, separating the regime into meniscus, mould contact, and

air-gap cooling. Secondly, they tested two methods for modeling of the liquid-solid phase change (**Figure 2.1**), and found that the equivalent specific heat method suffered from numerical instability due to the sharp jump at the liquidus. If the node spacing is too large some of the latent heat released could be lost. The enthalpy method is more stable, and hence able to track the solidification front more accurately.

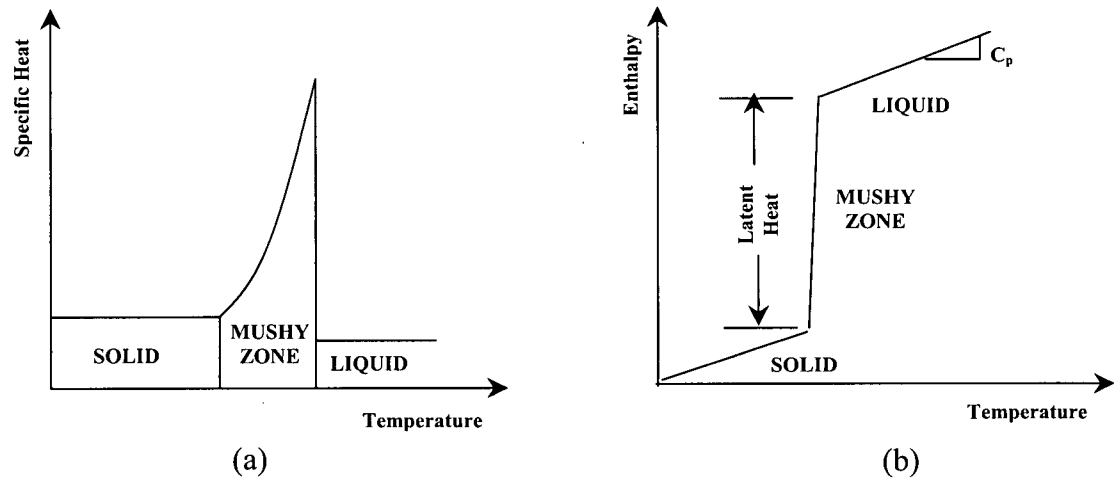

Figure 2.1 – Schematic representation of (a) Equivalent Specific Heat, and (b) Enthalpy method (after Devadas and Grandfield[10]).

In 1994, Grün *et al*[11] reported the use of a 3-D coupled thermal and fluid flow model to investigate the influence of nozzle-distributor systems on temperature and sump profile using FIDAP software code. However, their heat transfer analysis was oversimplified, in order to focus on the effect of geometry of metal distributor on the sump development.

In 1995, Jensen and Schneider[12] extended their earlier 2-D analysis[8, 9] to a 3-D model using ALSIM3, the 3-D finite element version of 2-D ALSIM2. Unfortunately, details of the thermal boundary conditions for this new 3-D model were not discussed in the paper. In the same year, El-Raghy *et al*[13] developed a 3-D finite difference model of a geometrically simplified cylindrical billet for AA6063 alloy. The cooling condition on the outer surfaces of the billet was assumed to be purely convective (h = 10,000 $Wm^{-2}K^{-1}$), and was not discussed in detail. Heat loss due to radiation and convection from the top surface of the billet was neglected because it represents only 0.6% of the total heat removed from the system. In the mushy zone, the effect of latent heat of fusion and the solidified fraction were used to calculate an equivalent specific heat

term applied over the solidus-to-liquidus temperature range. The authors did not report any numerical instability in their model, which was experienced by Devadas and Grandfield[10] while using this method. Temperature fields were not verified experimentally, but the liquid/solid interface (or sump) profiles were found to correlate with the measured data reasonably.

In 1996, Watanabe and Hayashi[14] used a 3-D thermal model to calculate the temperature profiles during the initial unsteady and steady states of the D.C. casting process. The thermal boundary conditions were investigated using experimental data from D.C. cast pure aluminum slabs. The authors stressed the fact that heat transfer to the cooling water depends not only on the temperature of the ingot surface but also on the vertical position on the slab surface. Hence, two different heat transfer curves were used: one for the water impingement zone and the other for region below this zone. The use of Al-50%Zn tracer in the metal pool and subsequent etching of slices taken from the cast ingot were used to measure the sump profiles. These were compared with the model results and found to be satisfactory. However, temperature profiles were not compared with either experimental or industrial data.

In the same year, Wiskel and Cockcroft published the details of a 2-D inverse heat transfer model[15], which used measurements made on an AA5182 rolling ingot instrumented with embedded thermocouples placed at key locations in the vicinity of the ingot face near its base, as an input. The model calculates heat transfer as a function of surface temperature curves in the direct water impingement regime. The findings indicated that the flow of heat is influenced by the surface morphology and water flow conditions during the start-up phase.

A 2-D finite element (FE) analysis[16] of the start-up phase employed these calculated flux/surface temperature relationships to predict the thermal fields developed in the ingot. Model predicted ingot shell thickness at the point of water contact was found to reach a maximum value early in the casting process. The location of this maximum coincided with the position where surface cracks are routinely found to initiate. Further, this maximum was found to also coincide with the position at which the rate of butt curl begins to slow down. The authors concluded that cracks on the ingot face form due to excessive shell thickness during transient start-up conditions and their occurrence could be reduced by an optimal combination of water flow rate and casting speed during cast start-up.

2.3 Coupled Thermal and Stress Models

The earliest work on coupled thermal and stress modeling of D.C. casting reported in literature is by Janin[17] in the year 1986. He developed a 2-D fully coupled axisymmetric simulation using the commercial FE package MARC. The paper does not give any details of the thermal boundary conditions employed. The residual hoop stresses in the billet were found to compare very well with in-situ measurements, although the methodology of residual stress measurement was not explained. In 1989, Flood *et al*[18] described a 3-D thermal and fluid flow model using PHOENICS, a commercial CFD package, and used the thermal fields to compute the stress distribution using ANSYS, a commercial FE package. The thermal model was validated against measured solidification front profiles using zinc prints. The details of the thermal boundary conditions were not discussed. The authors found that the ratio of the calculated equivalent stress (or von Mises stress) to the yield stress as a function of temperature was highest at the centre of the ingot, indicating the susceptibility of this region to cracking.

In 1990, Fjær and Mo[19, 20] reported comprehensive studies on the thermomechanical behavior of aluminum during D.C. casting. In their study, the authors developed the FE mechanical model ALSPEN, specifically for the analysis of the D.C. casting process. A 2-D axisymmetric formulation was applied to an extrusion billet with a simplified base. The temperature field input to the stress model was calculated using the FE code ALSIM2. Although heat transfer to the bottom block was assumed to vary with time and position, the thermal history was independent of stress calculations. The authors also discuss the incremental addition of material associated with the withdrawal of the ingot and the state of strain of the material. In their algorithm, elements are added to the analysis domain as they cool to within a specified amount of the metal coherency temperature†. The authors do not show or discuss the validation of the stress model other than to say that the residual stresses agree in quality with the published values. Furthermore, the deformation of ingot base or butt curl was not compared to industrial data.

In 1991, Brobak *et al*[22] applied Fjær and Mo's model to address the possibility of predicting centre cracks in aluminum billets. They found that increasing the values of casting speed and casting temperature lead to increasing values of centre stresses. Also, application of

† The temperature at which a continuous dendritic network in the solidifying metal offers a mechanical resistance to deformation, thus resulting in a behavior close to that of a solid. Above this temperature, the grains are free to move and the solid-liquid mixture is treated like a liquid[21].

the conventional bowl shaped bottom block to the calculation domain leads to a peak in the centre stresses during the start-up phase. Both the scenarios result in increased cracking tendency. In 1992, Fjær *et al*[23] used the same model to study the influence of two different industrial secondary cooling conditions on the thermal stress and strain fields generated in AA6063 billets and found that their model was effective in qualitatively predicting industrial observations (i.e. presence of hot tears).

The sequentially coupled thermal and stress analysis of Fjær and Mo did not include the effect of butt curl on heat transfer between the bottom block and ingot. To address this issue, Hannart *et al*[24] developed a fully coupled 3-D thermomechanical model, to predict the temperature and stress distributions in an AA2024 rolling ingot during the start-up phase using the commercial software package MARC. The model, reported in 1992, employed surface temperature-dependent heat transfer correlations to account for the primary and secondary cooling and a displacement-based boundary condition on the base of the ingot to account for the influence of butt curl on the heat transfer. The ingot geometry was simplified to be a rectangle and the bottom block was treated as a surface with a constant temperature of 100 °C. The butt curl predictions of the model were shown to agree fairly well with displacements measured in the industry, as indicated in **Figure 2.2**. Further, the model predicted a maximum in principal stress at the lowest part of the ingot, perpendicular to the rolling faces, consistent with cold cracking tendency. However, no comparison was made to ingot temperature measurements and no attempt was made to compare the measured and predicted residual stresses.

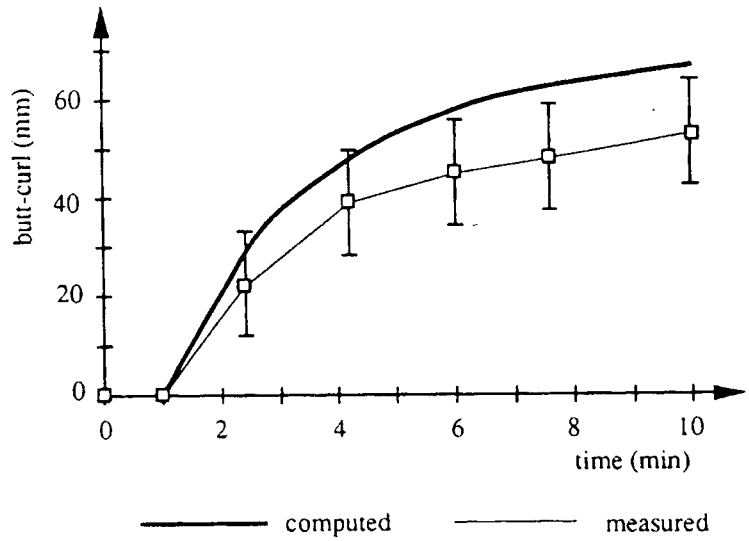

Figure 2.2 – Comparison between measured evolution of butt curl and computed values from Hannart *et al*'s[24] model.

In 1995, Fjær and Jensen[25] used the 3-D thermal model ALSIM3 and stress model ALSPEN3 (3-D version of ALSPEN) to mathematically model the butt curl deformation of AA1050 sheet ingots of dimensions 600 mm x 200 mm. Although the bottom block was not included in either analysis, vertical contact forces from the bottom block, which counterbalances the gravity forces, was imposed on the bottom side of ingot as a quickly decaying function of the calculated vertical displacement in the stress model. Overall a good agreement between calculated and measured butt curl values (and butt curl velocity) was achieved by this study, as indicated in **Figure 2.3**.

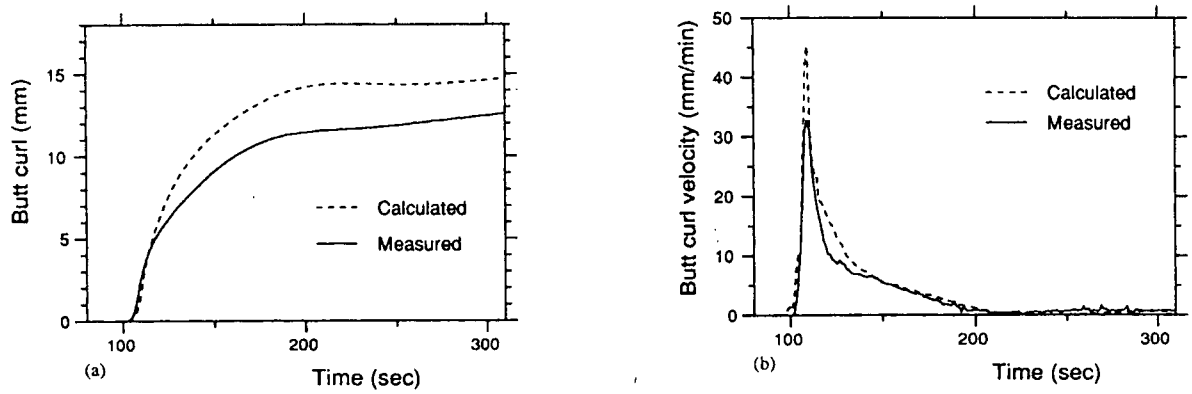

(a) (b)

Figure 2.3 – Comparison of measurements and calculated results from Fjær and Jensen's model[25]; (a) butt curl, and (b) corresponding butt curl velocity.

Fjær and Jensen observed that asymmetric evolution of butt curl, "rocking" of the ingot butt during the initial stages, and possible effects of sticking and friction in the experimental scenario will introduce discrepancies between the measured and predicted butt curl values. They found that butt curl evolution is highly sensitive to the thermal boundary conditions; reducing the heat transfer in the secondary cooling zone or enhancing the heat transfer to bottom block has a remarkable effect on the evolution in butt curl, as shown in **Figure 2.4**. This clearly underlines the fact that accurate thermal modeling is very important in order to reasonably predict the butt curl and stresses generated in the ingot. A qualitative study was presented in the paper with regards to the stress, strain, and strain rate predictions to study the butt curl mechanism in two different bottom block designs. These results were not compared to any experimental measurements. Fjær and Håkonsen[26] used the above model to investigate the pull-in phenomena observed during the D.C. casting process. The authors reported that as steady state casting conditions are approached, a gradually increasing effect of the pull-in leads to the thickness decreasing with cast length at the central regions of the rolling faces. This is known as "butt swell", and schematically shown in **Figure 2.5**.

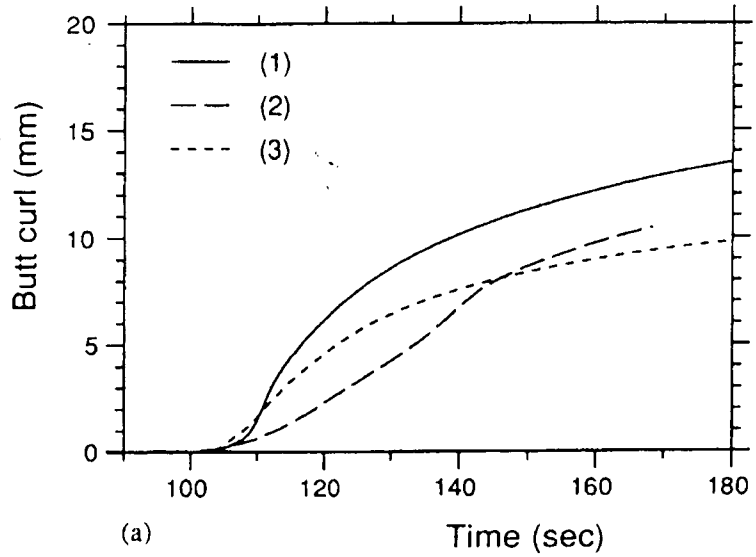

Figure 2.4 – Calculations from Fjær and Jensen's model[25]: butt curl for cases: (1) as shown in Figure 2.3, (2) with reduced secondary cooling, and (3) with increased ingot and bottom block interface cooling.

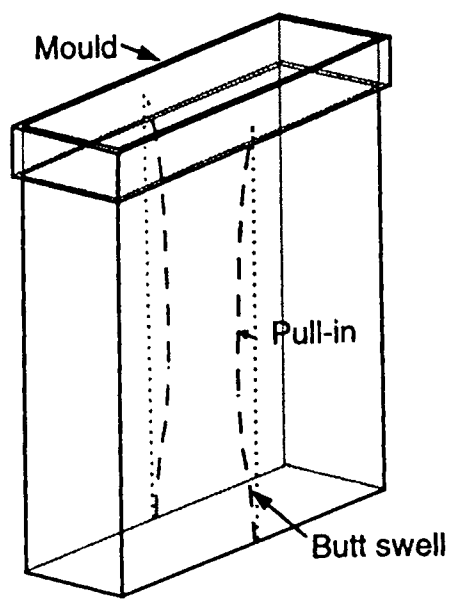

Figure 2.5 – Schematic illustration of the "pull-in" and "butt swell" phenomena for a D.C. cast sheet ingot.[26]

In 1995, Drezet and Rappaz reported that both 2-D[27, 28] and 3-D[29-31] fully coupled thermal/stress models were developed, using the commercial FE code ABAQUS to study the steady state inward pull-in of the rolling faces of AA1201 ingots. Their model was similar in many aspects to that of Hannart *et al*'s and includes a displacement dependent bottom block boundary condition. The bottom block was treated as a surface with a constant temperature of 100 °C in both the models. The cross sectional geometry of the ingot is more realistic but the ingot base geometry has been simplified. The value of thermal conductivity of liquid aluminum was increased from 90 $Wm^{-1}K^{-1}$ to 400 $Wm^{-1}K^{-1}$ to account for liquid convection in the sump†.

A major drawback of the Drezet and Rappaz model is that it adopts a positionally dependent heat flux calculated from thermocouple measurements during steady state operation to describe primary and secondary cooling in the thermal model. Thus the model cannot address thermal behavior during the start-up phase at which time the ingot surface temperatures at the point of water contact may vary significantly with time. One interesting conclusion of this work is that all of the inelastic strain is accumulated in the interior of the ingot and very little is accumulated at the surface where cracks are routinely observed. The computed and measured[32] steady state ingot cross-sections after complete cooling were compared for two different casting speeds, shown in **Figure 2.6**, for the purpose of model validation.

In the same year, Rogers *et al*[33] reported thermal and stress models developed using FE packages PHOENICS and ELFEN, respectively, to study the start-up phase behavior of commercially pure aluminum billets and ingots. The bottom block was again treated as a surface, and the effect of butt curl on the heat transfer was not described. Comparison between experimental and predicted temperature and butt curl data were presented.

† Weckman and Niessen[1] found that integrating the effect of fluid flow in numerical models has very little influence on the position of solidus line of alloys and pure metals, but has a pronounced effect on the position of the liquidus line. They also concluded that errors in the prediction of the liquidus position would not influence the accuracy of any subsequent stress analysis.

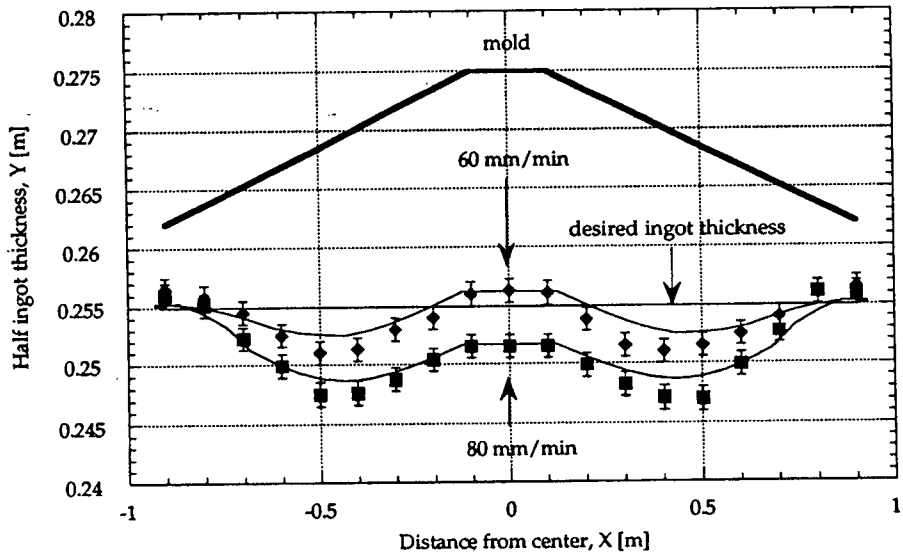

Figure 2.6 – Measured (diamonds and squares) and calculated (lines) steady state ingot cross-section for AA1201 ingots cast at two different casting speeds (after Drezet and Rappaz[31]).

In 1998, Du *et al*[34] outlined the development of a fully coupled 3-D thermomechanical analysis, which included the bottom block, for a 1351 mm x 406 mm AA7xxx ingot. They employed a temperature and water flow rate dependent relationship to quantify secondary cooling heat transfer based on temperature measurements obtained during steady state operation. Interface elements were used at the ingot base/bottom block interface to link heat transfer to base deflection. A functional relationship between the heat transfer coefficient and interfacial gap opening was used. The authors compared the model predictions with experimentally measured temperature and butt curl.

In 1999, Fjær *et al*[35] investigated the heat transfer conditions at cast start-up using a transient 3-D simulation, which coupled thermal, stress, and fluid flow phenomena for AA5005 sheet ingots. The boundary condition applied at the ingot base/bottom block interface accounted for air gap formation and included the effects of conduction and radiation. The heat transfer coefficient was assumed to depend on the surface temperature of ingot base and normal pressure fields computed by the stress analysis. The effect of water incursion was also included in the analysis. Those areas of the base in contact with water adopt a high heat transfer coefficient in the range of 2000-3500 $Wm^{-2}K^{-1}$. A provision has been added for the ejection of water from the

ingot base at high temperatures due to film boiling, which drops the heat transfer coefficient to 200 $Wm^{-2}K^{-1}$. The predicted temperatures at the base of the ingot and inside the bottom block were compared to measured values, and were found to agree reasonably. Fjær *et al* experienced two difficulties while validating their thermal model: (i) most of the thermocouples near the ingot base failed during the evolution of butt curl, and (ii) fine tuning the heat transfer coefficients for ingot base cooling was not possible due to the long computing times.

In 2000, Droste *et al*[36] published their work on the development of a 3-D thermomechanical model for a 1650 mm x 600 mm AA1050 sheet ingot, which employs a heat flux boundary condition dependent on water flow rate and surface temperature, for the ingot vertical sides. The authors included the effect of water incursion along the ingot base. They argued that a modeling strategy, which simply increases the gap conductance between the ingot base and bottom block, when water starts to intrude, is partially wrong since the intruding water represents a heat sink for both. Models, which do not account for that, deliver butt curl results, which are too small compared to measured data. The authors proposed a more realistic model, which entails removal of contact elements along the interface where water intrudes, and application of a special boundary condition on both sides of the interface, assuming a constant heat transfer coefficient and water temperature.

2.4 Development of a Comprehensive Thermal Model: Key Issues

Based on the literature review of modeling activities related to the D.C. casting process, it is obvious that the mathematical thermal and stress models have been continually evolving over the past two decades. Several layers of complexity have been added over time by various researchers to develop a fundamental understanding of the thermal behavior of the ingot during the start-up phase. However, there are certain "gray areas", which still need further scrutiny, in order to develop a thermal model that can be effectively used for process optimization. These are:

(i) The boiling curves used in most of the thermals models represent steady state regime of the D.C. casting process. At the most, analysis has been extended to use of boiling curves dependent on the distance from the point of water impingement. Although it is known that the secondary cooling conditions vary with the use of different casting recipes, little work has been done to produce

validated models, which can be used for optimization of the start-up phase. Moreover, the phenomenon of film boiling on the ingot surfaces observed in the industry has been completely ignored while implementing secondary cooling boundary condition in the available models.

(ii) Although the bottom block geometry has been included in a few models (the general trend is to treat it as a surface at a constant temperature), its role in cooling the ingot base during the transient phase has not been explored. Also, there is a need to develop a robust procedure to implement the effects of butt curl and water incursion, if the bottom block geometry is included in the thermal model. This is a key factor, which has to be addressed while developing models to optimize the design of the bottom block.

(iii) Most thermal models use simplified ingot geometry, which do not represent actual ingots produced by the industry. Simplifying the geometry of the ingot base will not accurately predict the extent of ingot base cooling, and if model validation has to be done by freezing thermocouples near the ingot base, ignoring a realistic geometry can be a possible source of error.

(iv) Most thermal models have been indirectly validated by comparison of butt curl predictions with measured data. No attempt has been made so far to validate the thermal model by measuring temperatures along the ingot rolling and narrow faces, under industrial casting conditions. There is only one work available in the literature[35], which validated the ingot base cooling by use of industrial thermocouple data recorded at the ingot/bottom block interface.

(v) Although the representation of secondary cooling by use of boiling curves have been discussed extensively in literature, the details regarding the implementation of primary cooling boundary conditions in the thermal model have been rarely addressed.

The following sections present a detailed discussion on the more important phenomena described above.

2.4.1 Mechanism of Heat Transfer by Secondary Cooling

During the D.C. casting process, removal of heat from aluminum ingots in the secondary cooling zone is achieved by chill water quenching, during which time the heat transfer coefficient has a strong relationship with the ingot surface temperature. This correlation is usually described by an idealized boiling curve such as shown in **Figure 1.6**. Referring to the figure, four mechanisms of heat transfer can be distinguished, which, in order of decreasing surface temperature, are:

- Film boiling at high temperatures (> 350°C),
- Transition boiling between 200-350°C,
- Nucleate boiling between 100-200°C, and
- Convective cooling at temperatures lower than 100°C.

Two distinct features of the boiling curve are:

- The critical heat flux (and heat transfer coefficient), which determines the ability of the water film to cool the ingot by nucleate boiling, and
- The Leidenfrost temperature, which determines whether the heat transfer mode will switch from film to nucleate boiling on cooling.

Over the last few years, several studies have been conducted to quantify the heat transfer by secondary cooling. Kraushaar *et al*[37], Langlais *et al*[38], Maenner *et al*[39], Larouche *et al*[40, 41], Opstelten and Rabenberg[42], Zuidema Jr. *et al*[43], Li *et al*[44, 45], and Kiss *et al*[46] conducted experimental quench tests in which samples were cooled by a water film to determine boiling curves by inverse heat transfer analysis. Bakken and Bergström[5], Jensen *et al*[6], Watanabe and Hayashi[14], Wiskel and Cockcroft[15], and Drezet *et al*[47] also used inverse heat transfer analysis to obtain heat transfer characteristics from thermocouples embedded in ingots during casting. Weckman and Niessen[1] developed empirical relationships instead. Grandfield *et al*[48] described other relationships available in the literature. Recently, Sørheim *et al*[49] has suggested a new method for inverse heat transfer analysis for a 3-D situation.

From the above studies, the following conclusions can be made:

1. Although the critical heat transfer coefficient is relatively insensitive to increasing water flow rate, the heat transfer coefficient corresponding to Leidenfrost temperature is very sensitive to water flow rate at low flow rates. The Leidenfrost temperature is observed to increase with increasing water flow rate. This behavior is consistent with an increase in

momentum of the water jet and its enhanced ability to break through the stable film layer as it strikes the ingot surface. These relationships, shown in **Figure 2.7**, underline the importance of the water flow rate at the start of the cast in determining whether stable film boiling (or water ejection) will occur or not[40].

2. The variation of the critical heat flux has a strong functional relationship with the distance from the impingement point. As indicated in **Figure 2.8**, it is low in the region of back flow above the impingement point, and increases rapidly to a maximum value corresponding to the position where the water jet has a maximum momentum. Finally, it decreases rapidly to a stable value as the water film loses momentum[40].
3. Two distinct zones can be distinguished on the ingot surface, in the absence of stable film boiling: (a) the water impingement zone (usually 10-15 mm in length depending on the diameter of water holes at the base of the mould and angle of impingement) where abrupt cooling happens due to the direct contact with water, and (b) the streaming zone located below (a) where the heat flux density diminishes because the water film loses momentum as the distance from the impingement point increases.
4. The rate of heat extraction is also a strong function of ingot temperature at the point of water impingement. The dependence on impingement point temperature is reported to be related to the capacity of the ingot to supply heat, and is shown in **Figure 2.9**[44].
5. There is a general agreement on the critical heat flux (and heat transfer coefficient) determined by different techniques. The critical heat flux measured by researchers[1, 5, 7, 14, 15, 37, 45] falls between 1.0 and 5.0 MWm^{-2}, and the critical heat transfer coefficient measured by researchers[37, 39, 41, 46, 47] lies between 40.0 and 50.0 $kWm^{-2}K^{-1}$.

During the start-up phase, it is typical to have stable film boiling develop at certain locations on the ingot surface below the impingement zone. In the presence of film boiling, heat transfer becomes more complicated as a portion of the water curtain may be ejected away from the ingot surface. This process is illustrated schematically in **Figure 2.10**[40]. During water ejection, the heat transfer rate is significantly lower below the point of water ejection, as there is little or no contact of the water film with the ingot surface. The stable film layer then gradually collapses as the casting proceeds and water flow rates are increased. The film boiling area appears as a visible "dome" on the ingot surfaces, with a parabola shaped steam barrier profile demarcating the nucleate and film boiling heat transfer zones. This visual manifestation of water ejection, which

is only observed during the start-up phase, is illustrated in **Figure 2.11**[50]. In the industry, it is a common practice to deliberately maintain a low water flow rate at the cast start-up in order to keep the ingot relatively hot for a certain period of time in order to avoid intense cooling and stress build up, which could lead to severe butt curl[40, 41]. However, extensive film boiling can lead to formation of local hot spots and sub-surface hot tears[38].

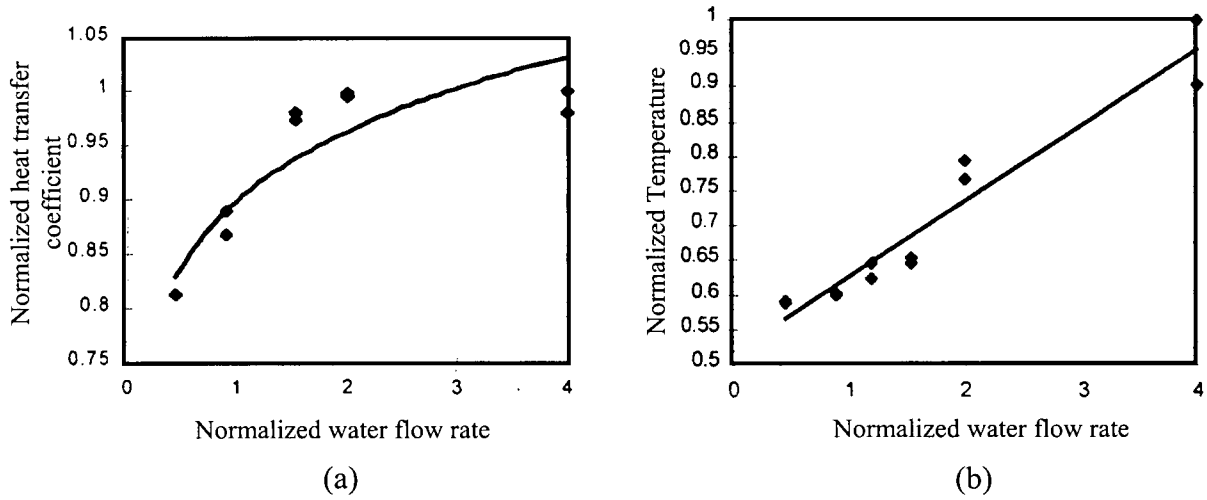

(a) (b)

Figure 2.7 – Effect of water flow rate on (a) Leidenfrost heat transfer coefficient at the impingement point, and (b) Leidenfrost temperature at impingement point.[40]

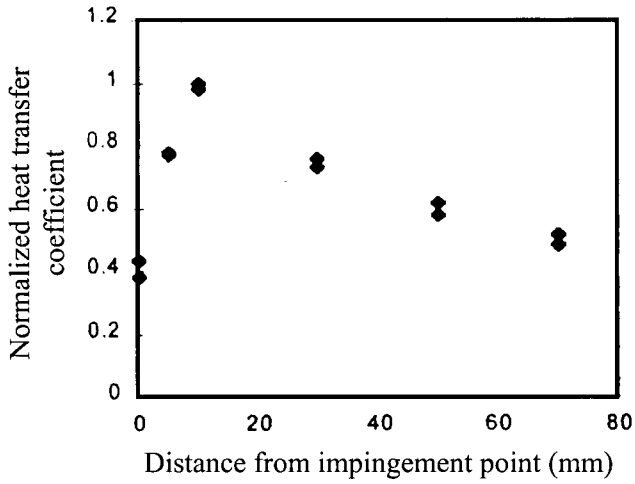

Figure 2.8 – Variation of critical heat transfer coefficients with the distance from the impingement point.[40]

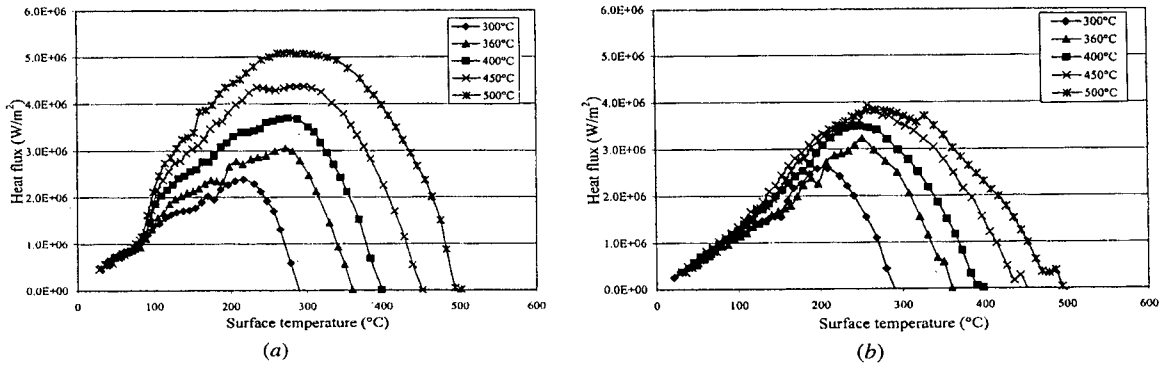

Figure 2.9 – The effect of initial sample temperature (as-cast AA5182, water flow rate = 0.38 ls^{-1}) on the calculated boiling curves for: (a) the impingement zone, and (b) the streaming zone.[45]

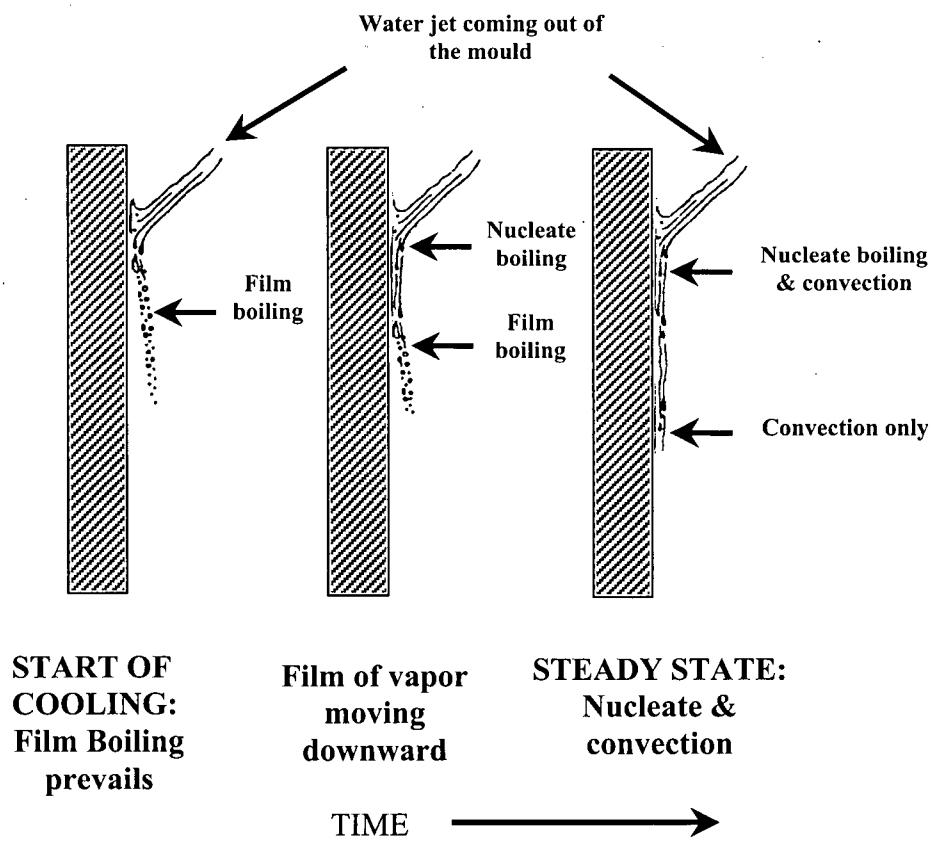

Figure 2.10 – Phenomenon of water ejection or film boiling observed on the ingot surface during cast start-up.[40]

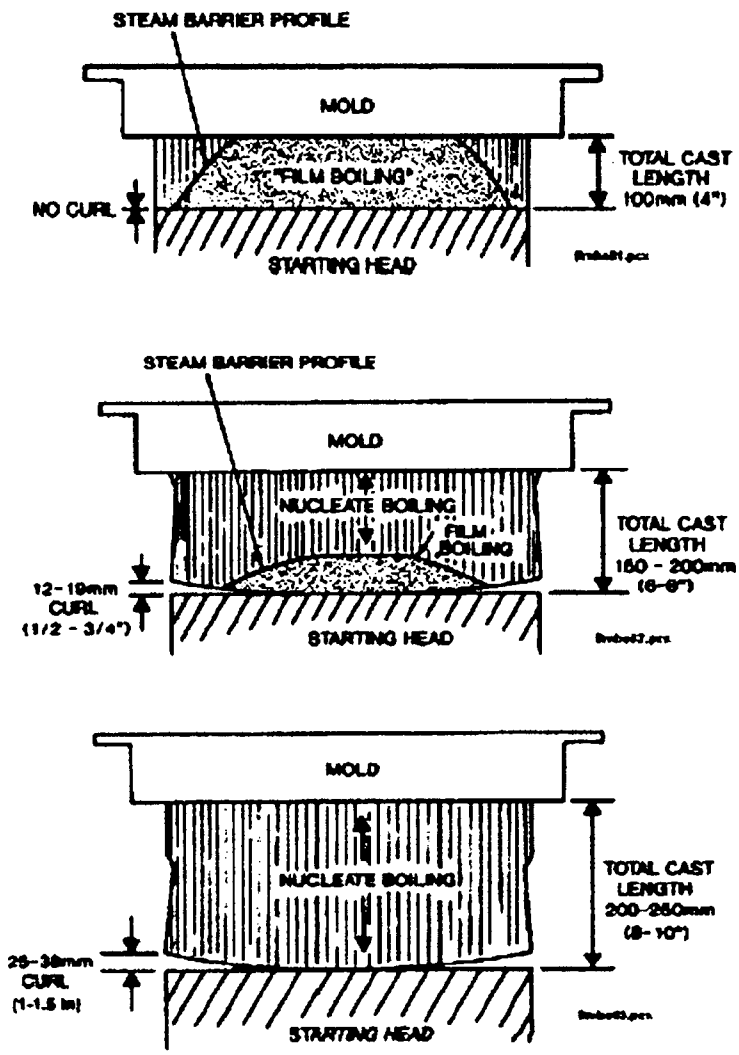

Figure 2.11 – Dynamic evolution of parabola shaped steam barrier in response to ingot surface temperature during a film boiling driven start-up phase.[50]

2.4.2 Ingot Base Cooling Conditions

At the beginning of the start-up phase of the D.C. casting process, when the liquid metal enters the bottom block, the rate of heat transfer from the molten metal to the cold bottom block will be high. After a short time, a small gap at the interface will form due to solidification and the rate of heat transfer will drop. This gap will remain relatively small until the ingot begins to withdraw from the mould and the ingot base deforms in response to the direct contact of the ingot sides with water (the ingot base or "butt" curls in response to the contraction of the vertical faces of the ingot). As a result of this gradual evolution of butt curl, the heat transfer experienced

at different locations over the ingot base can be expected to vary significantly[24,34,35]. For example, the region surrounding the centre of ingot base remains in relatively good physical and thermal contact with the bottom block, whereas, in the vicinity of ingot corners, where large vertical displacement is observed, the heat transfer may be expected to drop significantly. However, as the base continues to deform (or curl), water falling down the side may enter the gap and enhance the heat transfer from the ingot base[36]. This in turn will influence the deformation of the base, or butt curl.

The heat transfer during this process of water incursion is governed by the boiling curves, wherein the heat transfer coefficient is a function of the surface temperature of the ingot base[35]. It is likely that the intensity of the base cooling by water incursion is dependent on the rate of removal of the entrained water by the drainage holes in the bottom block. The details of the interfacial heat transfer processes active near the base of the ingot is schematically shown in **Figure 2.12**.

Recently, Sengupta *et al*[51, 52] included the bottom block geometry in a 3-D sequentially coupled thermomechanical analysis for AA5182 sheet ingots and included the competing effects of the butt curl and water incursion to represent the base cooling. They showed that the bottom block plays a significant role in the heat transfer from the base of the ingot during start-up, and thus contributes to the mechanical behavior of the ingot base in this phase of the process. The authors found that predicted stress/strain results were significantly sensitive to the rate of heat transfer from the base of the ingot to the bottom block. They concluded that it is essential to include the bottom block in thermal analysis of the start-up phase.

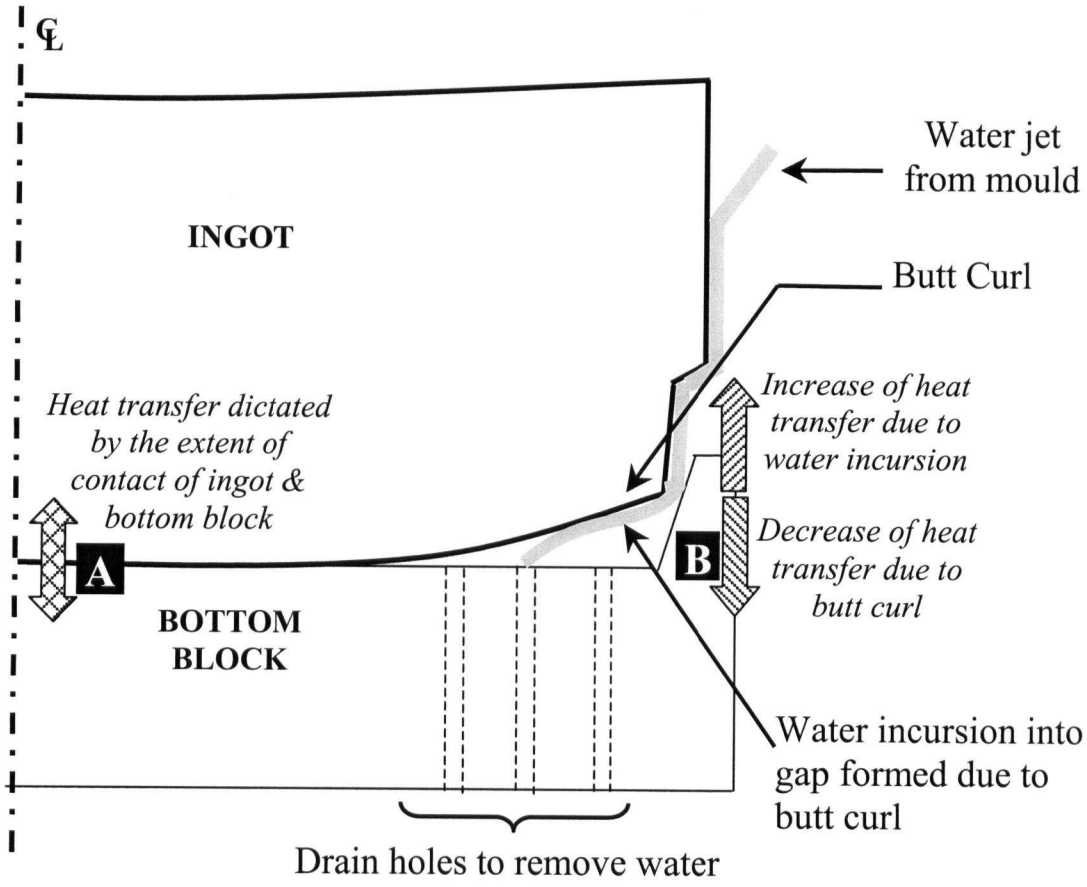

Figure 2.12 – The details of the ingot base cooling conditions during the start-up phase, showing the various heat transfer processes occurring near the centre of the ingot (Region A), and the outer edges (Region B).

2.4.3 Mould Cooling Conditions

The heat transfer associated with the primary cooling to the mould can be further subdivided into two regions of behaviour: 1) mould/metal contact or meniscus cooling and 2) air gap cooling[53]. In the beginning, the liquid metal is in good physical contact with the mould, and heat transfer is high. The duration of this stage is quite brief, and ends with the formation of an air gap between the metal and mould when the solid shell contracts. Once the gap has formed, the mechanisms of heat transfer are conduction through the air in the gap, and radiation through the gap. The phenomenon is illustrated in **Figure 2.13**. The lateral pull-in[26] of the ingot faces that occur during butt curl may complicate the primary cooling, by altering the length of air gap. Despite representing less than 20% of the total heat extracted from the solidifying ingot[54], the

heat transfer in the mould is critical as it has a significant impact on the ingot surface quality[55]. Moreover, it also determines the surface temperature of the ingot at the point of exit from the mould, which subsequently influences the mode of boiling water heat transfer (film/nucleate boiling)[4].

Ho and Pehlke[56] and Nishida *et al*[57] did fundamental work on the mechanisms of mould cooling. The heat transfer between the solidifying metal and mould usually varies with time. This variation is related to the interaction between the metal and mould. A high heat transfer coefficient is observed for conditions of intimate mould/metal contact (meniscus cooling). The heat transfer is substantially decreased in the air gap zone, where heat is primarily transferred through radiation/conduction. Under these conditions (air gap cooling), the solidifying shell may re-melt, which results in a "recalescence" in the thermal field associated with the ingot. The peak heat transfer coefficient reported for aluminum contacting a chilled mould ranges from 2000-4000 $Wm^{-2}K^{-1}$. By comparison, in the air gap, the heat transfer coefficient may be as low as approximately 150 $Wm^{-2}K^{-1}$ in the air gap[56].

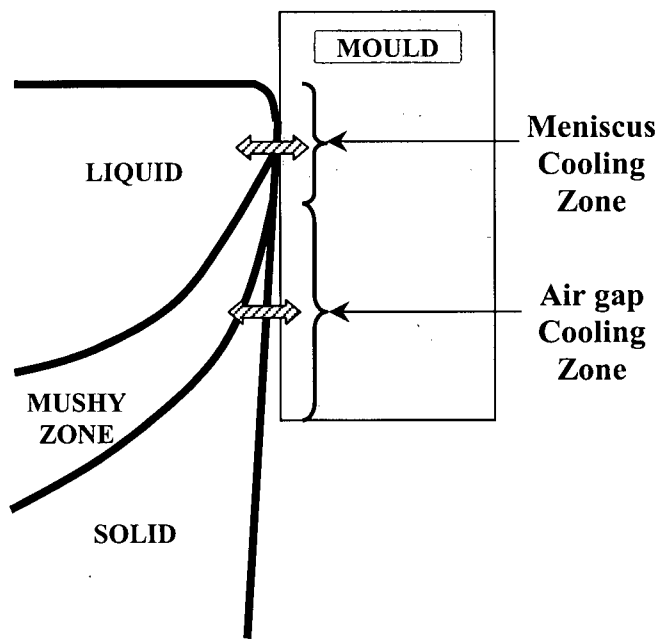

Figure 2.13 – Heat transfer zones for the ingot rolling and narrow faces showing mould cooling.

2.5 Summary

There is a clear trend toward the use of fundamentally based mathematical models to analyze the thermomechanical behavior of ingots during the transient start-up phase of the D.C. casting process. While industry has historically tended to adopt a trial-and-error approach towards process optimization, more recently there has been recognition on the part of industry for the need of a well-validated and flexible D.C. casting model. This need is being driven by the desire to economically cast various aluminum alloys at high production rates. Such a model will significantly reduce the number of trials required to understand and eliminate defects in the cast product. The basic tools or methods required to analyze defect formation are available and well established. However, the application of FE heat transfer models require a thorough understanding of the thermal boundary conditions. Based on literature review, it is clear that several complex heat transfer phenomena must be included in the analysis to accurately describe the primary, secondary, and base cooling conditions that prevail during the start-up phase of the D.C. casting process.

References

1. Weckman, D.C., and Niessen, P., *Mathematical Models of the D.C. Continuous Casting Process,* Canadian Metallurgical Quarterly, 1984, **23**(2), pp. 209-216.
2. Jensen, E.K., *Mathematical Model Calculations in Level Pour D.C. - Casting of Aluminum Extrusion Ingots,* Light Metals 1980, The Minerals, Metals and Materials Society, Warrendale, USA, 1980, pp. 631-642.
3. Katgerman, L., *A Mathematical Model for Hot Cracking of Aluminum Alloys during D.C. Casting,* Light Metals 1981, The Minerals, Metals and Materials Society, Warrendale, USA, 1981, pp. 845-853.
4. Weckman, D.C., and Niessen, P., *A Numerical Simulation of the D.C. Continuous Casting Process Including Nucleate Boiling Heat Transfer,* Metallurgical Transactions B, 1982, **13B**, pp. 593-602.
5. Bakken, J.A., and Bergstrom, T., *Heat Transfer Measurements during D.C. Casting of Aluminum Part I: Measurement Technique,* Light Metals 1986, The Minerals, Metals and Materials Society, Warrendale, USA, 1986, pp. 883-889.
6. Jensen, E.K., Johansen, S., Bakken, Bergstrom, T., and Bakken, J. A., *Heat Transfer Measurements during D.C. Casting of Aluminum Part II: Results and Verification for Extrusion Ingots,* Light Metals 1986, The Minerals, Metals and Materials Society, Warrendale, USA, 1986, pp. 891-896.
7. Tarapore, E.D., *Thermal Modeling of D.C. Continuous Billet Casting,* Light Metals 1989 (Ed. P. G. Campbell), The Minerals, Metals and Materials Society, Warrendale, USA, 1989, pp. 875-879.
8. Jensen, E.K., and Schneider, W., *Investigations about Starting Cracks in D.C.-Casting of 6063-type Billets Part II: Modeling Results,* Light Metals 1990 (Ed. C. M. Bickert), The Minerals, Metals and Materials Society, Warrendale, USA, 1990, pp. 937-943.
9. Schneider, W., and Jensen, E. K., *Investigations about Starting Cracks in D.C. Casting of 6063-type Billets Part I: Experimental Results,* Light Metals 1990 (Ed. C. M. Bickert), The Minerals, Metals and Materials Society, Warrendale, USA, 1990, pp. 931-936.
10. Devadas, C., and Grandfield, J. F., *Experiences with Modeling D.C. Casting of Aluminum,* Light Metals 1991 (Ed. E. L. Rooy), The Minerals, Metals and Materials Society, Warrendale, USA, 1991, pp. 883-892.

11. Grun, G.-U., Eick, I., and Vogelsang, D., *3D-Modeling of Fluid Flow & Heat Transfer for D.C. Casting of Rolling Ingots,* Light Metals 1994 (Ed. U. Mannweiler), The Minerals, Metals and Materials Society, Warrendale, USA, 1994, pp. 863-869.

12. Jensen, E.K., and Schneider, W., *Development of a New Starting Block Shape for the D.C. Casting of Aluminum Sheet Ingots Part II: Modeling Results,* Light Metals 1995 (Ed. J. Evans), The Minerals, Metals and Materials Society, Warrendale, USA, 1995, pp. 969-978.

13. El-Raghy, T.S., El-Demerdash, M. F., Ahmed, H. A., and El-Sheikh, A. M., *Modeling of the Transient and Steady State Periods during Aluminum D.C. Casting,* Light Metals 1995 (Ed. J. Evans), The Minerals, Metals and Materials Society, Warrendale, USA, 1995, pp. 925-929.

14. Watanabe, Y., and Hayashi, N., *3-D Solidification Analysis of the Initial State of the D.C. Casting Process,* Light Metals 1996 (Ed. W. Hale), The Minerals, Metals and Materials Society, Warrendale, USA, 1996, pp. 979-984.

15. Wiskel, J.B., and Cockcroft, S. L., *Heat-flow-based Analysis of Surface Crack Formation during the Start-up of the Direct Chill Casting Process: Part I. Development of the Inverse Heat-Transfer Model,* Metallurgical Transactions B, 1996, **27B**, pp. 119-127.

16. Wiskel, J.B., and Cockcroft, S. L., *Heat-flow-based Analysis of Surface Crack Formation during the Start-up of the Direct Chill Casting Process: Part II. Experimental Study of an AA5182 Rolling Ingot,* Metallurgical Transactions B, 1996, **27B**, pp. 129-137.

17. Janin, B., *Simulation of Thermal Stresses in Continuous Casting of Al Alloys Billets,* Proceedings of the European Materials Society Symposium, Strasbourg, France, 1986, pp. 305-314.

18. Flood, S.C., Katgerman, L., Langille, A. H., Rogers, S., and Reed, C. M., *Modeling of Fluid Flow and Stress Phenomena during D.C. Casting of Aluminum Alloys,* Light Metals 1989 (Ed. P. G. Campbell), The Minerals, Metals and Materials Society, Warrendale, USA, 1989, pp. 943-947.

19. Fjær, H.G., and Mo, A., *ALSPEN - A Mathematical Model for Thermal Stresses in D.C. Casting of Aluminum Billets,* Metallurgical Transactions B, 1990, **21B**, pp. 1049-1061.

20. Fjær, H.G., and Mo, A., *Mathematical Modeling of Thermal Stresses during D.C. Casting of Aluminum Billets,* Light Metals 1990 (Ed. C. M. Bickert), The Minerals, Metals and Materials Society, Warrendale, USA, 1990, pp. 945-950.

21. Arnberg, L., and Backerud, L., *Solidification Characteristics of Aluminum Alloys*, Edited by S.P. Thomas, American Foundrymen's Society, Inc.

22. Brobak, T.J., Fjær, H. G., Jensen, E. K., and Mo, A., *Mathematical Predictions of Center Crack Formation in D. C. Casting of Aluminum billets,* Light Metals 1991 (Ed. E. L. Rooy), The Minerals, Metals and Materials Society, Warrendale, USA, 1991, pp. 869-876.

23. Fjær, H.G., Jensen, E. K., and Mo, A., *Mathematical Modeling of Heat Transfer and Thermal Stresses in Aluminum Billet Casting: Influence of the Direct Water Cooling Conditions,* Proceedings of the 5th International Aluminum Extrusion Technology Seminar, Aluminum Association Edition, 1992, pp. 113-120.

24. Hannart, B., Cialti, F., and Schalkwijk, R. V., *Thermal Stresses in D.C. Casting of Aluminum Slabs: Application of a Finite Element Model,* Light Metals 1994 (Ed. U. Mannweiler), The Minerals, Metals and Materials Society, Warrendale, USA, 1994, pp. 879-887.

25. Fjær, H.G., and Jensen, E. K., *Mathematical Modeling of Butt Curl Deformation of Sheet Ingots: Comparison with Experimental Results for Different Starter Block Shapes,* Light Metals 1995 (Ed. J. Evans), The Minerals, Metals and Materials Society, Warrendale, USA, 1995, pp. 951-959.

26. Fjær, H.G., and Hakonsen, A., *The Mechanism of Pull-in during D.C.-Casting of Aluminum Sheet Ingots,* Light Metals 1997 (Ed. R. Huglen), The Minerals, Metals and Materials Society, Warrendale, USA, 1997, pp. 683-690.

27. Drezet, J.-M., and Plata, M., *Thermomechanical Effects during Direct Chill and Electromagnetic Casting of Aluminum Alloys Part I: Experimental Investigation,* Light Metals 1995 (Ed. J. Evans), The Minerals, Metals and Materials Society, Warrendale, USA, 1995, pp. 931-940.

28. Drezet, J.-M., Rappaz, M., and Krahenbuhl, Y., *Thermomechanical Effects during Direct Chill and Electromagnetic Casting of Aluminum Alloys Part II: Numerical Simulation,*

Light Metals 1995 (Ed. J. Evans), The Minerals, Metals and Materials Society, Warrendale, USA, 1995, pp. 941-950.

29. Drezet, J.-M., and Rappaz, M., *Modeling of Ingot Distortions during Direct Chill Casting of Aluminum Alloys,* Metallurgical Transactions A, 1996, **27A**, pp. 3214-3224.

30. Drezet, J.-M., and Rappaz, M., *Modeling of Thermomechanical Effects during Direct Chill Casting of AA1201 Aluminum Alloy,* Materials Science Forum, 1996, **217-222 (1996)**, pp. 305-310.

31. Drezet, J.-M., and Rappaz, M., *Direct Chill Casting of Aluminum Alloys: Ingot Distortions and Mold Design Optimization,* Light Metals 1997 (Ed. R. Huglen), The Minerals, Metals and Materials Society, Warrendale, USA, 1997, pp. 1071-1080.

32. Drezet, J.-M., Rappaz, M., Carrupt, B., and Plata, M., *Experimental Investigation of Thermomechanical Effects during Direct Chill and Electromagnetic Casting of Aluminum,* Metallurgical Transactions B, 1995, **26B**, pp. 821-829.

33. Rogers, S., Flood, S., Hughes, D., and Rance, J., *Solidification and Deformation during the Start of an Aluminum D.C. Cast,* Modeling of Casting, Welding and Advanced Solidification Processes VII (Ed. M. Cross and J. Campbell), The Minerals, Metals & Materials Society, Warrendale, USA, 1995, pp. 287-294.

34. Du, J., Kang, B. S-J., Chang, K-M., and Harris, J., *Computational Modeling of D.C. Casting of Aluminum Alloy Using Finite Element Method,* Light Metals 1998 (Ed. B. Welch), The Minerals, Metals and Materials Society, Warrendale, USA, 1998, pp. 1025-1029.

35. Fjær, H.G., Mortensen, D., Hakonsen, A, and Sorheim, E., *Coupled Stress, Thermal, and Fluid Flow Modeling of the Start-up Phase of Aluminum Sheet Ingot Casting,* Light Metals 1999 (Ed. C. E. Eckert), The Minerals, Metals and Materials Society, Warrendale, USA, 1999, pp. 743-748.

36. Droste, W., Drezet, J-M., Grun, G-U., and Schneider, W., *3-D Modeling of Ingot Geometry Development of D.C.-Cast Aluminum Ingots During the Start-up Phase,* Continuous Casting (Ed. K. Ehrke and W. Schneider), Wiley-VCH, 2000, pp. 177-183.

37. Kraushaar, H., Jeschar, R., Heidt, V., Jensen, E. K., and Schneider, W., *Correlation of Surface Temperatures and Heat Transfer by D.C. Casting of Aluminum Ingots,* Light

Metals 1995 (Ed. J. Evans), The Minerals, Metals and Materials Society, Warrendale, USA, 1995, pp. 1055-1059.

38. Langlais, J., Bourgeois, T., Caron, Y., Beland, G., and Bernard, D., *Measuring the Heat Extraction Capacity of D.C. Casting Cooling Water,* Light Metals 1995 (Ed. J. Evans), The Minerals, Metals and Materials Society, Warrendale, USA, 1995, pp. 979-986.

39. Maenner, L., Magnin, B., and Caratini, Y., *A Comprehensive Approach to Water Cooling in D.C. Casting,* Light Metals 1997 (Ed. R. Huglen), The Minerals, Metals and Materials Society, Warrendale, USA, 1997, pp. 701-707.

40. Larouche, A., Caron, Y., and Kocaefe, D., *Impact of Water Heat Extraction and Casting Conditions on Ingot Thermal Response during D.C. Casting,* Light Metals 1998 (Ed. B. Welch), The Minerals, Metals and Materials Society, Warrendale, USA, 1998, pp. 1059-1064.

41. Larouche, A., Langlais, J., Bourgeois, and Gendron, A., *An Integrated Approach to Measuring D.C. Casting Water Quenching Ability,* Light Metals 1999 (Ed. M. Bouchard and A. Faucher), MetSoc, Warrendale, USA, 1999, pp. 235-245.

42. Opstelten, I.J., and Rabenberg, J. M., *Determination of the Thermal Boundary Conditions during Aluminum D.C. Casting from Experimental Data using Inverse Modeling,* Light Metals 1999 (Ed. C. E. Eckert), The Minerals, Metals and Materials Society, Warrendale, USA, 1999, pp. 729-735.

43. Zuidema Jr., J., Katgerman, L., Opstelten, I. J., and Rabenberg, J. M., *Secondary Cooling in D.C. Casting: Modeling and Experimental Results,* Light Metals 2001 (Ed. J. L. Anjier), The Minerals, Metals and Materials Society, Warrendale, USA, 2001, pp. 873-878.

44. Li, D., Wells, M. A., and Lockhart, G., *Effect of Surface Morphology on Boiling Water Heat Transfer During Secondary Cooling of the DC Casting Process,* Light Metals 2001 (Ed. J. L. Anjier), The Minerals, Metals and Materials Society, Warrendale, USA, 2001, pp. 865-871.

45. Wells, M.A., Li, D., and Cockcroft, S. L., *Influence of Surface Morphology, Water Flow Rate, and Sample Thermal History on the Boiling-Water Heat Transfer during Direct-Chill Casting of Commercial Aluminum Alloys,* Metallurgical Transactions B, 2000, **32B**, pp. 929-939.

46. Kiss, L.I., Meenken, T., Charette, A., Lefebvre, Y., and Levesque, R., *Experimental Study of the Heat Transfer along the Surface of a Water-film Cooled Ingot,* Light Metals 2002 (Ed. W. Schneider), The Minerals, Metals and Materials Society, Warrendale, USA, 2002, pp. 981-985.

47. Drezet, J.-M., Gruen, G-U., and Gremaud, M., *Determination of Thermal Properties and Boundary Conditions in the D.C. Casting Process Using Inverse Stationary Methods,* Light Metals 2000 (Ed. R. D. Peterson), The Minerals, Metals and Materials Society, Warrendale, USA, 2000, pp. 585-590.

48. Grandfield, J.F., Hoadley, A., and Instone, S., *Water Cooling in Direct Chill Casting: Part I. Boiling Theory and Control,* Light Metals 1997 (Ed. R. Huglen), The Minerals, Metals and Materials Society, Warrendale, USA, 1997, pp. 691-699.

49. Sorheim, E.A., Mortensen, D., Benum, S., and Stette, C., *Inverse Analysis of Space and Time Variations in the Boundary Heat Flux during Water Film Cooling,* Light Metals 2002 (Ed. W. Schneider), The Minerals, Metals and Materials Society, Warrendale, USA, 2002, pp. 679-686.

50. Grealy, G.P., Lee Davis, J., Jensen, E. K., Tondel, P. A., and Moritz, J., *Advances for DC Casting: Part 2 - Heat Transfer and Casting Results,* Light Metals 2001 (Ed. J. L. Anjier), The Minerals, Metals and Materials Society, Warrendale, USA, 2001, pp. 813-821.

51. Sengupta, J., Maijer, D., Wells, M. A., and Cockcroft, S. L., *Modeling of the Thermomechanical Effects During the Start-up Phase for DC Casting of Aluminum Sheet Ingots,* Proceedings of the Brimacombe Memorial Symposium, TMS, MetSoc, and ISS, Canada, 2000, pp. 673-684.

52. Sengupta, J., Maijer, D., Wells, M. A., Cockcroft, S. L., and Larouche, A., *Mathematical Modeling of the Thermomechanical Behavior of a 5182 Aluminum Ingot During the Start-up Phase of the DC Casting Process: The Role of Bottom Block,* Light Metals 2001 (Ed. J. L. Anjier), The Minerals, Metals and Materials Society, Warrendale, USA, 2001, pp. 879-885.

53. Trovant, M., and Argyropoulos, S., *A Technique for the Estimation of Instanteneous Heat Transfer at the Mould/Metal Interface during Casting,* Light Metals 1997 (Ed. R.

Huglen), The Minerals, Metals and Materials Society, Warrendale, USA, 1997, pp. 927-931.

54. Drezet, J.-M., *Direct Chill and Electromagnetic Casting of Aluminium Alloys: Thermomechanical Effects and Solidification Aspects*, Ph.D. Thesis, Department of Materials, Ecole Polytechnique Federale de Lausanne, Lausanne, Switzerland, 1996.

55. Schneider, W., and Reif, W., *Present Situation of Continuous Casting for Aluminum Wrought Alloys,* Proceedings of the 6th Arab International Aluminum Conference (ARABAL 93), Arab Federation for Engineering Industries, 1994, pp. 173-190.

56. Ho, K., and Pehlke, R. D., *Metal-Mold Interfacial Heat Transfer,* Metallurgical Transactions B, 1985, **16B**, pp. 585-594.

57. Nishida, Y., Droste, W., and Engler, E., *The Air-gap Formation Process at the Casting-Mold Interface and the Heat Transfer Mechanism through the Gap,* Metallurgical Transactions B, 1986, **17B**, pp. 833-844.

CHAPTER 3

SCOPE AND OBJECTIVES

3.1 Scope of the Research Programme

The overall goal of this research programme was to develop fundamental knowledge to describe the thermal behavior of AA5182 aluminum sheet ingots during the start-up phase of the D.C. casting process. Ingot cooling during this transient phase is determined by complex interplay between the primary, secondary, and base cooling processes, depending upon the type of cast recipe being used. The thermal fields generated in turn control the final stress and strain states in the solidified ingot. Hence, the research programme focused mainly on the heat transport phenomena during casting.

3.1.1 Model Development

To achieve this goal, fundamentally based 2-D and 3-D mathematical models were developed to predict the evolution of temperature field during the solidification and cooling of ingot castings. The uncoupled thermal models, capable of computing the transient temperature distribution during the initial stages of the D.C. casting process, were developed using the commercial FE code, ABAQUS. The non-linear solution capabilities in ABAQUS are well developed and robust making it well suited to solve the complex heat transfer problem. Additional features of the code relevant to this research programme include the ability to handle multiple thermal load steps, which involve addition and removal of elements from the computational domain, so that the evolution of cast length with time that is consistent with the ingot withdrawal rate could be simulated. The recently introduced sparse matrix solver enables larger geometrically complex 3-D models to be tackled in reasonable execution times. ABAQUS also permits the incorporation of boundary conditions through the development of user programmable subroutines as an option. The complex thermal boundary conditions specific to the start-up phase of the D.C. casting process were formulated using these external user subroutines written in FORTRAN language.

The development of the thermal model entailed the implementation of appropriate boundary and initial conditions, and finally, verification of the temperature predictions. The

computational domain included the liquid metal, mushy zone, and solid metal. Model development was done in stages, with each stage providing an increase in complexity of the model and its boundary conditions. For the 3-D formulation, a quarter section of the ingot was modeled to reduce the computation size of the problem by assuming that symmetry could be realistically applied to the whole domain. The geometry used for the ingot and the bottom block were geometrically realistic (*viz.* the geometry included the bottom block thickness, depth, and lip), although not as detailed as actual production geometry owing to proprietary considerations. Thermal contact surfaces were implemented in the model to account for the exchange of heat between the base of the ingot and bottom block. The details of the process parameters: pour temperature, filling rate, casting speed and water flow rate, provided by Alcan International Ltd. (Alcan) were generic *i.e.* they did not reflect the standard operating practice actually used in the industry. Thermo-physical properties required by the thermal model were readily available in literature. Boiling curves suitable for use in the start-up phase and fraction solidified *vs.* temperature relationships were provided by Alcan, since these were not available in published literature.

Figure 3.1 shows the overview of the modeling work specific to this research programme, which is a crucial part of the overall modeling activities related to the UBC-Alcan D.C. casting project mentioned earlier in Chapter 1.

3.1.2 Model Validation

To obtain data suitable for verification of the thermal and stress models, industrial trials were performed at Alcan's casting facilities on 711 mm x 1638 mm AA5182 ingots. The bottom block filling rate, and water flow rate were varied to produce two different start-up casting practices, so that the thermal model could be validated and tested for a wide range of ingot-cooling conditions. Thermocouples were "frozen" inside the vertical rolling and narrow faces of the ingot to measure temperatures for validating the primary and secondary cooling boundary conditions, which were incorporated in the thermal model. The ingot/bottom block interface boundary conditions were validated by comparing model predicted temperatures with measured data from thermocouples located near the base of ingot and on the top face of bottom block. Butt curl measurements were also done to incorporate the effects of air gap formation and water incursion between the ingot butt and bottom block into the model.

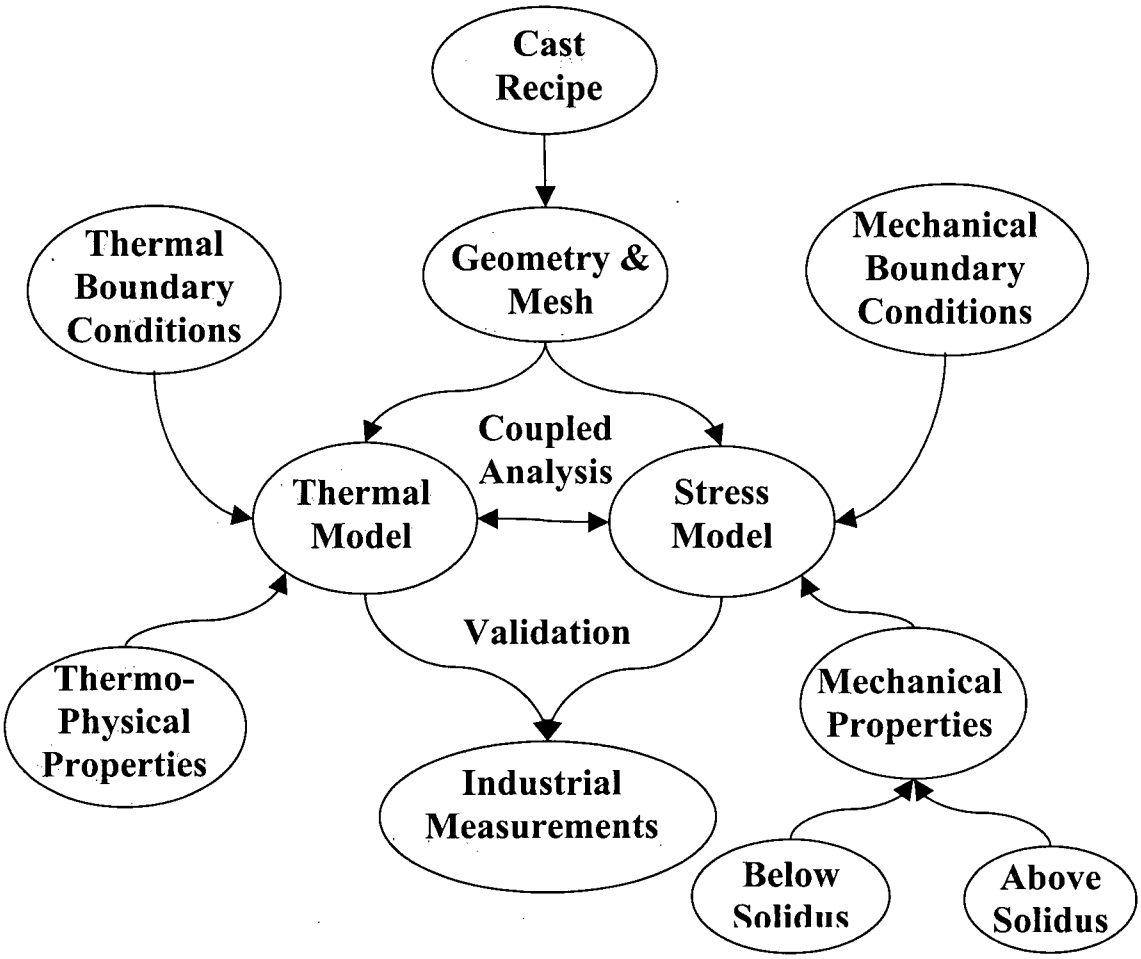

Figure 3.1 – Overview of the modeling work carried out in the research programme (shaded), which is a crucial part of the overall modeling activities related to the UBC-Alcan D.C. casting project.

3.2 Objectives of Research Programme

The primary objective of the present study is:

- To formulate, develop, and verify a mathematical model capable of predicting the temperature evolution in AA5182 aluminum sheet ingots during the transient start-up phase of the D.C. casting process.

In accomplishing the primary objective, the following sub-objectives were formulated:

- To develop and implement, within ABAQUS, equations describing the boundary conditions for the heat transfer processes active on the ingot and bottom block surfaces during the start-up phase.
- To validate the model predictions using temperature data measured on ingots (and bottom block) produced at Alcan's experimental casting centre.

Although thermal models describing the start-up phase of the D.C. casting process have been developed previously (as mentioned in Chapter 2), the uniqueness of the present study lies in:

- An algorithm to describe the phenomena of water ejection during cast start-up so that the extent of film boiling on the ingot surfaces can be predicted.
- A more detailed description of the role of bottom block on the cooling of the ingot during the start-up phase of the D.C. casting process. This included the use of a more geometrically realistic bottom block as well as the influence of butt curl and water incursion on the ingot base cooling process.
- Extensive validation of the thermal model using data measured at a variety of thermocouple positions on both the narrow and rolling faces as well as near the base of the ingot. In addition, temperature in the bottom block was also measured and compared with model predictions.

CHAPTER 4
INDUSTRIAL MEASUREMENTS

4.1 Introduction

An experimental campaign was conducted to acquire thermal and mechanical data from AA5182 sheet ingots during the start-up phase of the D.C. casting process. The casting recipes used during the campaign were non-standard (compared to those used in the production). The non-standard recipes included a "cold" cast and a "hot" cast in order to gather data reflecting a broad range of cooling conditions to validate the thermal model. The thermocouple measurements served to help characterize the boundary conditions active on the ingot and bottom block surfaces, as well as to provide overall validation of the heat transfer model. The butt curl measurements were used to incorporate the effects of air gap formation and water incursion between the ingot butt and bottom block into the model. The next two sections discuss the experimental method and results of the two castings produced in collaboration with Alcan.

4.2 Industrial Casting Trials

The industrial casting trials were conducted at Alcan's casting facilities located in the Saguenay area of Québec, during a visit there in August 2000. The author was responsible for the design of experiments and was present during all the casting trials. The casting facility is fully equipped with melting and holding furnaces, metal treatment systems, casting equipment, and automated casting control systems. It is capable of producing industrial scale casts with the aid of sophisticated instrumentation for measuring temperatures and displacements. The casting control system includes control loops for liquid metal level in the mould, water flow rate, and casting speed. The metal level control system regulates the liquid metal height in the mould precisely, using non-contact metal level sensors placed above the liquid metal. It allows metal level adjustment during the cast as specified by the filling sequence, and automatically starts the withdrawal of the cast when the metal reaches a pre-determined level in the mould. The water cooling control system is designed to regulate the start, intermediate, and final mould water flow rates based on cast length, with linear ramps between the values specified by the casting practice. Motor-driven hydraulic flow control valves provide precise monitoring of the rate of bottom

block descent, thereby controlling the casting speed for the process. The function of the casting speed control system is similar to the mould water control ramps. Cast speeds are specified in the practice at cast lengths, with linear ramps between set points. Customized software packages are used to provide operator interface graphics screens for continuous display and monitoring of all the process variables.

4.2.1 Cast Material

Aluminum alloy AA5182 was chosen for study in this research programme because it is currently being used in the automotive industry for manufacturing body panels[1], and is a hard-to-cast alloy owing to its propensity to form cracks during cast start-up. AA5182 has a long freezing range (536-637°C)[2], which makes it very susceptible to hot tearing[3]. The cracks tend to form in the vicinity of the bottom block lip, along the base of ingot, and along the surface of the rolling face[4]. The face crack is the most serious; as once initiated, it can extend through the entire length of the casting, rendering the ingot unsuitable for further processing.

4.2.2 Ingot, Bottom Block and Mould Geometry

The bottom block and mould used during the trials were similar in shape to those used by Alcan for their commercial castings. The details of the ingot and bottom block geometry used in the casting trials are shown in **Figure 4.1**. The rectangular cross-section of the cast ingots had the dimensions of 711 mm x 1638 mm. The ingots were cast up to a length of ~500 mm since only the start-up phase was under scrutiny. A bowl-shaped bottom block was used, which had a height of 304.8 mm. The inner edges of the bottom block were rounded off with a fillet radius. A lip around the ingot base restricted the relative movements between the ingot and bottom block during the casting process. A rectangular water-chilled mould was used.

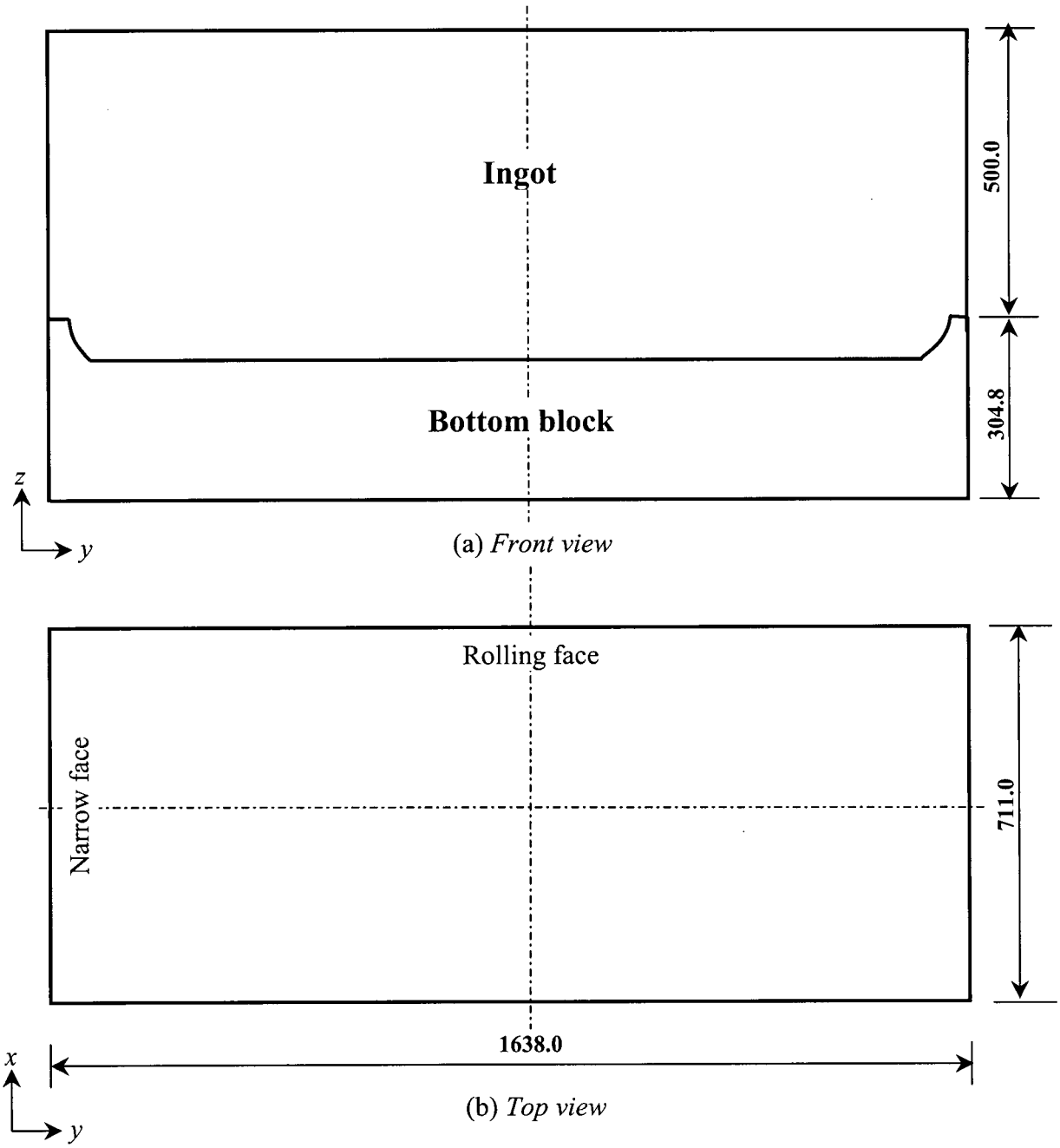

Figure 4.1 – The front (a) and top (b) views of the geometry of the bowl-shaped bottom block, and the ingot produced during the casting trials. The Cartesian coordinate system is defined by the narrow face direction (*x* axis), the rolling face direction (*y* axis), and the vertical direction (*z* axis). *Note: Units are in mm.*

4.2.3 Cast Start-up Procedure

At the beginning of the casting process, the bottom block was placed such that the top edge was ~20-35 mm inside the mould, which was located just above the casting pit (refer to **Figure 4.2**). Lubricating oil was applied to the mould surfaces, and mould water was turned on. Superheated liquid aluminum filled the bottom block through the metal feeding system *via* the distribution bag. The metal level in the bottom block was monitored by non-contact sensors placed above the liquid metal, which measured the distance, N, between the sensor and the liquid metal. The level was slowly increased as specified by the casting practice, until the liquid metal was in contact with the mould faces. The bottom block moved downwards at a pre-determined casting speed, as soon as the metal level sensor reading reached a critical value of N_{start}. The incoming metal flow rate was adjusted such that the mould metal level reached a constant value after ~0.1 normalized time. Meanwhile, the casting speed and water flow rates were linearly ramped as per the predetermined casting practice. The casting process continued until the desired cast length was achieved, at which time the incoming liquid metal flow, and the downward movement of the bottom block were interrupted. The chill water continued to flow from the mould, until the cast ingot was completely solidified. Finally, the casting was removed from the pit, and set aside to cool down to room temperature.

During the industrial trials, the mould filling practice, casting speed, and water flow rate were varied to produce a non-typical "cold" cast (Casting Practice No. 1) and a non-typical "hot" cast (Casting Practice No. 2). The casting practices for the two casts were designed to generate two extreme start-up ingot cooling conditions, and are not used by Alcan as standard operating practice (SOP) for production of ingots. The cold cast was intended to produce an ingot that experiences little or no water ejection from the vertical surface, a large amount of base deformation (butt curl), and a substantial amount of water incursion during start-up. The hot cast was intended to produce an ingot that experiences film boiling and water ejection on the surface, a comparatively small amount of base deformation, and little or no water incursion.

Figures 4.3, 4.4, and 4.5 show the details of the filling practice, casting speed, and water flow rate, respectively, which were used for the two casting practices. It is obvious from these figures that a faster filling rate and a lower water flow rate were used for the hot cast. Non-contact sensors also recorded the evolution of cast length with time for both the casts, as shown in **Figure 4.6**. The casting was stopped at ~0.78 normalized time for the hot cast, to prevent the

possibility of a break out since the temperature of the ingot would be considerably higher than what is normally observed during production.

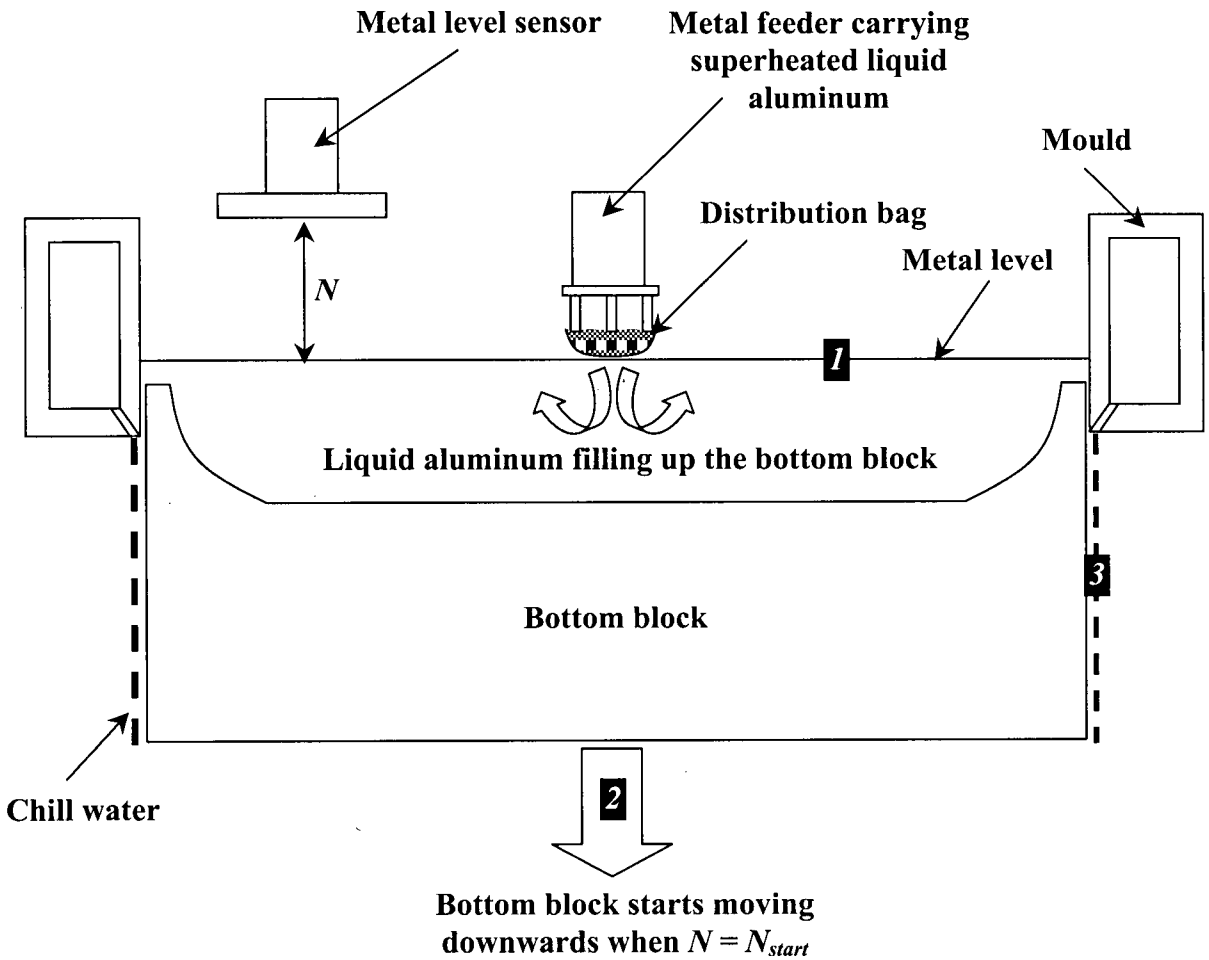

Figure 4.2 – Schematic illustrating the locations of casting equipment at the cast start-up for the industrial trials. The casting parameters, which control the heat transfer process during the start-up, are (1) metal level in the mould, (2) casting speed, and (3) water flow rate. The metal level sensor records the distance, *N*, between the sensor and liquid metal level inside the mould.

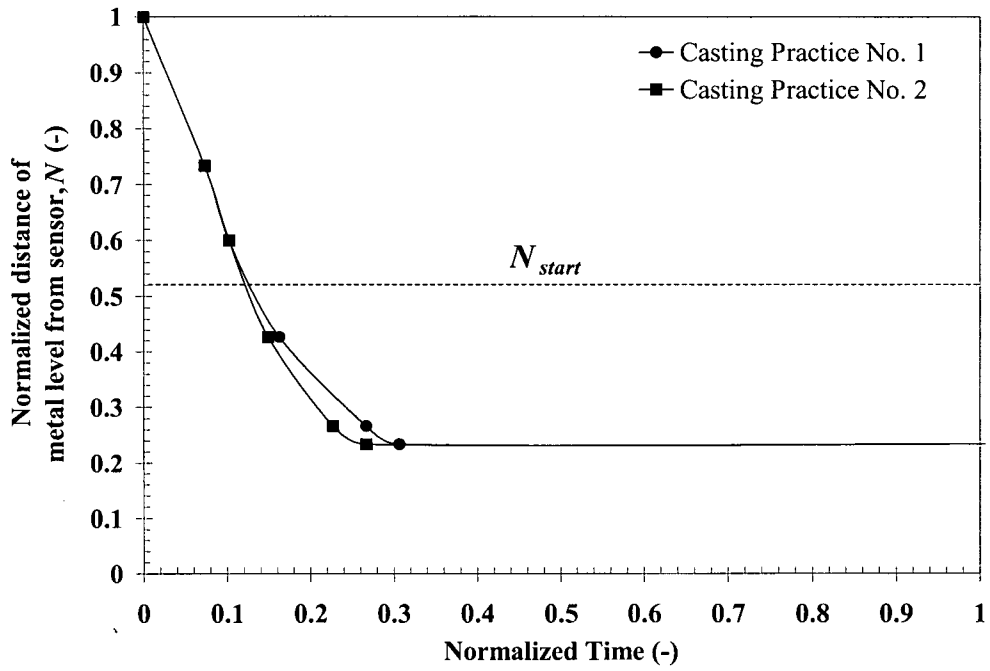

Figure 4.3 – Bottom Block filling practice (normalized) employed by Casting Practice Nos. 1 and 2, for the cold and hot casts, respectively.

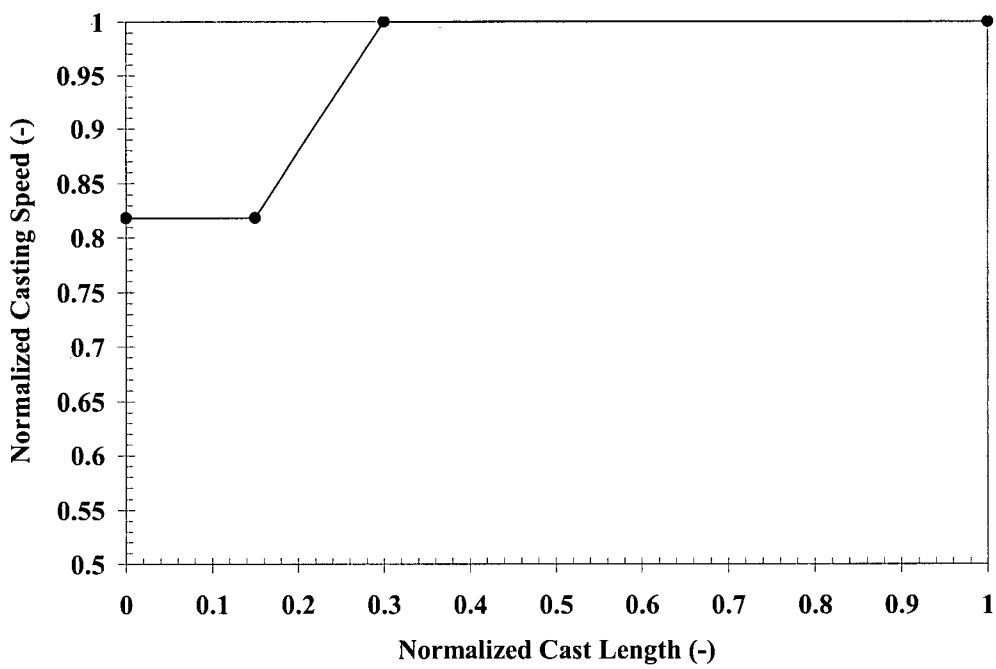

Figure 4.4 – Casting speed (normalized) employed by both Casting Practice Nos. 1 and 2, for the cold and hot casts, respectively.

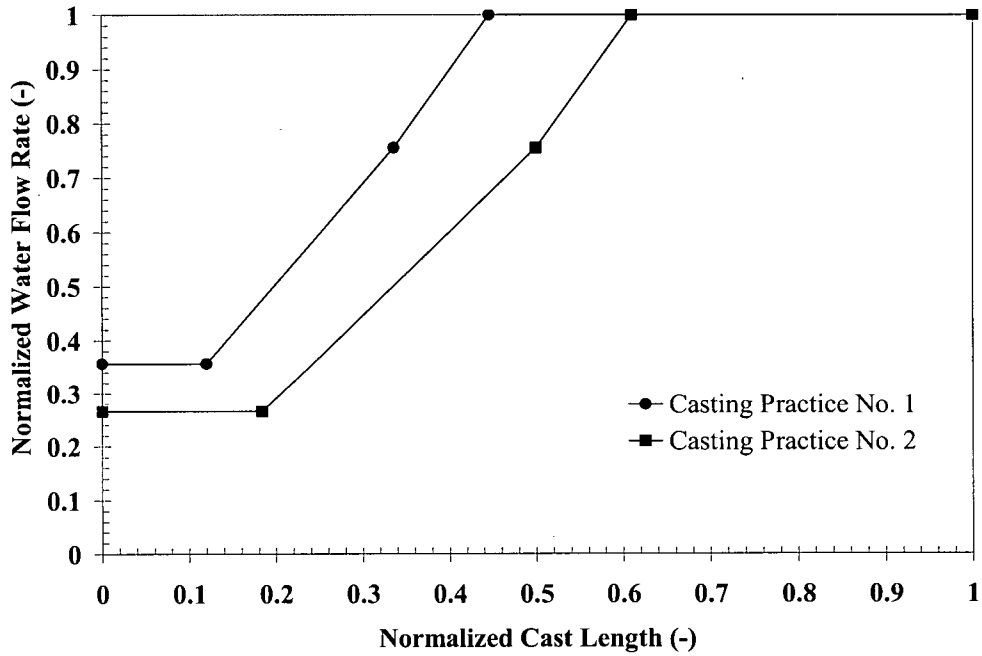

Figure 4.5 – Water flow rates (normalized) employed by Casting Practice Nos. 1 and 2, for the cold and hot casts, respectively.

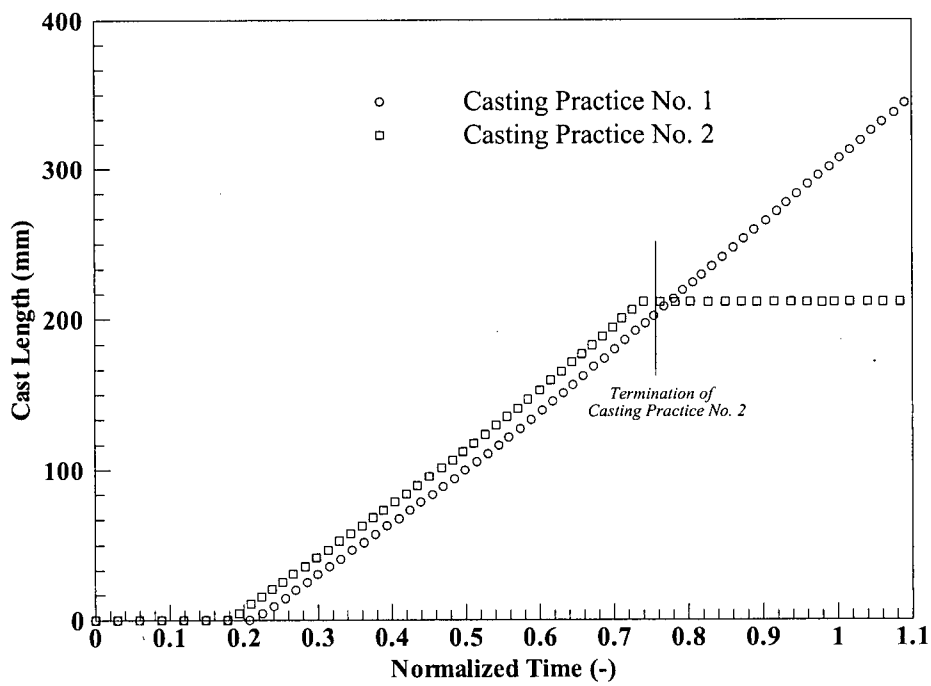

Figure 4.6 – Evolution of cast length with time for the cold and hot casts produced by Casting Practice Nos. 1 and 2, respectively. Casting Practice No. 2 was terminated at ~0.78 normalized time owing to safety considerations.

4.2.4 Casting Instrumentation

The instrumentation system, thermocouples employed to monitor the thermal history of the cast ingots, and transducers used to measure the displacement of the ingot base were provided by Alcan. Meniscus temperatures were recorded at fifteen locations around one half of the ingot (**Figure 4.7**) for both the cold and hot casts. The thermocouples were placed 12.5 mm deep in the molten metal, and were located 12.5 mm away from the mould and along the rolling and narrow faces of the ingot. The spacing between each thermocouple was 165 mm on the rolling face, and 175 mm on the narrow face.

Mould temperatures were recorded at four different heights (**Figure 4.8**) along the inner wall of the mould and at the centre of the rolling face for both the casts. Sub-surface temperatures in the ingot were recorded at four different heights (*i.e.* 10, 60, 110, and 160 mm) above the lip for both the rolling and narrow faces, as indicated in **Figure 4.9**. The thermocouples were placed 5 mm from the ingot faces and were held in place by metal wires, which were "frozen" in the solidifying ingot. For the rolling face, the thermocouples were placed 280 mm away from the center, whereas for the narrow face, they were placed along the centreline.

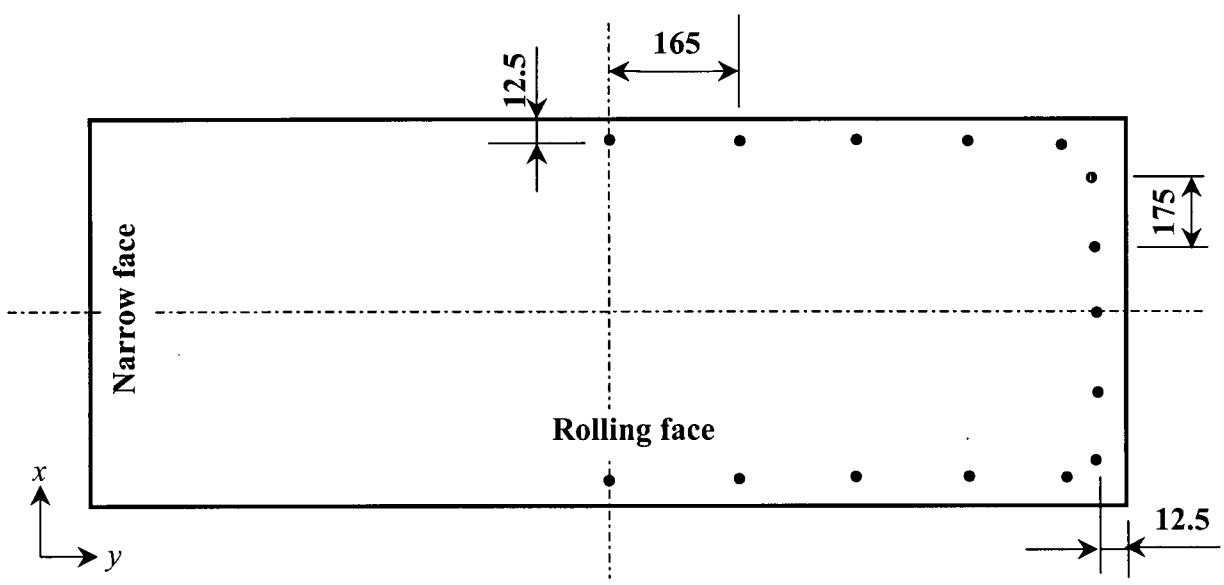

Figure 4.7 – Schematic of the arrangement of thermocouples instrumented 12.5 mm below the metal meniscus inside the mould. ***Note: Units are in mm.***

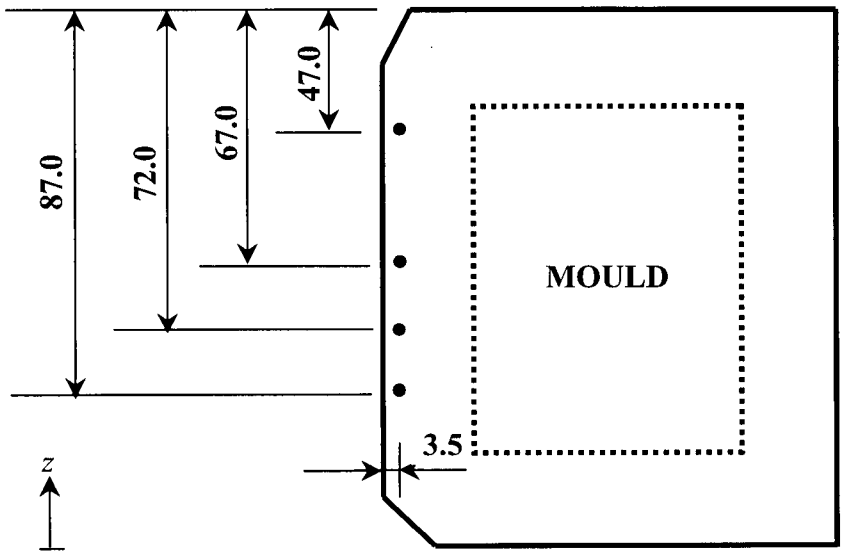

Figure 4.8 – Schematic of the arrangement of thermocouples instrumented along the inner edge of the mould. ***Note: Units are in mm.***

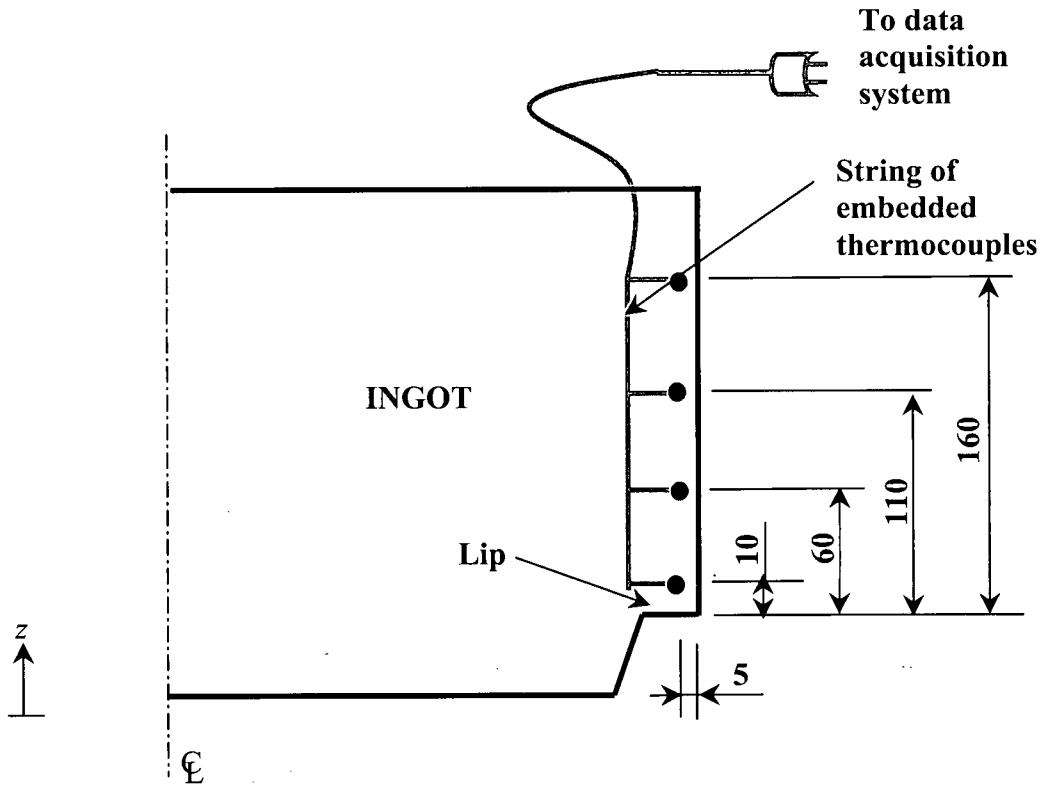

Figure 4.9 – Schematic of the arrangement of thermocouples instrumented adjacent to the ingot rolling and narrow faces. ***Note: Units are in mm.***

Two sets of thermocouples were used to record temperatures at the ingot base and the top surface of the bottom block. The thermocouples in the ingot base set were frozen along the base of the solidifying ingot, and those in the bottom block set were embedded along the top face of the bottom block. All the thermocouples were placed at a distance of 5 mm from the ingot/bottom block surface. The position (Location Nos. 2-8) of these thermocouple sets along the cross-section are schematically presented in **Figure 4.10**. Location No. 4 near the centre of the cross-section was not accessible in the case of the ingot due to the position of the distribution bag and metal feeder. As a result, temperature data for this location at the base of the ingot was not recorded. Temperatures were also recorded for both the ingot and bottom block at Location Nos. 1, 9, and 10 near the ingot lip as shown in **Figures 4.10** and **4.11**.

The thermocouples employed in the trials were a type-K (Nickel/Chrome-Nickel) thermocouple with a diameter of 1/16 inch. The thermocouples were protected from oxidation and/or corrosion by an Inconel sheath. A computer based data acquisition system was employed to record the thermocouple data at a frequency of 5 Hz. The calibration of the individual thermocouples was undertaken by Alcan personnel. Alcan's expertise was also utilized to ensure that there was minimum movement of the thermocouple assemblies during the casting process.

The measurement of butt curl was carried out using displacement transducers by employing well-established techniques described in the literature[5]. The displacement data acquisition rate was also 5 Hz.

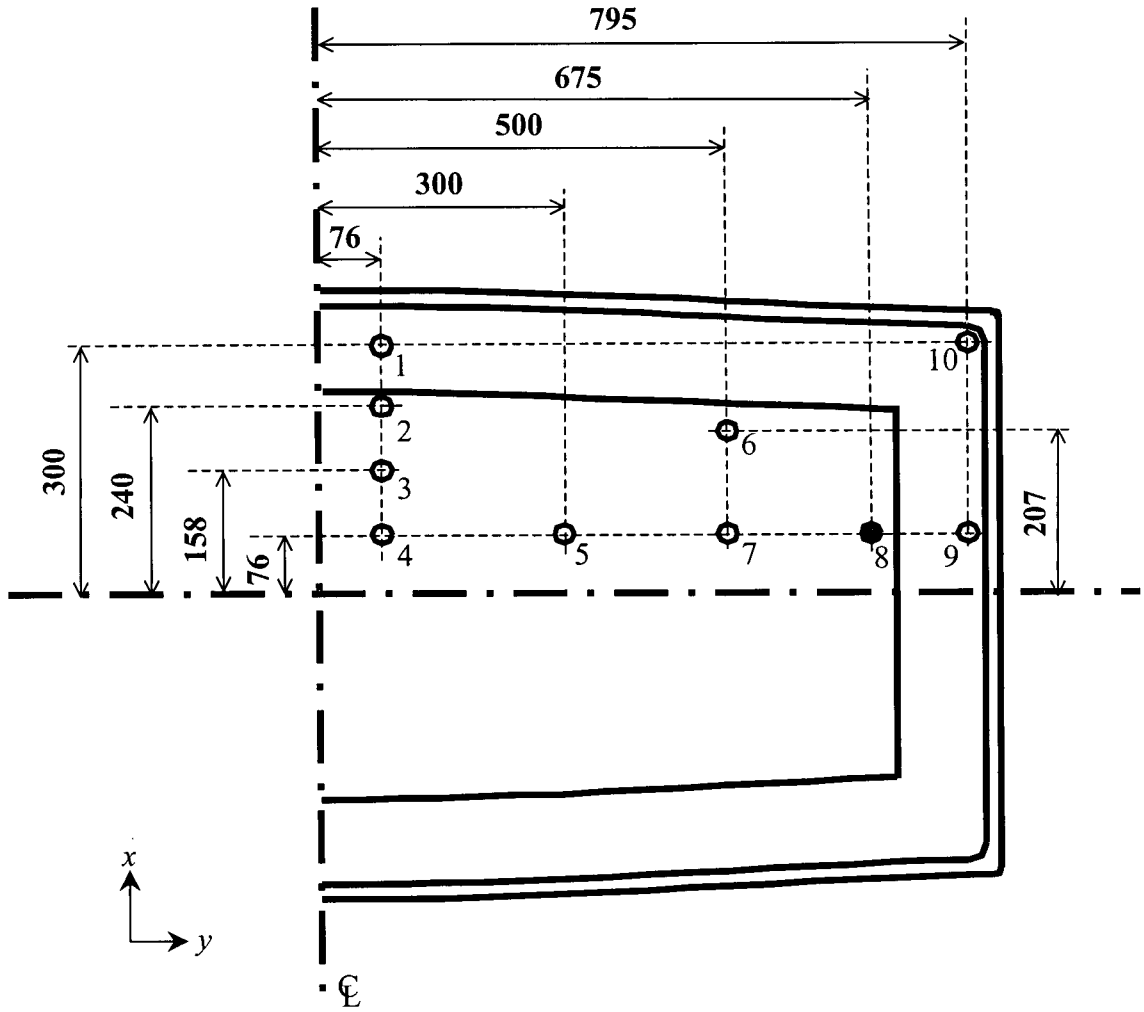

Figure 4.10 – Schematic of the arrangement of two thermocouple sets: one along the ingot base ,and the other along top face of the bottom block (cross-sectional view).

Note: Units are in mm.

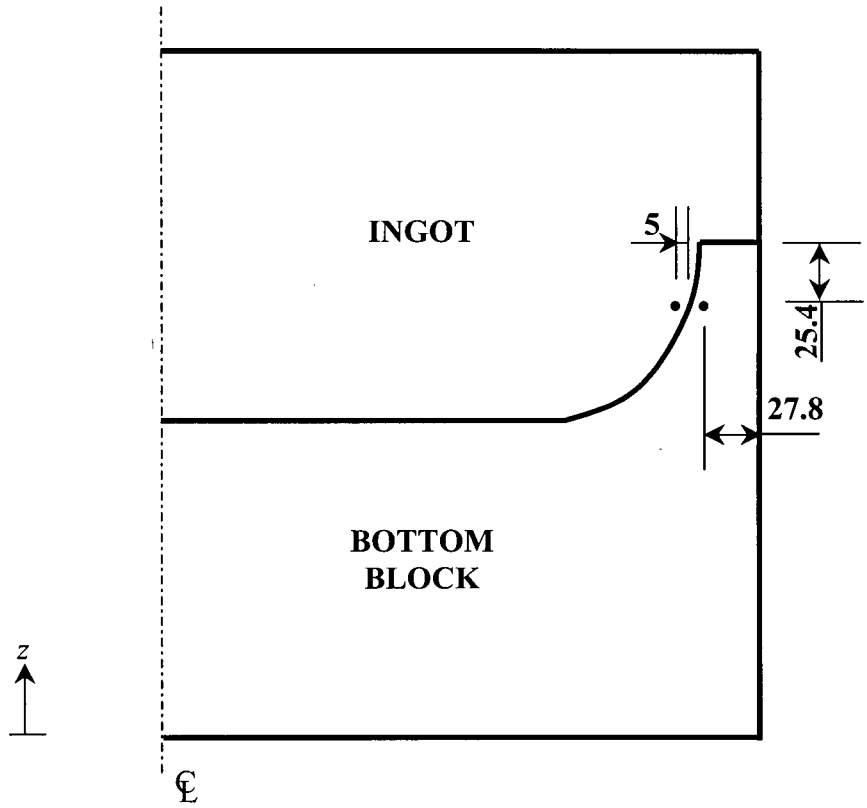

Figure 4.11 – Position of thermocouple placed at Location Nos. 1, 9, and 10 (refer to Figure 4.10) near the ingot lip. ***Note: Units are in mm.***

4.3 Results

In the following sections, the thermal responses of various thermocouples obtained from the two experimental casts are presented and discussed.

4.3.1 Temperature Measurements below the Metal Meniscus

Temperatures recorded by thermocouples placed in the molten metal near the centre of the rolling and narrow faces (refer to **Figure 4.7**) for the cold cast, are shown in **Figure 4.12**. It is interesting to note that the meniscus temperature near the narrow face is on average higher than that near the rolling face. This effect could be due to an error in the placement of the thermocouples below the meniscus. However, it is more likely that the higher temperature near the narrow face was due to the way the molten metal was distributed into the mould since the outflow was oriented directly towards the narrow face. Owing to a relatively smaller amount of circulation of metal occurring near the rolling face, a "dead zone" was formed, which explains

the lower temperature fluctuations near the rolling face. The initial temperature of the metal was assumed to be 660 °C for the heat transfer analysis, based on **Figure 4.12**.

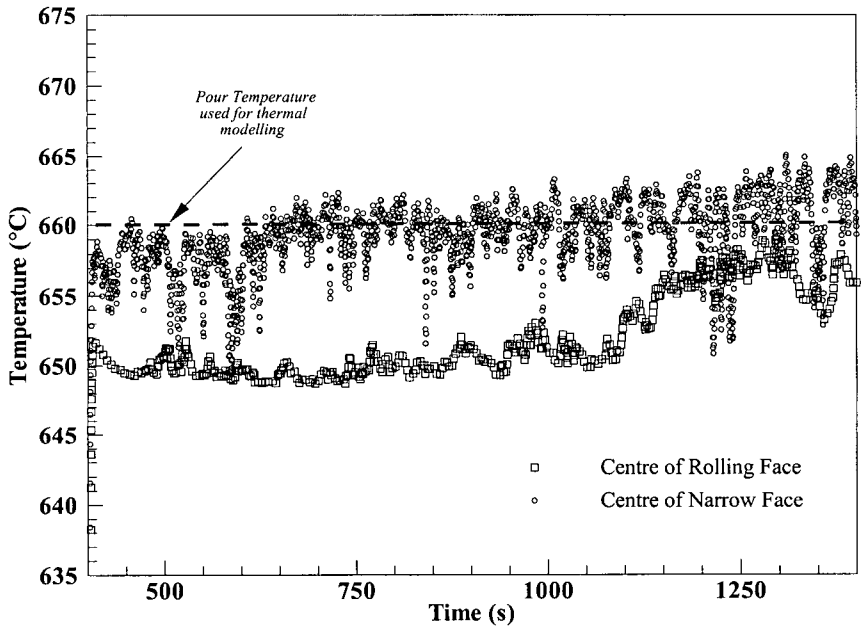

Figure 4.12 – Meniscus temperatures recorded for the cold cast.

4.3.2 Temperature Measurements on the Mould Inner Face

Figures 4.13 and **4.14** show the evolution of temperature with time along the mould wall (refer to **Figure 4.8**), for the cold and hot casts, respectively. Referring to these figures, it can be observed that there is an early rise in temperature measured by the thermocouple closest to the mould base when the liquid metal filled up the bottom block and made direct contact with the mould. As the liquid metal gradually filled up the mould itself, progressive heating of the other thermocouples away from the mould base is observed in the thermal response. It is evident from the figures that for both the cold and hot casts, the mould temperature was not stable during the first ~0.6 normalized time, owing to the periodic rise of the metal level and solidification/re-melting of the shell on the mould face. This transient behaviour associated with the mould cooling process in the initial stage of the start-up phase switched abruptly to a steady state behaviour as soon as the water flow rate was ramped to a maximum value and held constant for the rest of the casting period (refer to **Figure 4.5**). The small oscillations observed during the steady state regime are related to the "waves" of hot melt overflowing the meniscus and

solidifying at the mould surface. These oscillations, which were observed during the transient and steady state regimes, have also been reported in literature[6].

From **Figures 4.13** and **4.14**, it can also be concluded that the response of the thermocouples in the steady state regime is dramatically different for the two casts. In the case of the cold cast, it is evident from **Figure 4.13** that the rate of heat transfer in the steady state regime was higher near the top face of the mould (corresponding to meniscus cooling) as compared to the rate of heat transfer near the mould base (corresponding to air gap cooling). The variation of temperature along the mould face near the base may be due to the fact that the thickness of the air gap was not uniform along the vertical inner face of the mould for this cast; rather it was largest near the base and tapered down along the vertical direction. For the hot cast, all the four thermocouples show similar response in the steady state regime indicating the formation of a much smaller air gap along the vertical inner face of the mould compared to the cold cast, as can be seen from **Figure 4.14**. As will be discussed later in this chapter, this can be due to the effect of a considerably lower magnitude of butt curl that was observed during the hot cast. For the cold cast, the vertical faces of the ingot were pulled away from the mould wall to a greater extent owing to the larger macroscopic deformation of the ingot base, thus increasing the air gap.

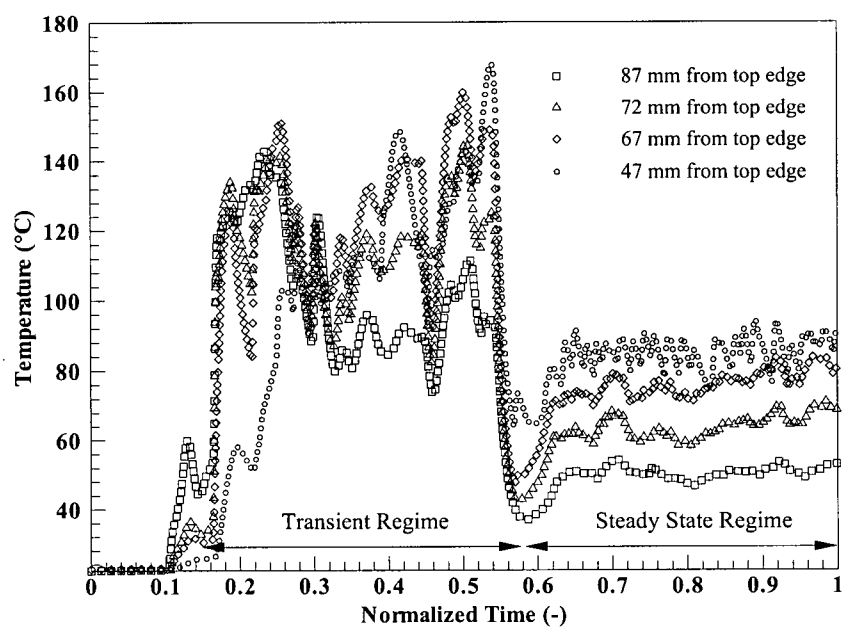

Figure 4.13 – Mould temperatures recorded for the cold cast.

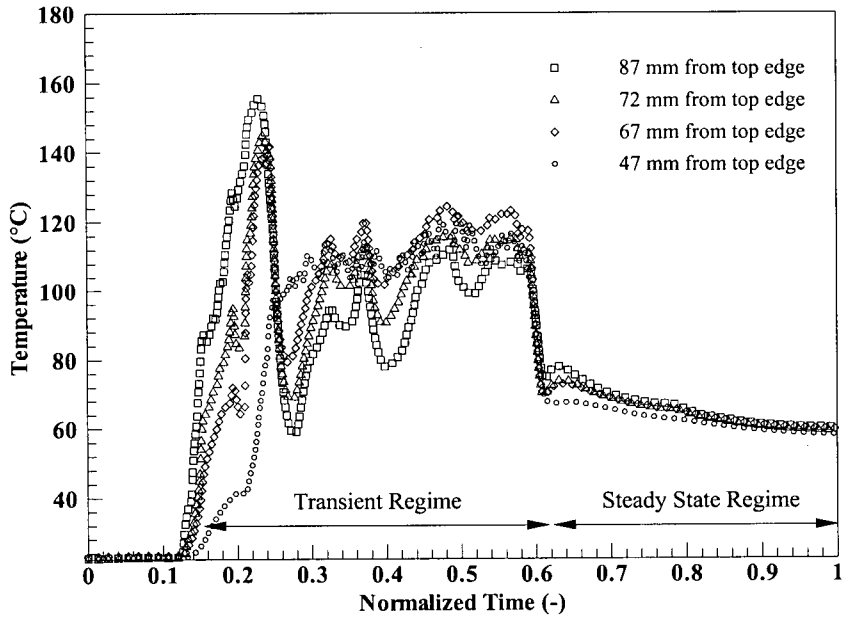

Figure 4.14 – Mould temperatures recorded for the hot cast.

4.3.3 Temperature Measurements on the Ingot Rolling and Narrow Faces

Figure 4.15 shows the variation in ingot sub-surface temperature obtained from the thermocouple located on the rolling face 10 mm above the lip, for the cold cast and for the hot cast. The thermocouple responses for both the casts also indicate an initial sharp drop in temperature, from 660 to ~ 520 °C, due to meniscus cooling, followed by a rebound after ~100 s owing to the decrease in the rate of heat transfer after the formation of air gap. It is evident from a comparison of the two plots that little or no drop in temperature is observed at the point of water contact (~0.3 normalized time) in the hot cast, compared with a significant drop observed in the cold cast (approximately 450 °C). The substantial difference in heat transfer observed in these two cases was due to the presence of stable film boiling observed in the hot cast. In addition to the thermocouple evidence, the presence of stable film boiling was observed on the surface of the ingot during casting and was indicated by substantial amounts of steam generation and a stable ejection front below which the ingot appeared "dry".

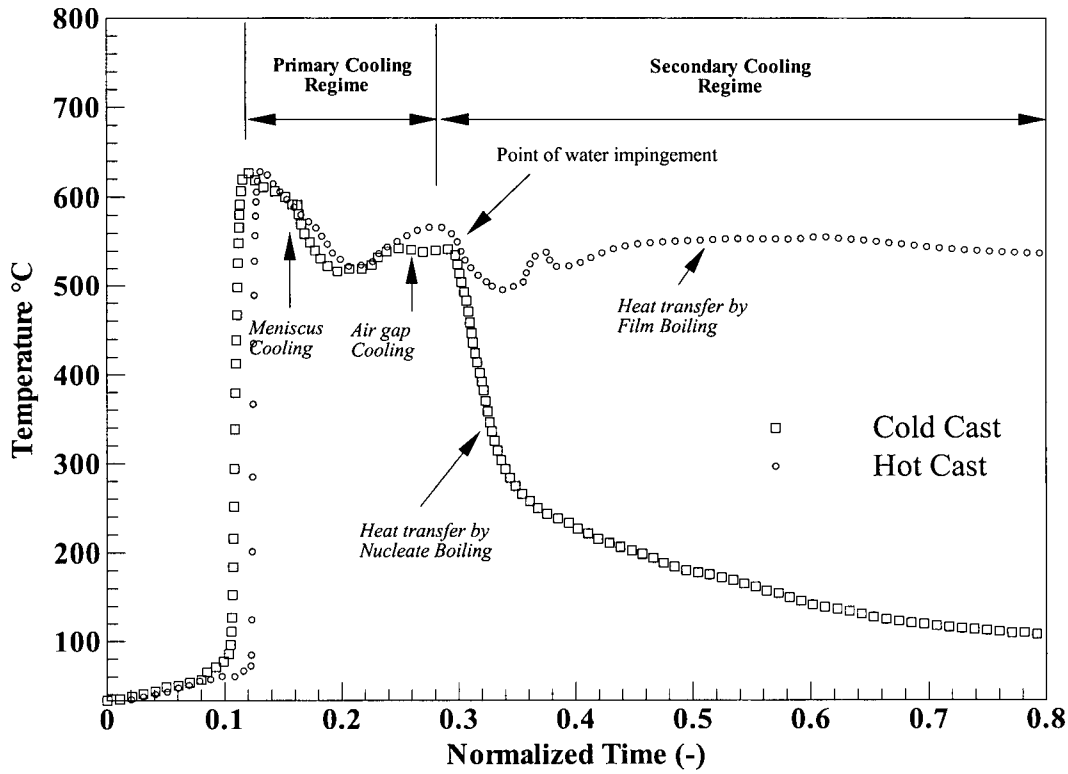

Figure 4.15 – Ingot sub-surface temperature profiles adjacent to the rolling face and 10 mm above the ingot lip for the cold and hot casts, illustrating the different secondary cooling rates experienced by the ingot for the two different start-up conditions.

Figures 4.16 and **4.17** show the recorded temperatures, along the rolling and narrow faces, respectively (refer to **Figure 4.9**), for the cold cast. **Figures 4.18** and **4.19** show the recorded temperatures, along the rolling and narrow faces, respectively, for the hot cast. For the cold cast, referring back to **Figure 4.16**, it is evident that the thermocouple placed adjacent to the rolling face, at a distance 110 mm above the lip, was damaged as soon as it came in contact with the liquid metal. The two distinct heat transfer zones of primary and secondary cooling are evident in the data collected from the thermocouples in the cold cast. It can also be observed that the two thermocouples near the lip (at 10 and 60 mm) recorded locally reduced temperatures near the end of the casting process.

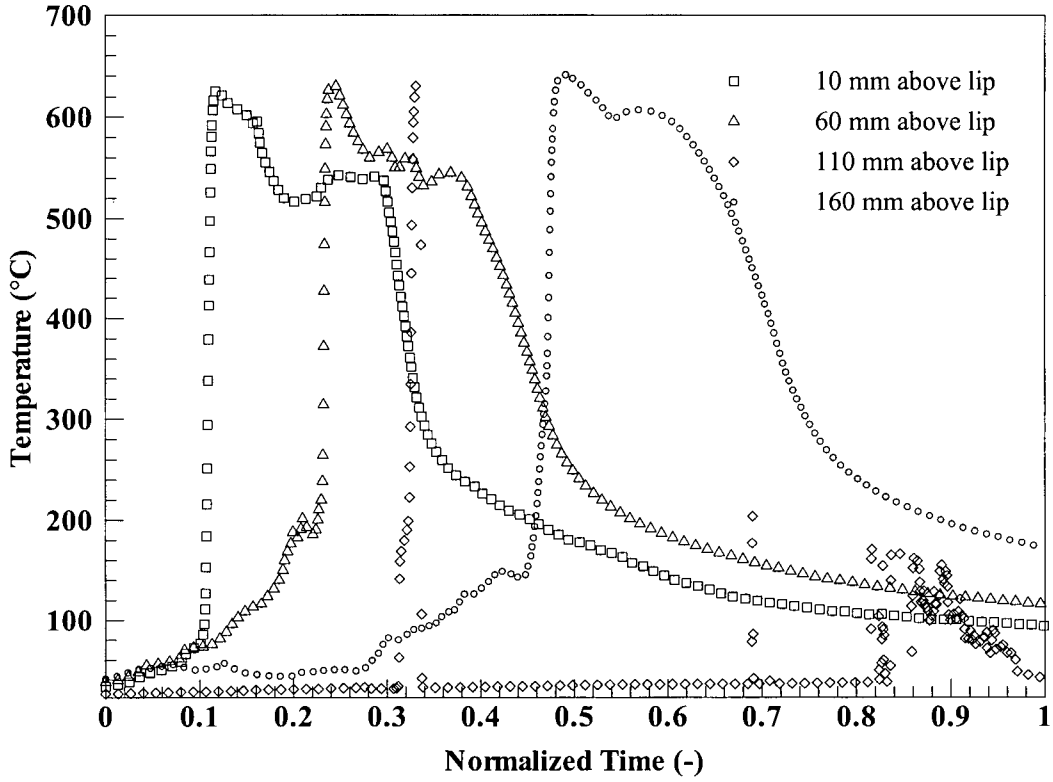

Fig 4.16 – Temperatures recorded by the thermocouples adjacent to the ingot rolling face for the cold cast.

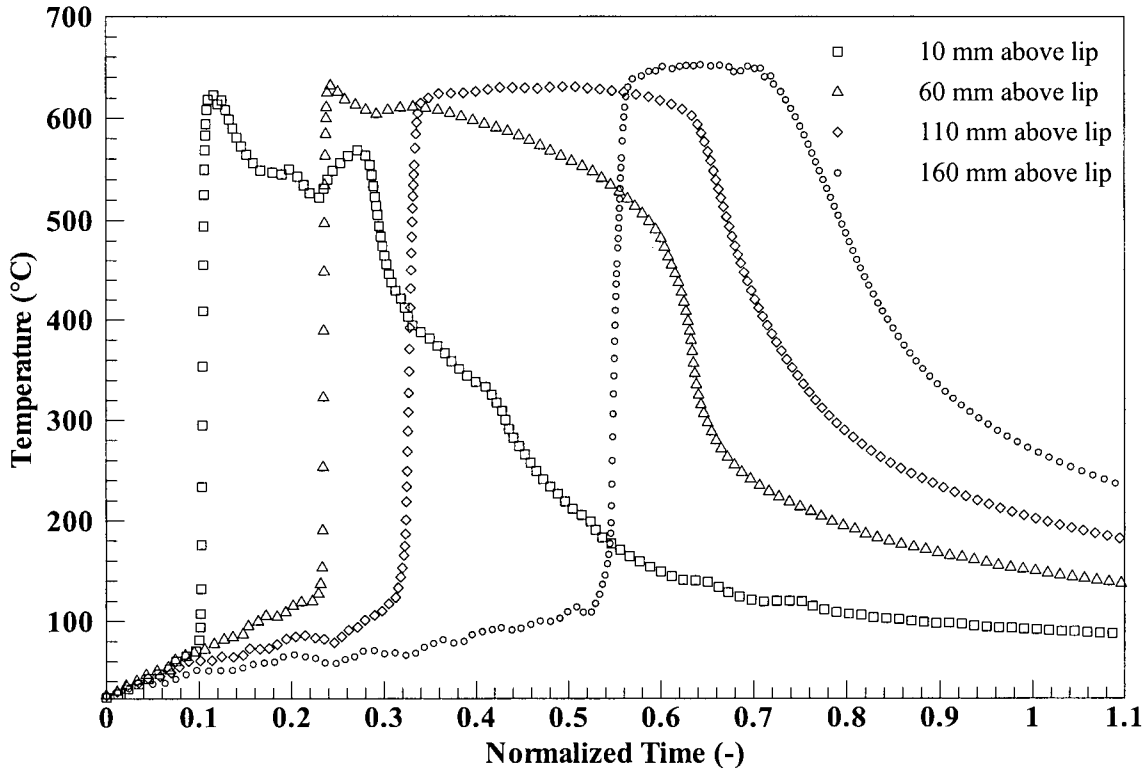

Fig 4.17 – Temperatures recorded by the thermocouples adjacent to the ingot narrow face for the cold cast.

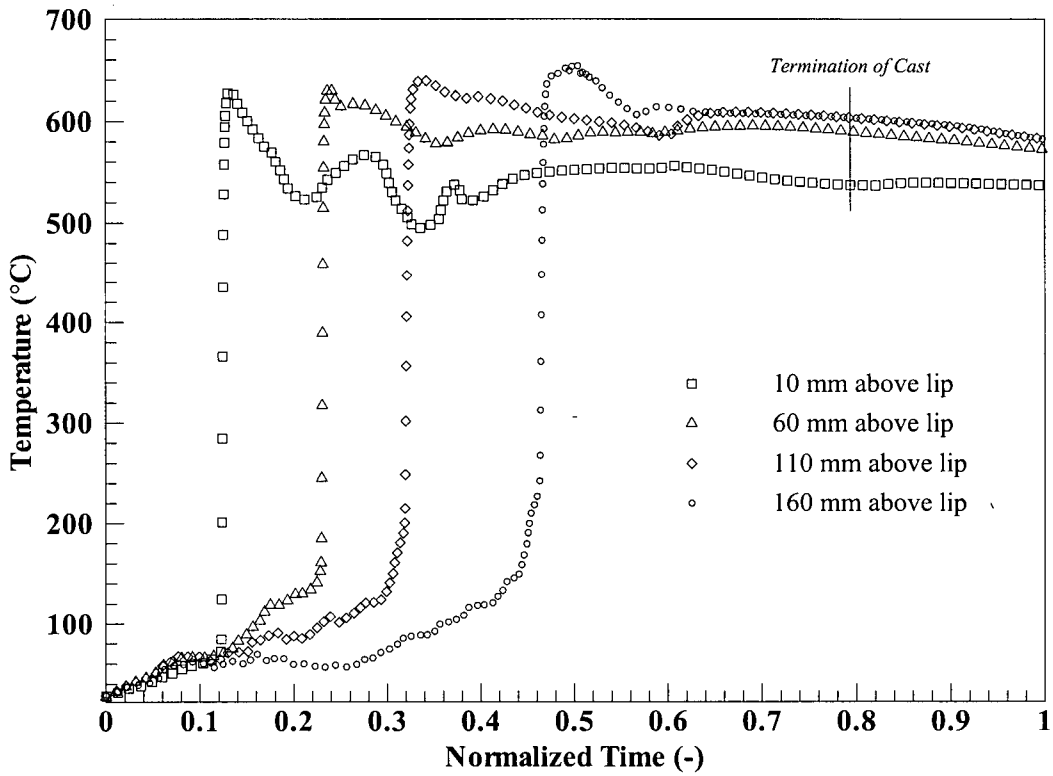

Fig 4.18 – Temperatures recorded by the thermocouples adjacent to the ingot rolling face for the hot cast.

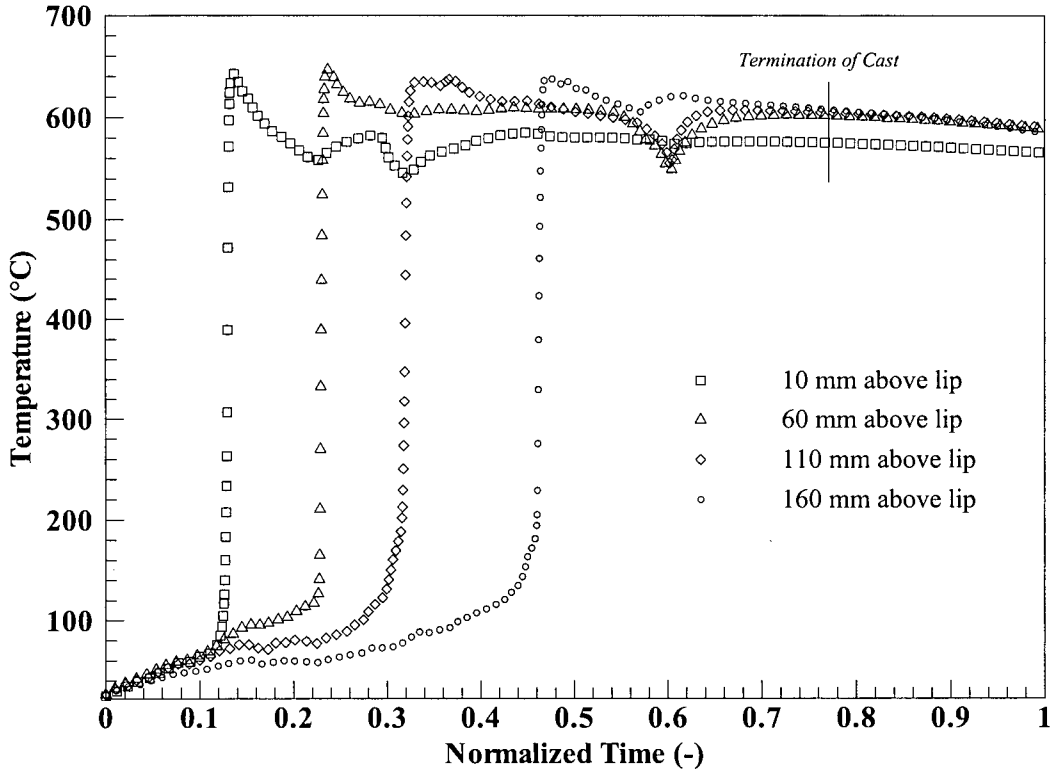

Fig 4.19 – Temperatures recorded by the thermocouples adjacent to the ingot narrow face for the hot cast.

Comparing the responses of the thermocouples placed at 60, 110, and 160 mm above the lip for the rolling face in **Figure 4.16**, and for the narrow face in **Figure 4.17**, it appears that the narrow face remained at a higher temperature for a longer period of time. In fact, the primary cooling effect was not observed for the thermocouples adjacent to the narrow face and further away from the lip. This phenomenon can be explained by the fact that the magnitude of butt curl for the narrow faces of the ingot is considerably higher than that for the rolling faces, owing to the rectangular geometry of the ingot cross-section. As the narrow faces curled, the thermocouples adjacent to this face moved upwards relative to the corresponding thermocouples adjacent to the rolling face. Hence, these thermocouples did not move downwards at a rate determined by the casting practice, rather their movement was "slowed down" by the effect of butt curl acting in the opposite direction. It was, therefore, quite possible that these thermocouples spent a longer time in the liquid metal, which may explain the flattening out

observed in their initial response. The reader is cautioned here that this effect displayed by narrow face thermocouples for the cold cast should not be misinterpreted as that caused by the film boiling phenomenon, which was observed during the hot cast.

For the hot cast, referring to **Figures 4.18** and **4.19**, it is evident that the central region of both the rolling and narrow faces of the ingot experienced severe film boiling phenomenon, which caused the water film in these regions to be ejected from the surface keeping the temperatures between 550 – 625 °C, throughout the casting period. This observation is further substantiated by the presence of a steady film boiling dome on the ingot exterior surfaces, which was clearly visible during the industrial trial, as shown in **Figure 4.20**.

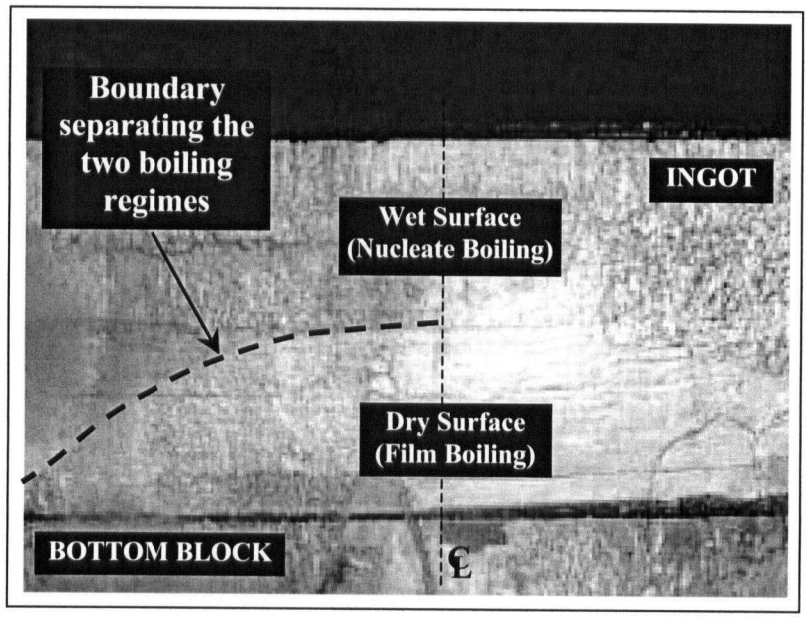

Figure 4.20 – The phenomenon of film boiling observed for the hot cast during the industrial trials. The parabola-shaped boundary, separating the film and nucleate boiling regimes, collapsed towards the centre-line as the casting progressed.

4.3.4 Temperature Measurements near the Ingot Base

The thermocouple responses of the ingot base for the hot cast were dramatically different from those observed during the cold cast. This can be easily seen in **Figure 4.21**, which compares the responses of the thermocouple placed near the centre of the narrow face at Location No. 9 (refer to **Figure 4.10**) for the two castings. Referring to this figure, the sharp drop in the temperature at ~0.32 normalized time (i.e. a few seconds after the chill water contacted the

vertical ingot faces) observed in the cold cast can be attributed to the intensive cooling caused by water entering the air gap between the ingot base and bottom block due to butt curl. This effect is not observed in the hot cast, which remained hotter for the entire casting period. This response is indicative of the absence of water incursion as a result of the lower magnitude of the butt curl. It can thus be concluded that the effect of water incursion, which was specifically observed for the cold cast, can significantly alter the cooling conditions near the ingot base during the start-up phase. Further, this behaviour points to the need for a fully coupled thermal/stress analysis as ingot base cooling is strongly influenced by the mechanical deflection of the ingot base.

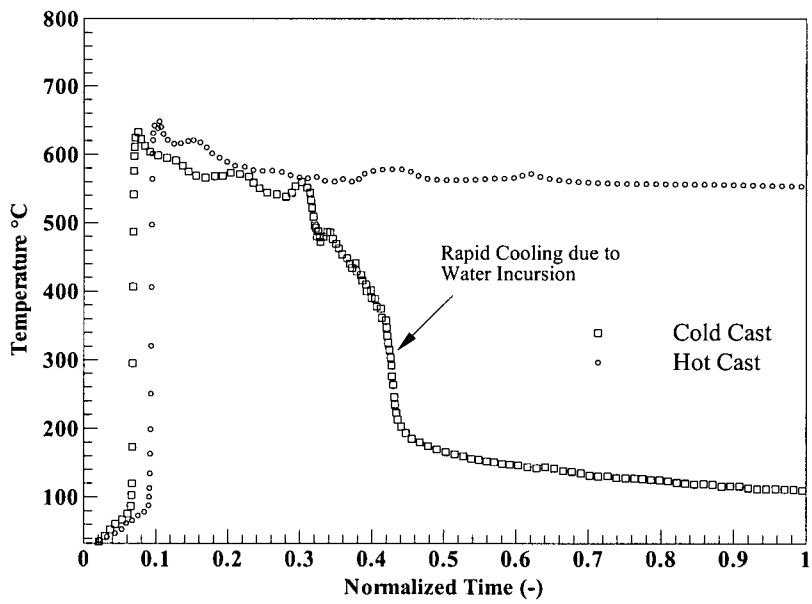

Figure 4.21 – Comparison between the responses of the thermocouple placed at Location No. 9 (refer to Figure 4.10) near the ingot base for the two castings.

The temperatures recorded along the ingot base perpendicular to the rolling and narrow faces, and along the diagonal from the corner (refer to **Figures 4.10** and **4.11**) are presented in **Figures 4.22**, **4.23** and **4.24**, respectively for the cold cast. **Figures 4.25**, **4.26**, and **4.27** show the corresponding data for the hot cast.

For the cold cast, the effect of water incursion at the base is clearly visible from the sharp drop in temperature observed in the response of thermocouples at Location Nos. 1, 9, and 10 in **Figures 4.22-24**, which were located very close to the ingot lip. It is evident that water enters

into the gap formed between the ingot and bottom block due to butt curl, and reached the thermocouple at Location No. 1 (refer to **Figure 4.22**) along the rolling face, the thermocouple at Location No. 7 (refer to **Figure 4.23**) along the narrow face, and the thermocouple at Location No. 6 (refer to **Figure 4.24**) along the diagonal to the cross-section. This is due to the fact that the narrow face shows more deformation than the rolling face, as explained earlier. The gradual decrease in the rate of cooling for the thermocouples at Location No. 7 to Location No. 9 in **Figure 4.22** is indicative of the fact that the extent of water incursion (or the process of "wetting") between the bottom block and ingot decreased gradually from the exterior edge of the narrow face to the centre. The thermocouples located near the center of ingot (*i.e.* Location Nos. 2, 3, and 5) stayed hot for a long time, owing to the absence of water incursion.

It is evident from **Figures 4.25-4.27** that the temperature of the entire ingot base for the hot cast was above 500 °C throughout the casting time, owing to the absence of water incursion along all the four edges of the ingot base.

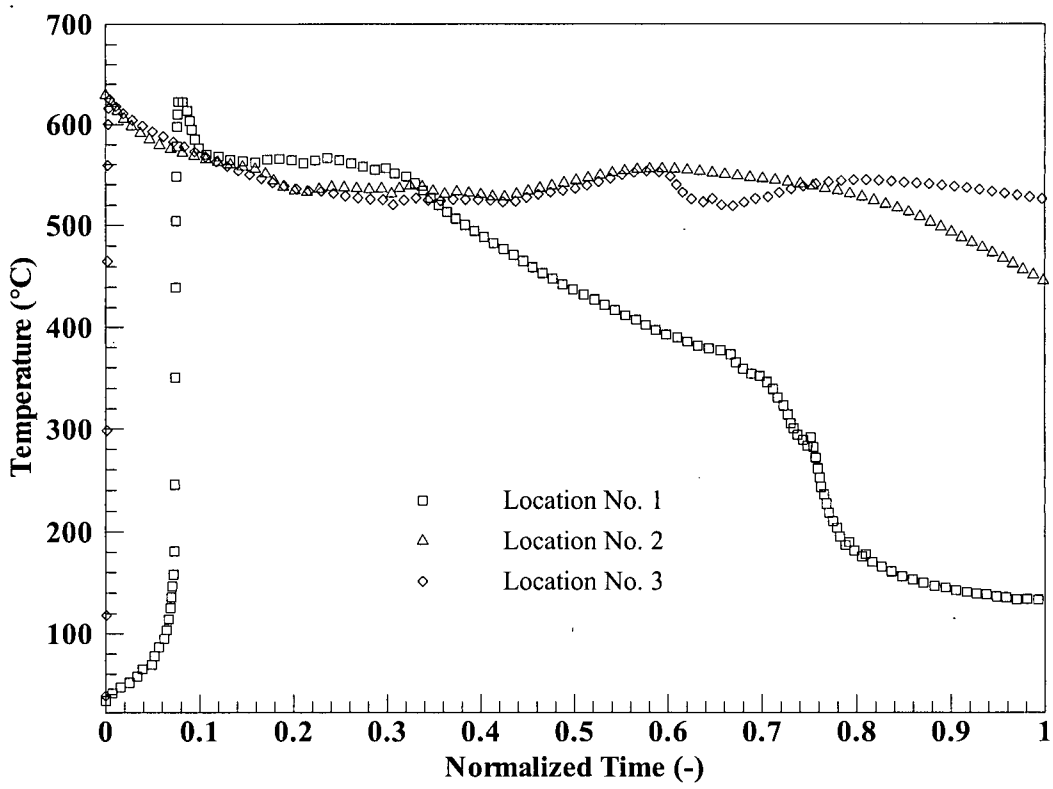

Figure 4.22 – Temperatures recorded by the thermocouple placed at Location Nos. 1, 2, and 3 (refer to Figure 4.10) near the ingot base for the cold cast.

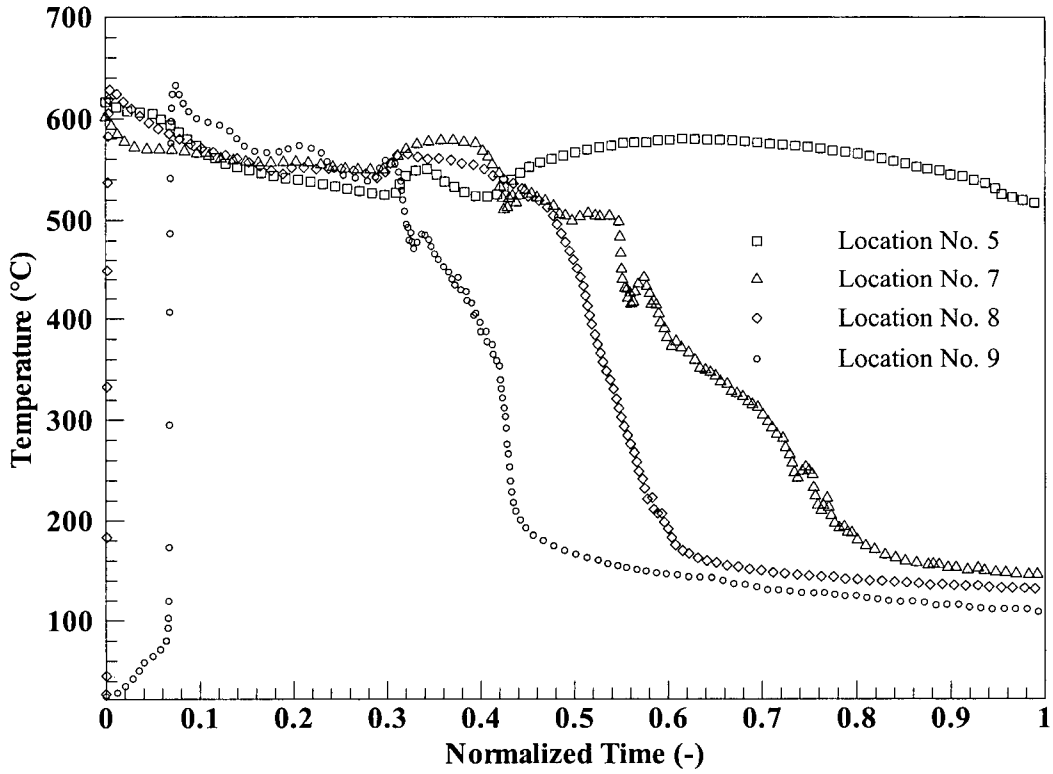

Figure 4.23 – Temperatures recorded by the thermocouple placed at Location Nos. 5, 7, 8, and 9 (refer to Figure 4.10) near the ingot base for the cold cast.

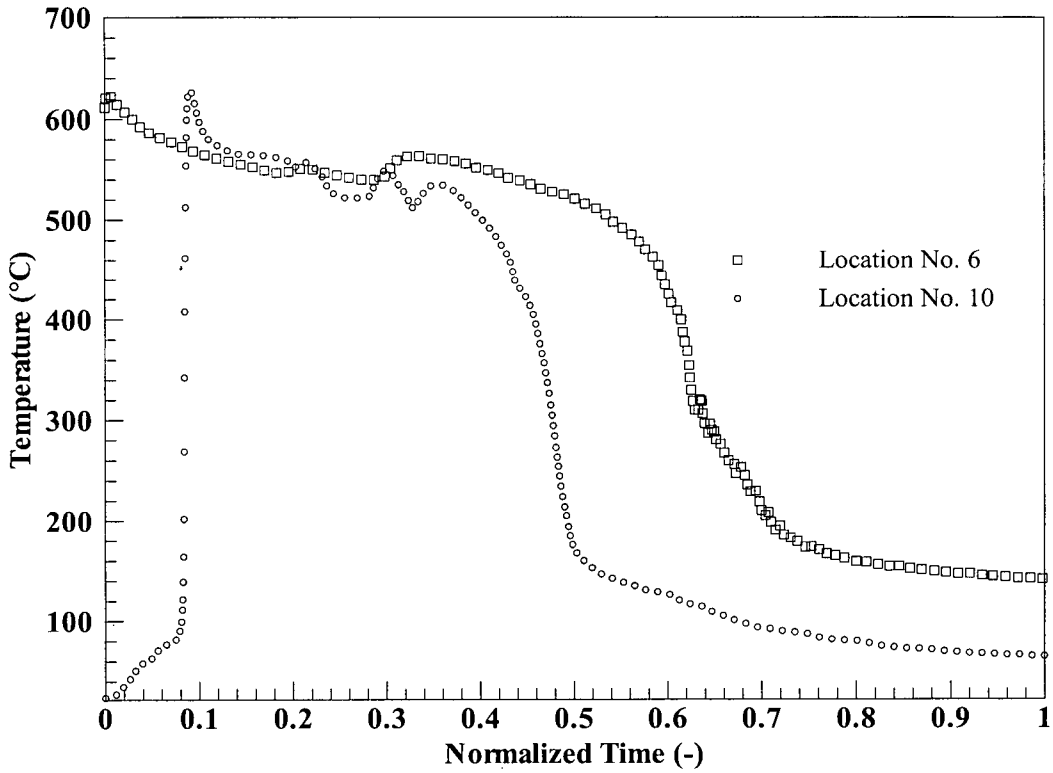

Figure 4.24 – Temperatures recorded by the thermocouple placed at Location Nos. 6, and 10 (refer to Figure 4.10) near the ingot base for the cold cast.

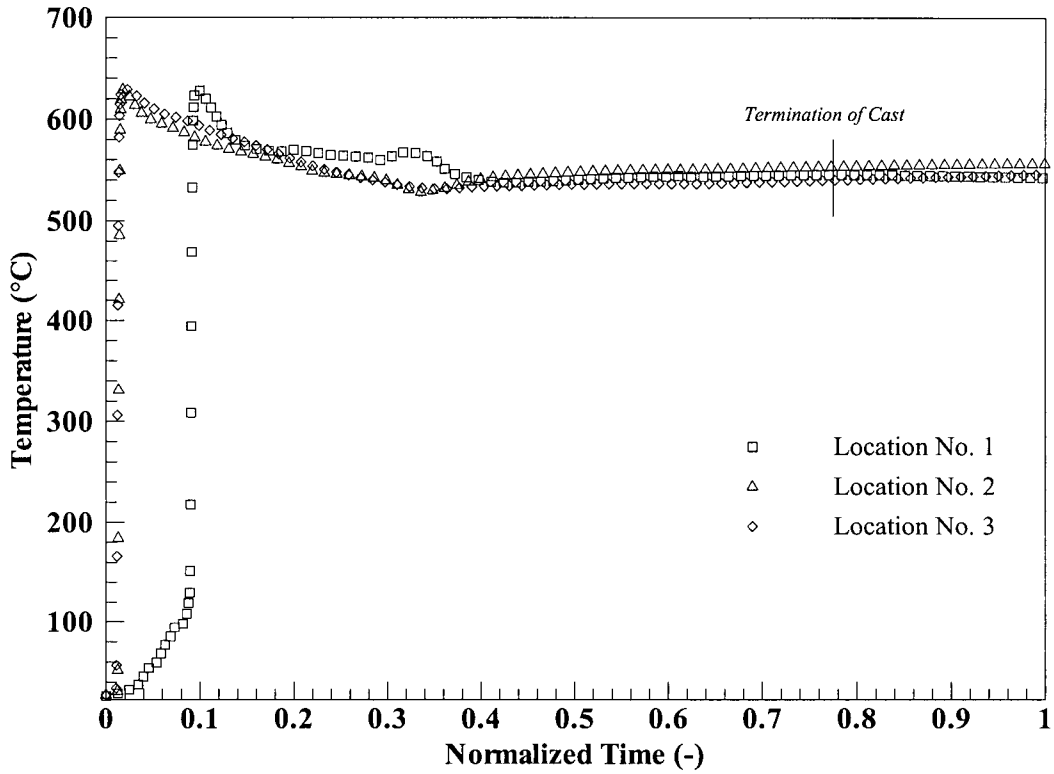

Figure 4.25 – Temperatures recorded by the thermocouple placed at Location Nos. 1, 2, and 3 (refer to Figure 4.10) near ingot base for the hot cast.

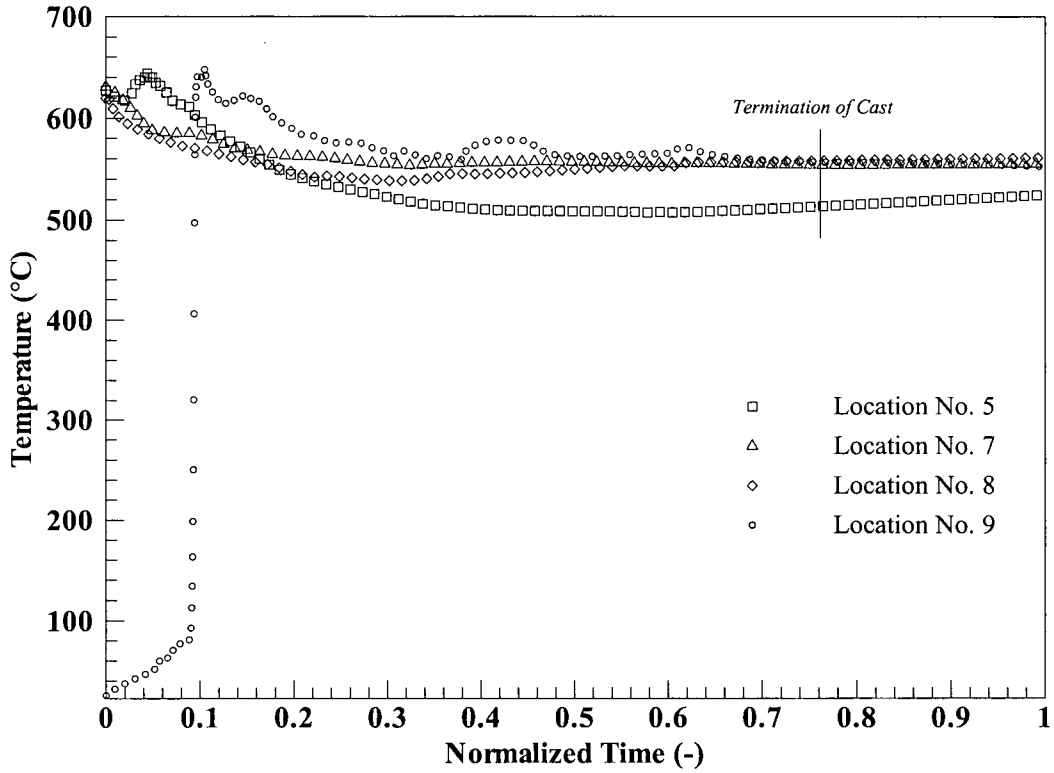

Figure 4.26 – Temperatures recorded by the thermocouple placed at Location Nos. 5, 7, 8, and 9 (refer to Figure 4.10) near the ingot base for the hot cast.

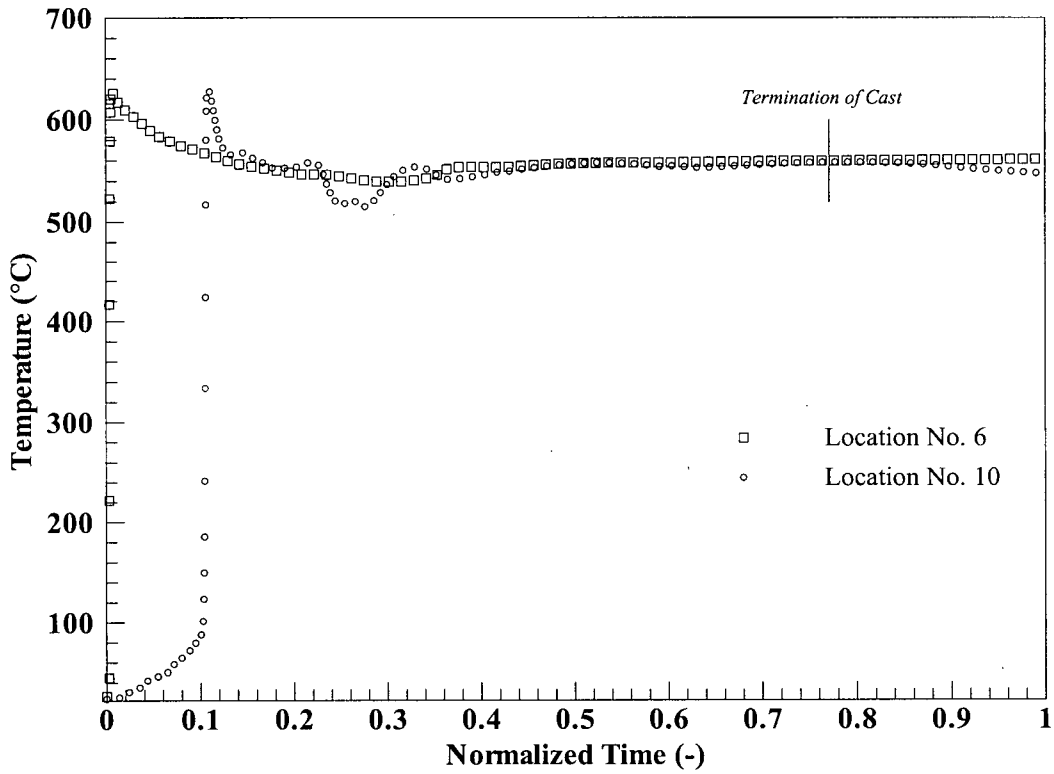

Figure 4.27 – Temperatures recorded by the thermocouple placed at Location Nos. 6, and 10 (refer to Figure 4.10) near the ingot base for the hot cast.

4.3.5 Temperature Measurements near the Top Face of the Bottom Block

The temperatures recorded near the top surface of the bottom block along a line perpendicular to the rolling and narrow faces, and along the diagonal from the corner (refer to **Figures 4.10** and **4.11**) are shown in **Figures 4.28**, **4.29** and **4.30**, respectively for the cold cast. **Figures 4.31**, **4.32**, and **4.33** show the corresponding data for the hot cast. The rise in temperature (up to ~250 °C) observed in the response of the thermocouples for both the casts during the first few seconds of the casting was due to the conduction of heat from the liquid metal entering the bottom block. For the cold cast, rapid cooling recorded by thermocouples at Location Nos. 1, 9, and 10 (refer to **Figures 4.28-4.30**) was due to water entering the air gap between the ingot and bottom block from the exterior edges. As the water dripping from the narrow faces of the ingot rolled down the top surface of the bottom block, the thermocouples at Location Nos. 5, 7, and 8 were progressively cooled, as seen in **Figure 4.29**. The intensity of

cooling decreased towards the centre as the holes in the bottom block gradually drained out the water. This cooling effect was not recorded by the thermocouple at Location Nos.1 through 4 (refer to **Figure 4.28**), since the water could not reach these locations owing to the smaller size of air gap between the ingot and bottom block.

The effects of water incursion observed in the case of the cold cast were absent in the data recorded by thermocouples for the hot cast, in which case the chill water was ejected away from the ingot faces, and did not enter the gap. Consequently, the bottom block remained at a higher temperature (~300 °C) for the entire casting time, owing to the continuous conduction of heat from the ingot base, as indicated by the thermocouples at Location Nos. 2-8 in **Figures 4.31-4.33**. The decrease in temperature observed in the responses of thermocouple at Location Nos. 1, 9, and 10 for the hot cast was not due to water incursion; rather they were subjected to cooling by the chill water running down the bottom block sides prior to being ejected from the ingot vertical faces. As the process of water ejection began, the temperature rose again as the ingot base continued to heat up the bottom block, and the vertical sides of the bottom block were now cooled by natural convection to air instead of conduction to the chill water.

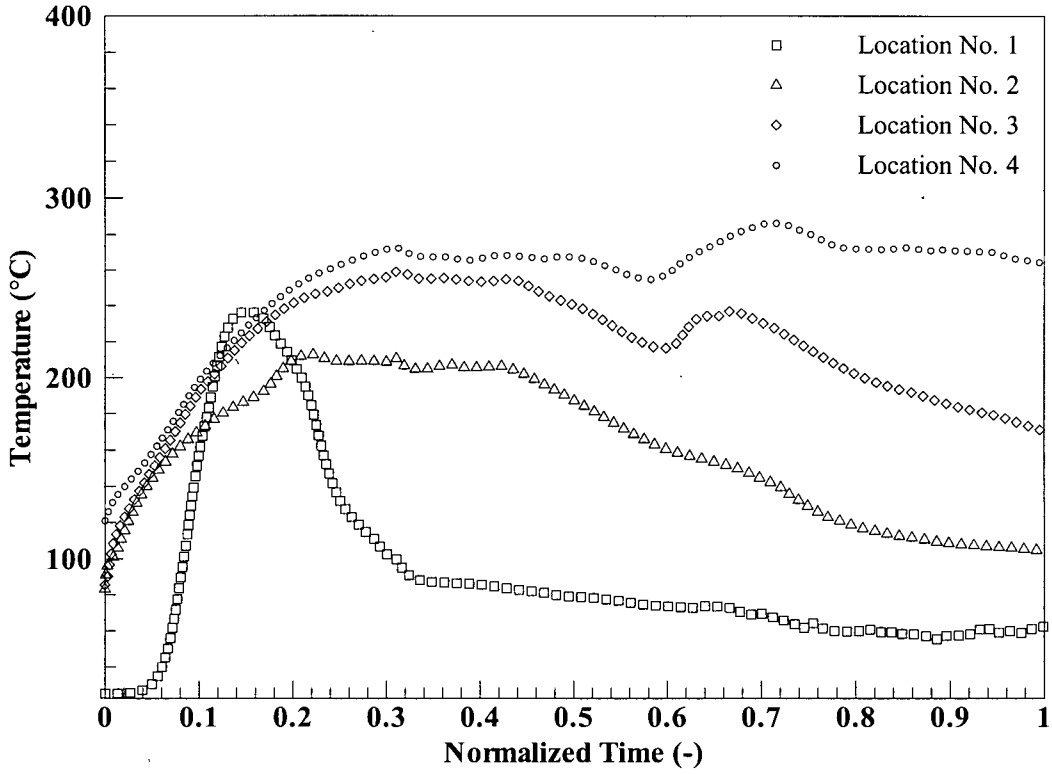

Figure 4.28 – Temperatures recorded by the thermocouple placed at Location Nos. 1, 2, 3, and 4 (refer to Figure 4.10) near the bottom block top face for the cold cast.

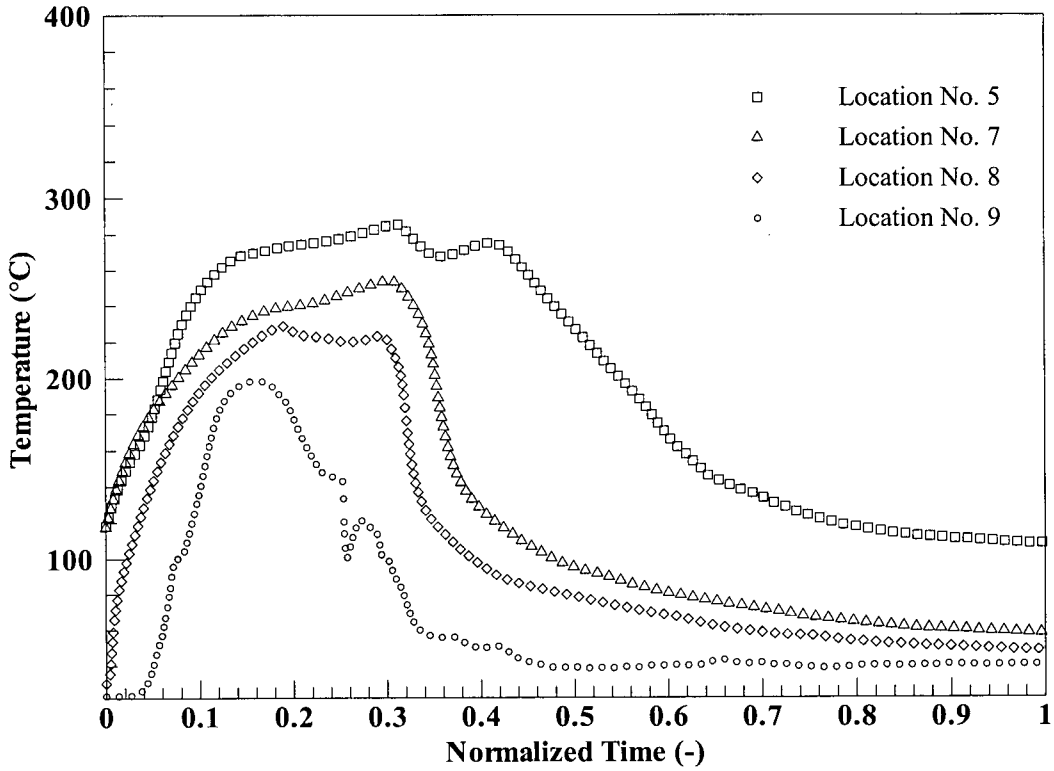

Figure 4.29 – Temperatures recorded by the thermocouple placed at Location Nos. 5, 7, 8, and 9 (refer to Figure 4.10) near the bottom block top face for the cold cast.

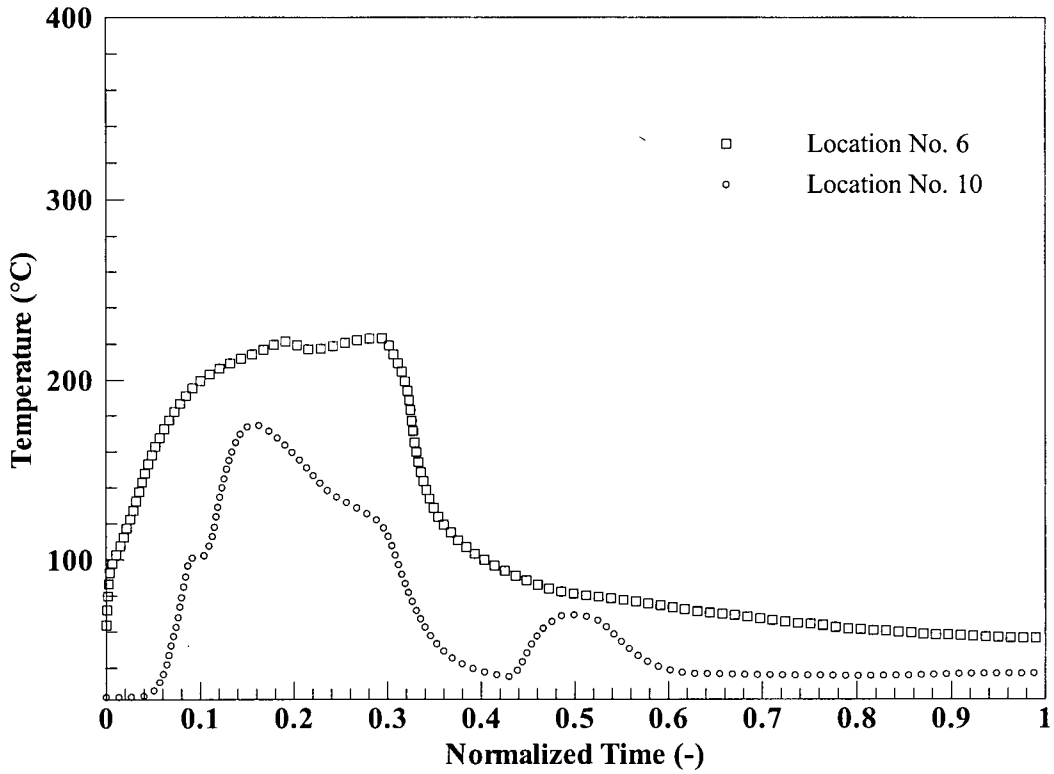

Figure 4.30 – Temperatures recorded by the thermocouple placed at Location Nos. 6, and 10 (refer to Figure 4.10) near the bottom block top face for the cold cast.

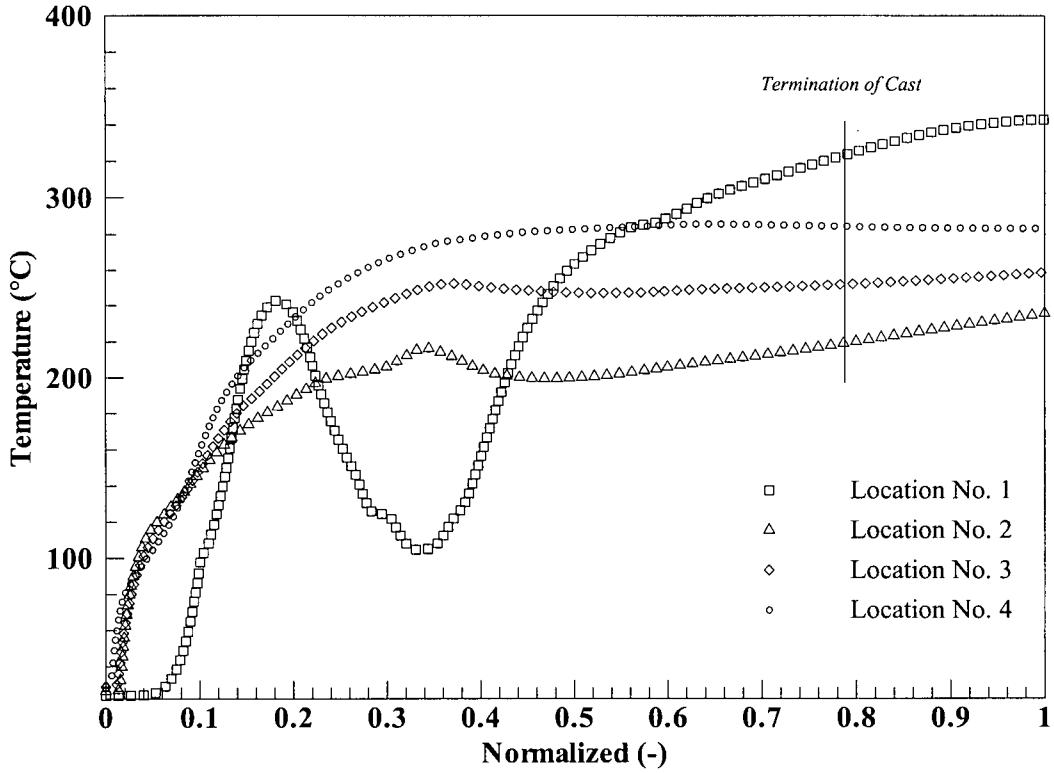

Figure 4.31 – Temperatures recorded by the thermocouple placed at Location Nos. 1, 2, 3, and 4 (refer to Figure 4.10) near the bottom block top face for the hot cast.

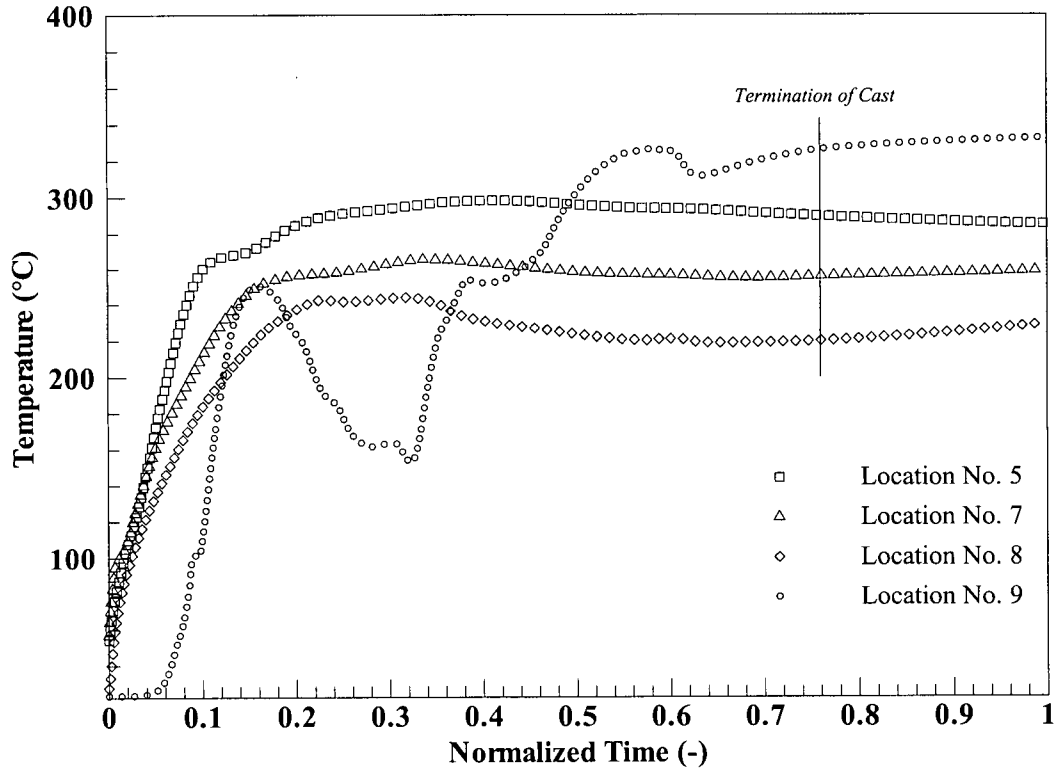

Figure 4.32 – Temperatures recorded by the thermocouple placed at Location Nos. 5, 7, 8, and 9 (refer to Figure 4.10) near the bottom block top face for the hot cast.

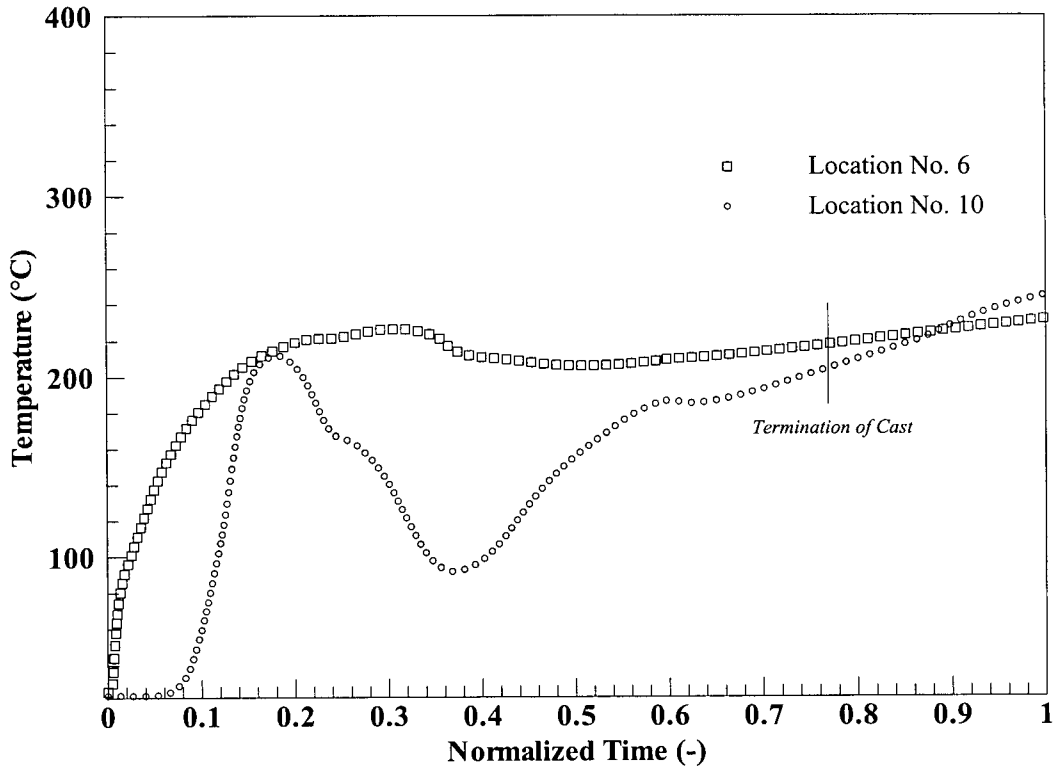

Figure 4.33 – Temperatures recorded by the thermocouple placed at Location Nos. 6, and 10 (refer to Figure 4.10) near the bottom block top face for the hot cast.

4.4 Butt Curl Measurements

Butt curl was measured near the centre of the narrow face for both the castings. A comparison of the evolution in the ingot base displacement for the two castings is shown in **Figure 4.34**. As can be seen, the colder casting resulted in a substantial increase in the base deflection in comparison to the hot casting. The distinctly different macroscopic deformations of the ingot base for the two cases can also be observed easily in **Figure 4.35**, which shows the two ingots cast during the industrial trial.

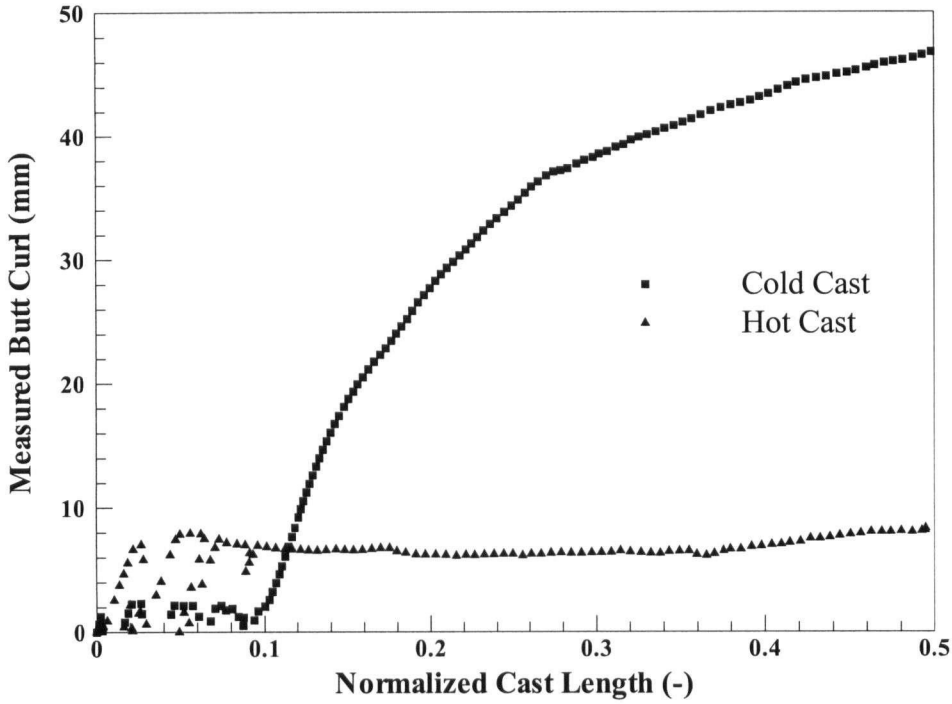

Figure 4.34 – Evolution of ingot base displacement (butt curl) at the centre of the narrow face for the two castings.

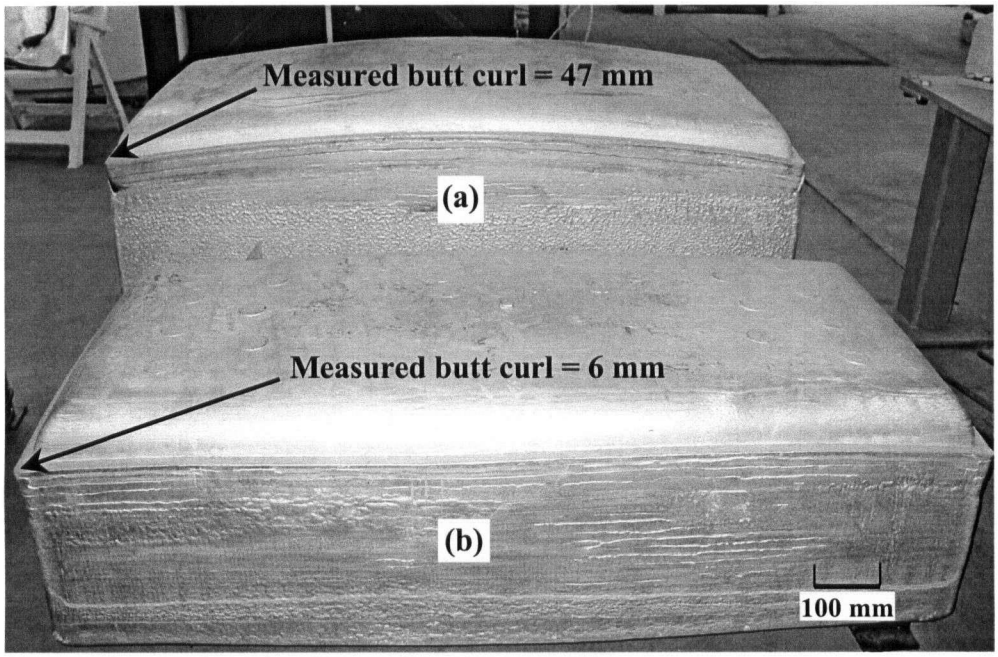

Figure 4.35 – Ingots produced during the casting trials for (a) cold cast, and (b) hot cast.

4.5 Summary

The trials conducted at Alcan's casting facility were a success. Two distinctly different casting recipes (cold and hot) produced ingots that displayed contrasting thermomechanical behaviour during the start-up phase. The thermocouples located on the ingot and bottom block were able to capture all the complicated heat transfer processes active during the first 350-500 mm of the D.C. casting process. The effects of water incursion between the ingot and bottom block, and water ejection along the ingot rolling and narrow faces were clearly observed in the cold and hot cast, respectively. Also, the butt curl values measured for the two castings represented two extremities in the mechanical deformation behavior of the ingot. Hence, the industrial experiments successfully provided a broad range of useful data for the model development and validation.

References

1. Hatch, J.E., *Aluminum: Properties and Physical Metallurgy*, First edition, 9th Reprint, 1999, American Society for Metals, Materials Park, Ohio, pp.373.
2. Arnberg, L., and Backerud, L., *Solidification Characteristics of Aluminum Alloys*, ed. S.P. Thomas, American Foundrymen's Society, Inc.
3. Clyne, T.W., and Davies, G.J., *The Influence of Composition on Solidification Cracking Susceptibility in Binary Alloy Systems,* The British Foundrymen, 1981, **74**, pp. 65-73.
4. Wiskel, J.B., *Thermal Analysis of the Startup Phase for D.C. Casting of an AA5182 Aluminum Ingot*, Ph. D. Thesis, Dept. of Metals and Materials Engineering, University of British Columbia, Vancouver, B.C., 1996.
5. Droste, W., and Schneider, W., *Laboratory Investigations about the Influence of Starting Conditions on Butt Curl and Swell of DC Cast Sheet Ingots,* Light Metals 1991 (Ed. E.L. Rooy), The Minerals, Metals & Materials Society, Warrendale, USA, 1991, pp. 945-951.
6. M-Hamdi, M., Mo, A., Mortensen, D., and Fjær, H. G., *Modeling of Air Gap Development and Associated Surface Macro-segregation in D.C. Casting of Aluminum Sheet Ingots,* Light Metals 2002 (Ed. W. Schneider), The Minerals, Metals & Materials Society, Warrendale, USA, 2002, pp. 695-701.

CHAPTER 5
MODEL DEVELOPMENT

5.1 Introduction

In line with the goals of the research, a mathematical model capable of solving the governing heat conduction equations was required in order to predict the temperature field in the ingot and bottom block during the start-up phase of the D.C. casting process. Based on the review of modeling activities to date, it is clear that the finite element (FE) method provides a convenient procedure to mathematically model the thermal behaviour of the ingot and bottom block during the cast start-up. The commercial FE software, ABAQUS was employed as a solution platform for this problem. ABAQUS was chosen because it provides highly developed nonlinear solution procedures and a well-documented method for extending the program's capabilities to integrate spatially and temporally changing heat transfer conditions in the thermal model via user written subroutines.

The thermal model employed in this study to predict the evolution of temperature in the ingot and bottom block solved the nonlinear heat transfer problem that resulted from the inclusion of temperature dependent material properties, evolution of latent heat, and application of thermal boundary conditions. The approach adopted in the present study was to incorporate the effects of butt curl and water incursion on the ingot base heat transfer based on the measured displacement data. This chapter provides an overview of the FE concepts relevant to the formulation of thermal models for the start-up phase of the D.C. casting process. A detailed description of the FE method will not be presented because these algorithms were not developed during the course of this programme.

5.2 Finite Element Formulation

Referring to **Figure 5.1**, the generalized concept of FE analysis is to obtain an approximate solution, $\hat{\phi}$, for a problem (represented by $A(\phi) = 0$) in the domain Ω, with boundary conditions (represented by $B(\phi) = 0$) on the boundary Γ, using a series of differential equations developed for sub domain regions Ω^e (or elements). These FE equations may be derived either from variational principles or by the Galerkin weighted residual method. Using

this approach, it is possible to solve a wide variety of engineering problems dealing with phenomena such as heat transfer. In heat transfer problems, the desired solution is usually the temperature throughout the domain, resulting from heat flux or prescribed temperature boundary conditions. The reader is referred to the text by Zienkiewicz and Taylor[1] for a complete explanation and discussion of the issues related to the finite element solution procedures.

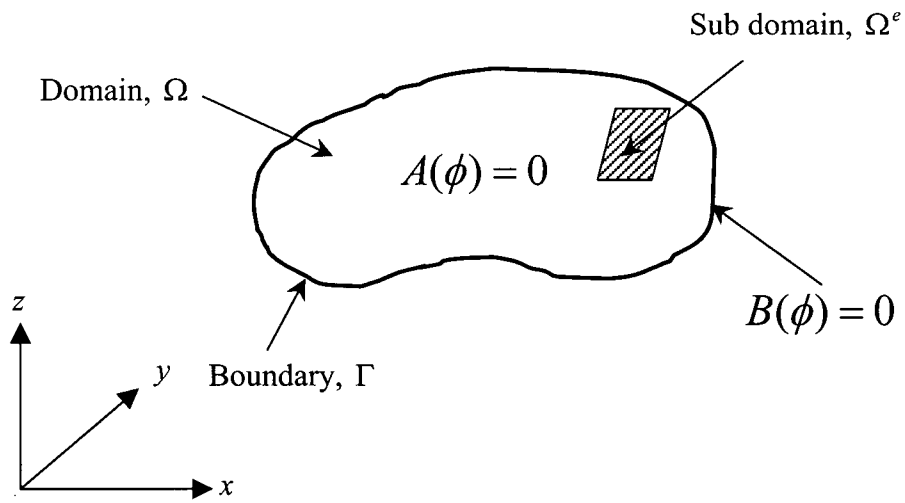

Figure 5.1 – Schematic of problem domains as they apply to FE method.[1]

5.2.1 Finite Element Interpolation

An essential component of the FE method are the interpolating functions used to approximate the exact solution $\phi(x,y,z)$, which satisfies the governing differential equation within the discretized domain Ω, by $\hat{\phi}(x,y,z)$. The approximate solution has the form:

$$\hat{\phi} = \sum_{i=1}^{n} N_i(x,y,z)\phi_i \tag{5.1}$$

where, N_i are the nodal interpolation functions defined in terms of the independent variables such as the spatial coordinates, n is the number of degrees of freedom, and ϕ_i are the unknown nodal solution values. These interpolation functions, which are also known as shape functions, may be linear or higher order polynomials, depending upon the number of degrees of freedom in the problem.

Interpolation functions are also used to map elements from arbitrary shapes in global coordinate space (x,y,z) to regular shapes in local coordinate space (ξ,ζ,η). **Figure 5.2** illustrates the elemental mapping for a few elements used in 3-D analyses. Elements are called isoparametric when the same shape functions are used for both the coordinate transformation and the solution function. In this study, 4-node quadrilateral and 8-node hexagonal isoparametric linear elements were employed for the 2-D and 3-D analyses, respectively.

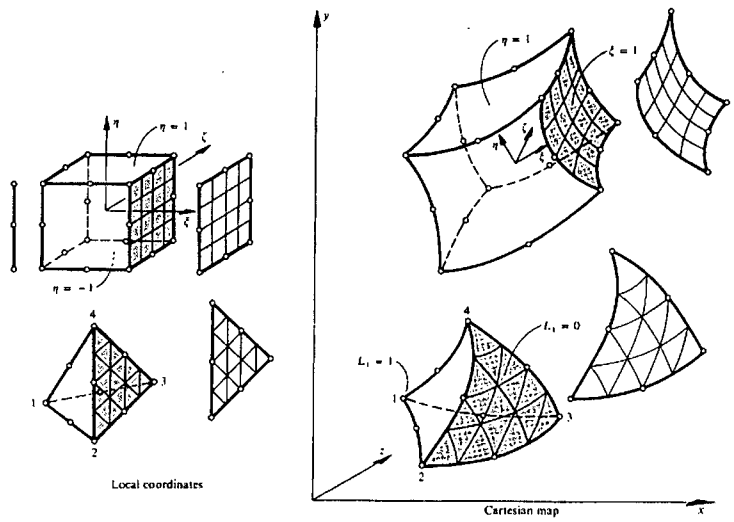

Figure 5.2 – 3-D mapping of different element types from the Cartesian (global) space (x,y,z) to a local coordinate system (ξ,ς,η). In particular, 8-noded isoparametric elements are always mapped to a unit cube in the local coordinate system.[1]

5.2.2 Numerical Integration

In order to assemble the matrix of elemental differential equations describing the global problem in domain Ω, numerical integration is required on an elemental basis. Of the techniques available for numerical integration, the Gauss quadrature method is particularly well suited to FE analysis because it requires the least number of function evaluations. In a 3-D domain, the Gauss quadrature integration of a function $f(\xi,\zeta,\eta)$ is described by the following expression:

$$\int_{-1}^{1}\int_{-1}^{1}\int_{-1}^{1} f(\xi,\zeta,\eta)d\xi d\zeta d\eta = \sum_{k=1}^{m}\sum_{j=1}^{m}\sum_{i=1}^{m} W_i W_j W_k f(\xi_i,\zeta_j,\eta_k) \tag{5.2}$$

where, W_i, W_j, *and* W_k are weighting coefficients at locations i, j, and k, respectively, ξ_i, ζ_j and η_k denote the Gauss integration points within an element, and m is the number of Gauss points in each direction. Employing this integration formulation, the 2-D quadrilateral elements and the 3-D hexagonal elements utilized in this study are defined with 2x2 and 2x2x2 integration points, respectively. The integration points provide one of the means by which spatially dependent variables can be addressed in FE models. For example, the heat transfer coefficient in a thermal problem, which can be a function of temperature and displacement, are calculated at the integration points.

5.2.3 Transient Response via Recurrence Relations

After the elemental differential equations have been assembled to describe the global problem in domain Ω, the procedure for determination of the transient response in the solution variable ϕ relies on deriving recursion formulas that relate the values of ϕ, and $\dot{\phi}$ at one instant of time, t, to the values of these quantities at a later time, $t+\Delta t$, where Δt is the time step for the analysis. The recursion formulas make it possible for the solution to be "marched out" in time, starting from the initial conditions at t=0 and continuing step by step until reaching the desired final time.

Most of the time marching algorithms are based on finite difference methods, and represent the first-order matrix equations by finite difference approximations at an intermediate time t_θ such that $t_\theta = t_n + \theta\Delta t$, where $0 \leq \theta \leq 1$, and t_n is a typical time in the response so that $t_{n+1} = t_n + \Delta t$. The following approximations can then be used:

$$\dot{\phi}_\theta = \frac{\phi_{n+1} - \phi_n}{\Delta t} \tag{5.3a}$$

$$\phi_\theta = (1-\theta)\phi_n + \theta\phi_{n+1} \tag{5.3b}$$

The global system of equations that incorporates these relationships, represent a general family of recurrence relations. The employment of a particular algorithm to compute the transient response depends on the value of θ selected. If $\theta = 0$, the algorithm is the forward difference method (or Euler method); if $\theta = ½$, the algorithm is the Crank-Nicolson method; and if $\theta = 1$, the algorithm is the backward difference method.

The family of algorithms, mentioned above, requires the solution of a set of simultaneous equations at each time step. A time marching algorithm that requires the repetitive solution of these equations at each time step is an implicit algorithm, and the computational effort for these transient solutions is considerably large. One method of reducing this computational effort is to employ an explicit algorithm, wherein the nodal unknowns at each time step are computed from uncoupled algebraic equations. However, this computational advantage is offset by the disadvantage that the time step selected must be less than a critical value for the response to be stable, and hence cannot be selected arbitrarily. The explicit algorithm is therefore well suited to solve high-speed dynamic problems that require many small increments to obtain a high-resolution solution (*e.g.* impact, blast and forming simulations). The implicit method is unconditionally stable and does not place an inherent limitation on the time increment size. The increment size is generally determined from accuracy and convergence considerations. Hence, this method is widely used for transient heat transfer and stress analyses.

5.2.4 Sources of Nonlinearity in FE Analysis

Most of the engineering problems usually encountered are nonlinear, *i.e.* the relationship between the applied loads and the response of the system is not constant. Sources of nonlinearity arise due to the changes in the material properties and boundary conditions during an analysis. In a thermal analysis, temperature dependence of the thermo-physical properties (heat capacity, thermal conductivity and density), evolution of latent heat, and spatial and temporal variation of the heat transfer processes (*e.g.* dependence of secondary cooling conditions on the ingot surface temperature during the D.C. casting process), and variation in thermal contact between two surfaces (*e.g.* the change in ingot base cooling conditions due to air gap formation between the ingot and bottom block due to butt curl) are major sources of nonlinearity.

5.2.5 ABAQUS Solution Method for Transient Nonlinear Problems

ABAQUS[2] is particularly well suited to solving heat transfer problems because its nonlinear solution capabilities are highly developed and robust. In a nonlinear analysis, an accurate solution cannot be calculated by solving the system of FE equations a single time, as would be done in a linear problem. Therefore, ABAQUS finds the approximate solution at the

end of each time increment. It often takes ABAQUS several iterations to determine an acceptable solution for a given time increment.

ABAQUS uses a modified Newton solution method to solve the nonlinear FE equations to obtain a convergent solution. The modified Newton method is an incremental solution algorithm that employs a series of piecewise approximation to approach a solution. An acceptable solution is obtained when the change in incremental solution becomes small relative to some tolerance.

Within a time increment, ABAQUS predicts a solution based on the material properties and loads (heat fluxes or forces) at the increment start. After updating the properties and loads based on the predicted solution, a second solution is calculated to check convergence. The convergence check ensures that the change in solution values and load levels are within their prescribed tolerances. If the convergence criteria have been satisfied, a new increment is started; otherwise another set of iterations is performed to find a solution based on the updated data. In extreme cases where a solution cannot be found within a reasonable number of iterations, the increment is started over with a reduced increment size. In highly nonlinear problems, ABAQUS may reduce the increment size repeatedly, thus requiring a lot of CPU time. Also, ABAQUS automatically increases the increment size if two consecutive increments quickly converge to the solution.

Since the modified Newton solution method relies on a series of incremental solutions, the resulting solution in a transient analysis will be sensitive to the time step. Thus, time step selection is an important issue and ABAQUS has addressed this through the implementation of an adaptive time step algorithm. When setting up the problem, the user supplies a maximum and minimum time step, as well as a tolerance for the maximum solution change within a time increment. Based on the solution change tolerance and the rates of convergence of the solution, ABAQUS adapts the time step to ensure solution accuracy while maintaining the largest acceptable time step.

5.3 Thermal Model

A transient heat conduction model was developed using ABAQUS to predict the temperature evolution in two AA5182 aluminum ingots cast with different non-standard start-up procedures. Thermal boundary conditions, which include the primary, secondary and ingot base

cooling effects during the cast start-up were formulated from knowledge of the D.C. casting process based on the literature review and industrial experiments. In the following sections, general issues related to the FE analysis of the heat transfer problem, and details outlining the development of the thermal model related to the start-up phase of the D.C. casting process will be presented.

5.3.1 FE Formulation of the Thermal Model in ABAQUS

Due to the time-dependent nature of the start-up phase of the D.C. casting process, the thermal model involves solving the transient heat transfer problem, which must account for a variation in temperature with time in the ingot and bottom block. In the thermal model, the governing partial differential equation[3] for a 3-D anisotropic domain Ω bounded by two surfaces Γ_1 and Γ_2 in the Cartesian coordinates (x,y,z), is shown in Equation 5.4:

$$\frac{\partial}{\partial x}\left(k_x(T)\frac{\partial T}{\partial x}\right)+\frac{\partial}{\partial y}\left(k_y(T)\frac{\partial T}{\partial y}\right)+\frac{\partial}{\partial z}\left(k_z(T)\frac{\partial T}{\partial z}\right)+\dot{Q}-\rho(T)c_p(T)\frac{\partial T}{\partial t}=0 \qquad (5.4)$$

with the initial condition:

$$T = T_o(x,y,z) \text{ in domain } \Omega, \text{ for time, } t = 0 \text{ s} \qquad (5.5)$$

and with the boundary conditions:

$$T = T^*(x,y,z,t) \text{ on surface } \Gamma_1, \text{ for } t > 0 \text{ s} \qquad (5.6)$$

and:

$$k_x(T)\frac{\partial T}{\partial x}n_x + k_y(T)\frac{\partial T}{\partial y}n_y + k_z(T)\frac{\partial T}{\partial z}n_z + q(x,y,z,t) + h(x,y,z,t)T = 0$$

$$\text{on surface } \Gamma_2, \text{ for } t > 0 \text{ s} \qquad (5.7)$$

where, $\dot{Q}$ ($Jm^{-3}s^{-1}$) is the internal heat generation rate per unit volume, $k(T)$ is the temperature dependent conductivity with the subscripts x, y, z representing its component in the three directions ($Wm^{-1}K^{-1}$), $\rho(T)$ is the temperature dependent density (kgm^{-3}), $c_p(T)$ is the temperature dependent specific heat ($Jkg^{-1}K^{-1}$) , T_o is the initial temperature, which may vary with position, n_x, n_y, and n_z are the direction cosines of the outward normal to the surface Γ_2, q is the specified heat flow rate per unit area (Neumann type boundary condition) (Wm^{-2}), h is a convective heat transfer coefficient (Cauchy type boundary condition) ($Wm^{-2}K^{-1}$) . Temperature dependent material properties and nonlinear boundary conditions signify that the problem is inherently nonlinear. To find the spatial and temporal distribution of temperature, $T(x,y,z,t)$, Equation (5.4)

can be solved by employing a finite element discretization of the spatial derivatives, as explained in the earlier sections. To derive the elemental equations from the energy equation, *i.e.* Equation 5.4, the Galerkin weighted residual method[1] is invoked, which requires

$$\int_{\Omega^e}\left[\frac{\partial}{\partial x}\left(k_x\frac{\partial T}{\partial x}\right)+\frac{\partial}{\partial y}\left(k_y\frac{\partial T}{\partial y}\right)+\frac{\partial}{\partial z}\left(k_z\frac{\partial T}{\partial z}\right)-\dot{Q}+\rho(T)C_p(T)\frac{\partial T}{\partial t}\right]N_i d\Omega=0 \tag{5.8}$$

After some manipulation, the resulting element equations become

$$\left[C^e\right]\left\{\frac{dT^e}{dt}\right\}+\left[\left[K_c^e\right]+\left[K_h^e\right]\right]\left\{T^e\right\}=\left\{R_Q^e\right\}+\left\{R_q^e\right\}+\left\{R_h^e\right\} \tag{5.9}$$

which is of the general form:

$$[C^e]\{\dot{T}\}+[K^e]\{T\}+\{R^e\}=0 \tag{5.10}$$

where, $[C^e]$ is the element capacitance matrix; $[K_c^e]$ and $[K_h^e]$ are the elemental conductance matrices and relate to conduction and convection, respectively; and, the vectors $\{R_Q^e\}$, $\{R_q^e\}$, and $\{R_h^e\}$, are heat load vectors arising from internal heat generation, specified surface heating and surface convection, respectively.

The transient response of the global nonlinear system of equations, which results from assembly of a system of element equations represented by Equation 5.10, is then calculated via step-by-step recurrence techniques. In the thermal model, temperatures are stored by ABAQUS at the nodal positions in a solution increment, and the temperatures are interpolated to the integration point locations before solving the elemental differential equations. Material properties that are temperature dependent are evaluated at these integration point locations based on the interpolated temperatures. Loads in the form of heat fluxes and prescribed temperatures are applied at specified positions within the model. The result of these calculations is a new set of temperatures at each node in the mesh. ABAQUS computes multiple temperature solutions in each time increment to ensure equilibrium equations are satisfied.

The first-order heat transfer elements provided by ABAQUS, such as the 4-node quadrilateral and 8-node brick elements used in this study, have a non-standard formulation. The integration points in these elements are located at the corners of the element rather than within the element as in standard formulations. This modification improves the performance of these elements when strong latent heat effects and nonlinear boundary conditions are present in a heat transfer problem. ABAQUS recommends that these first-order elements be employed for

problems involving latent heat evolution, and large thermal contact surfaces, such as the one between the ingot base and bottom block in this study.

ABAQUS uses the backward difference implicit algorithm for solving heat transfer problems because of the simplicity in its implementation and well-understood behaviour. The algorithm is unconditionally stable, and can be used over very long time periods. Although the Crank-Nicolson method has the highest accuracy, this method is not used by ABAQUS to avoid oscillations, which are generally observed in the early time solution.

5.3.2 Latent Heat Evolution

The evolution of latent heat, which is released upon solidification of molten aluminum, is a major source of nonlinearity in a heat transfer analysis. Hence, correct treatment of latent heat is necessary during the development of a thermal model in order to avoid computational instabilities. ABAQUS[2] provides two different methods of incorporating latent heat release in thermal models:

- The enhanced specific heat method, which involves modifying the $c_p(T)$ term in Equation 5.4 over a range of temperatures from a lower (solidus) temperature to an upper (liquidus) temperature. This is applicable to those problems wherein it is reasonable to assume that one or several phase changes occur within known temperature ranges during the solidification process, regardless of the local cooling conditions.
- The volumetric heat release method, which treats the latent heat as an internal heat source i.e. the $\dot{Q}$ term in Equation 5.4. This method is generally used to couple the heat released to a phase transformation kinetics relationship.

The general trend in the thermal models outlined in literature is to assume that the evolution of volume fraction of solid, f_s is linear between the liquidus, T_L, and solidus, T_S temperatures for aluminum alloys. Under this condition, the enhanced specific heat method can be applied to incorporate the latent heat, L (Jkg^{-1}) in the model by modifying the temperature dependent specific heat, c_p using the following relationship:

$$c_p(T) = c_p(T) + \frac{L}{(T_L - T_S)} \quad \text{for } T_L < \mathrm{T} < T_S \tag{5.11}$$

This assumption is in contrast to the measurements made by Aliravci and Pekgüleryüz[4], which revealed that most of the latent heat is released near the liquidus during the solidification of

several aluminum alloys. However, Drezet and Rappaz[5] confirmed that this assumption had no influence on the final stress-strain results predicted by their analysis; rather the early latent heat release resulted in a faster convergence of computations. A similar approach was thus adopted for the present study, and AA5182 was assumed to solidify linearly between 637 °C (T_L) and 536 °C (T_S)[6] and the latent heat released between these temperatures is 397.1 kJkg^{-1}[7].

5.3.3 Temperature Dependent Thermo-physical Properties

The ingot and bottom block experience a large temperature range during the start-up phase of the D.C. casting process. This necessitates the use of temperature dependent thermo-physical properties for the ingot and bottom block materials. In addition to the effect of latent heat evolution, this temperature dependence further adds to the overall nonlinearity of the thermal problem. The material of the bottom block, used for the industrial trials, was an AA6xxx aluminum alloy. However, in the thermal model, it was assumed to be the same material as the ingot, *i.e.* AA5182, due to the absence of published thermomechanical data for AA6xxx. ABAQUS allows the user to define a table of material properties, incorporating the temperature dependence. ABAQUS linearly interpolates between the tabular material property data when updating the material properties at an integration point.

Wiskel[7] compiled the thermo-physical properties for AA5182 from available literature, which are presented in **Table 5.1**, and were used as input to the thermal model. The density was not changed during the analysis to avoid altering the mass since the volume of the computational domain will not vary with time for the thermal analysis. Although fluid flow was not considered in the model, the conductivity values above the liquidus were increased artificially (up to ~4x) to take into account heat transport due to liquid convection in the liquid sump[5].

With reference to Equation 5.10, the incorporation of the influence of latent heat release and the effect of temperature on the thermo-physical properties for AA5182, allow the computation of $[C^e]$ and $[K^e]$ matrices at every material integration point in the thermal model. The thermal load vector $\{R^e\}$ is the only other quantity in the equation that remains to be determined in order to solve the transient heat transfer problem. The formulation of the boundary conditions for calculating the thermal loads is presented in the later sections.

Table 5.1 – Thermo-physical properties of AA5182 aluminum alloy used in the thermal model for the ingot and bottom block.[7]

T (°C)	k ($Wm^{-1}K^{-1}$)	T (°C)	c_p ($J\ kg^{-1}$)	ρ ($kg\ m^{-3}$)
50	122.32	27	909.2	2400
100	125.43	127	950.4	
250	134.78	227	999.6	
500	150.35	327	1044.8	
536	152.59	427	1090.0	
550	153.47	527	1135.2	
577	154.93	627	1112.1	
600	130.80	727	1097.0	
632	96.39			
637	200.00			
660	400.00			

5.3.4 Calculation Domain Geometry and FE Mesh

The calculation domain for the thermal analysis included the ingot and bottom block, which were used for the industrial trials, as shown in **Figure 4.1**. The basic features of the ingot and bottom block geometries were incorporated into the calculation domain. These features include the ingot lip, and a bowl-shaped bottom block, which has a finite depth and thickness, and a fillet radius at the corners.

As part of a step-wise model development approach, with each stage providing an increase in complexity of the model and its boundary conditions, a quick-to-run 2-D thermal model was initially developed. This 2-D model analyzed the heat transfer in a plane normal to the rolling face of the ingot, and was utilized to implement and adjust the thermal boundary conditions in order to bring the model predictions closer to measured thermal data. The calculation domain used for the model was a 2-D slice taken perpendicular to the rolling face at the centre of the face (Section *A-A* along the symmetry face *x-z* indicated in **Figure 5.3**). This domain allowed the model to capture all the complex phenomena related to primary and

secondary cooling on the vertical face, and base cooling on the ingot. Due to the inherent symmetry in heat transfer, only a half-section of the 2-D slice was modeled for both the ingot and bottom block. The FE mesh for the 2-D model comprised of 4-noded isoparametric elements, which utilized 4 gauss integration points, located at the element nodes. The size of the elements used for both the ingot and bottom block was approximately 8 mm (width) x 4 mm (height). The 2-D FE mesh for the ingot and bottom block is shown in **Figure 5.4**.

Once the preliminary 2-D thermal analysis was successfully completed, and a level of confidence was gained in implementing the boundary conditions describing the heat transfer processes active during the start-up phase of the D.C. casting process, the thermal analysis was extended to a 3-D formulation. Taking advantage of the symmetry in heat transfer perpendicular to the rolling and narrow faces during the casting process, the calculation domain employed in the 3-D analysis was reduced to a quarter section of the ingot and the bottom block, as indicated by the shaded section in **Figure 5.3**. This ¼ section bisected the rolling and narrow faces of the ingot vertically. The FE mesh for the 3-D model, presented in **Figure 5.5**, consisted of 8-noded isoparametric brick elements, each with 8 gauss integration points. To increase the stability and efficiency of the FE solution, a graduated meshing technique was used to generate nodes and elements along the rolling and narrow face directions. The elemental length used for generating the FE mesh for the ingot along the vertical direction was fixed at ~4 mm. The width of the coarser elements near the centre of the ingot was ~12.5 mm, whereas the width of the finer elements near the corner was ~5 mm. The graduated meshing technique was also used to generate elements in the vertical direction for the bottom block in order to reduce the computational size of the problem. The elemental length near the top surface was ~4 mm, as compared to a length of ~12.5 mm near the bottom surface. **Table 5.2** summarizes the details of the FE meshes used for the 2-D and 3-D thermal analyses.

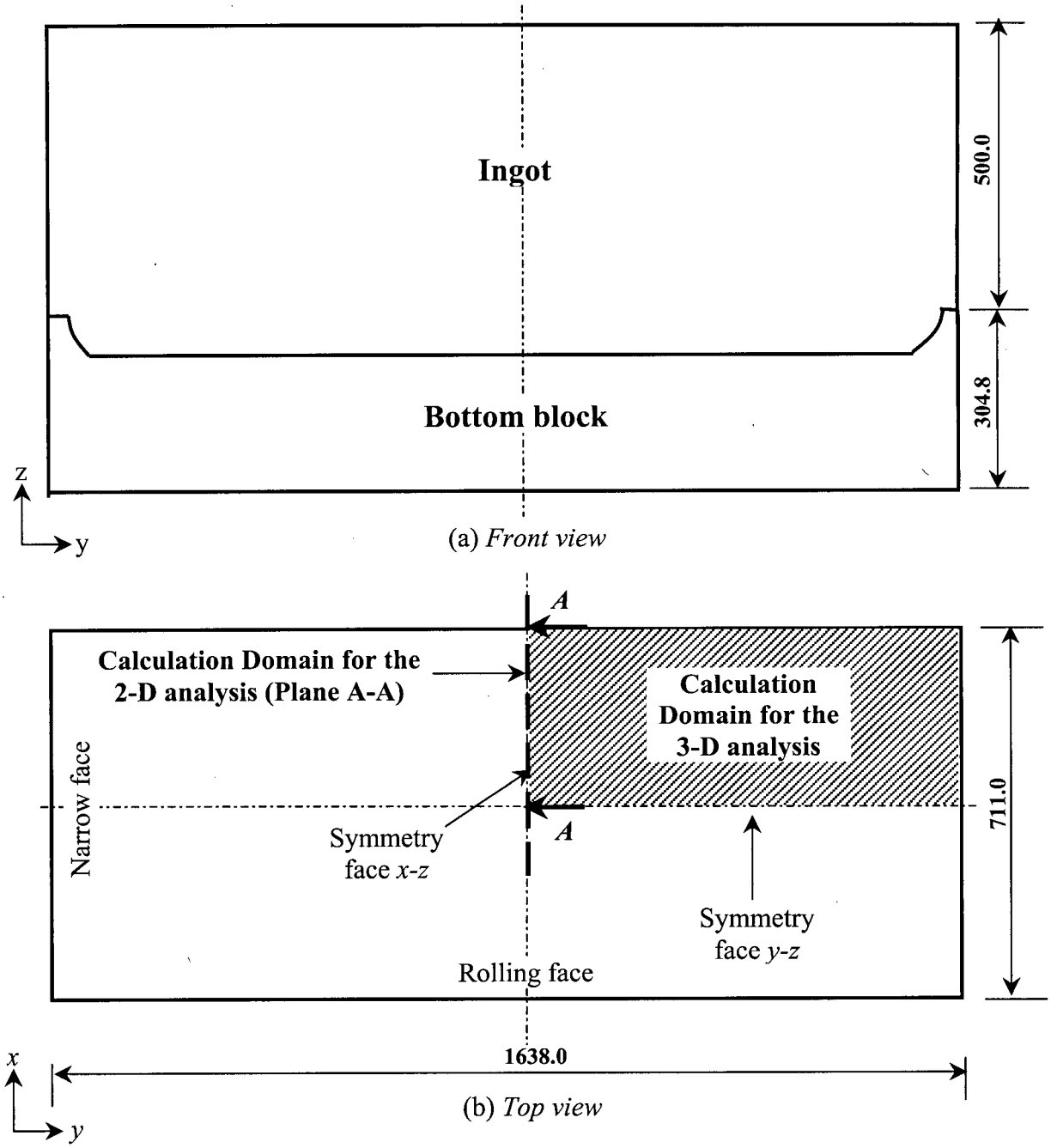

Figure 5.3 – Calculation domain for the 2-D and 3-D thermal analyses.

Note: Units are in mm.

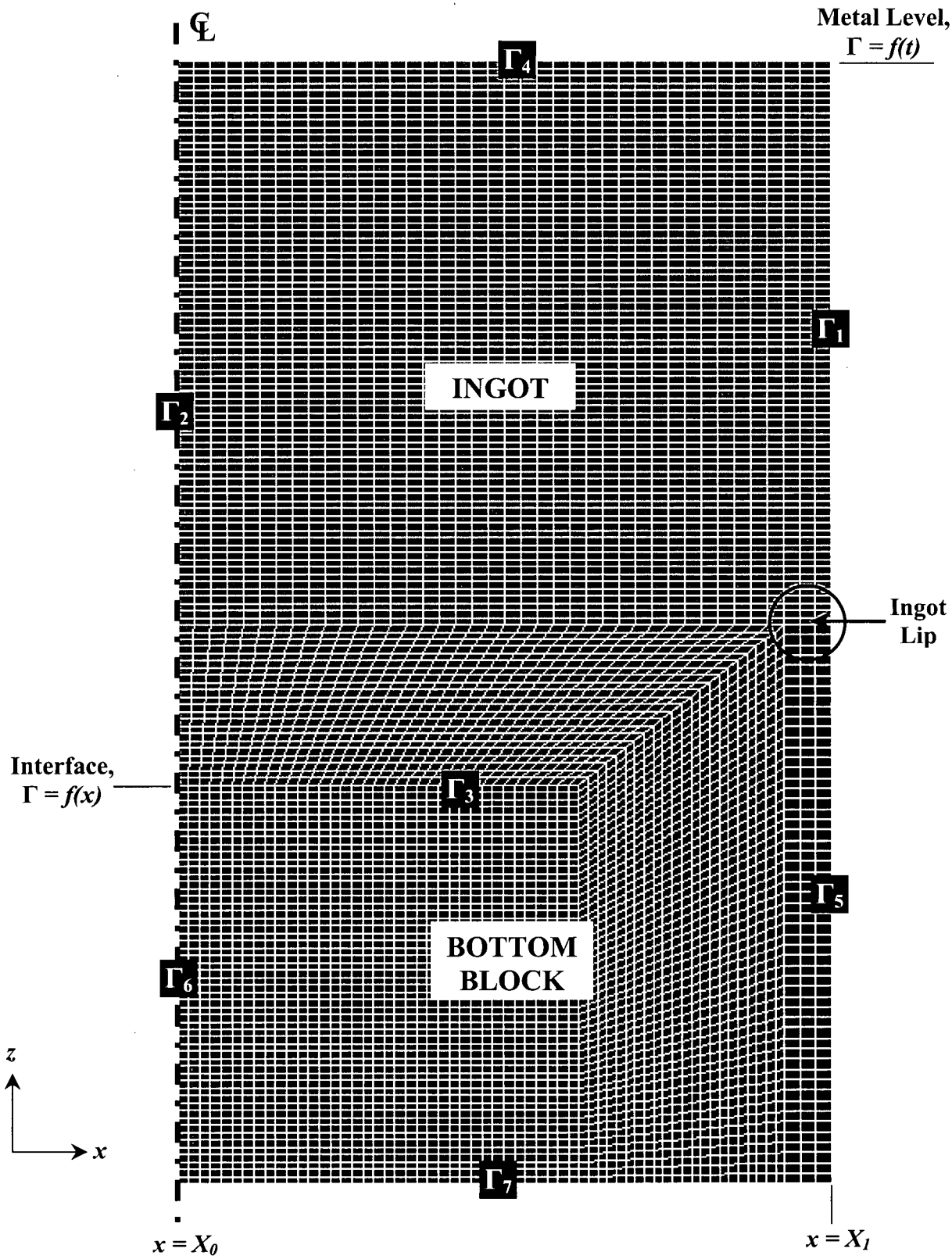

Figure 5.4 – The 2-D FE mesh for the ingot and bottom block. The various faces in the domain, on which thermal boundary conditions were applied, have also been indicated.

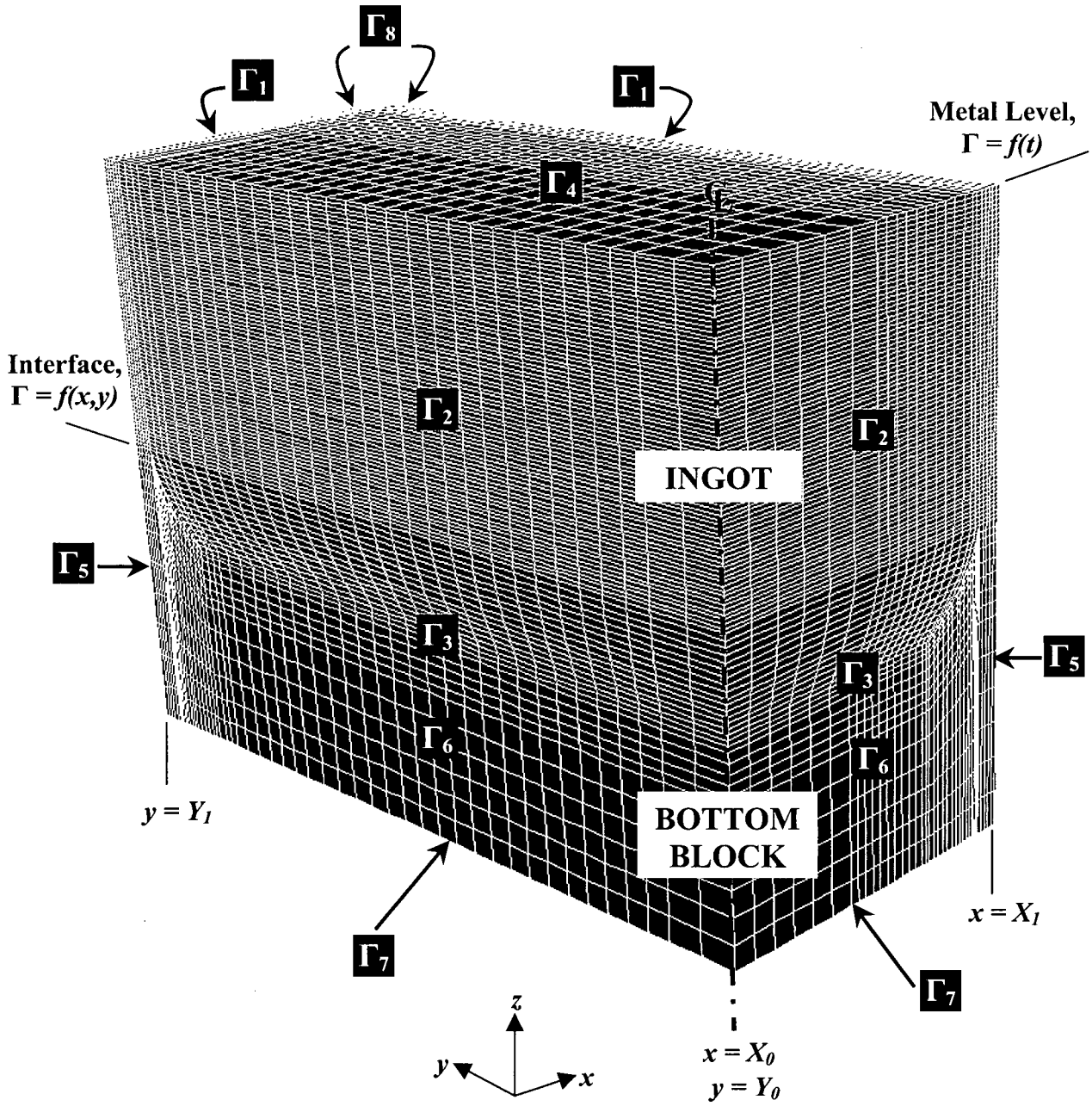

Figure 5.5 – The 3-D FE mesh for the ingot and bottom block. The various faces in the domain, on which thermal boundary conditions were applied, have also been indicated.

Table 5.2 - Summary of details for the FE meshes used in the 2-D and 3-D thermal analyses.

	2-D Model		3-D Model	
Domain	No. of Nodes	No. of Elements	No. of Nodes	No. of Elements
Ingot	5,242	4,934	83,752	70,470
Bottom block	3,575	3,348	28,785	21,882
Total	8,817	8,282	112,537	92,352

The use of linear temperature elements for both the 2-D and 3-D models required a high mesh density along the vertical z direction to ensure proper accounting of the non-linear and transient boundary conditions along the rolling and narrow faces of the ingot. The upper bound of the resolution was limited by the thickness of the water impingement zone, which was assumed to be ~10 mm. The lower bound of the vertical resolution was limited by computational time and cost. A 2-D sensitivity analysis revealed that the model predicted temperatures were not sensitive to any decrease in the vertical resolution below 10 mm. However, a vertical resolution of 4 mm was chosen so as to include at least 3 integration points within the water impingement zone at any time during the analysis, to effectively incorporate the impingement cooling effect in the models, albeit at the cost of computation time.

The mesh corresponding to the ingot and bottom block was generated with coincident nodes at the contact region between the ingot base and the bottom block top surface to form a thermal interface. This formulation provides flexibility for defining spatially and temporally varying interfacial boundary conditions, which control the thermal interaction between the ingot and bottom block during the casting process.

To facilitate the implementation of the complicated start-up procedures in the FE analysis, the ingot mesh for the both the 2-D and 3-D models was developed such that it consisted of horizontal layers of elements, as can be seen in **Figures 5.4** and **5.5**. Using this methodology, the gradual evolution of the metal level in the mould as well as the application of the boundary conditions at correct times could be achieved during the analysis. The methodology used for simulating the continuous formation of the ingot (or the evolution of cast length with time), illustrated by **Figure 5.6**, was to incrementally add these horizontal layers of elements to

the calculation domain as the analysis moved forward in time. These layers were added at certain time intervals, which were consistent with the start-up procedure. The time for addition of each layer was determined by calculating the time interval (or thermal load step) required for each layer addition in the model based on the mould filling times and casting speeds shown in **Figures 4.3** and **4.4**.

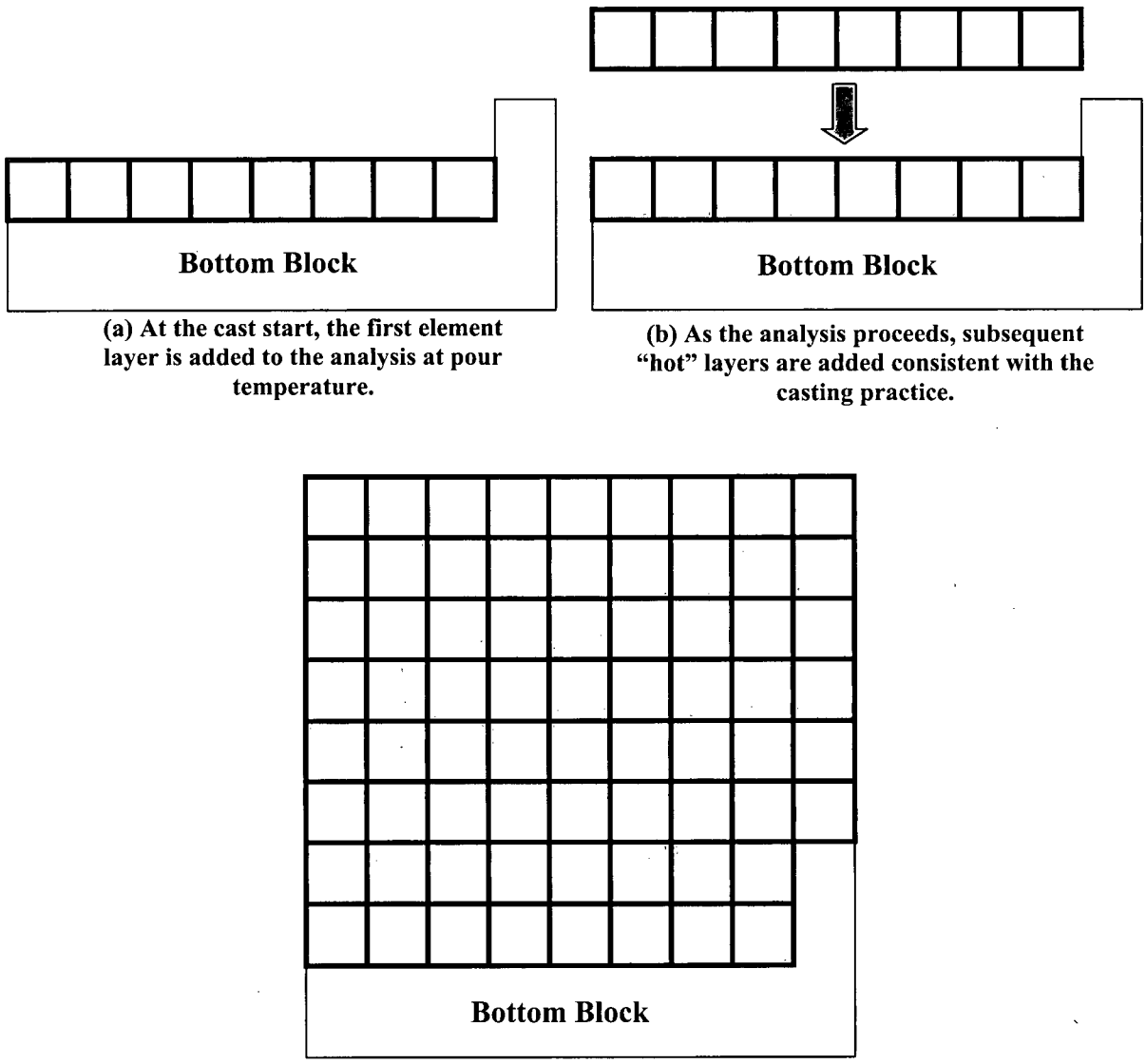

(a) At the cast start, the first element layer is added to the analysis at pour temperature.

(b) As the analysis proceeds, subsequent "hot" layers are added consistent with the casting practice.

(c) The analysis is completed after all the layers in the model have been added.

Figure 5.6 - Schematic representation of the casting simulation sequences (a) through (c), illustrating the process of incremental addition of elements to the calculation domain.

5.3.5 Thermal Boundary Conditions

Description

Ingot - Referring to **Figures 5.4** and **5.5**, the external rolling and narrow faces of the ingot (surface, Γ_1) extending above the bottom block lip was treated using a Cauchy-type boundary condition according to Equation 5.12:

$$-k\left.\frac{\partial T}{\partial n}\right|_{x=X_1,y=Y_1} = h(T_{Surf} - T_{Sink}) \tag{5.12}$$

where, k is the thermal conductivity ($Wm^{-1}K^{-1}$), $\frac{\partial}{\partial n}$ is the outward pointing derivative normal to the ingot surface, h is the effective heat transfer coefficient ($Wm^{-2}K^{-1}$), T_{Surf} is the ingot surface temperature, T_{sink} is the far field or sink temperature, X_1 is half the thickness of the ingot (= 355.5 mm), and Y_1 is half the width of the ingot (= 819 mm). The process for evaluating the appropriate heat transfer coefficient, h, is described in detail in the subsequent section on implementation.

Owing to symmetry, the interior vertical faces (surface, Γ_2) were assumed to be adiabatic according to Equation 5.13:

$$-k\left.\frac{\partial T}{\partial n}\right|_{x=X_0,y=Y_0} = 0 \tag{5.13}$$

The base of the ingot in contact with the bottom block (interface, Γ_3) was treated with a combination of a Cauchy-type boundary condition to describe interface gap conductance and a Cauchy-type boundary condition to describe heat transfer to water, present due to the process of water incursion described earlier. The expression employed in the model is given below in Equation 5.14:

$$-k\left.\frac{\partial T}{\partial n}\right|_{\Gamma=f(x,y)} = f_{wet}h_{water}(T_{Ingot} - T_{water}) + h_{gap}(T_{Ingot} - T_{Bottom\ Block}) \tag{5.14}$$

where h_{water} represents the heat transfer coefficient to any water that may or may not be present ($Wm^{-2}K^{-1}$) and h_{gap} represents the gap conductance at the interface ($Wm^{-2}K^{-1}$). The variable $T_{Bottom\ Block}$ appearing in the second term on the left hand side of Equation (5.14) represents the temperature in the bottom block directly adjacent to the point on the ingot base being processed. The term f_{wet} represents a factor used to account for the degree to which the ingot bottom surface is wetted by the incursion water.

The top of the ingot (surface, Γ_4) was assumed to be adiabatic according to Equation 5.15:

$$-k\frac{\partial T}{\partial n}\bigg|_{\Gamma=f(t)} = 0 \tag{5.15}$$

Bottom Block – Referring to **Figures 5.4** and **5.5**, the external rolling and narrow faces of the bottom block (surface, Γ_5) were treated with a Cauchy-type condition of form shown in Equation 5.12 with the term T_{surf} now set equal to the bottom block temperature. The interior vertical faces (surface, Γ_6) were assumed to be adiabatic due to symmetry and were treated with an expression of the form shown in Equation 5.13. Heat transfer from the top face of the bottom block (interface, Γ_3), which is initially in contact with the ingot, was accounted for using an expression similar to that appearing in Equation 5.14. However, in the 1st term on the right side, the variable T_{ingot}, is replaced with $T_{bottom\ block}$ and in the 2nd term on the right hand side, the variables T_{ingot} and $T_{bottom\ block}$ have been interchanged – i.e. to reflect that the ingot is now the far field or sink temperature. Heat transfer from the bottom face of the bottom block (surface, Γ_7) was treated with an expression of the form shown in Equation 5.12.

Implementation

For the vertical rolling and narrow faces of the ingot (surface, Γ_1), the magnitude of the heat transfer coefficient appearing in Equation 5.12 was adjusted to describe the various heat transfer regimes shown schematically in **Figure 5.7**. The calculation was implemented within ABAQUS using the *sfilm.f* † subroutine. Three regions of heat transfer were defined based on position relative to the top of the thermal analysis domain. They are:

Mould cooling: - Referring to **Figure 5.7**, this was applied to those regions of the calculation domain located above the base of the mould, at time *t*. In this regime, the heat transfer coefficient is assumed to vary with fraction solidified (temperature) according to Equation 5.16:

$$h = h_{contact}(1 - f_s) + h_{air\ gap}(f_s) \tag{5.16}$$

† *sfilm.f* is a user subroutine provided by ABAQUS, which can be accessed by a user to implement non-linear Cauchy-type heat transfer coefficients on different surfaces within the FE model.

where, $h_{contact}$ was in the range of 1000 to 2000[8] $Wm^{-2}K^{-1}$ and was intended to reflect good thermal contact, $h_{air\ gap}$ was in the range of 50 to 200[8] $Wm^{-2}K^{-1}$ to reflect poor thermal contact associated with air gap formation inside the mould, and f_s is the volume fraction of solid, which was assumed to be linear between the liquidus, T_L, and solidus, T_S temperatures for the AA5182 aluminum alloy.

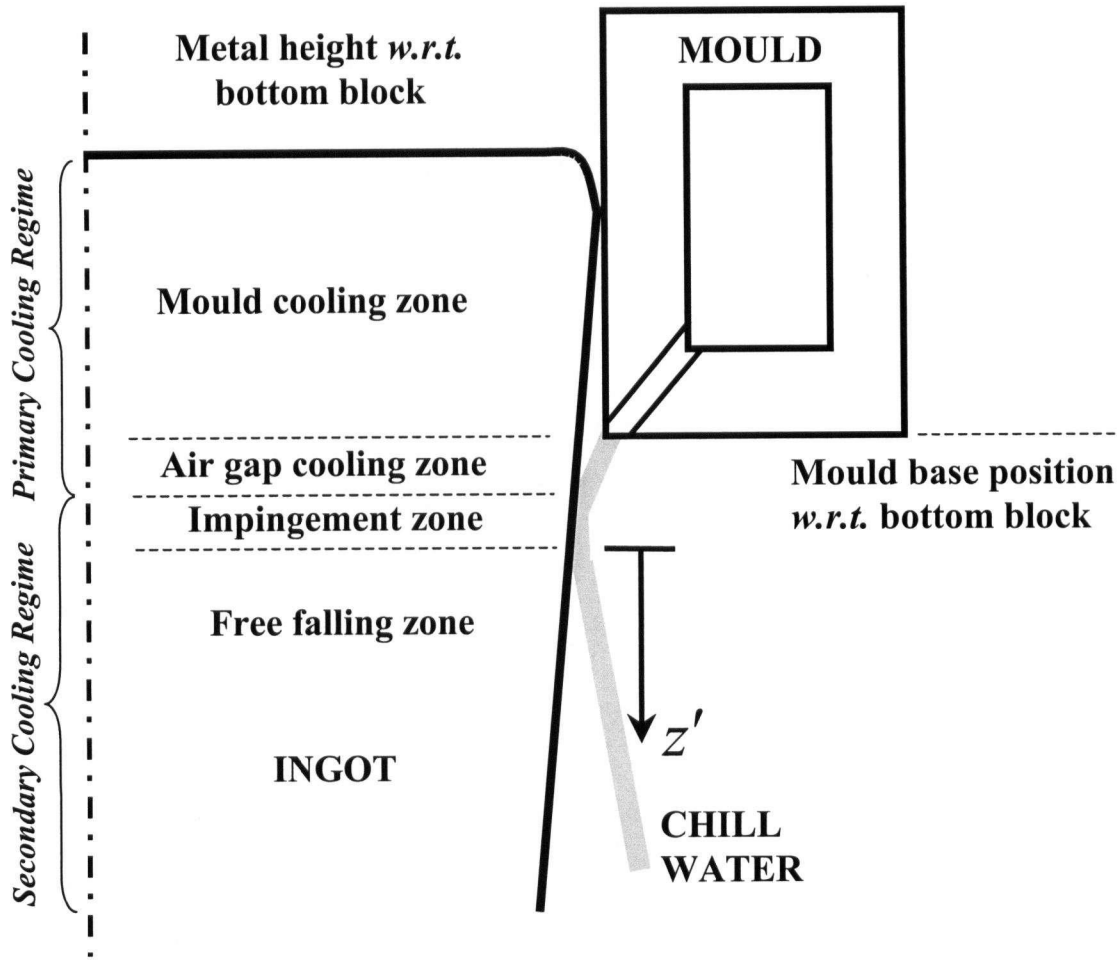

Figure 5.7 - Primary and secondary cooling regimes on the vertical face of the ingot.

Air gap cooling: - Referring to **Figure 5.7**, this was applied to those regions of the calculation domain located below the base of the mould and above the water impingement zone, at time t. In this regime, the heat transfer coefficient was assumed to be constant at, h = 50 to 200 $Wm^{-2}K^{-1}$.

Secondary cooling†: - Referring to **Figure 5.7**, this condition was applied to the portion of the calculation domain located below the air gap, at time t. In this regime, the heat transfer coefficient is a function of the ingot surface temperature, temperature at water impingement point, water flow rate (Q), and vertical distance below the impingement point (z'). Correlations developed by Alcan to account for these various dependencies were implemented in *sfilm.f* within ABAQUS. Example boiling curves are presented in **Figure 5.8** for a low water flow rate at $z' = 0$ mm and for a high water flow rate at $z' = 0$ and 50 mm, for the case where the impingement point temperature is 575 °C. The peak heat transfer coefficient in the figure lies between 50 to 100 $kWm^{-2}K^{-1}$. The effect of impingement point temperature on the boiling curve was added to the correlations obtained from Alcan, which is illustrated in **Figure 5.9**. The figure shows boiling curves for impingement point temperatures of 575 and 485 °C (Q and z' held constant). During transient behaviour in the start-up regime, the ingot surface temperature at the impingement point varies with time, and hence, each point on the surface of the casting was assigned its own unique boiling curve dependent on the impingement point temperature experienced by that point on the ingot surface.

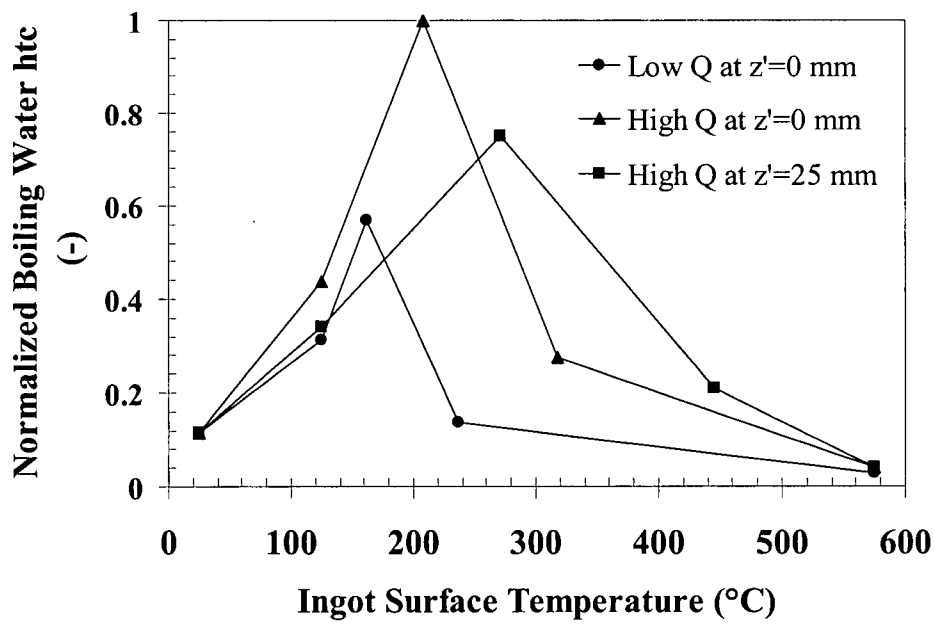

Figure 5.8 – Normalized boiling curves for different values of Q and z', which have been used to describe the secondary cooling process in the model.

† Secondary cooling was not applied at regions adjacent to the corner of the ingot, represented by surface, Γ_8 in **Figure 5.5**, due to the absence of water holes in the mould at this location. For this surface, the secondary cooling was replaced by $h = \sim 200\ Wm^{-2}K^{-1}$.

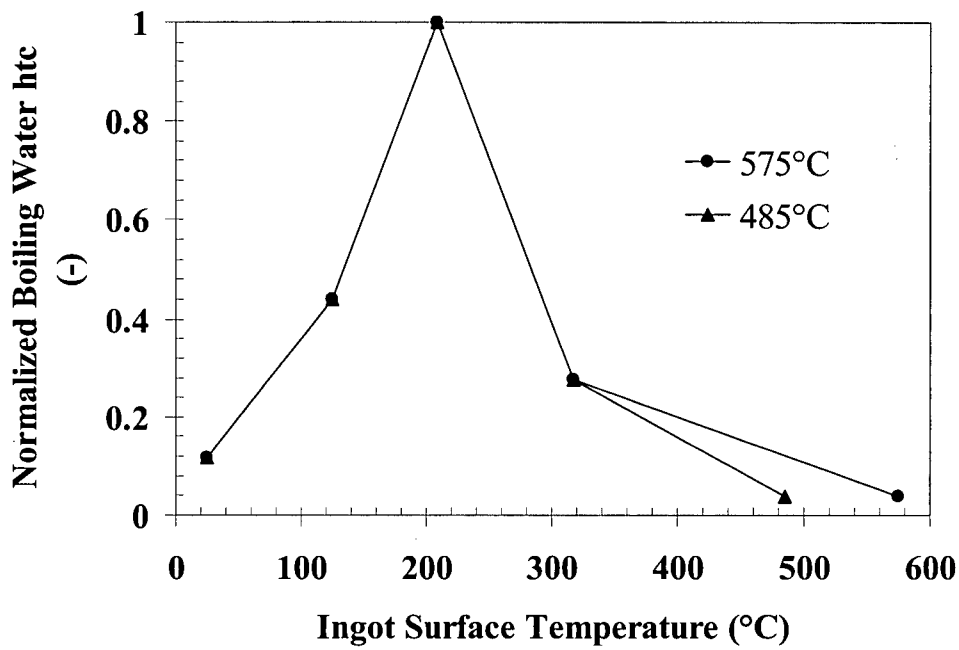

Figure 5.9 - Boiling curves for impingement point temperatures of 575 and 485°C (Q and z' held constant).

A provision for ejecting the water film from the ingot vertical edges due to film boiling was implemented in the subroutine for the domain just below the impingement zone, which is commonly referred to as the free falling zone (shown in **Figure 5.7**). For this purpose, the vertical ingot surfaces were divided into several streams, represented by columns of material integration points. For any stream, represented by a counter, i, the location of any integration point was referred to as stream position, represented by another counter, j. Hence, any material integration point on the surface, Γ_1, could be referenced by the array $[i, j]$, in terms of discrete streams of water flowing down the vertical surfaces of ingot in the free falling zone. This formulation for the 3-D analysis is schematically illustrated in **Figure 5.10**. The 2-D case is a trivial form of the 3-D formulation, wherein $i = 1$.

The algorithm used in the model to simulate the ejection of water from the ingot surface in the free falling zone is presented schematically in **Figure 5.11** (left hand side water ejection, right hand side no water ejection). In *sfilm.f*, the temperature at every stream position (as determined at the material integration points for every element on the vertical ingot surface) was compared with the Leidenfrost temperature (*i.e.* the temperature on the boiling water cooling

curve above which the film boiling process is predominant) at the beginning of every time increment. If at a certain stream position, the temperature exceeded the Leidenfrost temperature, all the stream positions below it were assigned a lower heat transfer coefficient of approximately 200[8] $Wm^{-2}K^{-1}$, to simulate reduced heat transfer associated with the ejection of water. All the stream positions above it were cooled as per the boiling curve described above.

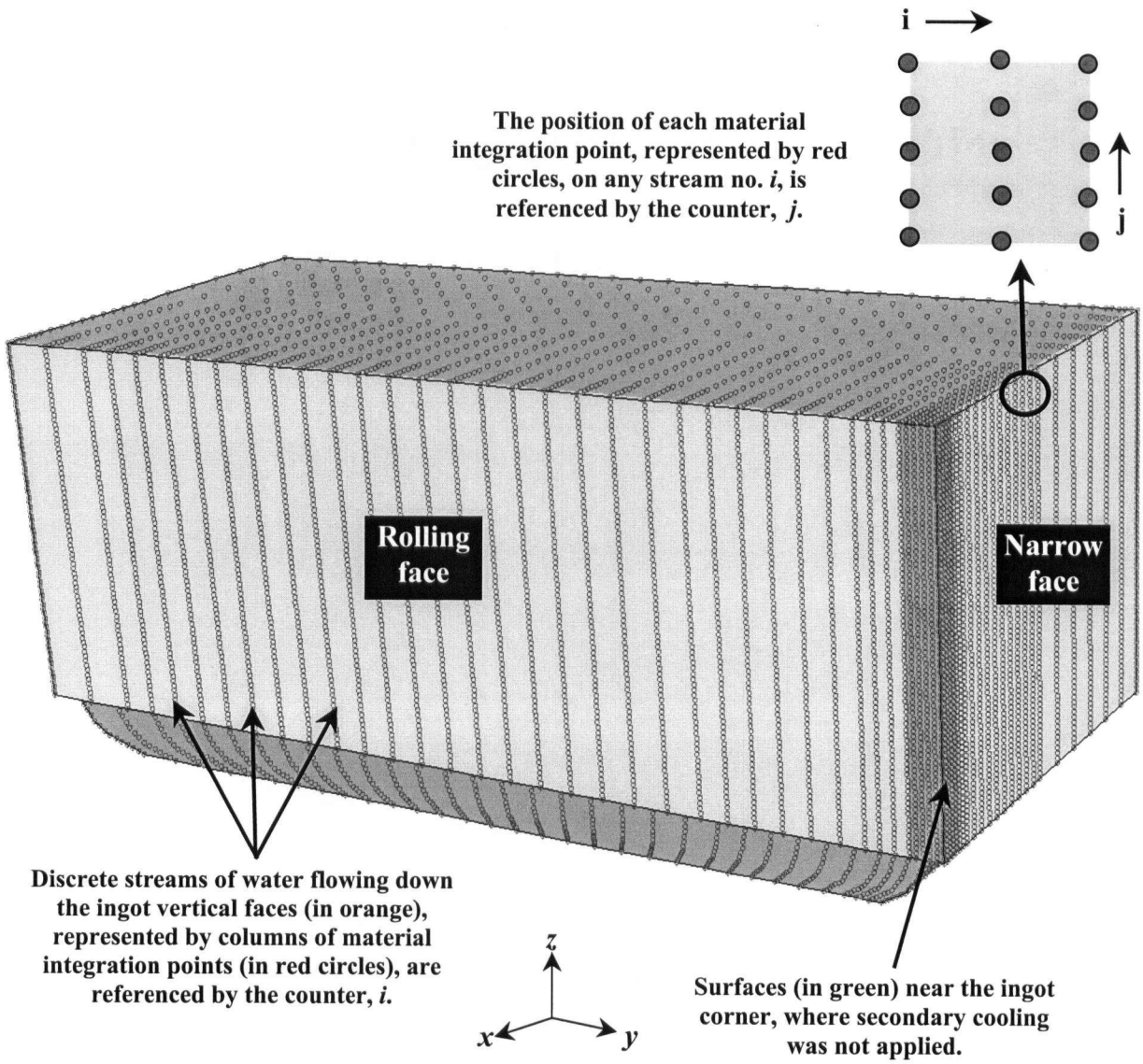

Figure 5.10 – Schematic representation of discrete water streams flowing down the ingot vertical surfaces (in light gray) in the 3-D FE thermal model, the formulation of which was required to implement the process of water ejection in the free falling zone. The surfaces shown in red (*e.g.* near the corner) are not included in the formulation.

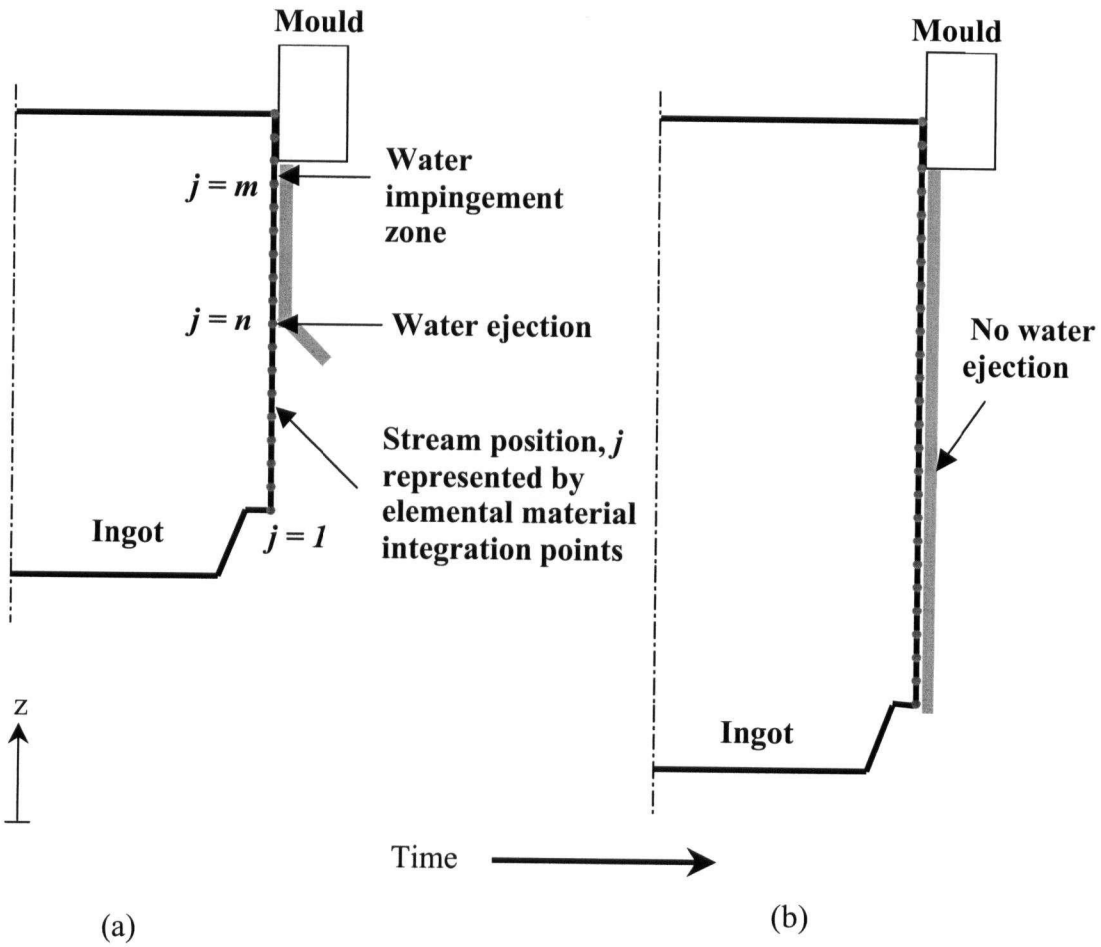

Figure 5.11 - Schematic illustration of (a) water ejection at stream location $j = n$ and (b) no water ejection, for any stream no. i.

For the vertical exterior face of the bottom block (surface, Γ_5), the heat transfer coefficient applied in Equation 5.12, was identical to that used for the ingot vertical face subject to secondary (water) cooling – the reader is referred to previous description and to **Figures 5.8** and **5.9**. Finally, for the bottom face of the bottom block (surface, Γ_7) the heat transfer coefficient appearing in Equation 5.12 was set equal to 25 $Wm^{-2}K^{-1}$ to reflect natural convection to air.

For the boundary condition at the ingot-bottom block contact surface (interface, Γ_3), Equation 5.14, both the gap conductance term, h_{gap}, and heat transfer coefficient to water term, h_{water}, were ramped linearly with vertical displacement (butt curl). In the model, h_{gap} was ramped

from 750 to 50 $Wm^{-2}K^{-1}$ within the subroutine *gapcon.f* † in ABAQUS. The term h_{water} was ramped from 0 to a value corresponding to the boiling curve applicable at the local temperature within the subroutine *sfilm.f* (Q as per cast practice, $z' = 70$ mm, impingement temperature = 600°C, $f_{wet} = 0.25$ for ingot & 0.5 for bottom block). In this manner, the loss in contact heat transfer due to increasing gap formation (butt curl) was offset by the increase in heat transfer due to water incursion. The gap conductance term, h_{gap} was always active at any time, t on interface, Γ_3 during the analysis. However, the water term, h_{water}, representing the process of water incursion was applied to only a portion of the interface, Γ_3 for both the ingot and bottom block, indicated by the regions in light gray and dark gray, respectively, in **Figures 5.12(a)** and **(b)**. Referring to these figures, the water term was active only on the vertical edges of the ingot base below the lip. It was assumed that water would enter the gap and flow along these edges, and then, drip over to the bottom block, due to gravity. It was also assumed that water entering the bottom block through the air gap from narrow faces of the ingot would only "wet" the top face of the bottom block up to the point where all the water was removed by the drainage holes (*i.e.* Y_3 = ~500 mm), as indicated in **Figure 5.12(b)**. For the water entering the bottom block from the rolling faces of the ingot, the wetted region was assumed to be limited to X_3 = ~250 mm, in order to match the model predicted results with measured data from the bottom block top face thermocouples for the cold cast.

The vertical displacement of the base of the ingot was assumed to obey a parabolic relationship for both the cold and hot casts with the largest displacement occurring at the edges of the ingot, which evolves with time, and no displacement occurring at the centre. With reference to **Figures 5.13(a)** and **(b)**, the spatial variation of displacement along the ingot base (*e.g.* for the cold cast), which is of the form: $\Gamma = f(x,y)$ (refer to **Figure 5.5**), was then calculated from this relationship, and a polynomial fitted to the evolution in base displacement with time, $z_{max} = f(t)$, as measured at the centre of ingot narrow face for the cold and hot casts.

† *gapcon.f* is a user subroutine provided by ABAQUS, which can be accessed by a user to implement non-linear heat transfer coefficients active between two surfaces, which are in thermal contact with each other.

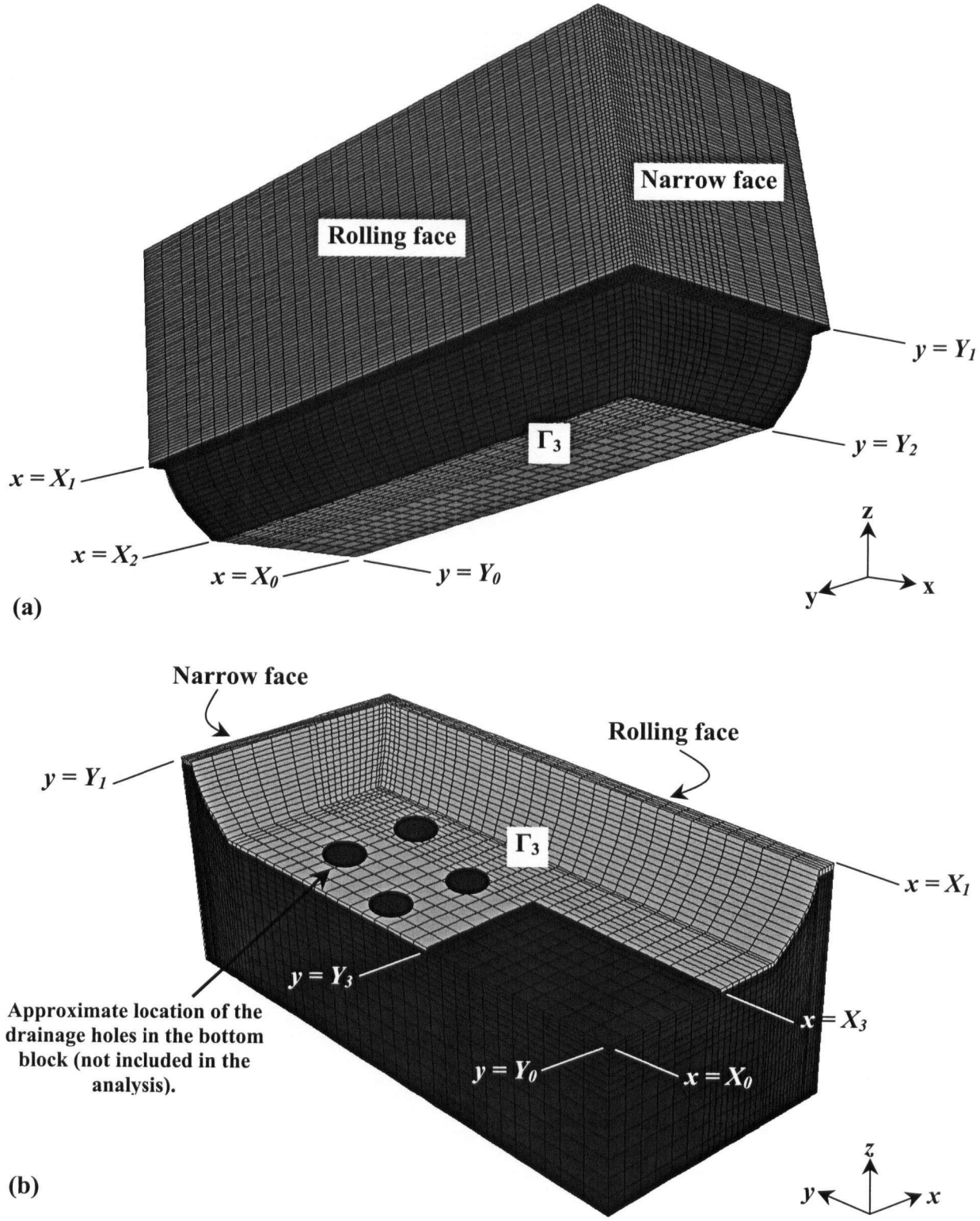

Figure 5.12 - Regions on the ingot-bottom block interface, Γ_3, which were assumed to be in contact with water entering the air gap during the process of incursion - for (a) ingot (in light gray), and (b) bottom block (in dark gray).

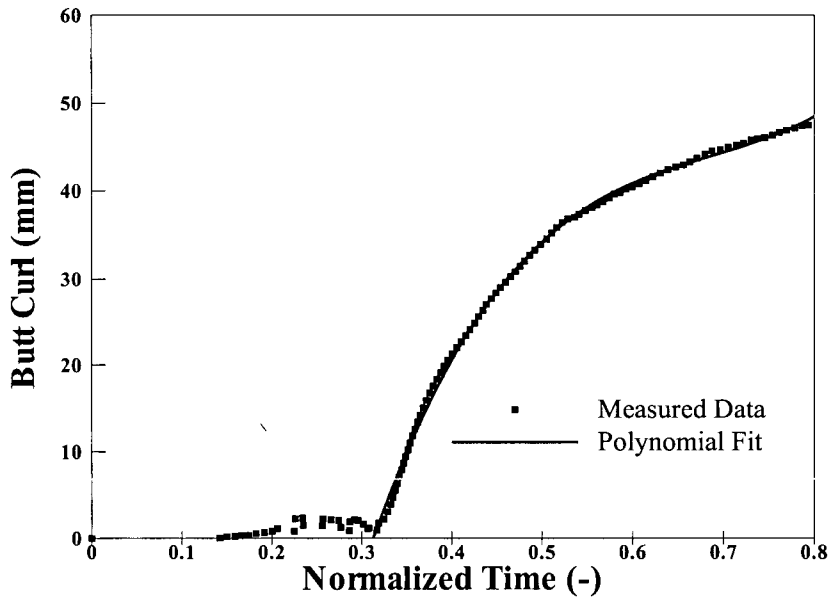

(a)

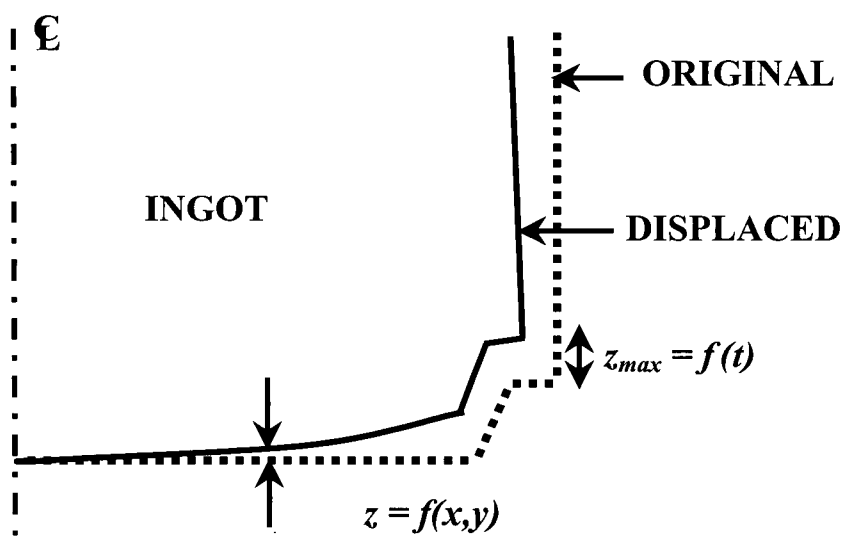

(b)

Figure 5.13 – (a) The measured butt curl (for the cold cast) at the centre of ingot narrow face and the polynomial fit to that data. (b) The spatial variation of the butt curl (in *x* & *y* directions) along the base of the ingot calculated assuming a parabolic relationship.

Note: The Figure is a schematic, and not to scale.

5.4 Summary

The geometry, FE mesh, and boundary conditions for the 2-D and 3-D thermal models to study the heat transfer processes active during the start-up phase of the D.C. Casting process have been presented. The thermal boundary conditions include primary cooling to the mould, secondary cooling to water, and ingot base cooling. With respect to primary cooling, the boundary conditions include: (i) meniscus effect, and (ii) dependence on air gap formation. With respect to secondary cooling, these include: (i) surface temperature and impingement point temperature dependence, (ii) water flow rate dependence, (iii) position dependence (relative to the point of water impingement), and (iv) dependence on presence or absence of water ejection due to film boiling. With respect to heat transfer from the ingot base, these include: (i) the bottom block temperature dependence, (iii) ingot base/bottom block gap dependence, and (iv) dependence on water incursion. The application of these models on AA5182 ingots cast with two distinctly different start-up recipes will be discussed in the following chapter.

References

1. Zienkiewicz, O.C., and Taylor, R.L., *The Finite Element Method*, 4th edition, 1994, McGraw-Hill Book Company.
2. *ABAQUS Theory Manual*, Version 6.2, 1997.
3. White, F.M., *Heat and Mass Transfer*, 1991, A-W Pub. Co.
4. Aliravci, C.A., and Pekguleryuz, M.O., *A Comparative Study of Fraction-Solid Evolution in Aluminum Alloys,* Light Metals 1998 (Ed. B. Welch), The Minerals, Metals and Materials Society, Warrendale, USA, 1998, pp. 1087-1096.
5. Drezet, J.-M., and Rappaz, M., *Modeling of Ingot Distortions during Direct Chill Casting of Aluminum Alloys,* Metallurgical Transactions A, 1996, **27A**, pp. 3214-3224.
6. Arnberg, L., and Backerud, L., *Solidification Characteristics of Aluminum Alloys*, ed, S.P. Thomas, American Foundrymen's Society, Inc.
7. Wiskel, J.B., *Thermal Analysis of the Startup Phase for D.C. Casting of an AA5182 Aluminum Ingot*, Ph.D. Thesis, Dept. of Metals and Materials Engineering, University of British Columbia, Vancouver, B.C., 1996.
8. Fjær, H.G., Mortensen, D., Hakonsen, A, and Sorheim, E., *Coupled Stress, Thermal, and Fluid Flow Modeling of the Start-up Phase of Aluminum Sheet Ingot Casting,* Light Metals 1999 (Ed. C. E. Eckert), The Minerals, Metals and Materials Society, Warrendale, USA, 1999, pp. 743-748.

CHAPTER 6

THERMAL MODEL APPLICATION

6.1 Introduction

The various heat transfer phenomena active during the start-up phase of the D.C. casting process were analyzed with the aid of the 2-D and 3-D thermal models described in the previous chapter. Comparison of the model predictions with the industrial measurements was used to "fine-tune" the analyses via the thermal boundary conditions. In the first instance, the parameters used to quantify these boundary conditions were taken from the literature and/or were provided by Alcan. The various boundary conditions were systematically modified in the model through the external user subroutines in ABAQUS in several stages during the research programme. During each stage, complexity was added incrementally to the functional relationships describing the boundary conditions such that the physics involved during the cooling process was represented appropriately. The sensitivity of the model predictions to the various parameters used to quantify the boundary conditions were then evaluated by comparing the nodal temperature outputs with the measured temperature data for both the cold and hot casts. A total of twenty-eight thermocouples were used for this purpose: eight on the ingot vertical surfaces, ten near the ingot base, and ten in the bottom block. Based on the sensitivity analysis, the specific model parameters were manipulated to align the model predictions with the measured data as closely as possible (*i.e.* within ~ ±50°C - as suggested by Alcan). This process combined with the fact that the conduction model is based on fundamental principles (conservation of energy) yielded a single set of parameters that could describe the two extreme casting conditions examined. While it is possible that this process did not yield a completely unique set of parameters, it is felt that they are reasonably close to being correct given the extent to which the various physical phenomena within the process have been included.

The quick-to-run 2-D analysis was used to test the effectiveness of the water ejection and water incursion algorithms when applied to two distinctly different start-up conditions represented by the cold and hot casts. These algorithms were extended to the 3-D model, which were then extensively validated through comparisons with the measured data for both the castings. The application of the thermal models to the cold and hot castings is now discussed.

6.2 Implementation of the Start-up Casting Recipes

The approach adopted in the model was to hold the coordinate system for the FE mesh stationary (although the FE mesh for the ingot is not "static" during the analysis), and move the boundary conditions associated with the primary and secondary cooling regimes (refer **Figure 5.7**) up the mesh at a rate consistent with the casting practice (*i.e.* the ramps associated with the mould filling rate and casting speed shown in **Figures 4.3** and **4.4**). Towards this goal, an algorithm that computes the evolution of metal height in the mould and cast length was incorporated in the *sfilm.f* subroutine, which was used to implement the thermal boundary conditions on the computational domain in ABAQUS. The algorithm was validated by comparing the calculated cast length data with the measured values for both the cold cast (using Casting Practice No. 1) and hot cast (using Casting Practice No. 2). The comparison is presented in **Figure 6.1** wherein the calculated values were found to lie within an acceptable range of ±0.5% of the measured data in both the cases. For the hot cast, the casting process was stopped at ~0.78 normalized time during the trials, owing to safety considerations, whereas in the simulation, the casting process was allowed to continue. Although the calculated values lie close to each other, the offset in the evolution of cast length for Casting Practice No. 1 compared with No. 2, observed during the trials, may be attributed to the delay in the response of the metal level sensor placed above the mould (refer **Figure 4.2**), which could only detect the metal after it had completely covered the top surface of the bottom block.

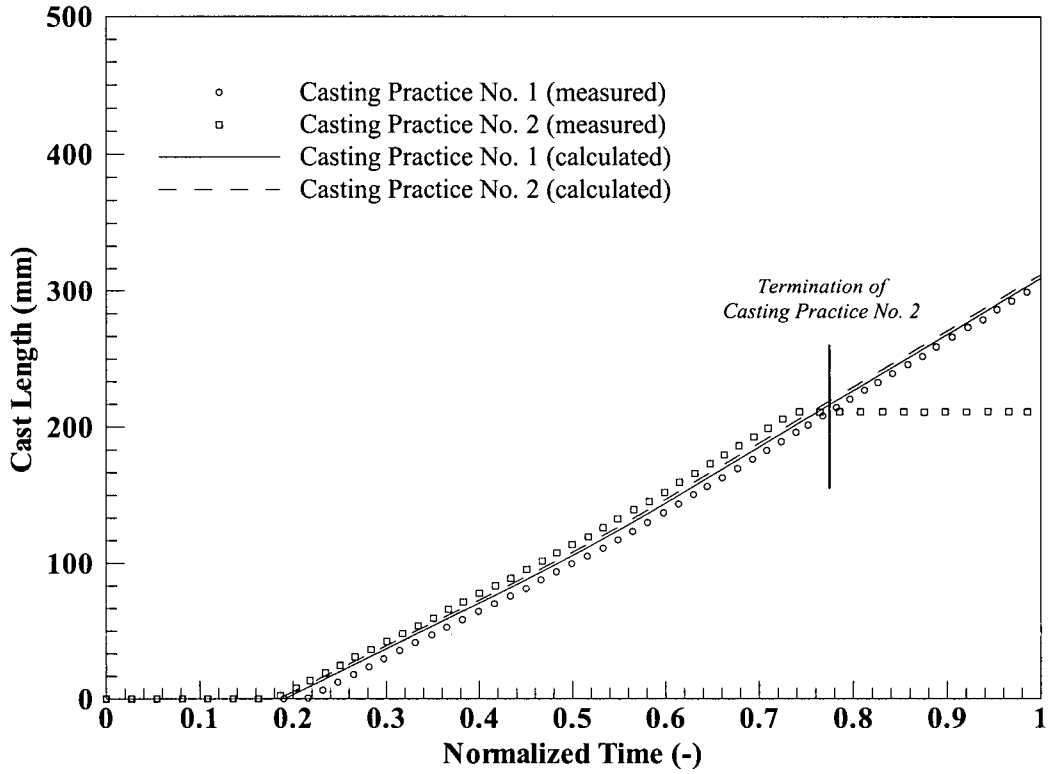

Figure 6.1 – Comparison of measured and calculated cast length data for Casting Practice No.1 and 2.

6.3 Application of the 2-D model†

The 2-D thermal model, which was computationally less intensive compared to the 3-D analysis, and therefore had a quicker run time, was developed to implement and test the water ejection and water incursion subroutines, as a part of step-wise approach in model development. The model was developed using ABAQUS version 5.8, and was run on an SGI Origin™ 200 machine equipped with four 175 MHz MIPS® 64-bit R10000 microprocessors. The CPU time to simulate the total casting time was approximately 8 hrs. The following sections discuss the results from this 2-D analysis.

† This section has been accepted for publication in the 2002 special issue of Journal of Light Metals, Elsevier Science, and was presented at the 131st Annual Meeting & Exhibition of TMS 2002 held in Seattle, USA.

6.3.1 Model Predictions and Verification

The results showing the model predictions for the cold cast and hot cast are presented in **Figures 6.2** and **6.3**, respectively. Referring to **Figure 4.9**, which shows thermocouple placement, **Figures 6.2** and **6.3** show a comparison between the model predictions for positions 10, 60 and 160 mm above the ingot lip, at a location, 5 mm below the surface of the rolling face. The thermocouple data for the same locations have also been plotted for comparison. As can be seen, the agreement between the model predictions and the measurements is good at the various locations examined on the rolling face. The secondary cooling heat transfer conditions in the absence of film boiling have been accurately described (**Figure 6.2**). In addition, the conditions that both trigger the occurrence of water ejection and its subsequent effect on secondary cooling heat transfer have also been captured (**Figure 6.3**).

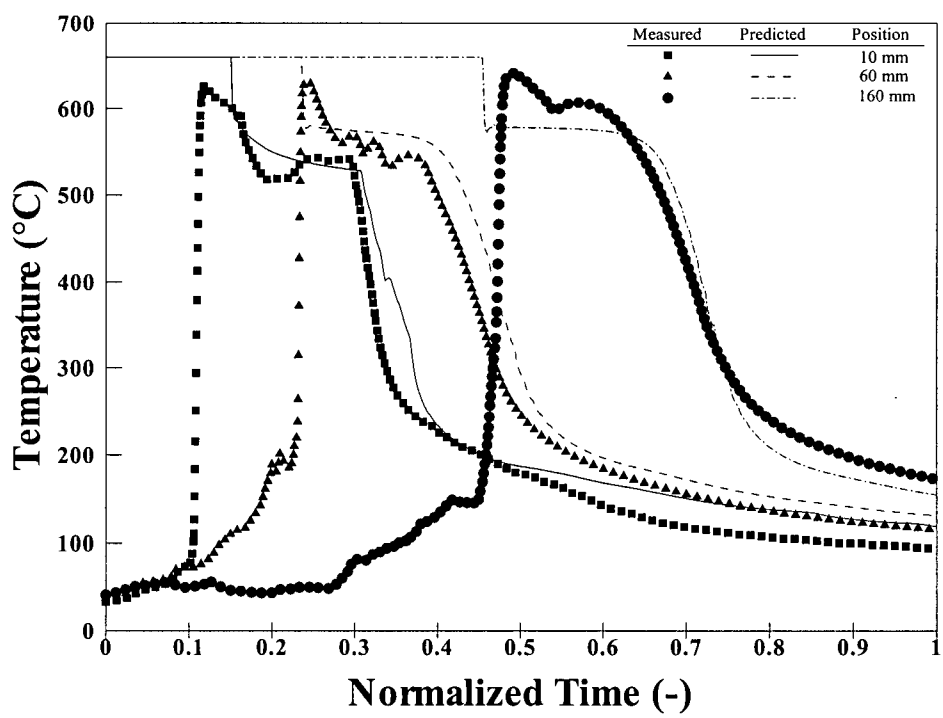

Figure 6.2 - Comparison of measured and model predicted temperatures at different heights (mm) above the ingot lip (refer to Figure 4.9), near the centre of rolling face for the cold cast.

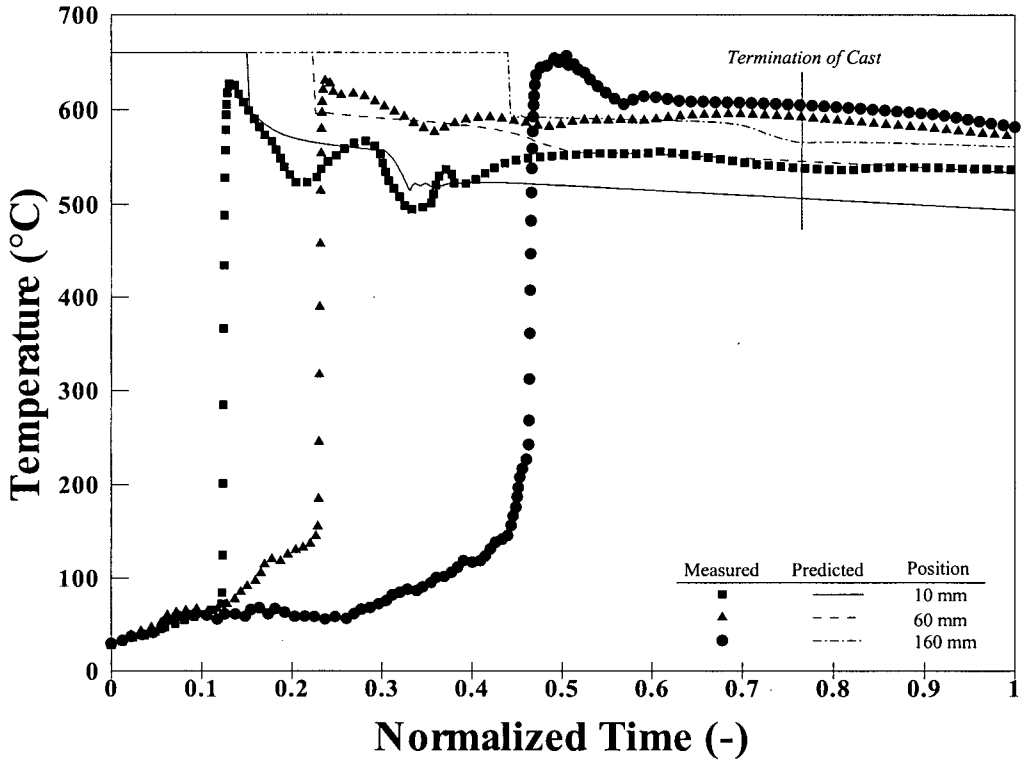

Figure 6.3 - Comparison of measured and model predicted temperatures at different heights (mm) above the ingot lip (refer to Figure 4.9), near the centre of rolling face for the hot cast.

The variation in temperature with time predicted by the model, 5 mm above the base of the ingot for the cold cast, is presented in **Figure 6.4**. Referring to **Figure 4.10**, the results for two locations: one, near the centre of the ingot (*i.e.* Location No. 3 in the figure) and the other, near the rolling face edge (*i.e.* Location No. 1) are presented. The thermocouple data obtained at the same locations have also been plotted for comparison. It is evident from the thermocouple data that the location near the edge experiences a greater rate of heat extraction than the center of the casting. This behaviour is related to the incursion of water near the edge as it pulls away from the bottom block due to base deflection and also to heat conduction from the impingement zone. The location at the centre remains in good physical and thermal contact with the bottom block. Based on these results it would appear that the loss in contact heat transfer at the edge is more than offset by an increase in heat transfer associated with water incursion. As can be seen, the

model also predicts this behaviour fairly accurately although there is a tendency to under predict the cooling due to water incursion.

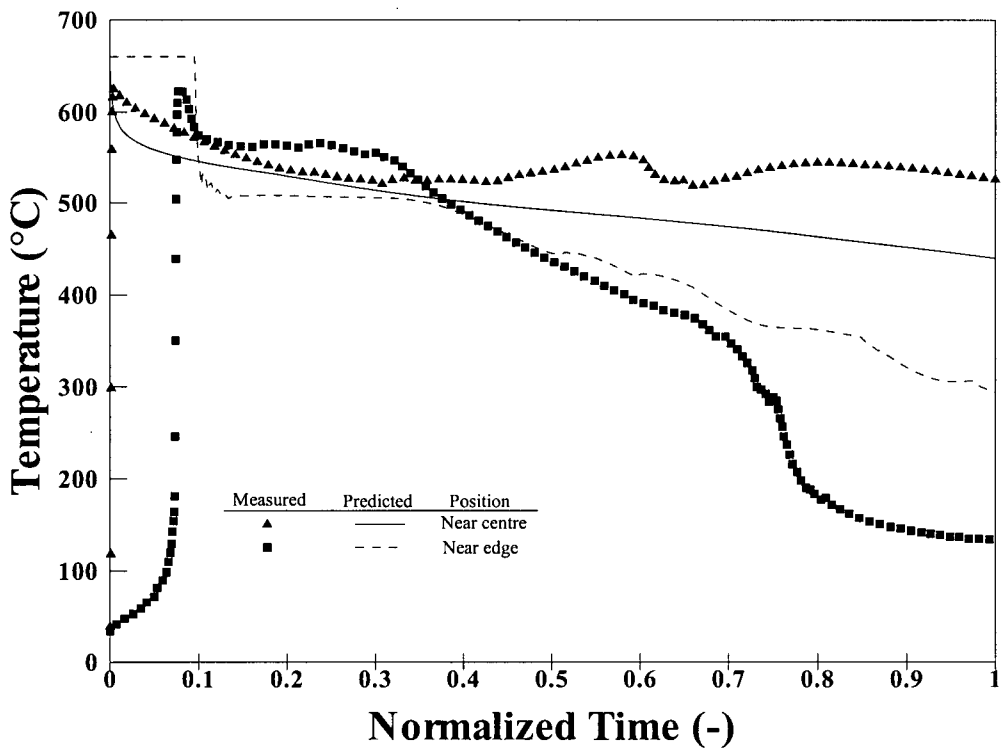

Figure 6.4 - Comparison of measured and model predicted temperatures at the base of the ingot near the centre (Location No. 3) and near the edge (Location No. 1) for the cold cast (refer to Figure 4.10).

The variation in temperature with time predicted by the model, 5 mm below the top face of the bottom block for the cold cast, is presented in **Figure 6.5** for locations near the centre of the ingot and near the rolling face edge. The thermocouple data obtained at the same locations have also been plotted for comparison. In this case, it is evident that the location near the edge on the bottom block experiences an even greater rate of heat extraction due to water incursion. The model also predicts this behaviour well although there is a tendency to under predict the heat transfer to the bottom block during the initial ~0.15 normalized time, and also, to predict the drop in temperature due to water incursion too late.

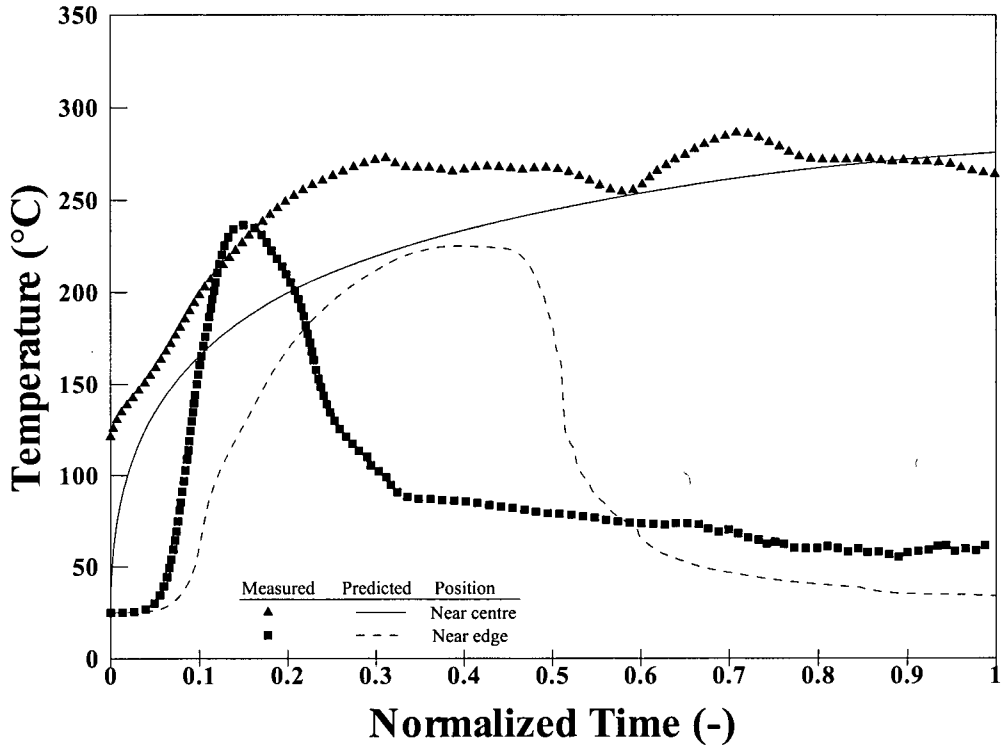

Figure 6.5 - Comparison of measured and model predicted temperatures at the top face of the bottom block near the centre (Location No. 4) and near the edge (Location No. 1) for the cold cast (refer to Figure 4.10).

6.3.2 Sensitivity Analysis

To better examine the effect of water ejection and water incursion and the interdependence of the two, a sensitivity analysis was conducted with the model. In the sensitivity analysis, two runs were completed. In the first run (Case I), the operating conditions for cold cast (*i.e.* Casting Practice No. 1) were used but, the water incursion algorithm was switched off – i.e. the heat transfer coefficient to water, h_{water}, appearing in Equation (5.14) was set to zero. In the second run (Case II), the operating conditions for hot cast (*i.e.* Casting Practice No. 2) were used, but with the water ejection algorithm switched off – i.e. the empirical relationships for secondary water cooling were used without the facility to reduce the heat transfer coefficient associated with the conditions for water ejection from the surface.

Figure 6.6 shows the variation in temperature with time for Case I predicted at three positions adjacent to the rolling face located 10, 60 and 160 mm above the lip. The model

predictions now indicate the presence of film boiling occurring at the 10 and 60 mm locations. Failure to extract the heat associated with water incursion has caused the ingot surface temperature on the rolling face to rise above the Leidenfrost temperature resulting in water ejection and a delay in cooling. The film then collapses as a result of the ramp up in water flow rate that occurs with increasing cast length (the water flow rate is gradually increased with increasing cast length in Casting Practice No.1).

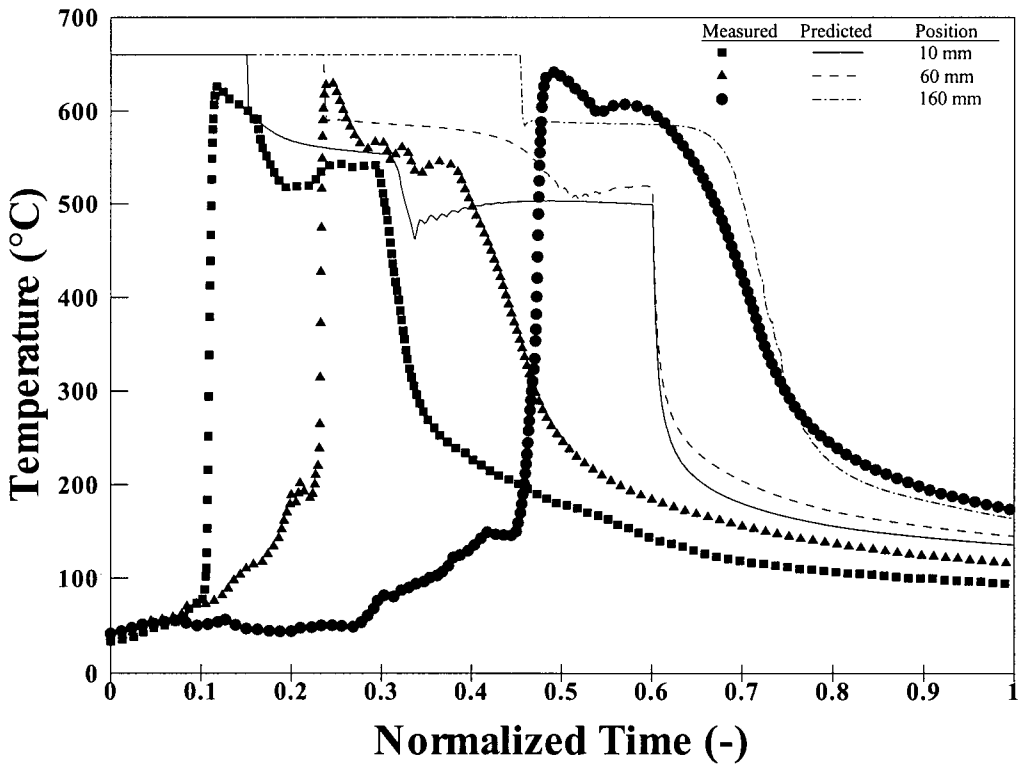

Figure 6.6 - Comparison of measured and predicted temperatures at different heights (mm) above the ingot lip (refer to Figure 4.9), near the centre of rolling face for Case I – no water incursion (compare with Figure 6.2).

The effect of switching off water incursion on the heat transfer from the ingot base and bottom block can be seen in **Figures 6.7** and **6.8**. From these plots, it is obvious that the ingot base and bottom block are substantially hotter, particularly near the rolling face edge, compared with results predicted with the water incursion switched on – see **Figures 6.4** and **6.5**. This in turn reduces diffusive heat transfer within the ingot to the base, giving rise to hotter rolling face

temperatures. As a result, there is water ejection and a significant reduction in the heat transfer from the sides of the ingot predicted by the model. The extent to which heat transfer from the sides and base of the ingot are coupled during the start-up phase of the process appears to be significant.

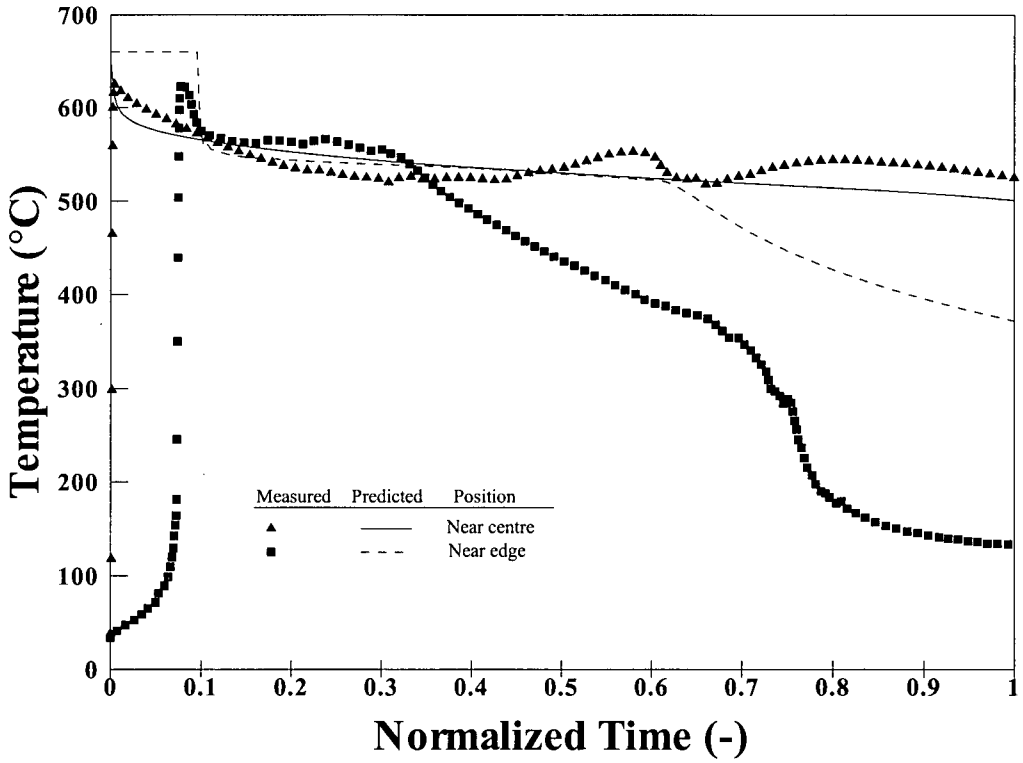

Figure 6.7 - Comparison of measured and model predicted temperatures at the base of the ingot near the centre (Location No. 3) and near the edge (Location No. 1) for Case I (refer to Figure 4.10, and compare with Figure 6.4).

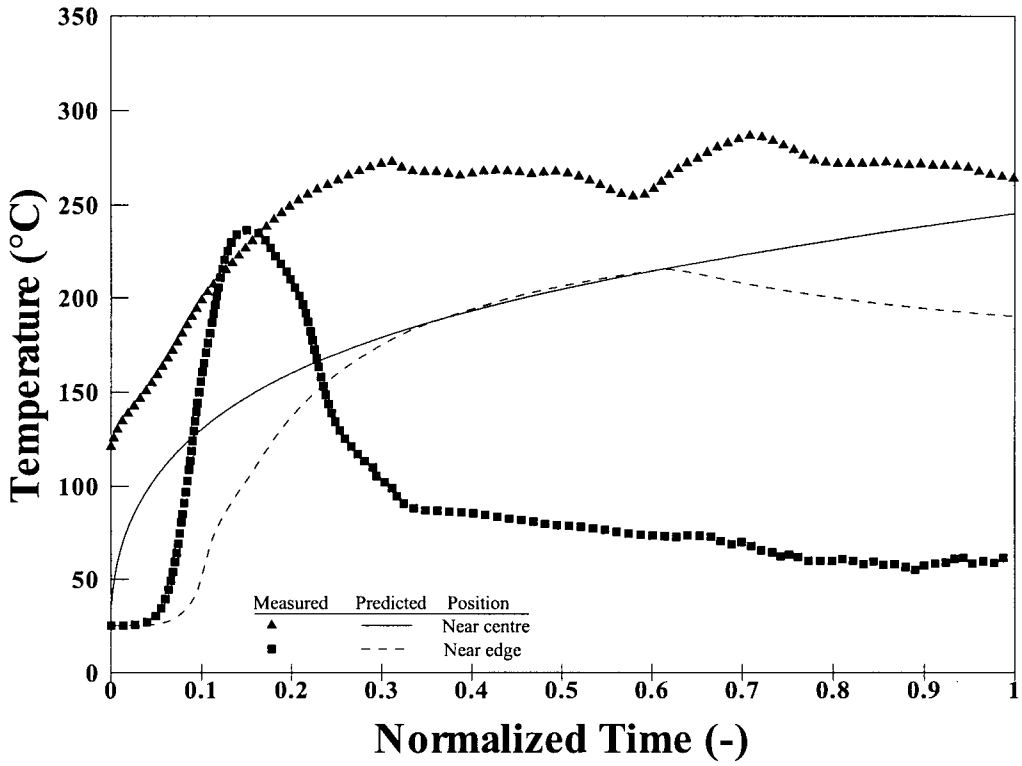

Figure 6.8 - Comparison of measured and model predicted temperatures at the top face of the bottom block near the centre (Location No. 4) and near the edge (Location No. 1) for Case I (refer to Figure 4.10, and compare with Figure 6.5).

The results for Case II are presented in **Figure 6.9** together with the original thermocouple data from the hot cast. The figure shows the variation in temperature with time for the three positions adjacent to the rolling face located 10, 60 and 160 mm above the lip. As can be seen, removing the effect of water ejection results in a substantial increase in heat transfer causing the model predictions to diverge significantly from the measured response.

The results from the sensitivity analysis clearly illustrate the importance of water incursion and water ejection in terms of their ability to influence heat transfer during the start-up phase of the DC casting process. It is also evident that these processes are coupled in that changes to the heat transfer from the base of the ingot can result in significant changes to the secondary cooling heat transfer.

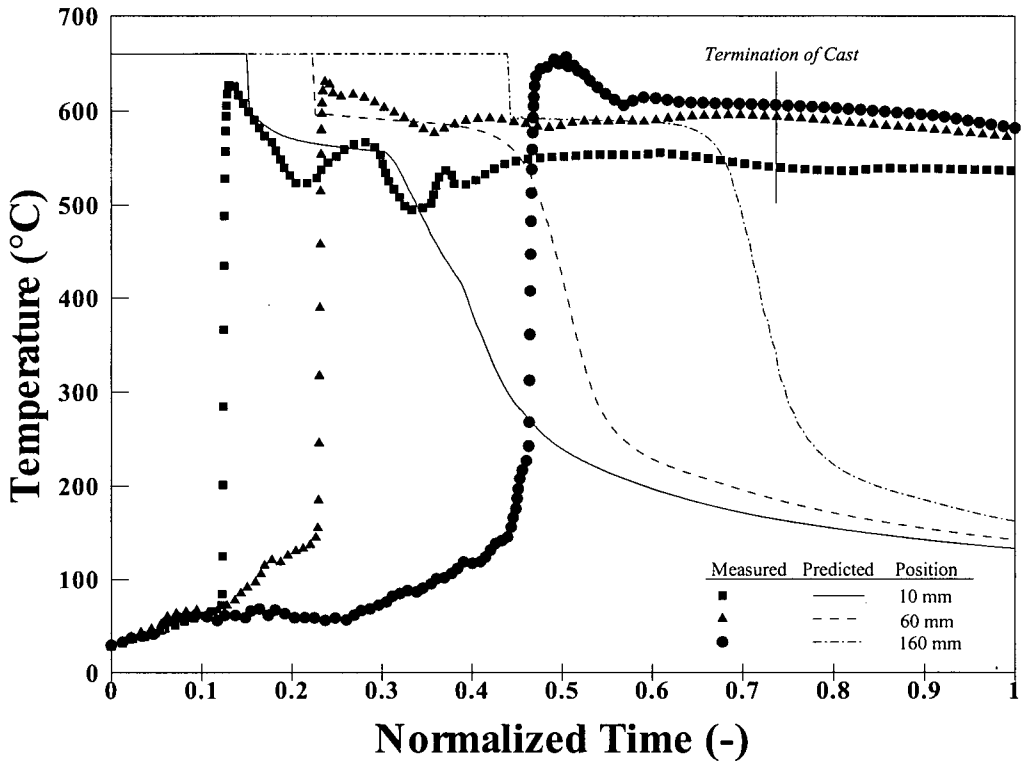

Figure 6.9 - Comparison of measured and model predicted temperatures at different heights (mm) above the ingot lip (refer to Figure 4.9), near the centre of rolling face for Case II (compare with Figure 6.3).

Model predictions indicate that the 2-D longitudinal model is limited to the analysis of heat transfer in a plane normal to the rolling face, and does not completely describe the three-dimensional heat transfer processes active during the start-up phase. Therefore, a 3-D analysis is required to capture the spatial and temporal variations of temperatures along the ingot rolling and narrow faces, ingot base, and bottom block top surface. However, the 2-D model is computationally less intensive, and is "quick-to-run" (the 2-D model took 1 hour to run on the HP Alphasystem^{TM} machine). Hence, it can be used effectively for sensitivity analysis and has the potential of being used as a powerful tool for making predictions during the actual production process.

6.4 Application of the 3-D model[†]

Once the preliminary 2-D analysis was completed, the study was extended to a 3-D thermal model in order to adequately describe the heat transfer during the start-up phase of the D.C. casting process. The model was developed using ABAQUS version 6.2, and was run on an ES-45 HP AlphaSystem™ machine equipped with four 1.0 GHz Alpha® 64-bit microprocessors. The CPU time to simulate the total casting time was approximately 2 days. The following sections discuss the results from this 3-D analysis.

6.4.1 Model Predictions for Positions Adjacent to the Ingot Rolling and Narrow Faces

The results showing the model predictions for the cold cast at various positions adjacent to the ingot rolling and narrow face are presented in **Figures 6.10** and **6.11**, respectively. Referring to **Figure 4.9**, which shows thermocouple placement, these figures show a comparison between the model predictions for positions 10, 60, 110, and 160 mm above the ingot lip at a location 5 mm below the surface of the rolling face. The thermocouple data for the same locations have also been plotted for comparison. It is evident that the agreement between the model predictions and the measurements is good at the various locations examined on the rolling face. The model has correctly captured the secondary cooling heat transfer conditions *i.e.* the cooling of the ingot faces by the process of nucleate boiling is confirmed. However, the model tends to under predict the temperatures near the end of the casting process, which may be due to a higher value of heat transfer coefficient that was used in the model to quantify the nucleate boiling regime for the secondary cooling. Referring to **Figure 6.11**, which shows the comparison for the corresponding narrow face locations, the model seems to predict aggressive cooling by chill water on this face. However, as explained in Chapter 4, the downward motion of the thermocouples located on this face associated with the withdrawal of the ingot was "slowed down" by the effect of butt curl – *i.e.* the upward displacement of the ingot face. Hence, the temperature evolution at any location on the narrow face above the ingot lip cannot be directly compared with predicted data from one single node situated at a corresponding location in the model. Rather, it should be compared with "snapshots" obtained from several nodes situated above this node of interest. Using the casting recipe and butt curl measurement data, the apparent

[†] Parts of this section have been accepted for publication in Light Metals 2003, The Minerals, Metals and Materials Society, and will be presented at the 132nd Annual Meeting & Exhibition of TMS 2003 to held in San Diego, USA.

vertical position of the node of interest considering the effect of butt curl was computed. Temperature predictions were obtained from all the nodes below this apparent position and plotted out against the measured data. Snapshots were then extracted from these nodal data to obtain the final "predicted curve". After correcting the model predictions using this methodology, the comparison shown in **Figure 6.12** indicates there is good agreement between the measured and model predicted temperatures for this face.

The results showing the model predictions for the hot cast at various positions adjacent to the ingot rolling and narrow face are presented in **Figures 6.13** and **6.14**, respectively. The thermocouple data obtained at the same locations have also been plotted for comparison. The effect of the using a lower water flow rate in the casting recipe (refer to **Figure 4.5**) on start-up cooling condition has been appropriately captured by the model by predicting the process of water ejection on the ingot faces. Hence, the thermal model is sensitive to the start-up recipe that is being used to generate the ingot. It is interesting to note, that the model predicts the progressive collapse of the water ejection front beyond ~0.78 normalized time on the rolling and narrow faces of the ingot, albeit at an earlier time in the case of the narrow face. This may be due to the rectangular cross-section of the ingot, which causes the corners to cool faster than the centre of the rolling and narrow faces (this is referred to as the "corner effect"). Hence, the centre of narrow face cools quicker than the centre of rolling face, owing to its proximity to the ingot corners.

Referring back to **Figures 6.10, 6.12 6.13,** and **6.14**, it may also be observed that the model predicts intensive cooling in the early stages of the casting for the location near to the ingot lip (*i.e.* at a height of 10 mm). This may be due to the fact that the supply of heat towards the mould faces was assisted by the turbulence in the liquid metal during the initial stages of the mould filling process. The model was not able to capture this phenomenon since it did not include a fluid flow analysis.

Figure 6.15 and **6.16** show the contour plot of temperatures on the rolling and narrow faces of the ingot for the cold cast after ~0.56 and ~1.0 normalized analysis times, respectively. As can be seen from the figures, there is a small region near the centre of the rolling face of the ingot where film boiling prevails during the early period of the start-up phase. The ingot faces ultimately cool aggressively in the absence of film boiling phenomenon. **Figures 6.17-6.19** show the snapshots (at ~0.56, 0.78, and 1.0 normalized analysis times, respectively) of the contour plot

of temperatures on the ingot faces for the hot cast. The evolution and ultimate collapse of the parabola-shaped water ejection front that separates the film and nucleate boiling regimes on the ingot faces is clearly illustrated. The shape of the water ejection front predicted by the model is strikingly similar to that observed during the industrial trials, shown in **Figure 4.20**, which demonstrates the effectiveness of the 3-D model.

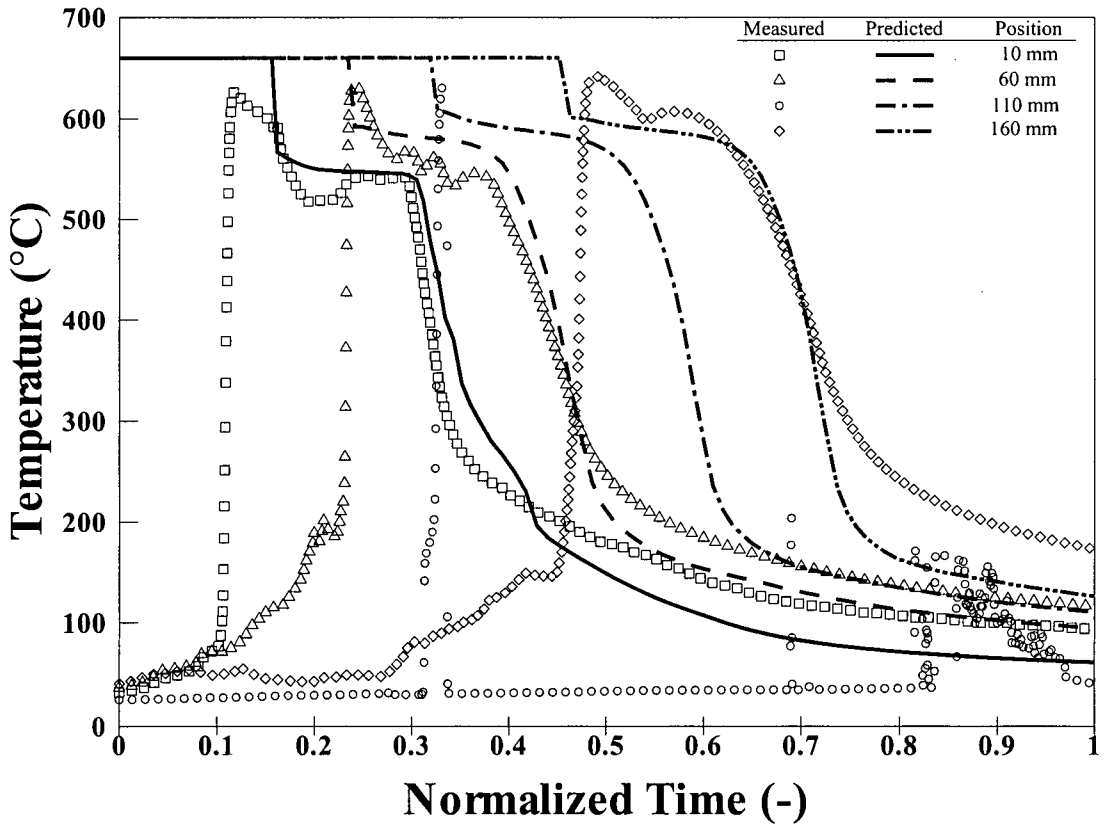

Figure 6.10 - Comparison of measured and model predicted temperatures at different heights (mm) above the ingot lip (refer to Figure 4.9), near the centre of rolling face for the cold cast.

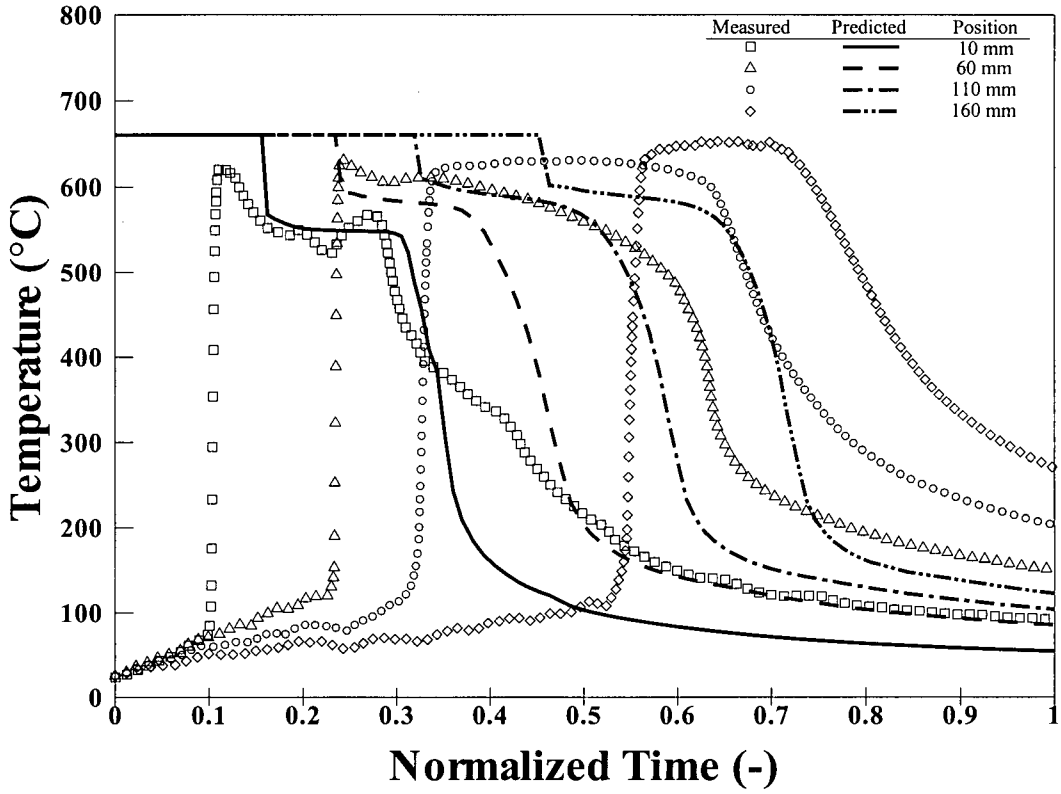

Figure 6.11 - Comparison of measured and model predicted temperatures at different heights (mm) above the ingot lip (refer to Figure 4.9), near the centre of narrow face for the cold cast.

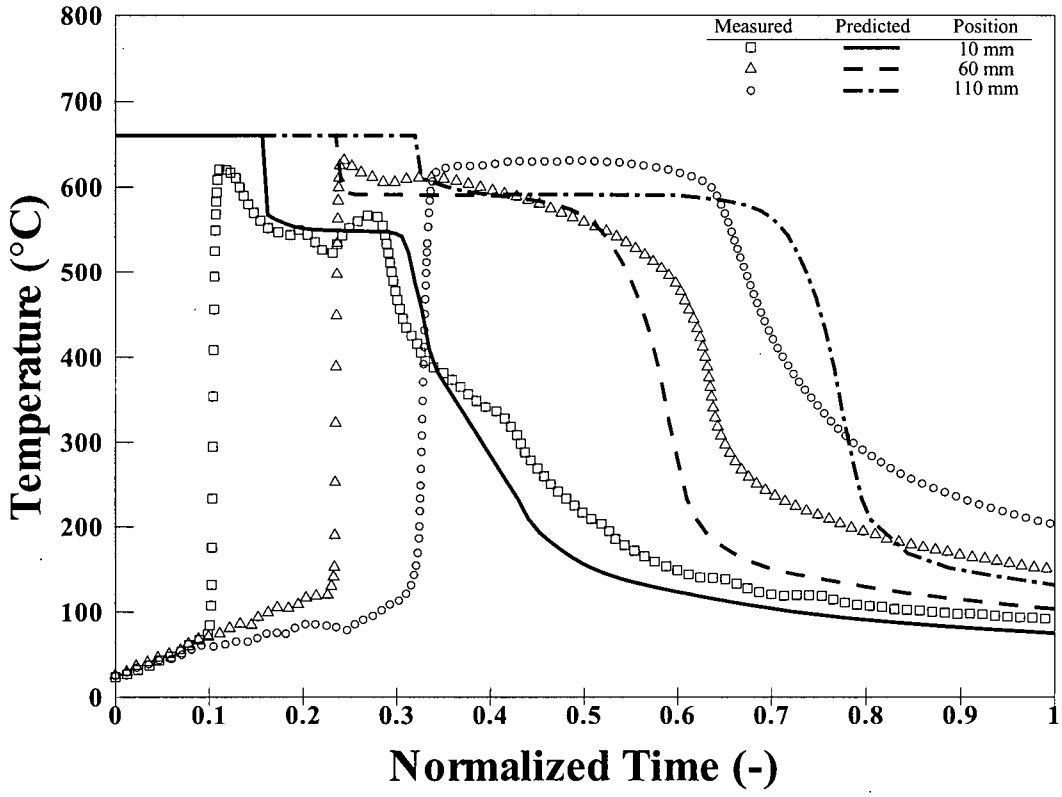

Figure 6.12 - Comparison of measured and model predicted temperatures at different heights (mm) above the ingot lip (refer to Figure 4.9), near the centre of narrow face for the cold cast, after including the correction for butt curl.

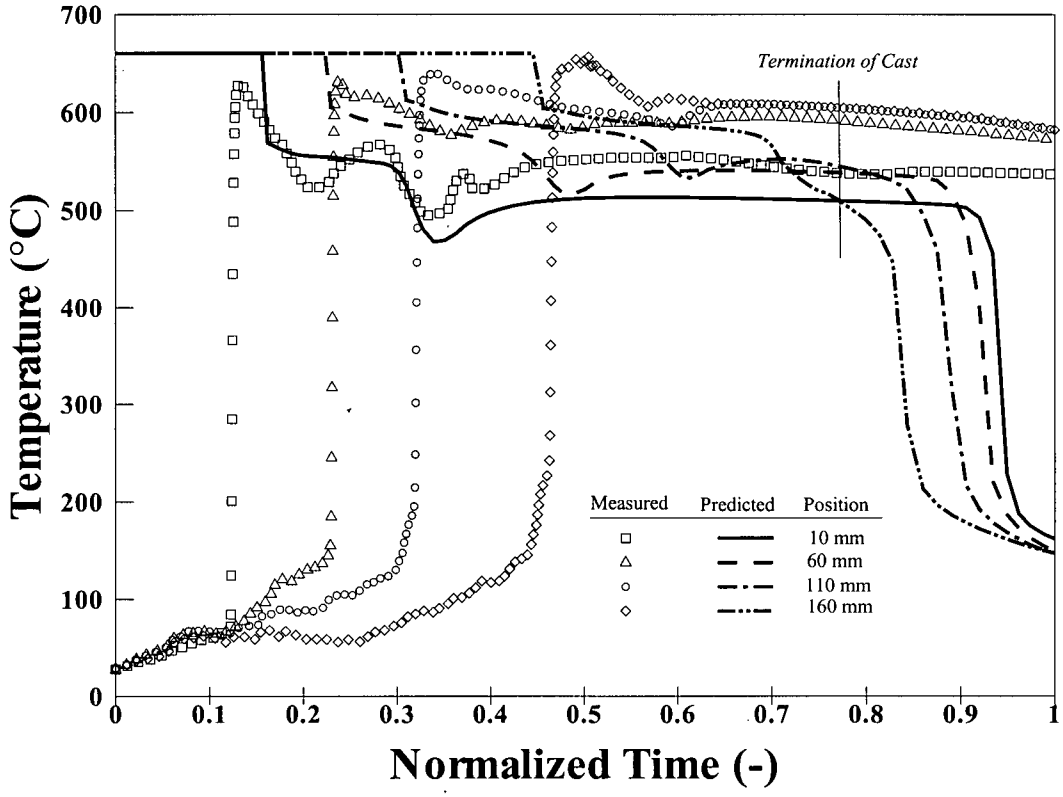

Figure 6.13 - Comparison of measured and model predicted temperatures at different heights (mm) above the ingot lip (refer to Figure 4.9), near the centre of rolling face for the hot cast.

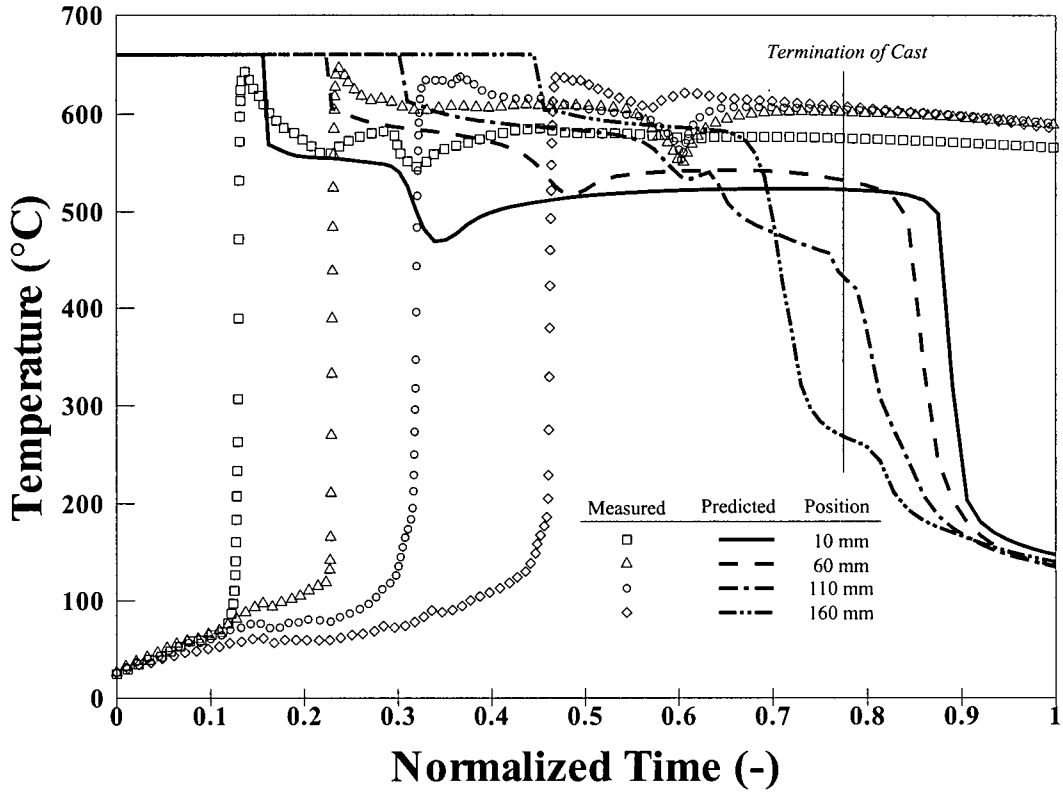

Figure 6.14 - Comparison of measured and model predicted temperatures at different heights (mm) above the ingot lip (refer to Figure 4.9), near the centre of narrow face for the hot cast.

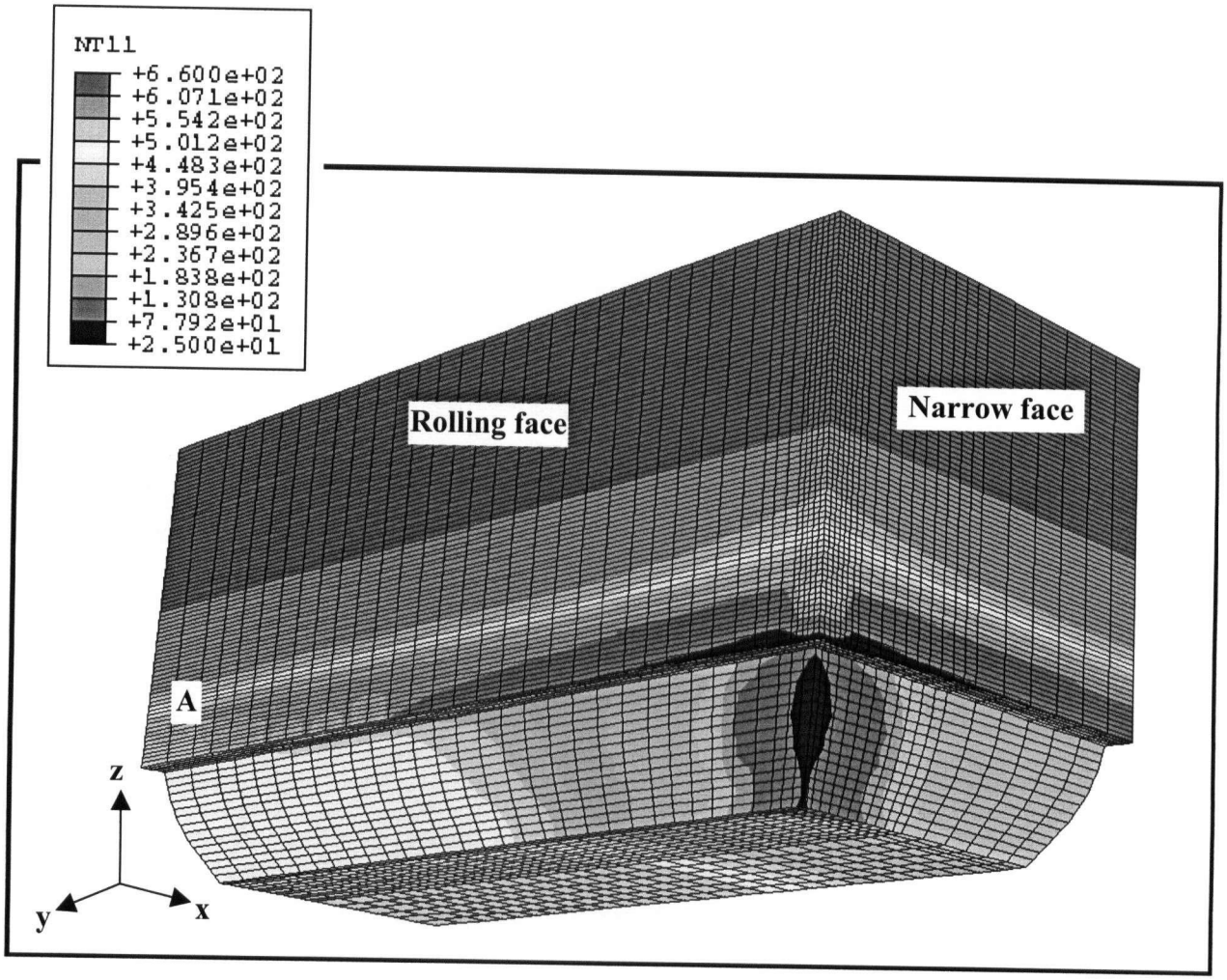

Figure 6.15 – Outer view of the computational domain showing the contour plot of temperature (NT11) along the rolling and narrow faces of the ingot for the cold cast after ~0.56 normalized analysis time. A small area (Region "A") of film boiling is predicted near the centre of the rolling face. Nucleate boiling prevails in the other areas cooled by chill water.

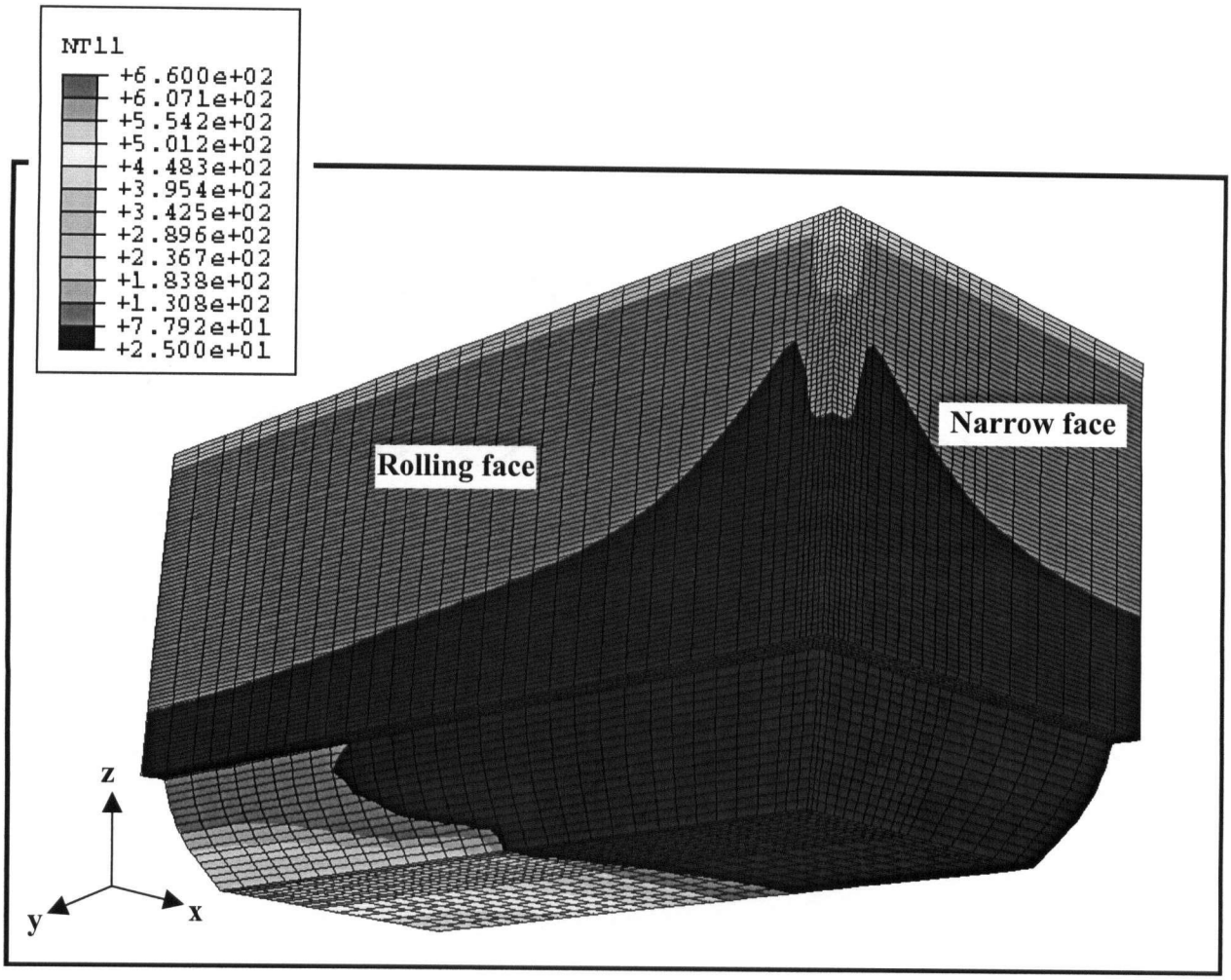

Figure 6.16 – Outer view of the computational domain showing the contour plot of temperature (NT11) along the rolling and narrow faces of the ingot for the cold cast at the end of the analysis *i.e.* after ~1.0 normalized analysis time. Both the faces of ingot cooled aggressively by nucleate boiling.

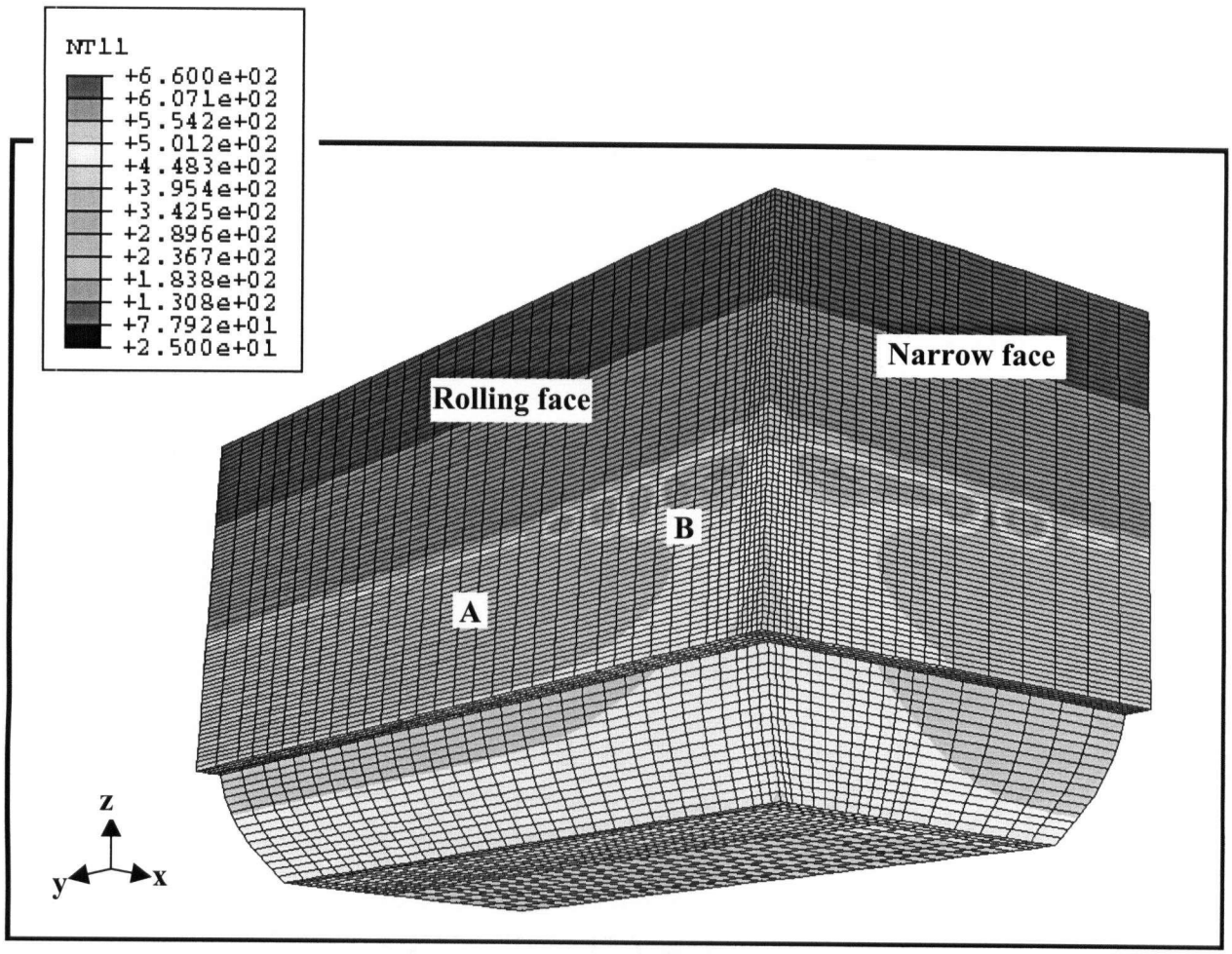

Figure 6.17 – Outer view of the computational domain showing the contour plot of temperature (NT11) along the rolling and narrow faces of the ingot for the hot cast after ~0.56 normalized analysis time. Both faces of ingot experience the process of water ejection, due to the process of film boiling (Region "A") on the rolling face. The process of transition/nucleate boiling has been initiated near the corner (Region "B") of the ingot.

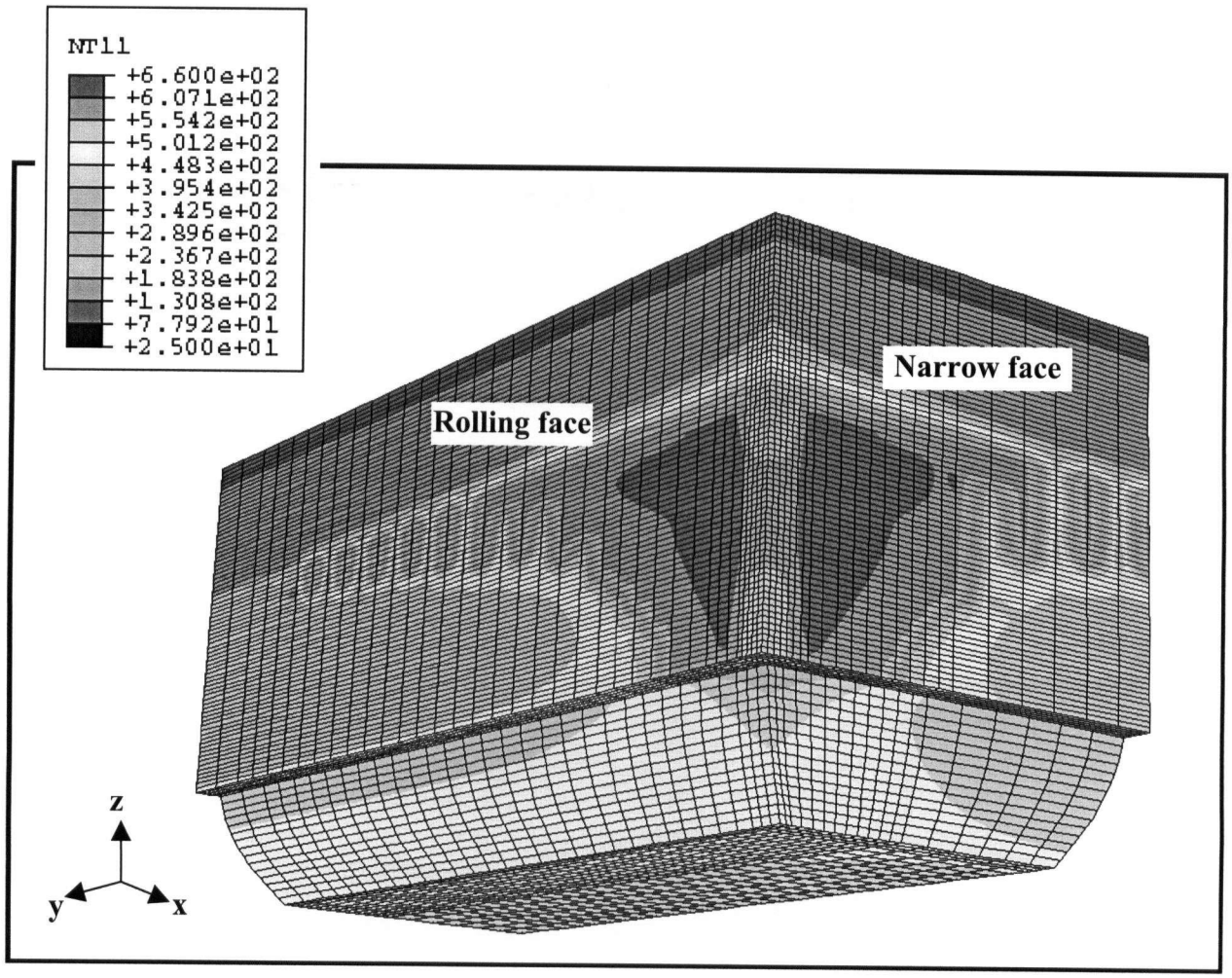

Figure 6.18 – Outer view of the computational domain showing the contour plot of temperature (NT11) along the rolling and narrow faces of the ingot for the hot cast at ~0.78 normalized analysis time. The parabola-shaped water ejection front (or dome) separating the film and nucleate boiling regimes is clearly visible on both the surfaces.

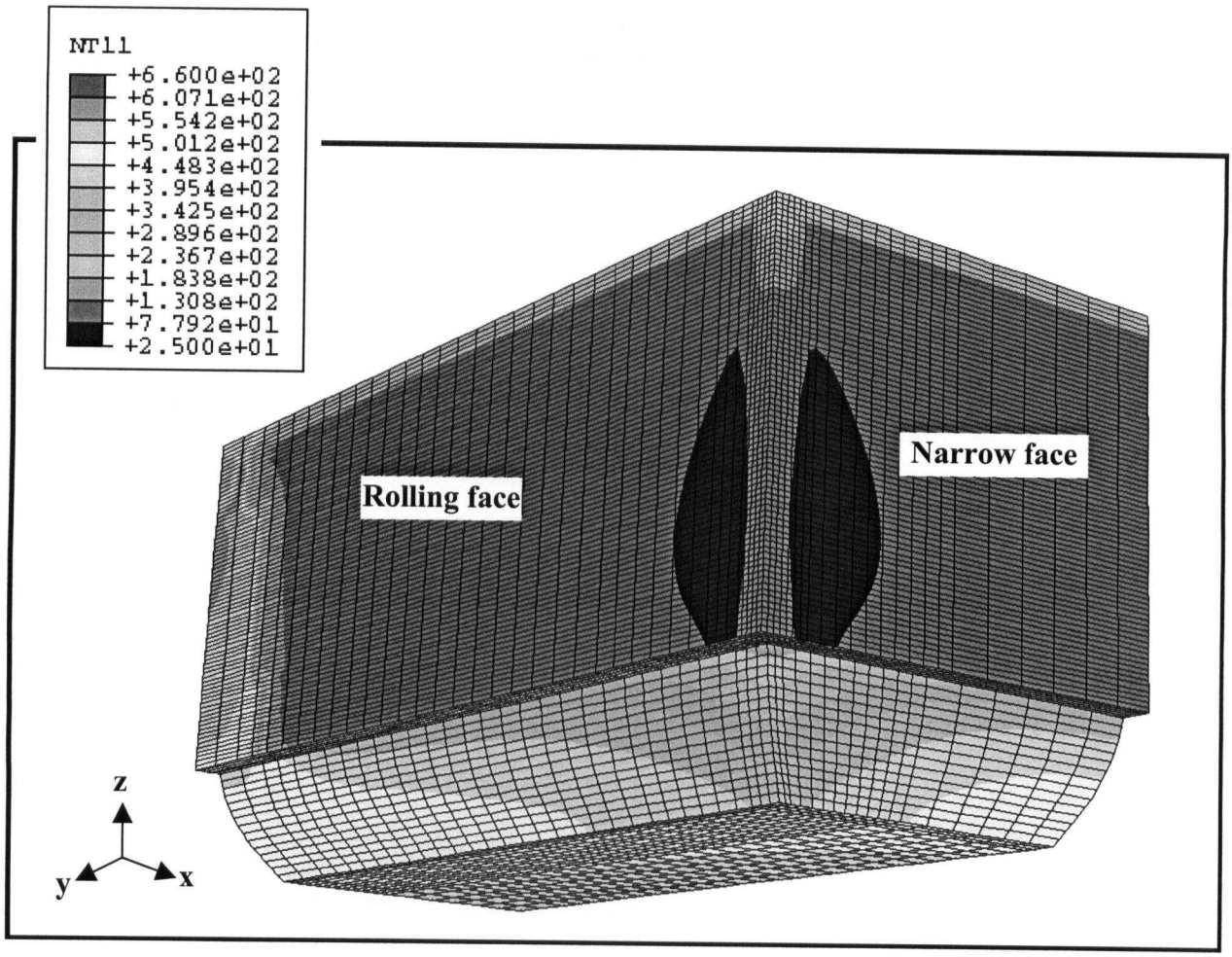

Figure 6.19 – Outer view of the computational domain showing the contour plot of temperature (NT11) along the rolling and narrow faces of the ingot for the hot cast at the end of the analysis *i.e.* ~1.0 normalized analysis time. The parabola-shaped water ejection front (or dome) separating the film and nucleate boiling regimes collapses towards the centreline on both the surfaces.

6.4.2 Model Predictions for Positions Adjacent to the Ingot Base

The variation in temperature with time predicted by the model 5 mm above the base of the ingot for the cold cast, and at various locations perpendicular to the rolling face (*i.e.* Location Nos. 1, 2, and 3 in **Figure 4.10**), and perpendicular to the narrow face (*i.e.* Location Nos. 5, 7, 8, and 9 in **Figure 4.10**) is presented in **Figures 6.20** and **6.21**, respectively. The thermocouple data obtained at the same locations have also been plotted for comparison. It is evident from the

thermocouple data that the model predicts the phenomenon of water incursion along the rolling (**Figure 6.20**), and narrow faces (**Figure 6.21**) quite accurately. However, the model under predicts the temperature for Location No. 2 owing to the over prediction of the gap formed between the ingot and bottom block (leading to increased cooling due to water incursion) based on the assumption that the spatial variation of the ingot base deflection obeys a parabolic relationship (refer to **Figure 5.13**). Also, the model does not capture the sudden drop in temperature at ~0.72 normalized time observed at Location No. 1, which may be a result of localized cooling specific to that location. **Figure 6.22**, which shows the contour plot of temperature at the end of the analysis for the ingot, clearly illustrates the extent of ingot base cooling (indicated by blue regions) due to water incursion along the narrow face, as a result of a higher magnitude of butt curl observed in this region.

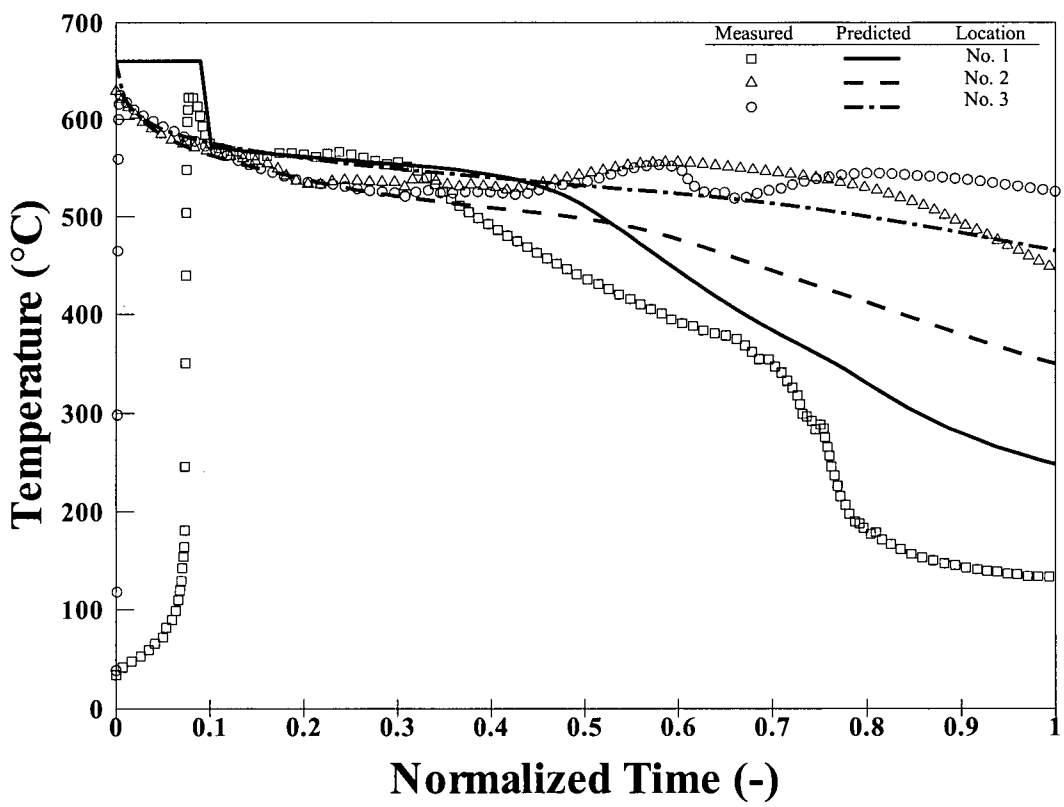

Figure 6.20 - Comparison of measured and model predicted temperatures at different locations 5 mm above the ingot base (refer to Figure 4.10), perpendicular to the rolling face for the cold cast.

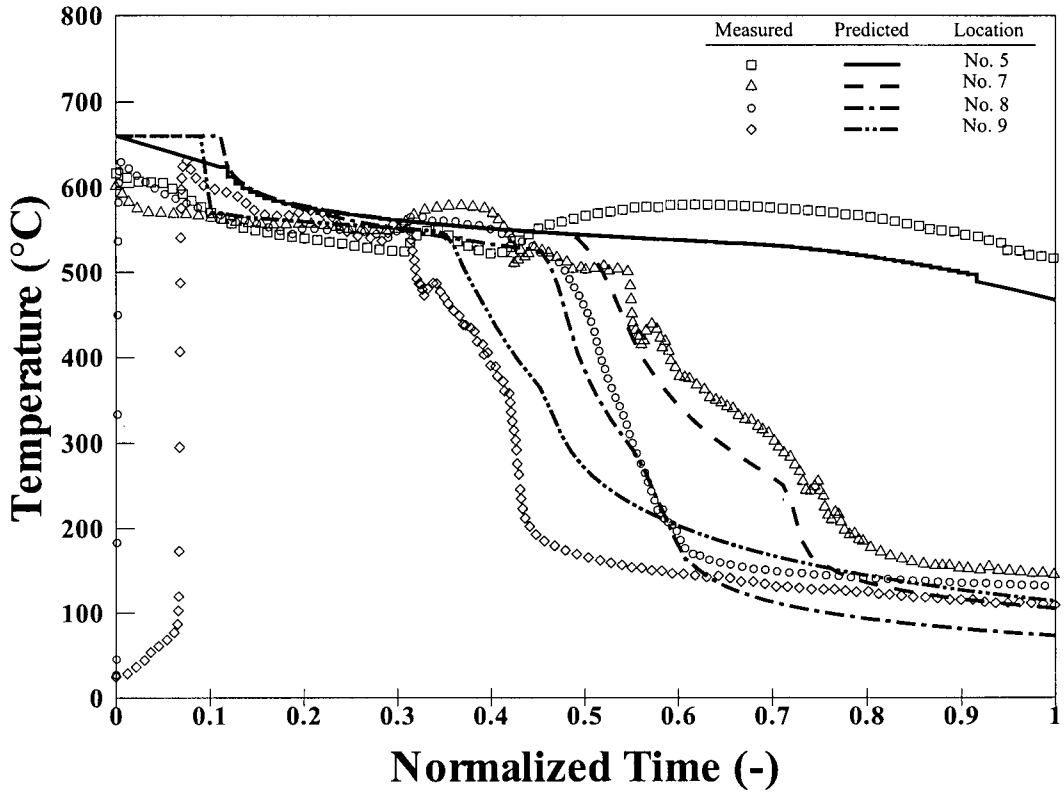

Figure 6.21 - Comparison of measured and model predicted temperatures at different locations along the ingot base (refer to Figure 4.10), perpendicular to the narrow face for the cold cast.

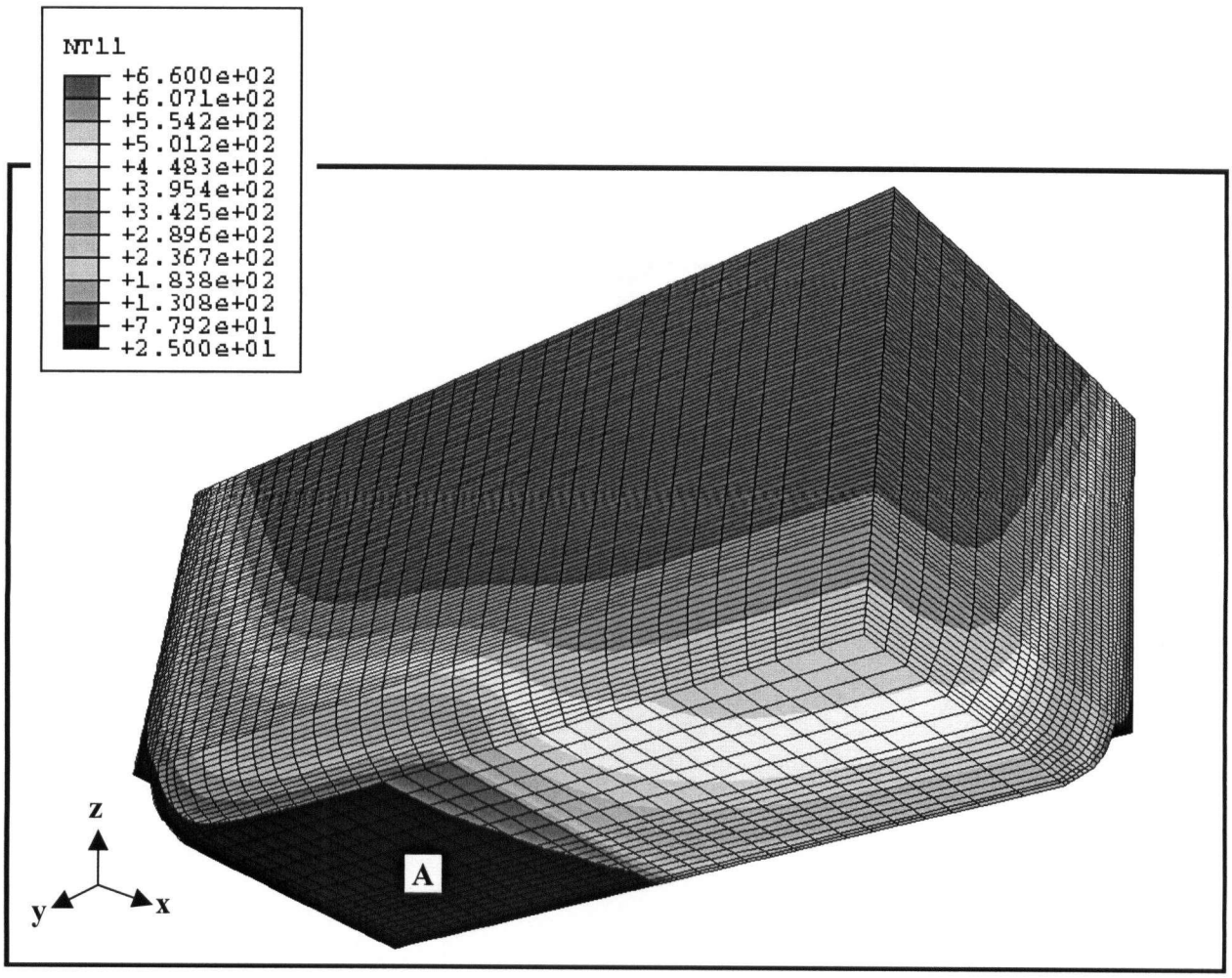

Figure 6.22 – Inner view of the computational domain showing the contour plot of temperature (NT11) along the symmetry faces of the ingot for the cold cast at the end of the analysis. Region "A" (area in blue) indicates the extent of ingot base cooling due to water incursion along the narrow face.

The variation in temperature with time predicted by the model 5 mm above the base of the ingot for the hot cast, and at various locations perpendicular to the rolling face (*i.e.* Location Nos. 1, 2, and 3 in **Figure 4.10**), and perpendicular to the narrow face (*i.e.* Location Nos. 5, 7, 8, and 9 in **Figure 4.10**) is presented in **Figures 6.23** and **6.24**, respectively. The thermocouple data obtained at the same locations have also been plotted for comparison. As can be seen, the model accurately predicts a hotter ingot base in the absence of water incursion due to the ejection of water along the ingot vertical faces and a lower magnitude of butt curl. This is also indicated in

Figure 6.25, which shows the contour plot of temperature at the end of the analysis for the ingot. Comparing **Figures 6.22** and **6.25**, the distinctly different cooling conditions experienced by the ingot base for the two different casts, which is accurately predicted by the model, can be easily delineated.

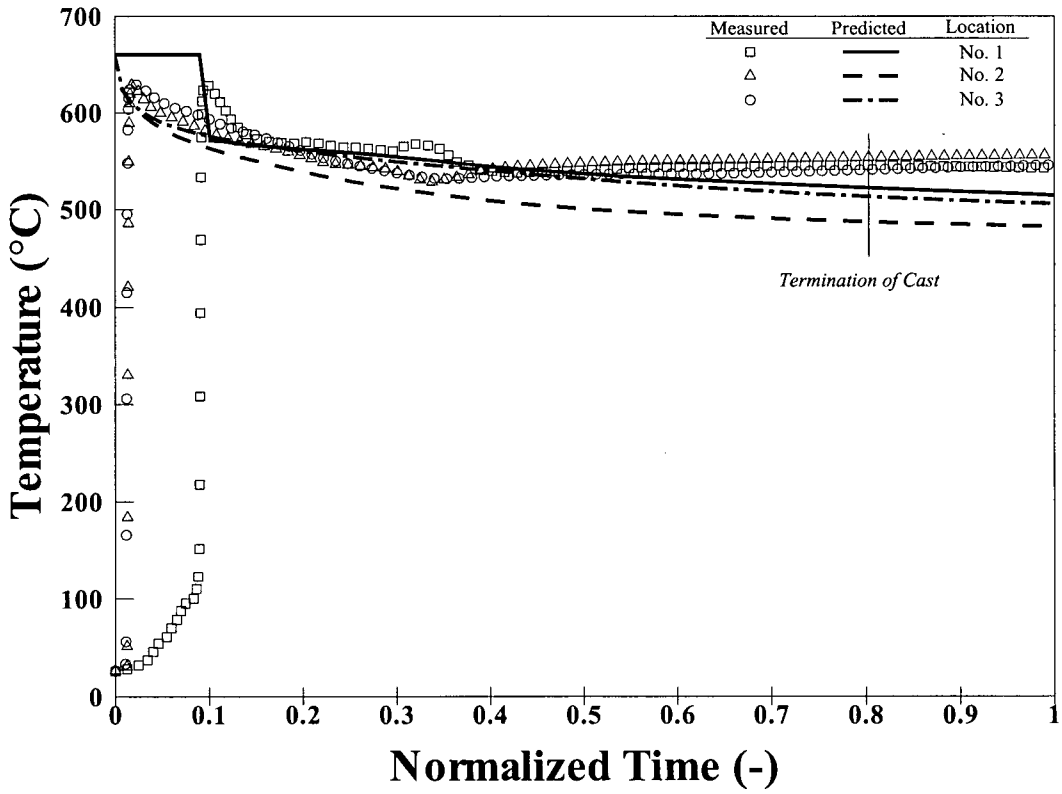

Figure 6.23 - Comparison of measured and model predicted temperatures at different locations 5 mm above the ingot base (refer to Figure 4.10), perpendicular to the rolling face for the hot cast.

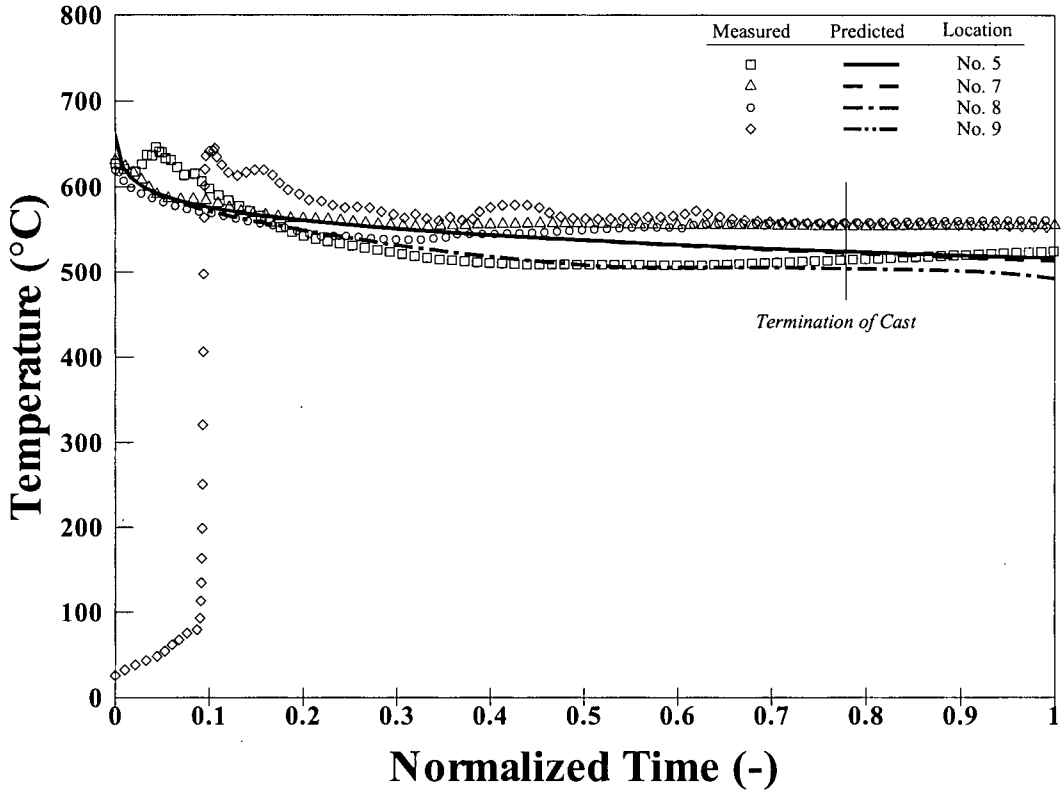

Figure 6.24 - Comparison of measured and model predicted temperatures at different locations 5 mm above the ingot base (refer to Figure 4.10), perpendicular to the narrow face for the hot cast.

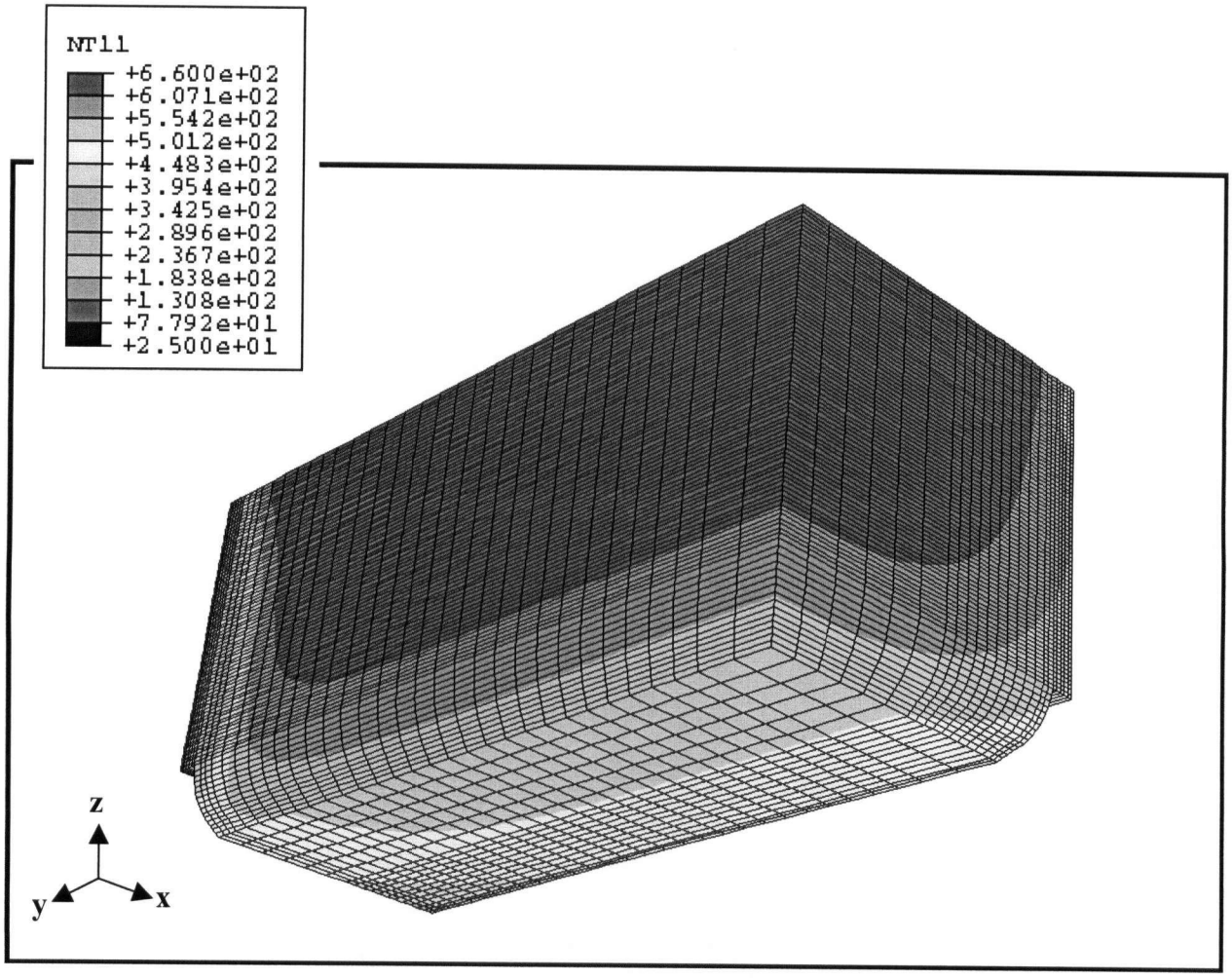

Figure 6.25 – Inner view of the computational domain showing the contour plot of temperature (NT11) along the symmetry faces of the ingot for the hot cast at the end of the analysis. The model predicts a hotter ingot butt in the absence of water incursion.

6.4.3 Model Predictions for Positions Adjacent to the Bottom Block

The variation in temperature with time predicted by the model 5 mm below the top face of the bottom block for the cold cast, and at various locations perpendicular to the rolling face (*i.e.* Location Nos. 1, 2, and 3 in **Figure 4.10**), and perpendicular to the narrow face (*i.e.* Location Nos. 5, 7, 8, and 9 in **Figure 4.10**) is presented in **Figures 6.26** and **6.27**, respectively. The thermocouple data obtained at the same locations have also been plotted for comparison. It is evident from the thermocouple data that the model predicts the phenomenon of water incursion along the rolling (**Figure 6.26**), and narrow faces (**Figure 6.27**) quite accurately. The model over predicts the temperatures at Location Nos. 2, 5, and 7, probably due to the fact that additional

cooling provided by the water running down the edges of the drainage holes was not included in the model. The model also predicts the combined cooling effect induced by the water flowing down the vertical edges of the bottom block and water incursion in the gap, at Location Nos. 1 and 9, although there is a tendency to predict the drop in temperature due to water incursion too late. The extent of cooling (indicated by blue regions) experienced by the bottom block due to water incursion is indicated in **Figure 6.28**, which shows the contour plot of temperature at the end of the analysis for the bottom block in the cold cast. It is evident that the narrow side of the bottom block is cooled to a greater extent due the increase in amount of entrained water between the gap between the ingot and bottom block, as a result of the higher magnitude of butt curl observed in this region.

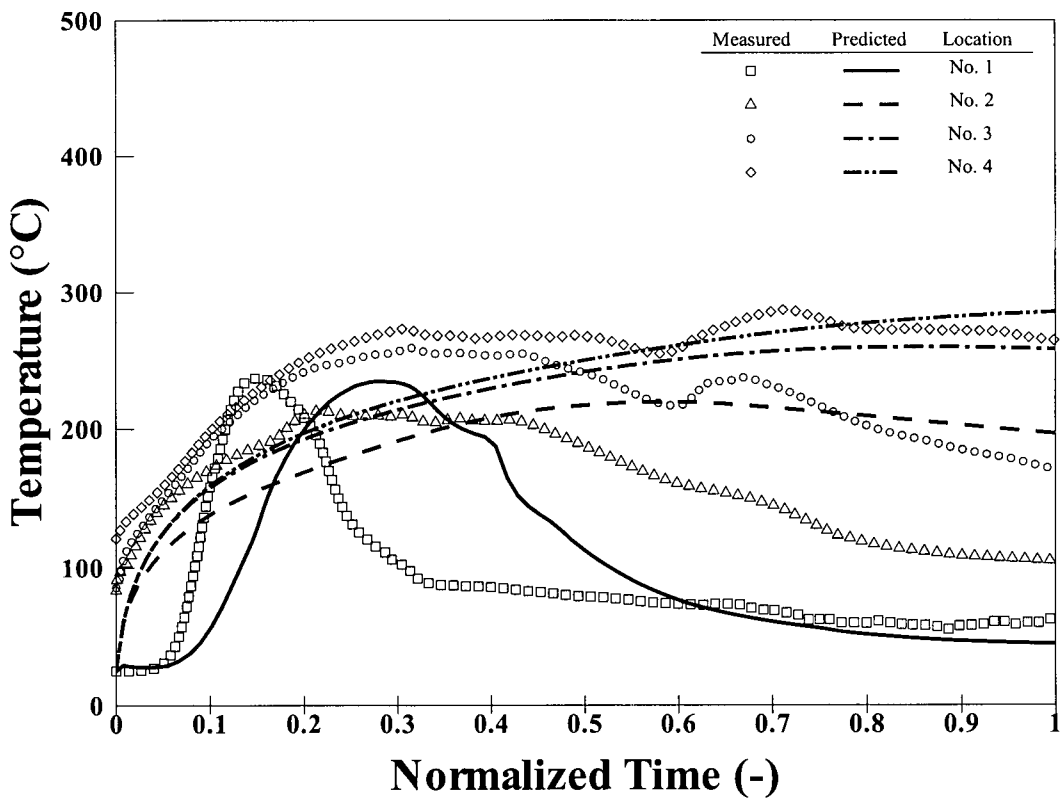

Figure 6.26 - Comparison of measured and model predicted temperatures at different locations 5 mm below the bottom block top face (refer to Figure 4.10), perpendicular to the rolling face for the cold cast.

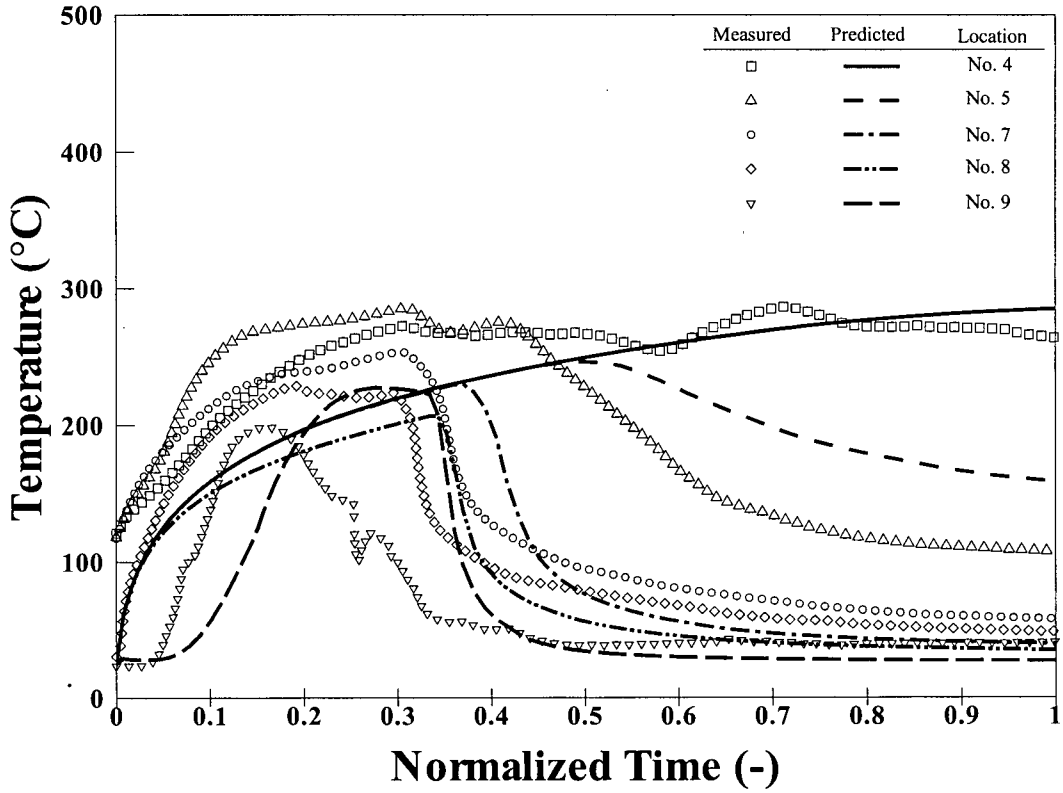

Figure 6.27 - Comparison of measured and model predicted temperatures at different locations 5 mm below the bottom block top face (refer to Figure 4.10), perpendicular to the narrow face for the cold cast.

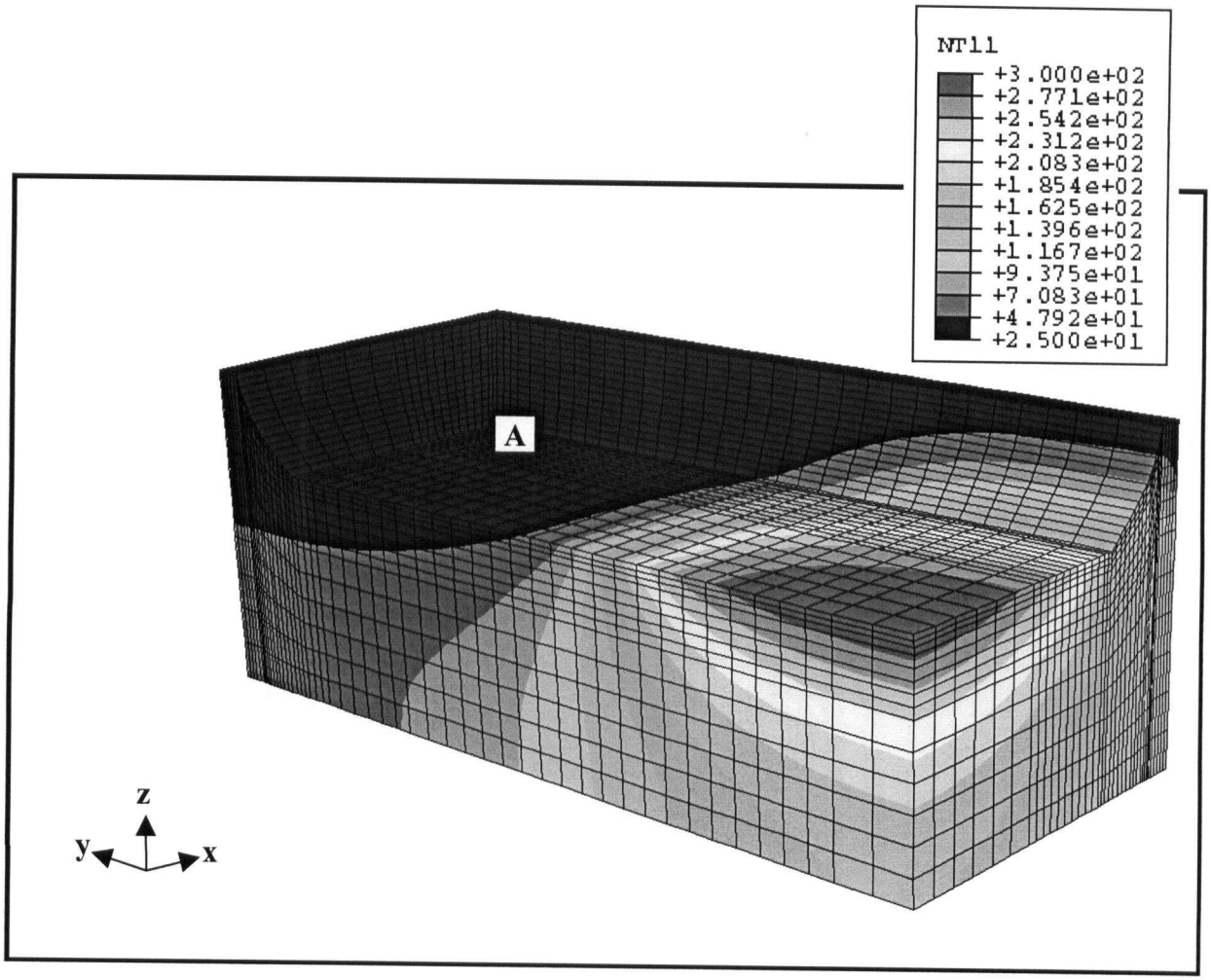

Figure 6.28 – Inner view of the computational domain showing the contour plot of temperature (NT11) along the symmetry faces of the bottom block for the cold cast at the end of the analysis. Region "A" (area in blue) indicates the extent of bottom block cooling due to water incursion along the rolling and narrow faces.

The variation in temperature with time predicted by the model 5 mm below the top face of the bottom block for the hot cast, and at various locations perpendicular to the rolling face (*i.e.* Location Nos. 1, 2, and 3 in **Figure 4.10**), and perpendicular to the narrow face (*i.e.* Location Nos. 5, 7, 8, and 9 in **Figure 4.10**) is presented in **Figures 6.29** and **6.30**, respectively. The thermocouple data obtained at the same locations have also been plotted for comparison. As can be seen, the model accurately predicts a hotter bottom block in the absence of water incursion due the ejection of water along the ingot vertical faces and a lower magnitude of butt curl. This is

also indicated in **Figure 6.31**, which shows the contour plot of temperature at the end of the analysis for the ingot in the hot cast. Comparing **Figures 6.28** and **6.31**, the distinctly different cooling conditions experienced by the bottom block for the two different casts, which is accurately predicted by the model, can be easily delineated. The model also accurately predicts the initial cooling effect induced by the water flowing down the vertical edges of the bottom block and water incursion in the gap, and the later rise in temperature in the absence of water incursion at Location Nos. 1 and 9 shown in **Figures 6.29** and **6.30**.

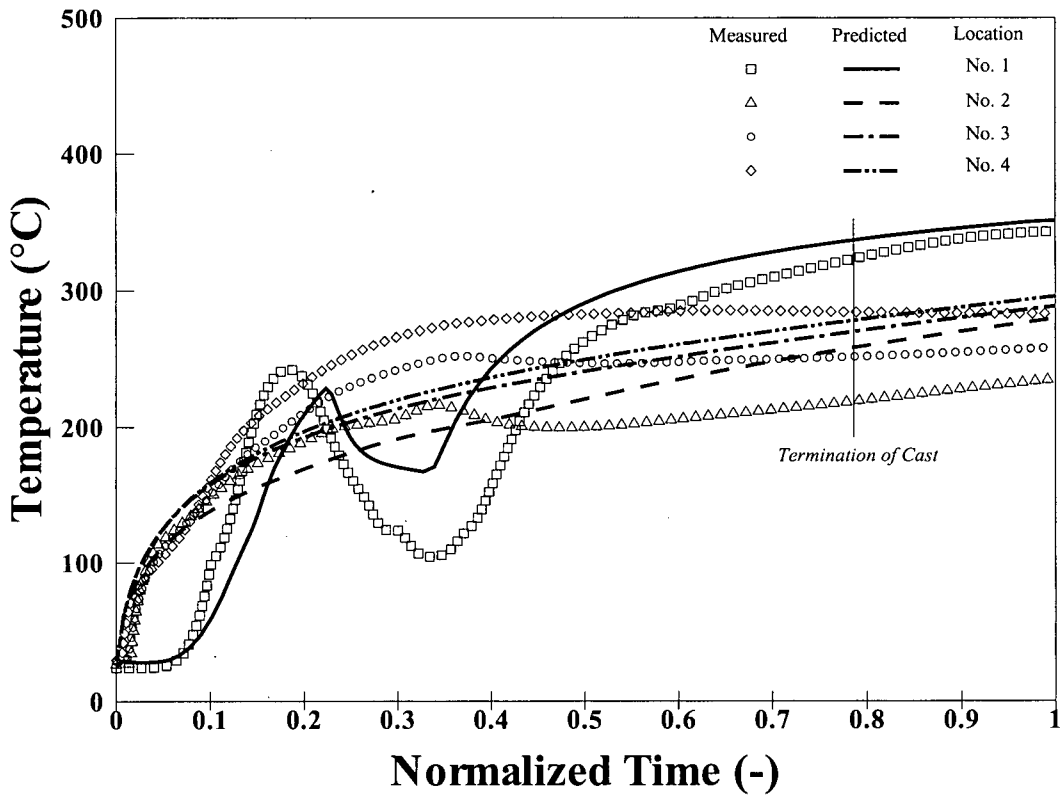

Figure 6.29 - Comparison of measured and model predicted temperatures at different locations 5 mm below the bottom block top face (refer to Figure 4.10), perpendicular to the rolling face for the hot cast.

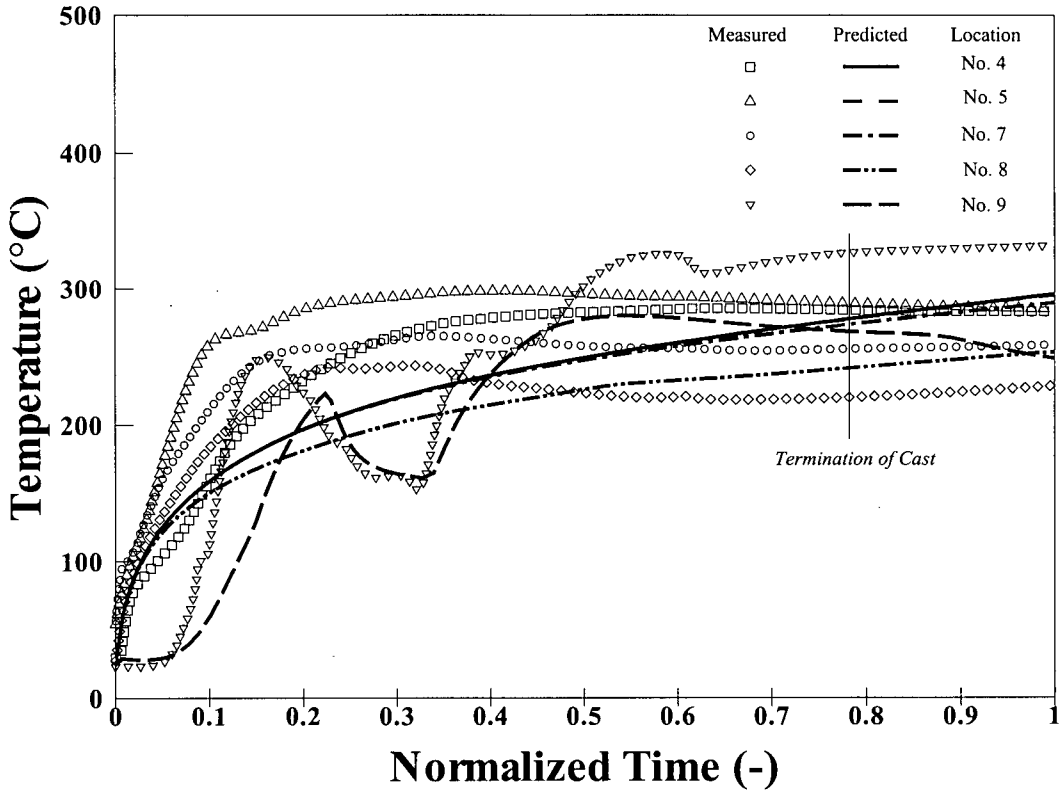

Figure 6.30 - Comparison of measured and model predicted temperatures at different locations 5 mm below the bottom block top face (refer to Figure 4.10), perpendicular to the narrow face for the hot cast.

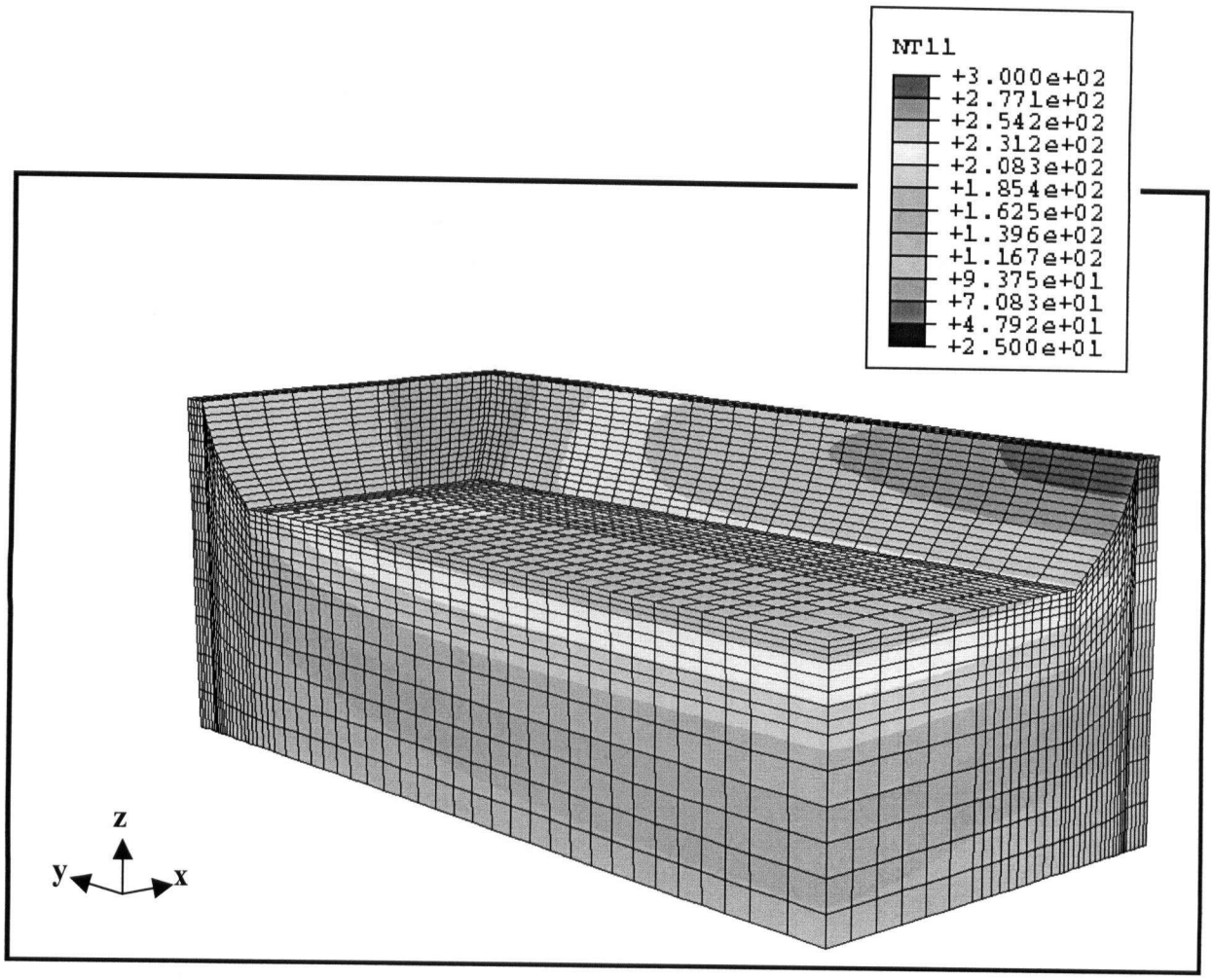

Figure 6.31 – Inner view of the computational domain showing the contour plot of temperature (NT11) along the symmetry faces of the bottom block for the hot cast at the end of the analysis. The model predicts a hotter bottom block in the presence of water ejection and absence of water incursion.

6.5 Implication for Hot Tearing

The 3-D thermal model coupled with a stress model can be used to study the formation of hot tears and cold cracks generated in the ingots during the D.C. casting process. From the standpoint of stress/strain state in the ingot, it is critical that the thermal model captures all the heat transfer phenomena, and correctly describes the evolution of temperature during the start-up phase, in order to predict the thermal loading (equivalent to mechanical loading) that the ingot

experiences. Moreover, correct thermal predictions are necessary to determine the material constitutive behaviour sensitive to temperature.

The effect of thermal phenomena such as collapse of the water ejection front (stable film boiling front) is likely to have a significant effect on the generation of thermal stresses and strains at the centre of the rolling face, which is normally the area prone to hot tearing (centre 1/3 of the face). Preliminary thermal stress calculations run with a thermal model that does not include water ejection has clearly established the presence of a zone of high plastic strain at the base of the ingot near the lip encompassing approximately ¾ of the rolling face (the reader is referred to reference [1]), which contains a detailed presentation of this preliminary thermal/stress model (this model was not included in this thesis for the sake of brevity). Within this region, it is quite conceivable that the collapse of the ejection front – refer to **Figure 6.32** – could lead to a concentration and intensification of plastic strain in the centre 1/3 of the rolling face (plastic strain is used in many of the published hot tear criteria – refer to references [11-14] in Chapter 1 - as an indicator of hot tearing susceptibility), which could bring the predictions more in-line with industrial experience. For example, the material cross-hatched within the centre of the face would be kept at a higher temperature for an extended period of time allowing more strain to accumulate, leading to pore cavitations and hot tearing. Obviously, this process is complex and will require a validated thermal/stress model in order to quantify the spatial stress/strain history within this region. In addition the validated model could also be used to conduct a sensitivity analysis to determine the effect of water ejection and the parameters that influence it on the generation of thermal stresses and strains.

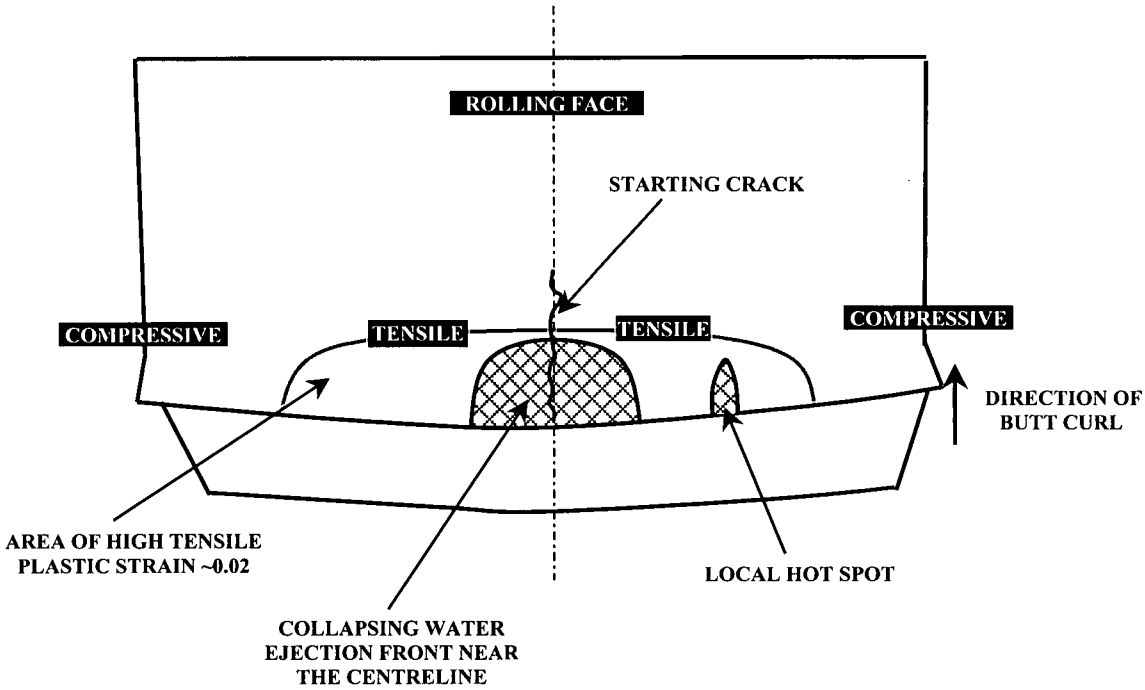

Figure 6.32 – The region of stable film boiling near the centre-line and local hot spots on the rolling face of the ingot, which lie within the region of high tensile plastic strain, may be potential sites for hot tears and starting cracks during the start-up phase of the D.C. casting process.

6.6 Summary

The influence of water ejection and water incursion on the evolution of temperature in the ingot and bottom block was examined with a 2-D thermal model. Comparison of the model predictions with the data collected from the embedded thermocouples indicated that the 2-D model was capable of describing the flow of heat in the early stages of the casting process in a region close to the centre of the rolling face. The sensitivity analysis completed with the model clearly identified the link between ingot base cooling and secondary water cooling heat transfer during the start-phase.

The 2-D longitudinal model was limited to the analysis of heat transfer in a plane normal to the rolling face, and did not completely describe the three-dimensional heat transfer processes

active during the start-up phase. A 3-D analysis was therefore necessary to capture the spatial and temporal variations of temperatures along the ingot rolling and narrow faces, ingot base, and bottom block top surface.

The temperature predicted by the 3-D model that also incorporated features, which capture phenomena such as water ejection and water incursion, showed satisfactory overall agreement with the measured temperature data for both the cold and hot casts, which were distinguished by the different start-up cooling conditions experienced by the ingot. The boundary conditions, which include specific phenomena describing the start-up phase of the D.C. casting process, were linked to the start-up casting practices *via* the *sfilm.f* subroutine in ABAQUS. The model adequately captured start-up conditions that trigger nucleate and film boiling on the ingot surfaces, and their subsequent effect on the secondary cooling heat transfer. The model qualitatively predicted the evolution and collapse of the parabola-shaped water ejection front, which was observed during the hot cast. The model also satisfactorily captured the influence of butt curl and entrained water on ingot base cooling during the start-up phase.

The distinctly different spatial variation in temperature for the bottom block predicted by the model for the cold and hot casts indicated that the bottom block played a significant role in dictating the heat transfer from the base of the ingot during the start-up phase. The thermal behaviour of the bottom block was clearly influenced by the evolution of the butt curl and the process of water incursion.

The model, owing to the limitation of the assumption that the spatial variation of the base deformation followed a parabolic relationship, under predicted the measured temperatures along the base of the ingot perpendicular to the rolling face. However, the predictions for other locations above the ingot base were found to be satisfactory. The uncoupled analysis is therefore limited by two factors: 1) the measured data for the evolution of butt curl at the centre of the rolling and narrow faces of the ingot are required as an input, and 2) the computation of the spatial distribution of the base deformation along the ingot base.

The model predicted the drop in temperature due to water incursion at locations near the bottom block edges too late compared to the actual observations. Aggressive cooling was predicted by the model in the regions close to the ingot lip and adjacent to the rolling and narrow faces of the ingot.

To the author's knowledge, this is the first time that a thermal model has been extensively validated against industrial data, and this research programme represents a significant improvement over existing models that do not quantitatively describe important phenomena specific to the start-up phase.

The temperature field from this validated thermal model can be utilized to run uncoupled stress models for computing stress/strain fields in the ingot. These thermal and stress models can then be used to evaluate process optimization techniques aiming at maximizing quality and productivity or to study new alloy systems.

References

1. Sengupta, J., Maijer, D., Wells, M. A., Cockcroft, S. L., and Larouche, A., *Mathematical Modeling of the Thermomechanical Behavior of a 5182 Aluminum Ingot During the Start-up Phase of the DC Casting Process: The Role of Bottom Block,* Light Metals 2001 (Ed. J. L. Anjier), The Minerals, Metals and Materials Society, Warrendale, USA, 2001, pp. 879-885.

CHAPTER 7
SUMMARY AND CONCLUSIONS

The control of the thermal cooling conditions at the start-up phase of the D.C. casting process for aluminum ingots is difficult, and is critical from the standpoint of defect formation. Firstly, boiling water heat transfer governs the secondary cooling experienced by the ingot surfaces as they emerge from the mould. This results in varying rates of heat transfer from the ingot faces as the surface temperature of the ingot changes with time during the start-up phase. Moreover, if the ingot surface temperature at locations below the point of water impingement is high enough to promote film boiling, the water is ejected away from the surface. Also, the chill water may enter into the gap formed between the ingot base and bottom block with the evolution of butt curl. This water incursion alters the heat transfer from the base of the ingot, and in turn affects the surface temperature of the ingot faces.

The complexity of the various heat transfer processes described above requires a tight control of the cooling of the ingot during the start-up phase. Optimization of the casting parameters such as withdrawal rate, water flow rate, and casting speeds has traditionally been achieved by empirical techniques. Recently, a number of computer-based thermal and stress models of the process have been developed with the intent that they can be applied to optimize the start-up practice and process design. It is critical that these tools capture all of the complexity of the industrial process if they are to ultimately be useful. Based on literature review, the thermal models reported in the past two decades suffer from several drawbacks. These are: (i) the phenomenon of film boiling has never been included in the thermal boundary conditions describing the secondary cooling, (ii) the role of the bottom block during the start-up phase has not been investigated thoroughly, and (iii) no attempt has been made so far to validate the thermal model by measuring ingot and bottom block temperatures within a broad range of industrial casting conditions.

To obtain data suitable for verification of the model, industrial trials were performed at Alcan's casting facility on two 711 mm x 1680 mm AA5182 aluminum ingots. The bottom block filling rate, casting velocity, and water flow rate were varied to produce a non-typical "cold" start and a non-typical "hot" start. Temperature data were recorded by thermocouples

cast/embedded at various locations along the ingot rolling and narrow faces, ingot base, and top surface of the bottom block. Ingot base deflection was also measured in order to obtain the evolution of butt curl with time.

The industrial trials conducted at Alcan revealed that variation in the water flow rate during the initial ~300-500 s of the casting process can significantly affect the start-up cooling conditions experienced by the ingot and the amount of butt curl observed at the ingot corner. Two process extremes were studied. On the one hand, at high water flow rate, the ingot base was cooler, but it experienced large butt curl deformation. On the other hand, at low water flow rate, the ingot base was hotter triggering the process of water ejection, which kept the ingot base above the solidus temperature throughout the start-up phase, while the corners experienced little macro-deformation.

A comprehensive mathematical model was developed to describe heat transfer during the start-up phase of the process. The model, based on the commercial finite element package ABAQUS, includes primary cooling to the mould, secondary cooling to water and ingot base cooling. The algorithm for primary cooling includes a weighting function based on the fraction solidified, which allows the transition between meniscus (high) and air gap (low) cooling. The algorithm used to account for secondary cooling to the water includes boiling curves that are a function of surface temperature, impingement point temperature, water flow rate and position relative to the point of water impingement. In addition, the secondary cooling algorithm accounts for water ejection, which can occur at low water flow rates (low heat extraction rates). The algorithm used to describe ingot base cooling, includes the drop in contact heat transfer due to base deformation (butt curl) and also the increase in heat transfer due to water incursion between the ingot base and the bottom block. The implementation of these phenomena specific to the start-up phase of the D.C. casting process is unique to this research programme, and represents a significant improvement over existing thermal models.

The two different start-up heat transfer conditions for the cold and hot cast were examined with the thermal model developed during this research programme. The model validation process involved "fine tuning" the thermal boundary conditions with the help of thermocouple data obtained from the ingot rolling and narrow faces, ingot base, and the top surface of the bottom block. Traditionally, thermal models for the start-up phase have been indirectly validated by comparing the butt curl predictions from uncoupled/coupled thermal and

stress models with measured data. To the author's knowledge, the extensive validation process for the thermal model by industrial measurements that was conducted during this research programme has never been reported in published literature to date.

Comparison of the model predictions to data collected from thermocouples cast/embedded in the ingot and bottom block lead to the following conclusions:

- Both the 2-D and 3-D models, which include the phenomena of water ejection and water incursion are capable of describing the flow of heat in the early stages of the casting process quite efficiently. However, the 2-D longitudinal model is limited to the analysis of heat transfer in a plane normal to the rolling face, and does not completely describe the three-dimensional heat transfer processes active during the start-up phase.
- Agreement between the model predictions and measured data indicate that the 3-D model was capable of capturing the conditions (*i.e.* low water flow rates) that encourage the shift from the nucleate boiling to film boiling phenomena, leading to the process of water ejection on the ingot rolling and narrow faces. The parabola-shaped ejection front, which collapses towards the centre-line of the face with time, was also predicted by the model at very low heat extraction rates. The 3-D model also effectively predicted the spatial variations in temperature adjacent to the ingot base and bottom block top surface, resulting from the combined effect of butt curl and water incursion.
- The 3-D uncoupled thermal model, owing to the limitation of the assumption that the spatial variation of the base deformation followed a parabolic relationship, requires: 1) the measured data for the evolution of butt curl at the centre of the rolling and narrow faces of the ingot is required as an input, and 2) the appropriate computation of the spatial distribution of the base deformation along the ingot base, to correctly predict the ingot base cooling process. Also, the model over estimated the heat transfer process due to primary cooling resulting in the initial sharp drop in temperature at locations adjacent to the rolling and narrow faces.

Finally, if the 3-D thermal model validated by industrial measurements is coupled with a stress model, it can be used as a powerful tool to optimize the start-up phase for producing zero defect ingots under controlled cooling conditions. It can also be used to study the formation of hot tears and cold cracks generated in the ingots during the start-up phase.

7.1 Recommendations for Future Work

The conclusions drawn from this research programme have been based primarily on the predictions from the FE thermal model describing the various heat transfer phenomena that occur during start-up phase of the D.C. casting process. However, a thorough understanding of the thermomechanical behaviour of the ingot during cast start-up requires the development of a stress model that is coupled with the thermal model, which has been formulated and validated during this programme. A 3-D stress model, which incorporates appropriate constitutive behaviour for AA5182 at both below- and above-solidus temperatures, could be validated by the butt curl and residual stress measurements made on the cold and hot casts. The validated thermomechanical model would then emerge as a comprehensive tool for optimizing the start-up phase and improving the quality of sheet ingots.

Presently, the uncoupled thermal model requires the measured data for the evolution of butt curl at the centre of the rolling and narrow faces of the ingot as an input, and thus, its applicability as a process optimization tool is limited. With the availability of newer versions of ABAQUS and enhanced computing facilities at UBC, an attempt can be made to couple the thermal and stress analysis together, which would result in simultaneous computation of the ingot base deformation and application of a displacement dependent Cauchy type heat transfer coefficient at the ingot-bottom block interface. This validated coupled analysis would then constitute a state-of-the-art technology that could revolutionize the D.C. casting industry. The coupled thermomechanical model would trigger new optimization techniques and hot tearing theories, resulting in an efficient process and high quality products. The coupled model would ultimately play a crucial role in removing the technological barriers involved in casting high strength aluminum sheet ingots that are slated for use in the automobile industry.